NGT-21-002-080

NGT-80001

DESIGN OF A RAM ACCELERATOR MASS LAUNCH SYSTEM

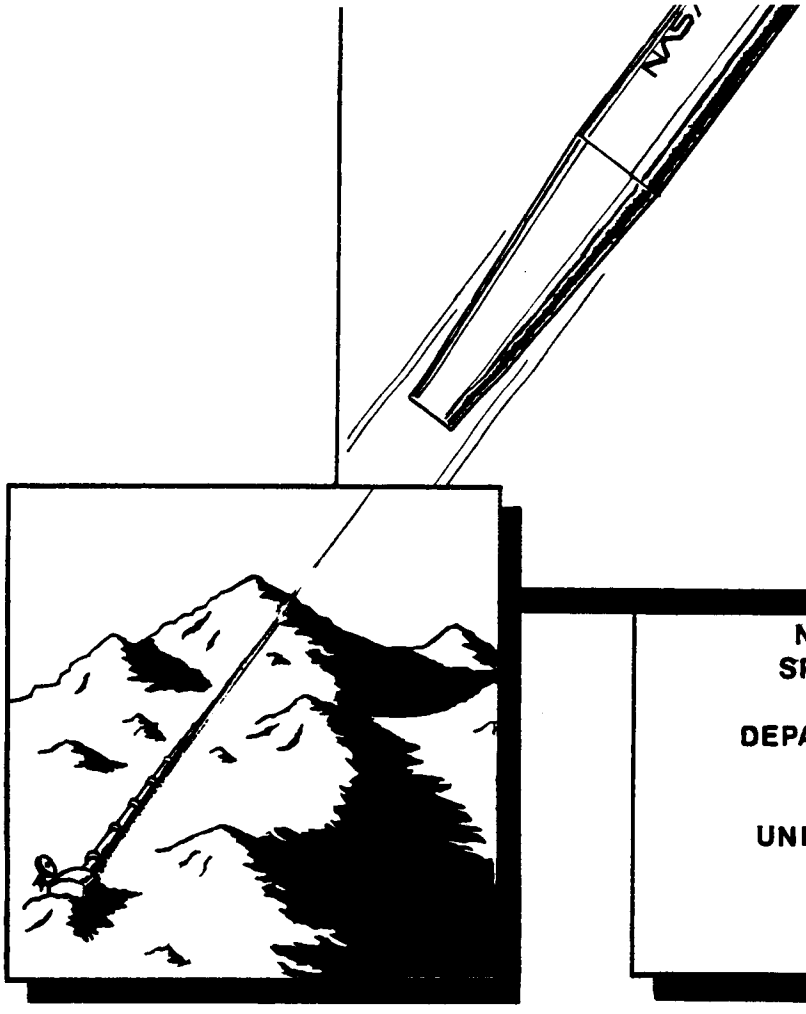

FINAL REPORT

NASA/USRA ADVANCED
SPACE DESIGN PROGRAM

DEPARTMENT OF AERONAUTICS
AND ASTRONAUTICS

UNIVERSITY OF WASHINGTON
SEATTLE, WA 98195

JUNE 1988

DESIGN OF A RAM ACCELERATOR MASS LAUNCH SYSTEM

FINAL REPORT

Spacecraft Systems Design, AA 420/499C
NASA/USRA Advanced Space Design Program

Prepared By:

Michael Aarnio
Calvin Armerding
Andrew Berschauer
Erik Christofferson
Paul Clement
Robin Gohd
Bret Neely
David Reed
Carlos Rodriguez
Fredrick Swanstrom
Seshu Vaddey
Jesse Vickers
Jack Wolda
LeAnne Woolf

Faculty Advisors

Adam P. Bruckner
Abraham Hertzberg

Department of Aeronautics and Astronautics
University of Washington, FS-10
Seattle, WA 98195

June 6, 1988

ABSTRACT

The viability of any large scale permanent space structure relies on the capability of being able to launch mass easily and efficiently into orbit. The ram accelerator mass launch system has recently been proposed to greatly reduce the costs of placing acceleration-insensitive payloads into low earth orbit.

The ram accelerator, conceived and experimentally demonstrated at the University of Washington, is a chemically propelled, impulsive mass launch system capable of efficiently accelerating relatively large masses from velocities of 0.7 km/sec to 10 km/sec. The principles of propulsion are based upon those of a conventional supersonic air-breathing ramjet; however the device operates in a somewhat different manner. The payload carrying vehicle resembles the center-body of the ramjet and accelerates through a stationary tube which acts as the outer cowling. The tube is filled with premixed gaseous fuel and oxidizer mixtures that burn in the vicinity of the vehicle's base, producing a thrust which accelerates the vehicle through the tube.

This study examines the requirements for placing a 2000 kg vehicle into a 500 km circular orbit with a minimum amount of on-board rocket propellant for orbital maneuvers. The goal is to achieve a 50% payload mass fraction.

The proposed design requirements have several self-imposed constraints that define the vehicle and tube configurations. Structural considerations on the vehicle and tube wall dictate an upper acceleration limit of 1000 g's and a tube inside diameter of 1.0 m. In-tube propulsive requirements and vehicle structural constraints result in a vehicle diameter of 0.76 m, a total length of 7.5 m and a nose-cone half angle of 7°. An ablating nose-cone constructed from carbon-carbon composite serves as the thermal protection mechanism for atmospheric transit.

Two modes of in-tube propulsion involving ramjet cycles are used in sequence to accelerate the vehicle to the desired launch tube exit velocity. The two modes that have been investigated are a thermally choked subsonic combustion mode, capable of accelerating the vehicle from 0.7 km/sec to 2.5 km/sec, and a mode which utilizes a stabilized oblique detonation wave for combustion to accelerate the vehicle from 2.5 km/sec to as high as 10 km/sec. An initial acceleration from zero to 0.7 km/sec, required to start the ramjet cycle, is provided by firing the vehicle into the launch tube using a combustion-driven gas gun. Nine different propellant mixtures, each at a fill pressure of 33 atm and a fill temperature of 300 K, are utilized in the ram accelerator to achieve the desired velocity. These propellants consist of methane or hydrogen as the fuel, oxygen as the oxidizer and carbon dioxide, nitrogen or hydrogen as diluents which tailor the heat release and speed of sound of each mixture. The acceleration of the projectile is kept near the design limit of 1000 g's at an average ballistic efficiency of 24% and an average thrust pressure ratio of 14%. The required total length of the stationary launch tube varies from 3.8 km at 8 km/sec to 6.7 km at 10 km/sec. Using high strength steel as the launch tube material, the wall thickness required for the thermally choked portion of the barrel is 12.7 cm while the wall thickness of the oblique detonation portion is 27.6 cm for the first 2.3 km and 24.8 cm for the remainder (using a yield safety factor of 3).

Once the necessary launch velocity of 8-10 km/sec is obtained, the vehicle traverses the atmosphere thermally protected by a carbon-carbon ablating nose cone. An aerodynamic heating analysis was carried out to determine the ablation mass loss and the velocity loss during atmospheric transit. Both turned out to be small. For example, for a 9 km/sec launch at the corresponding optimum launch angle of 20°, the vehicle retains 85% of its original launch velocity and suffers an ablative mass loss of only 1.3%. The drag coefficient increases from .058 at launch to .11 during the atmospheric transit. The aerodynamic stability of the vehicle was investigated by using small perturbation theory. The vehicle was found to be inherently unstable. Angular accelerations on the order of 164 rad/s^2 at the 4000

m launch altitude and .16 rad/s^2 at 40 km altitude were estimated. Stability augmentation devices, such as control surfaces or spinning the vehicle to provide the needed stability, will clearly be required.

After the vehicle exits the sensible atmosphere, an indirect orbital insertion maneuver with two rocket burns and aerobraking is performed to minimize the required on-board propellant mass. Analyses based on a proposed parking orbit altitude of 450 km and a final orbit of 500 km have been carried out. A launch site which offers a launch altitude of about 4000 m and lies very near the equator is proposed at Mt. Kenya in Kenya. The total velocity change needed from the on-board propellant for a 9 km/sec launch velocity at the optimum launch angle of 20° is approximately 780 m/s. The multi-step orbital maneuver with aerobraking allows a 40% savings in the orbital velocity change required from on-board propellant in comparison to a similar orbital maneuver without aerobraking. The optimum on-board propulsion system using current technology is an MMH-N_2O_4 bi-propellant rocket with an Isp of 297 sec and a total mass of approximately 670 kg.

The ram accelerator payload vehicle must structurally withstand an acceleration of 1000 g's, a maximum pressure of 1000 atm in the subsonic combustion mode and 1667 atm in the oblique detonation mode (using a 1-D analysis), and temperatures on the order of 3000 - 4000 K for brief periods (~1 second). A vehicle configuration incorporating T300/5208 graphite/epoxy resulted in minimum structural mass when approximating the composite material properties as isotropic. The analysis produced a structural mass of approximately 600 kg for a vehicle length of 7.5 m. A finite element analysis yielded similiar results. Estimates of the vehicle center of gravity place it 3.8 m behind the nose tip with a moment of inertia of 6,200 kg/m^2 about an axis perpendicular to the axis of the vehicle.

Each area of study was analyzed with the restriction that only current technology be employed. Considerable effort was also made in designing the vehicle to be reusable. It is demonstrated that no technological barrier hinders the development of the ram accelerator mass launch concept.

PREFACE

In 1980 the Department of Aeronautics and Astronautics at the University of Washington initiated an undergraduate design program in the field of space systems. Effective student participation in these space-design-related activities has been integrated as much as possible with the faculty's NASA-funded research program since the inception of the course. The inception of the NASA/University Pilot Program in 1985 and the selection of the University as one of the participants in both the Pilot Program and the formalized Advanced Space Design Program therefore enabled us to develop these efforts very productively. The student response has been excellent and the synergism with our research program highly beneficial.

Our course structure is aimed at exposing the students to a design situation which is "real world" as much as possible within the University framework. In addition, the course undertakes the responsibility of teaching the students those aspects of space engineering and science which would be needed for general space capability. Students are taught the fundamentals of propulsion, orbital mechanics, reentry physics, nuclear and solar power systems, structures and thermal management.† The design problems expose the students to a situation in which they must understand the inter-relationship and complete systems dependence of the structural components, thermal components, and environmental constraints particular to space.

The course offering consists of two 10-week academic quarters (Winter and Spring). The first course (AA420 Space Systems Design) is initially structured as a formal lecture/discussion series which meets 5 hrs/week. Formal lectures by the instructors and presentations by guest lecturers from industry and NASA provide the students with the fundamental background they need to carry out their design studies. By the second week of the quarter, the students are divided into design teams whose responsibility is to address

† The topics of propulsion, orbital mechanics and structures are covered in depth in other departmental courses. In the space design course selected topics in these areas are covered.

specific subsystems of the overall design. As the design progresses, more and more time is devoted to in-class discussions of the students' work. Teaching assistants supported by NASA/USRA funds work with the students and help the instructors with project management. The results of the design study are presented at the end of the quarter in the form of formal written reports, one by each of the design groups.

The Spring Quarter offering (AA499C - Independent Studies in Space Systems Design) is intended to refine and advance the design and to address key problem areas identified during the previous quarter. The class meets formally three hours a week in group discussion format. Early in the quarter the students are encouraged to submit papers on their projects to the AIAA Region VI Student Conference. In all cases to date, the reactions of the judges to the quality of our students' papers has been very favorable. At this year's conference our students garnered two third-place awards in the undergraduate division. At the end of the Spring Quarter the students submit a single final report on the overall design and make an oral presentation as part of the department's Undergraduate Seminar series.

The instructors are proud of the responsiveness of the students and feel that, while the students are terribly overworked, they are virtually unanimous in agreeing that this course provides them with a quality introduction to the world of design. A general competitive atmosphere is maintained wherever possible as an additional simulation of the real world. The feedback from the students to the instructors also has proved effective in stimulating the instructors. In addition, the basic research program carried out by the University has benefited by the recognition of the practical problems of design as they reflect back through the program.

The design problem selected during the 1985 instructional period, the first year of the NASA/University program, was a concept for a 150 kW_e solar dynamic space power system for future space factories, either in a roving mode or in space station orbits. The important condition of this design was that this power unit had to operate in an independent power package. A particularly significant finding of this study was the ability to combine the liquid

droplet heat exchanger concept with thermal energy storage in a unique fashion which tends to avoid many of the difficulties associated with existing thermal storage concepts.

During the 1986 period, an examination was carried out of future NASA space power needs, particularly in the high power region, i.e., greater than 1 MW. These studies led the students to conclude that nuclear power offered the most reasonable approach to such high power needs. A 3 MW_e power system was therefore elected as the subject of the design study. As we were able to perceive NASA's power needs, we felt that such high power systems will be required, particularly under the new thrust being set up by NASA based on the recent report from the National Commission on Space. One of the particular recommendations of this group is the utilization of extraterrestrial bodies such as the moon, Mars, and selected large asteroids as part of the supporting infrastructure for a future space culture. An important finding of our 1986 project was that space-based nuclear power systems readily adapt themselves to a surface environment without significant mass penalties. The liquid droplet radiator was found to be particularly adaptable to the moon due to the positive aspect of lunar gravity on the droplet collection process.

The project selected in 1987, as well as its continuation during the present academic year had its roots in the area of unconventional space transportation. Approximately 5 years ago we embarked on a long-range effort to develop a new propulsive technique, the ram accelerator, which is capable of both the velocities and the scale necessary for a viable direct-launch-to-orbit system. The ram accelerator is a ramjet-in-tube concept that makes use of chemical energy in an innovative manner to accelerate projectiles to superorbital velocities. With funding from the Air Force we have successfully carried out proof-of-principle experiments. The capabilities of this approach attracted the interest of NASA/OAST management and resulted in a grant (NAG-1-764), with United Technologies Research Center as the subcontractor, to explore the engineering feasibility and economic advantages that such a system may offer NASA. Simultaneously, we selected this topic as the 1987 design study for the NASA/USRA Advanced Space Design Program.

The encouraging results of last years' feasibility study, coupled with the results of the work under the separate NASA grant, led to our being invited to participate in a briefing at NASA Headquarters, in November 1987, on Unconventional Transportation Concepts. The favorable reception accorded to the ram accelerator concept, together with our advances on the experimental front prompted us to continue with a more detailed engineering study in our design course this year. The results of that study comprise the content of this report.

The combination of the USRA program with the NASA program has proved unusually effective, thereby proving a challenging and rewarding design experience for the students. As this concept continues to develop, it is expected to remain one that the students will surely respond to with creativity.

A.P. Bruckner
Research Associate Professor

A. Hertzberg
Professor

June 6, 1988

ACKNOWLEDGEMENTS

We would like to express our deep appreciation to NASA for selecting the University of Washington to participate in the NASA/University Advanced Space Design Program. Thanks are particularly due to Jack Sevier and Carol Hopf of the Universities Space Research Association for their skillful management of the Program and for the frequent informative discussions they had with the instructors, and to Karl Faymon of the NASA Lewis Research Center for his helpful comments and discussions, for providing the University with relevant literature and data, and for presenting topical seminars to our students. We are also indebted to Peter Kaloupis and Gilbert Chew, graduate teaching assistants, for their contributions and diligence throughout the duration of the course, and to Dean Brackett and Alan Kull, graduate research assistants, for their assistance with some of the computational aspects of the project. Many thanks are also due to Bruce Schmitz, Vice President for Research, Olin/Rocket Research Company, and to Paul Micheli, formerly with Aerojet General Corporation, for their very helpful discussions on the design of liquid and solid rocket propellant systems. We would also like to thank Prof. S. Eberhart of the University of Washington for his insightful advice on atmospheric transit at hypersonic velocities.

TABLE OF CONTENTS

I. INTRODUCTION

The viability of any large-scale, permanent space station relies on the capability of launching mass easily and efficiently into orbit. Present systems require the launch vehicle to carry all the propellant neccessary for launch and this reduces the amount of payload the vehicle can carry, thus increasing the launch costs to as much as $7000/lb for the space shuttle. Of prime importance for space stations would be water, propellants, consumables, and structural material, all of which are capable of withstanding high accelerations. Thus, research has turned toward the potential use of impulsive mass launchers, which impart the needed orbital kinetic energy at the earth's surface, eliminating the need for any on-board fuel during launch, except that for orbit circularization. The ram accelerator mass launch system is an impulsive launch concept conceived at the University of Washington for launching acceleration-insensitive payloads into a low earth orbit.[1,2]

The principles of propulsion of a ram accelerator are based upon those of a conventional supersonic air-breathing ramjet; however, the device operates in a somewhat different manner (see Fig. I-1 and I-2). The payload carrying vehicle resembles the center-body of a ramjet and accelerates through a stationary tube which acts as the outer cowling. The tube is filled with premixed gaseous fuel and oxidizer mixtures that burn in the vicinity of the vehicle's base, producing a thrust which accelerates the vehicle through the tube. In order to accelerate the vehicle to the desired launch tube exit velocity two different modes of in-tube propulsion involving ramjet cycles are used. The two modes that have been investigated are a thermally choked, subsonic combustion mode, which accelerates the vehicle to 2.5 km/sec, and a mode which utilizes a stabilized oblique detonation wave for combustion at higher velocities. Combined, these two modes are capable of accelerating the vehicle to a velocity as high as 10 km/sec. An initial combustion-driven, gas-gun type accelerator is used to impart the necessary initial velocity of 0.7 km/sec for the in-tube propulsive processes.

In previous work feasibility studies were done and proposals made on how to best

design the systems of this concept [1,2]. This year the design program has centered on a systems analysis based on the earlier proposals.

The design of the ram accelerator mass launch system presented in this report has been divided into six areas: 1) initial acceleration, 2) ramjet in-tube propulsion, 3) atmospheric transit, 4) orbital mechanics, 5) on-board propulsion, and 6) structural design of the vehicle and launch tube. This report details a systems analysis of these five areas. The analysis is done for the case study of placing a 2000 kg vehicle into a 500 km circular orbit with a minimum amount of on-board rocket propellant for orbital maneuvers. The goal is to achieve a 50% payload mass fraction. The proposed design requirements have several self-imposed parameters that define the vehicle and tube configurations. Due to structural considerations on the vehicle and tube wall, an upper limit of 1000 g's was imposed on the acceleration and the launch tube inside diameter was fixed at 1.0 m. In-tube propulsive requirements and vehicle structural constraints resulted in a vehicle diameter of 0.76 m, a total length of 7.5 m and a nose-cone half angle of 7°.

The initial accelerator system is detailed in Chapter II. The ramjet in-tube propulsion, which deals with imparting the necessary kinetic energy needed for launch, is discussed in Chapter III. It utilizes the ram accelerator concept which was conceived and experimentally demonstrated at the University of Washington [3]. The aerodynamics of the vehicle as it traverses the atmosphere after launch is discussed in Chapter IV. At the high hypersonic launch velocities of 8-10 km/sec the vehicle experiences severe aerodynamic heating and forces that will require adequate thermal protection and stability augmentation for controlled ascent. The thermal protection system used in the study is a carbon-carbon ablative nose cone. A transpiration cooling scheme was also considered but was ruled out as being too complex and heavy. The ablative nose cone and large pressure drag act to reduce the kinetic energy of the vehicle but high velocity retention is crucial for optimization of orbital maneuvers.

Once beyond the atmosphere orbital maneuvers have to be performed to place the

vehicle into the desired low earth orbit. As in any mass launch system, an on-board propulsion system is required in order to perform these maneuvers. Therefore, it is important that the orbital maneuvers be devised as efficiently as possible in order to minimize the mass penalty of the on-board rocket. Previous studies have indicated that a multi-step maneuver involving aerobraking offers the potential for minimum on-board propulsion system mass [2]. Therefore, the focus of this study is to integrate a multi-step maneuver with aerobraking into the ram accelerator launch concept. To increase the flexibility of this launch concept a parking orbit has been proposed to "store" the vehicle until it is needed at its final destination, e.g. a space station. The orbital mechanics analysis is presented in Chapter V.

The orbital requirements of the payload vehicle dictate the necessary velocity change and thrust performance for the on-board propulsion system. The optimization of the mass fraction of payload limits the size and mass specifications of the propellant system. Various propulsion systems exist for use on spacecraft, such as solid propellant rockets, liquid propellant rockets, and other concepts. The selection of a propulsion system which can meet the design criteria of vehicle mass and volume as well as system costs is treated in Chapter VI.

During the in-tube acceleration process the vehicle and launch tube experience high stagnation pressures and temperatures due to the propulsion modes. Of crucial importance to the feasibility of the ram accelerator launch concept is whether it is possible to design a vehicle and launch tube capable of withstanding the extreme conditions of launch, while maintaining the design criteria. Particular areas of concern are at the base of the vehicle during the thermally choked combustion mode and at the side wall of the vehicle during the oblique detonation mode. In addition, the vehicle must withstand the peak acceleration of 1000 g's. Analysis has centered around the use of lightweight, high yield stress graphite/epoxy composites for the vehicle and high strength steel for the launch tube. These structural studies are discussed in Chapter VII.

It should be noted that the present design study is not regarded as complete in that the

question of cost effectiveness in comparison to other launch methods has not been examined. However, to keep costs low, only current technology was employed, cheap propellants were selected, and a considerable effort was made to improve the reusability of the vehicle. Based on the success of the design and the depth to which the studies could be taken, a clear direction for system optimization in future studies can be defined.

REFERENCES

1. Hertzberg, A., Bruckner, A.P, eds., "The Ram Accelerator Concept: A Method for Direct Launch of Space Cargo to Orbit," Final Report, AA 420/499, NASA/USRA Advanced Space Design Program, University of Washington, Seattle WA., June 1987.

2. Bruckner, A.P., and Hertzberg, A., "Ram Accelerator Direct Launch System for Space Cargo," IAF Paper 87-211, 38th Congress of the International Astronautical Federation, Brighton, United Kingdom, October 10-17, 1987.

3, Hertzberg, A., Bruckner, A.P., Bogdanoff, D.W., "Ram Accelerator: A New Chemical Method for Accelerating Projectiles to Ultrahigh Velocities", AIAA Journal, Vol. 26, Feb. 1988, pp. 195-203.

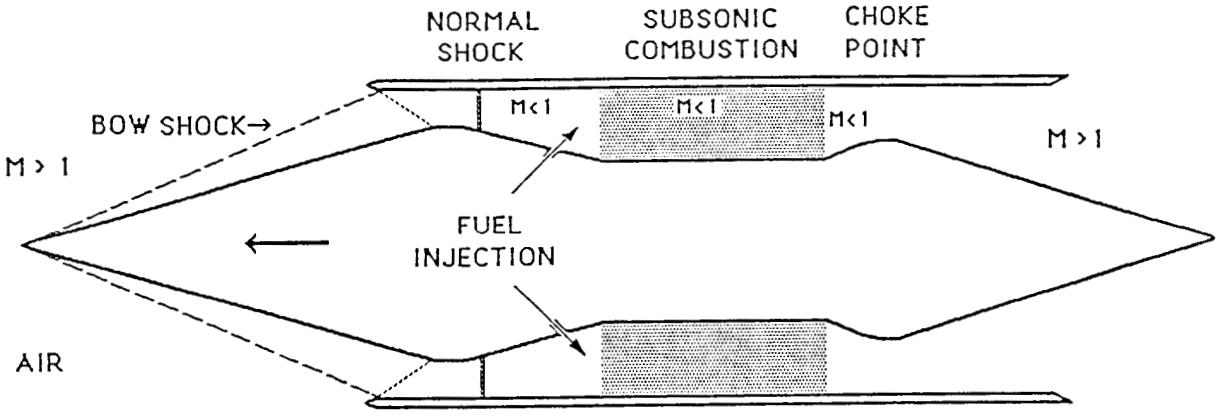

Fig. I-1 Schematic of a supersonic airbreathing ramjet.

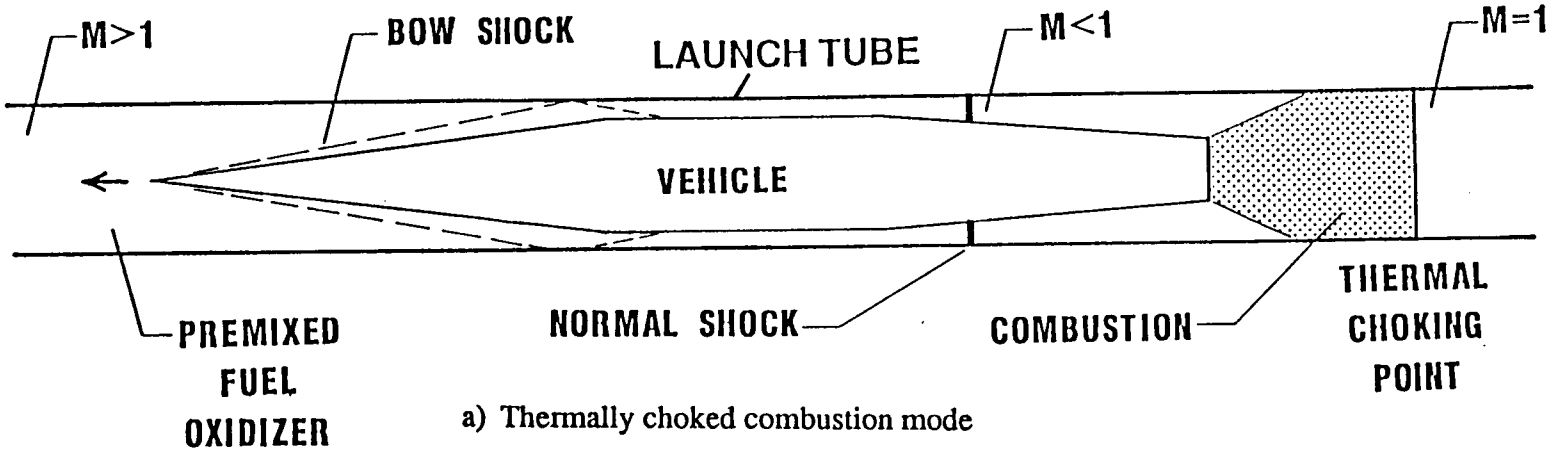

a) Thermally choked combustion mode

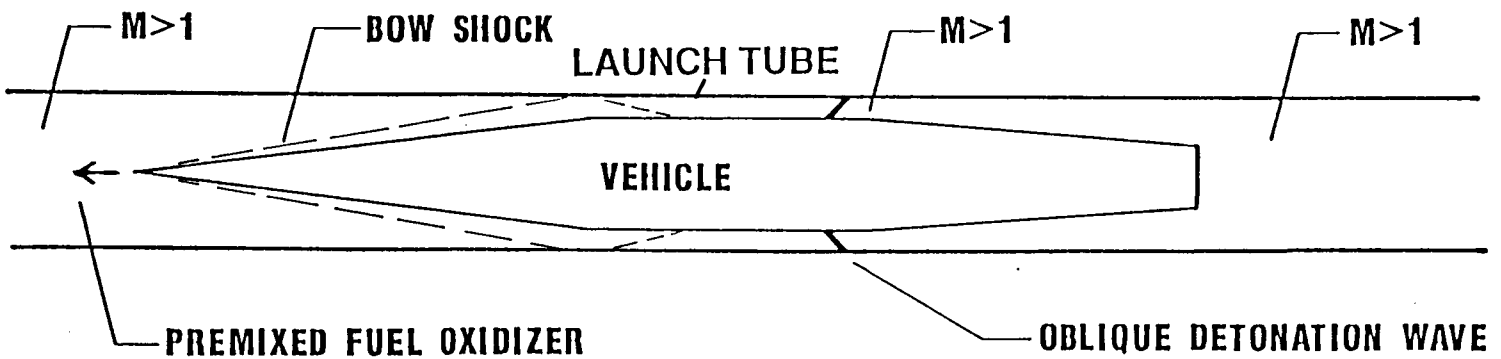

b) Oblique detonation mode

Fig. I-2 Schematic of the two propulsion modes for the ram accelerator

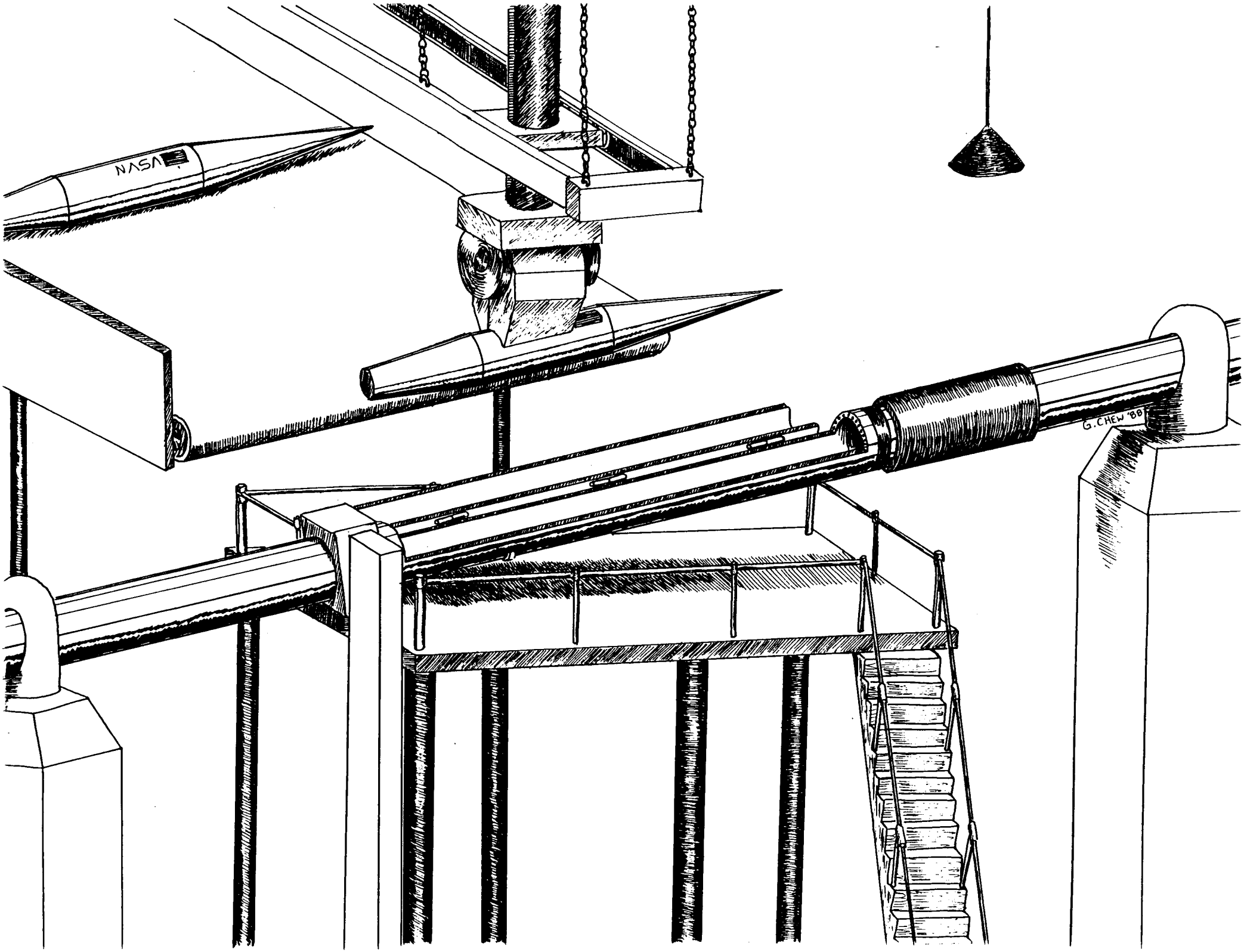
NASA
G. CHEW '88

II. INITIAL ACCELERATOR

Paul Clement

INTRODUCTION

An initial accelerator system must be employed to impart an initial velocity of 700 m/s to the vehicle so that the in-tube ramjet cycle may properly start. A combustion-driven gas gun is proposed which uses a stoichiometric methane-air mixture to initially accelerate the vehicle at a maximum of 1000 g's.

A combustion-driven gas gun uses the pressure created by the combustion of the fuel to accelerate the vehicle in much the same way a conventional powder gun accelerates a projectile. Given the vehicle size, mass, acceleration, and post-combustion gas properties one can determine the required barrel length, combustion chamber length, wall thickness, mass of propellant and mass of air.

To alleviate gun recoil upon firing, the combustion gases must be diverted through a muzzle blast deflector. This can be achieved by a simple design with very little increase in overall ram accelerator length. The performance parameters determined for the initial accelerator are: vehicle velocity versus the gas escape velocity, ballistic efficiency, and piezometric pressure ratio.

In addition to determining the basic dimensions, proposals for supporting systems are presented. Propellant-air mixing in a long tube is proposed as the most efficient method of delivering well-mixed stoichiometric gases into the combustion chamber. Ignition of the mixture is accomplished with an axial line ignition source made of tungsten wire. A closure between the combustion chamber and vehicle in the barrel is needed. This closure does not open until the required combustion pressure is reached to accelerate the vehicle at the initial maximum of 1,000 g's. It is shown that a simple, petalling metal diaphragm should suffice. Replacement of the diaphragm and vehicle before subsequent launches presents a unique problem that is solved by having the breech end of the barrel translate to one side for reloading.

THEORY

Initial Accelerator Basic Requirements

The basic requirement of the initial accelerator is to take a vehicle of given mass and diameter and impart to it a prescribed velocity without exceeding a given maximum acceleration. Combustion chamber and barrel sizing require the following calculations.* From Newton's Second Law,

$$F = m\,a \tag{1}$$

The maximum driving vehicle base pressure is then,

$$P_p = F / A \tag{2}$$

and occurs at the beginning of the acceleration process.

Combustion Chamber and Barrel Lengths

The sizing of the combustion chamber and barrel is accomplished assuming an isentropic process after combustion [1]. The irreversibilities associated with the rapid expansion of the gases are relatively small. That is, the gradients in an expansion process tend to decrease, whereas in a compression process they increase. Seigel [1] determined that the isentropic theory over-predicts the vehicle velocity by 2% for vehicle velocities of the order of the initial sound speed of the gas immediately following combustion.

The required barrel length to achieve a given projectile velocity in a combustion-driven gas gun is found from the following relation [1],

* The nomenclature follows the list of references in each chapter.

$$x_p = \frac{m\ a_o^2}{P_o A}\ \frac{2}{\gamma+1}\left\{\frac{\frac{2}{\gamma-1} - \frac{\gamma+1}{\gamma-1}\left[1 - \frac{u_p(\gamma-1)}{2a_o}\right]}{\left[1 - \frac{u_p(\gamma-1)}{2a_o}\right]^{\frac{\gamma+1}{\gamma-1}}} + 1\right\} \quad (3)$$

where the speed of sound immediately following combustion is,

$$a_o = (\gamma R T_o)^{1/2} \quad (4)$$

If rarefaction waves reflected from the breech reach the vehicle before it exits the end of the barrel, the driving pressure, and hence performance, is reduced. To ensure this does not occur, an effectively "infinite" combustion chamber is determined by [1],

$$x_o = a_o (x_p\, m / 3\, P_o\, A)^{1/2} \quad (5)$$

The pressure at the base of the vehicle may be related to a given vehicle velocity for the expansion of an ideal gas by [1],

$$P_p / P_o = \left\{1 - u_p / [2a_o / (\gamma-1)]\right\}^{2\gamma/(\gamma-1)} \quad (6)$$

The distance travelled down the barrel, x_p, for given vehicle velocities (0 to 700 m/s) may be calculated using Eq. 3. A dimensionless distance, x_d, can then be defined as,

$$x_d = x_p / \text{Barrel Length} \quad (7)$$

For a given vehicle velocity, a dimensionless velocity, u_{dp}, may be defined as the ratio of the given local vehicle velocity, u_p, to the maximum vehicle velocity u_{max},

$$u_{dp} = u_p / u_{max} \quad (8)$$

It can be seen from Eq. 6 that the pressure drops to a value of zero when the gas velocity reaches a value of $2a_o / (\gamma - 1)$. This velocity is called the "escape velocity" [1],

$$u_{esc} = 2\, a_o / (\gamma - 1) \tag{9}$$

If the gas expands to this velocity it can push no more since its pressure has dropped to zero. The escape velocity is one measure of the usefulness of a propellant. (This relation is valid for unchambered guns with effectively infinite combustion chambers as is the case here. An unchambered gun has a combustion chamber I.D. equal to the barrel I.D.). In practice, the vehicle can rarely obtain more than half the escape speed. This is due to the fact that at high vehicle speeds the pressure at the base of the vehicle becomes low enough that gas and frictional resistance and gas pressure ahead of the vehicle equal the pressure behind the vehicle, thus preventing further acceleration.

The ballistic efficiency of the initial accelerator may be defined as the ratio of the change in kinetic energy to the chemical energy invested,

$$\eta = \Delta KE / CE \tag{10}$$

The piezometric ratio, Q, is defined as the ratio of peak base pressure to average drive pressure. It is an important performance parameter because it provides a measure of the maximum pressure the vehicle and initial accelerator tube must regularly endure versus the initial accelerator's average driving pressure.

$$Q = P_o / P_{avg} \tag{11}$$

The average pressure over the length of the barrel may be determined from,

$$P_{avg} = (u_{max})^2\, m / 2\, A\, L \tag{12}$$

Methane-Air Stoichiometry and Combustion Properties

To calculate barrel and combustion chamber lengths, as well as required amounts of methane and air, the gas properties following combustion must be determined. Combustion of a methane-air mixture in the combustion chamber of the gun is a constant volume process. The gas properties for this process were determined by use of a computer combustion code [2]. Input data prior to combustion included reactant temperature, pressure, molecular composition of the air and methane, and equivalence ratio (i.e., the mass ratio of air to methane). Output data following combustion included product temperature, pressure, molecular composition, ratio of specific heats, and molecular weight.

From the ideal gas law the specific volume following combustion but before vehicle movement is,

$$v = R\,T_o / P_o \tag{13}$$

The chamber length multiplied by the tube area gives the combustion chamber volume. The volume divided by the specific volume gives a combustion product mass. From conservation of mass, the amount of combustion products is equal to the amount of reactants. For a stoichiometric air to fuel ratio, the mass of methane required is,

$$MASS_{CH4} = MASS_{mixture} / (AF + 1) \tag{14}$$

The partial pressures of methane and air are determined from,

$$P = n\,R_u\,T / V \tag{15}$$

Combustion Chamber and Barrel Wall Thickness

For simplicity, a uniform thickness is assumed for the entire length of the chamber and barrel. For safety, the chamber and barrel are designed to withstand detonation pressures. The tangential stress is largest at the inside radius. If the atmospheric pressure surrounding the gun is assumed negligible, the largest tangential stress in a thick-walled cylinder is [3],

$$\sigma_t = \left[r_1^2 P_o / (r_2^2 - r_1^2)\right] (1 + r_2^2 / r_1^2) \qquad (16)$$

RESULTS

Figure II-1 shows a schematic of the proposed gas gun system. To accelerate a 2,000 kg, 0.76 m diameter vehicle at a maximum of 1,000 g's a force of 19.6 MN is required. The required maximum driving pressure is thus 427 atm.

The combustion code determined that the stoiciometric mass ratio of air to methane is 17.12. The critical temperature of methane is 191.1 K, above which it will not condense, regardless of pressure [4]. With a propellant load temperature of 300 K, the methane will remain in a gaseous state.

The required masses of methane and air are 56 kg and 944 kg, respectively. The corresponding partial pressures are 5 atm and 42 atm. The total loading pressure of 47 atm results in a deflagration pressure of 427 atm, as required. The product temperature is 2725 K; molecular weight is 27.39; ratio of specific heats is 1.325 and the resulting sound speed is 982 m/s. Anticipating that the gun should safely handle accidental detonation of the stoichiometric mixture, the detonation pressure was determined to be 840 atm.

The combustion chamber length is 42 m and the barrel length is 48 m. Thus, the combined combustion chamber and barrel length is 90 m.

Figure II-2 is a plot of Eq. 6 versus Eq. 7. The base pressure remaining after the

vehicle reaches 700 m/s is 39% of the initial pressure of 427 atm, or 167 atm. Consequently, there is still a significant amount of pressure available for further acceleration.

For a_o = 982 m/s and γ = 1.325, a gas escape velocity of 6,043 m/s is obtained. With u_{max} = 700 m/s, the vehicle needs to achieve achieve only 11.5% of the escape velocity. Equations 8 and 9 are plotted versus Eq. 7 in Fig. II-3.

The change in kinetic energy for a 2,000 kg mass accelerating from 0 to 700 m/s is 490 MJ. The heating value for methane alone is 64.3 MJ/kg. With 56 kg of methane required, the chemical energy invested is 3,600 MJ. Thus, the ballistic efficiency is 14%.

For u_{max} = 700 m/s and a barrel length of 48 m, the average driving pressure is 222 atm. Thus, the piezometric efficiency is 1.93. The effect of the ambient air in the barrel ahead of the vehicle is very small, resulting in a velocity reduction of 1.5% (10.5 m/s) compared to an evacuated barrel [1].

Combustion Chamber and Barrel Design

Figure II-4 depicts the cross-sectional dimensions of the chamber and barrel combination. AISI 4340 (Nickel-Chromium-Molybdenum) steel is proposed. The ultimate strength is 1.98 GPa with 11% elongation. Rated yield strength is 1.86 GPa. With a safety factor of 4.05, the design stress is 459.3 MPa.

Setting σ_t equal to 459.3 MPa and knowing the inside radius, r_1=0.38 m, the wall thickness is calculated to be 7.83 cm. This yields a steel volume of 18.5 m^3 and a mass of 144 metric tons based on a steel density of 7,818 kg/m^3.

PROPOSALS FOR SUPPORTING SYSTEMS

In addition to the combustion chamber and barrel a number of additional systems are required, such as propellant loading, barrel closures, muzzle brake/blast deflector, ignition

system, and replacement of the barrel closure and vehicle.

Air-Propellant Mixing and Loading

As shown in Fig. II-1, the air and propellant are mixed in a tube prior to entering the combustion chamber. Quicker, more thorough mixing and a less complicated loading procedure is achieved in a tube compared to loading the constituents separately in the combustion chamber. Tube I.D. is arbitrarily set at 15.24 cm (6 inches) as a size to load the combustion chamber at a reasonable rate. Concentration fluctuations of less than one percent can be achieved in a tube length of 100 diameters [5], i.e. 15.34 m.

Also a consideration will be the presence of air at one atm pressure and in the mixing tube and combustion chamber prior to fuel loading. This air must be taken into account to ensure a stoichiometric mixture prior to ignition. The volume of the mixing tube and combustion chamber is 19.33 m^3. This yields 0.785 kg-moles, or 22.7 kg of ambient air. This figure must be deducted from the 944 kg of air required for a stoiciometric mixture. Therefore, about 921 kg of air must be added through the air pressure pump.

Since a combustible, stoichiometric mixture exists in the feed tube, it must be designed to withstand high pressures should accidental ignition occur. An automatic opening safety valve is installed to relieve pressure, should it significantly exceed loading pressures. However, the tube thickness is designed to withstand a full 840 atm detonation pressure. With the same allowable stress and 4.05 safety factor as in the chamber and barrel, a tube wall thickness of 3.14 cm is obtained. Hence, the weight of the mixing tube is 1,750 kg.

Ignition System

The NASA-Ames Research Center currently uses an experimental combustion-driven shock tube with hydrogen gas as the propellant [6]. The length of the combustion chamber is 22.86 m and has an I.D. of 0.43 m. These dimensions are of the order of the size of the initial accelerator proposed here. To discourage the formation of combustion

detonation waves, a 0.38 mm O.D. tungsten wire strung down the center of the combustion chamber is used. Ignition is accomplished by heating the wire with a large electric pulse derived from a 90 μf capacitor bank charged to 14.5 kV. The suddenly heated wire thus provides a line ignition source. It is proposed to use a similar arrangement for the initial accelerator described here. However, experiments using a full size combustion chamber should be conducted to precisely determine combustion behavior and to ensure reliable, repeatable, and detonation-free operation.

Barrel Closures

A closure is required between the combustion chamber and gun barrel as well as between the gun barrel and ram accelerator. The two options include a reusable valve or moving slide plate and a nonreusable bursting diaphragm. The time between consecutive launches is orders of magnitude longer than the launch itself. Together with the fact that a slide plate mechanism would be very heavy, a simple bursting diaphragm is preferred, as shown in Fig. II-5.

Using a metallic diphragm, scribing is done along radial lines. The use of a round shoulder around the circumferential edge of the diaphragm on the low pressure side promotes clean petalling [7-8]. This also helps to ensure that the petals fold back against the wall. References 7 and 8 found that best results are obtained if a pressure is created close to that of the natural bursting pressure. Those experiments inserted a plastic explosive into the grooves of a stainless steel diaphragm. The experiments resulted in opening times of less than one millisecond with a repeatability of better than 40 microseconds at about 30 atmospheres. Scaling to ram accelerator sizes should be experimentally tested but would be expected to yield similar results.

Muzzle Blast Deflector

To reduce launch tube recoil a multiple stage muzzle blast deflector is employed, as

shown in Fig. II-1. The deflector turns some of the propellant gas backwards causing the muzzle to be pulled forward, thereby decreasing the rearward force of the recoil.

Initially, the total required exhaust area is arbitrarily set to be five times the gun bore cross-sectional area of 0.4536 m^2, i.e. 2.27 m^2 (the exhaust area is arbitrarily picked and the blast deflector dimensions calculated to see if the dimensions are acceptable with regards to length and strength. If not, another exhaust area is picked until acceptable dimensions are achieved).

For this design ten exhaust stages are initially chosen; the exhaust area is then 0.227 m^2 per stage. Following this, if six holes per stage are selected, the exhaust area is 0.047 m^2 per hole. This results in a hole diameter of 24.5 cm. With six circumferential holes per stage, 91.7 cm is available for the six spaces between the six holes, i.e 15.3 cm between holes (based on the gun barrel I.D. of 76 cm). These dimensions appear to be suitable with regards to deflector length as well as the strength of the material between the holes. This aspect should be analysed in more detail to ensure a safe structure but significant increases in ram accelerator length will not result in any case.

Assuming steady, one-dimensional flow, the amount of gas diverted at each stage is proportional to the ratio of exhaust area to total exhaust-plus-bore cross-sectional areas. The exhaust area of each stage is 1/2 the bore cross-sectional area. Therefore, 1/3 of the incoming flow is exhausted at each stage.

The ten stages exhaust 98% of the combustion gas. The first stage exhausts 1/3 of the gases. The second stage exhausts 1/3 of (1 - 1/3) or 2/9 of the gases. The third stage exhausts 1/3 of (1 - 1/3 - 2/9) or 4/27 of the gases and so on up to ten stages. Using the above hole diameter and hole spacing, the resulting length of the muzzle blast deflector is 3.03 m.

Diaphragm and Vehicle Replacement

Figure II-6 depicts a suggested method for diaphragm and vehicle replacement. This

method combines movement of a minimum amount of barrel mass with a minimum length of joints to seal against combustion pressures. A section of the barrel would be translated laterally to one side by hydraulic rams. The used diaphragm would be removed from the aft end of the barrel section and a new vehicle inserted, followed by a replacement diaphragm. The hydraulic rams would then retract and align the barrel section with the rest of the initial accelerator. Sealing against combustion pressures could be accomplished using O-rings. The O-rings would lightly seal the barrel upon retraction. Combustion pressure would then automatically cause the O-rings to seal further.

The alternative would be to translate the 42 m combustion chamber to reload, somewhat like a conventional cannon. Clearly, the mass and size of the combustion chamber makes that scheme impractical.

CONCLUSION

There exists no fundamental technological barrier to constructing a combustion-driven gas gun to accelerate a 2000 kg, 0.76 m diameter vehicle to 700 m/s. The following are initial accelerator size requirements as well as fuel-air requirements:

* Combustion chamber length: 42 m
* Barrel length: 48 m
* Chamber and barrel wall thickness: 7.83 cm
* Chamber and barrel mass: 144,000 kg
* Muzzle blast deflector length: 3.03 m
* Load pressure of methane-air mix: 47 atm
* Mass of methane per launch: 56 kg
* Mass of air per launch: 944 kg

The following are suggested methods and designs to implement the above requirements:

*Propellant-air premixing in a feed tube .

*Line source axial ignition system using tungsten wire.

*Combustion chamber-barrel closure: pre-scored replaceable steel diaphragm.

*Breech end of barrel translates to the side to facilitate diaphragm and vehicle

replacement.

The effect of air in the barrel ahead of the vehicle was found to reduce the maximum velocity a neglible amount. The maximum vehicle speed of 700 m/s is only 11.5% of the escape velocity of the combustion products. Therefore, the methane-air combustion products are a suitable "pusher" for these accelerator requirements. The ballistic efficiency of the initial accelerator is 14% and the piezometric ratio is 1.93.

REFERENCES

1. Seigel, Arnold E., The Theory of High Speed Guns, North Atlantic Treaty Organization, Advisory Group for Aerospace Research and Developement (AGARD), no. 91, May 1965, pp. 69-79.
2. Pratt, D.S., Calculation of Equilibrium Product Composition Resulting From Combustion of Hydrocarbon Fuels, computer program, Department of Mechanical Engineering, University of Washington, Seattle, WA, 1988.
3. Baumeister, T., Marks, L.S., Mechanical Engineers' Handbook, 6th edition, McGraw-Hill Book Company, New York, 1958, pp. 5-65 to 5-66.
4. Chemical Rubber Company, CRC Handbook of Chemistry and Physics, 46th edition, The Chemical rubber Company, Cleveland, Ohio, 1965.
5. Breidenthal, R.E., Department of Aeronautics and Astronautics, University of Washington, Seattle, WA, private communication, May 1988.
6. Bogdanoff, D.W., NASA-Ames Research Center, private communication, April, 1988.
7. Montgomery, R. and Abell, J.H., Metal Diaphragm Released Explosively NOLTR 66-77, April 1955.
8. Merrit, D. and Aronson, P.M., Experimental Studies of Shock Shock Interactions on a 9^{o} Cone, NOLTR 67-182, January 1968.

NOMENCLATURE

A	cross-sectional area of accelerator tube
AF	air to fuel ratio (by mass)
a	acceleration
a_o	maximum post-combustion sound speed
CE	chemical energy
F	force
ΔKE	change in kinetic energy
L	barrel length
m	mass
n	number of moles
P_p	vehicle base pressure
P_{avg}	average pressure
P_o	maximum post-combustion pressure
Q	piezometric pressure ratio
R	local gas constant
R_u	universal gas constant, 0.08205 (liter-atm) per (mole-degrees K)
r_1	cylinder inside radius
r_2	cylinder outside radius
T	temperature
T_o	maximum post-combustion temperature
u_{max}	maximum velocity
u_{dp}	dimensionless local vehicle velocity with respect to maximum vehicle velocity
u_{esc}	escape velocity of a gas
u_p	vehicle velocity
V	volume
v	specific volume

x_d	dimensionless vehicle distance with respect to maximum vehicle distance
x_o	combustion chamber length
x_p	distance vehicle travels down the barrel for a given velocity
η	ballistic efficiency
γ	ratio of specific heats, c_p/c_v
σ_t	tangential stress

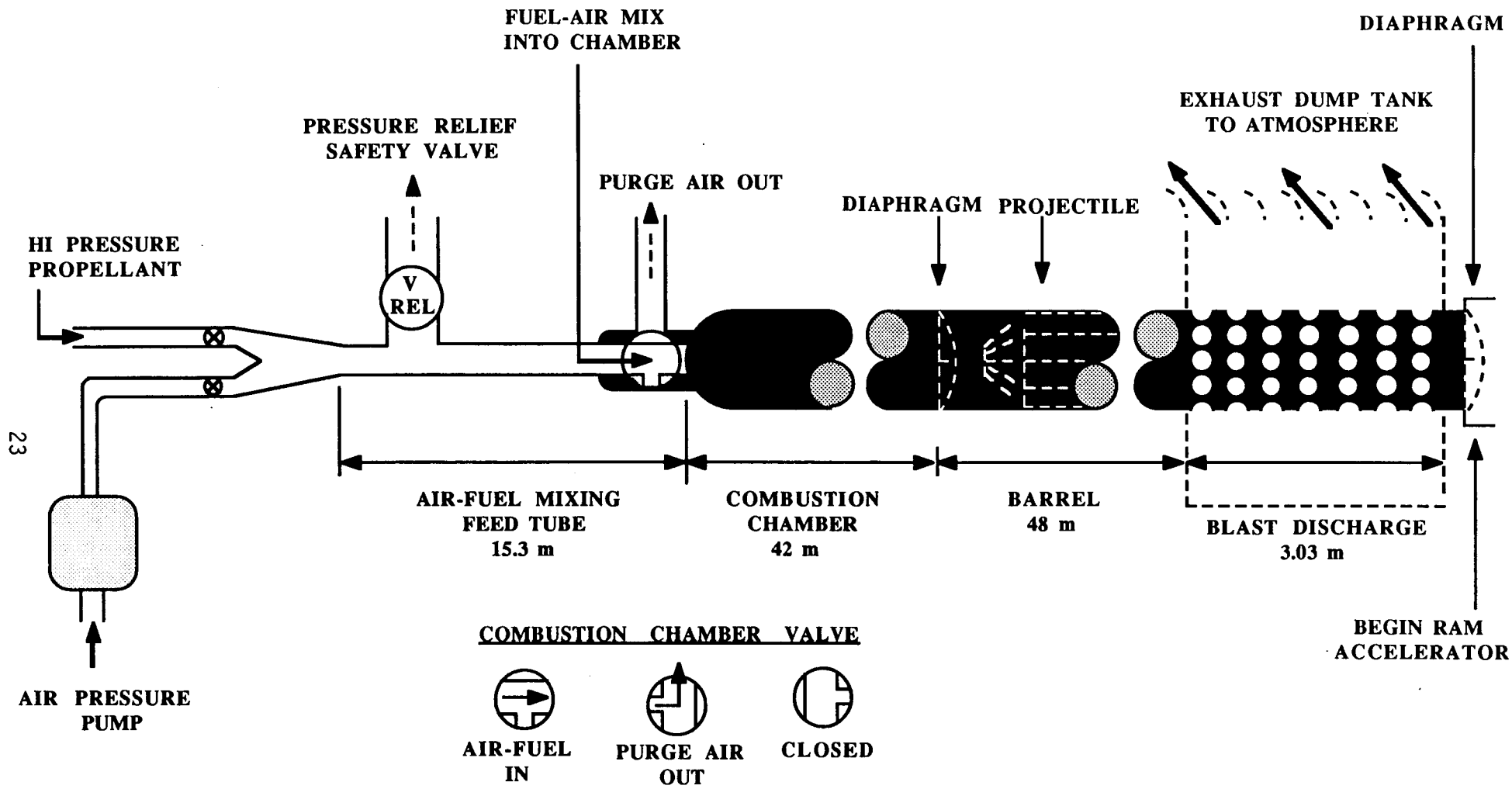

FIG. II-1. SCHEMATIC DIAGRAM OF THE INITIAL ACCELERATOR.

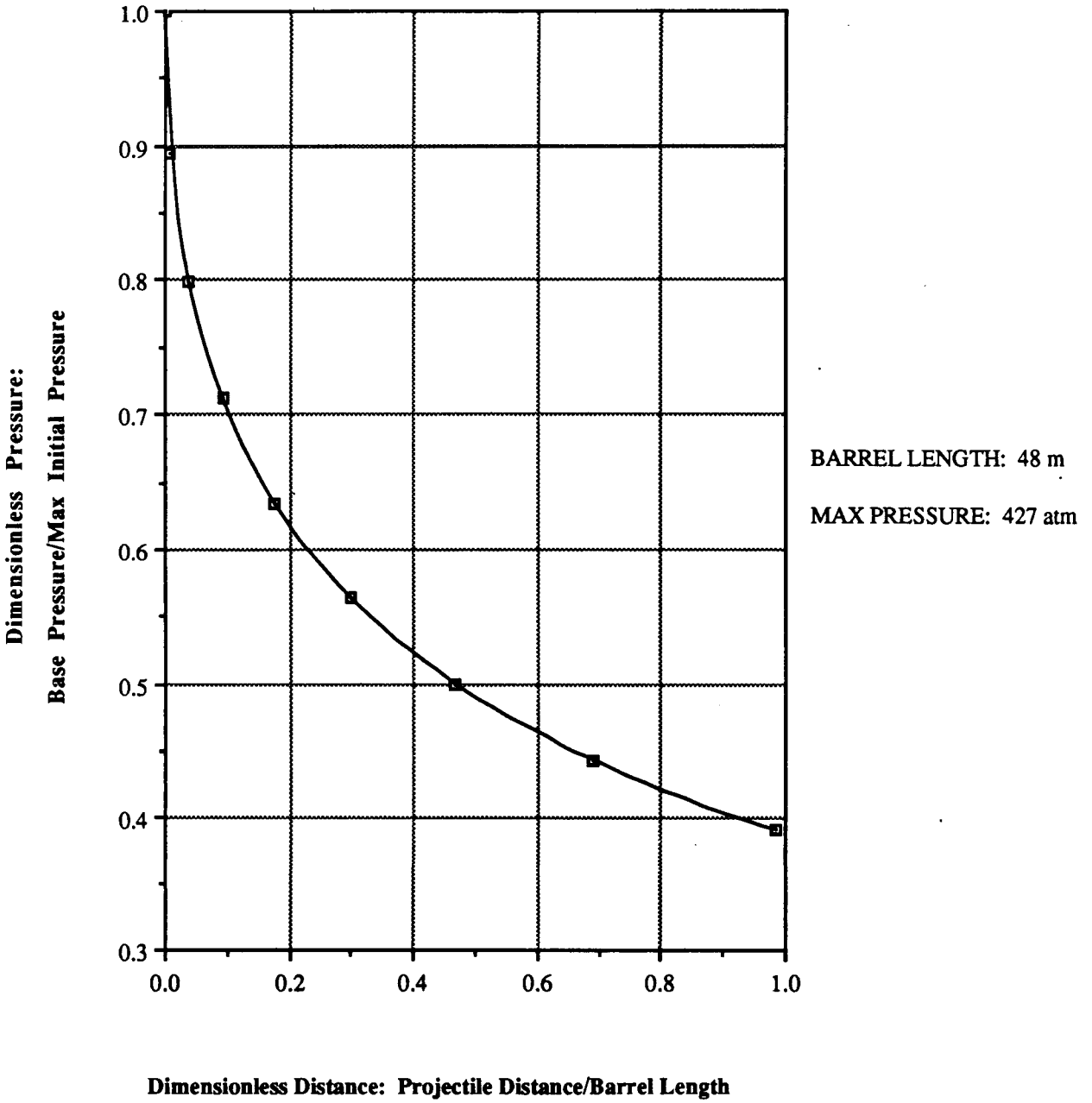

FIG. II-2. VEHICLE BASE PRESSURE vs VEHICLE TRAVEL.

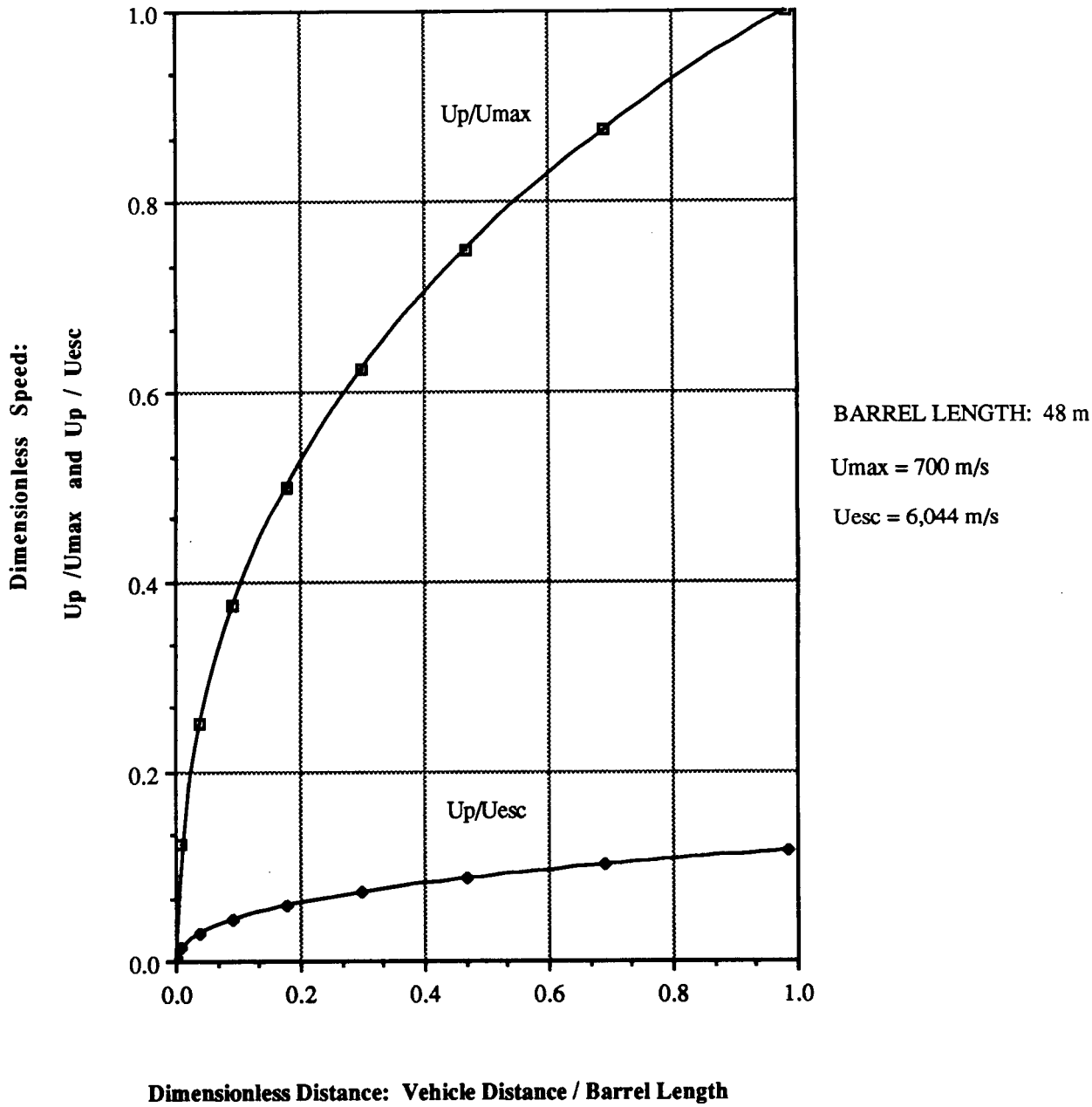

FIG. II-3. LOCAL VEHICLE SPEED COMPARED TO GAS ESCAPE SPEED.

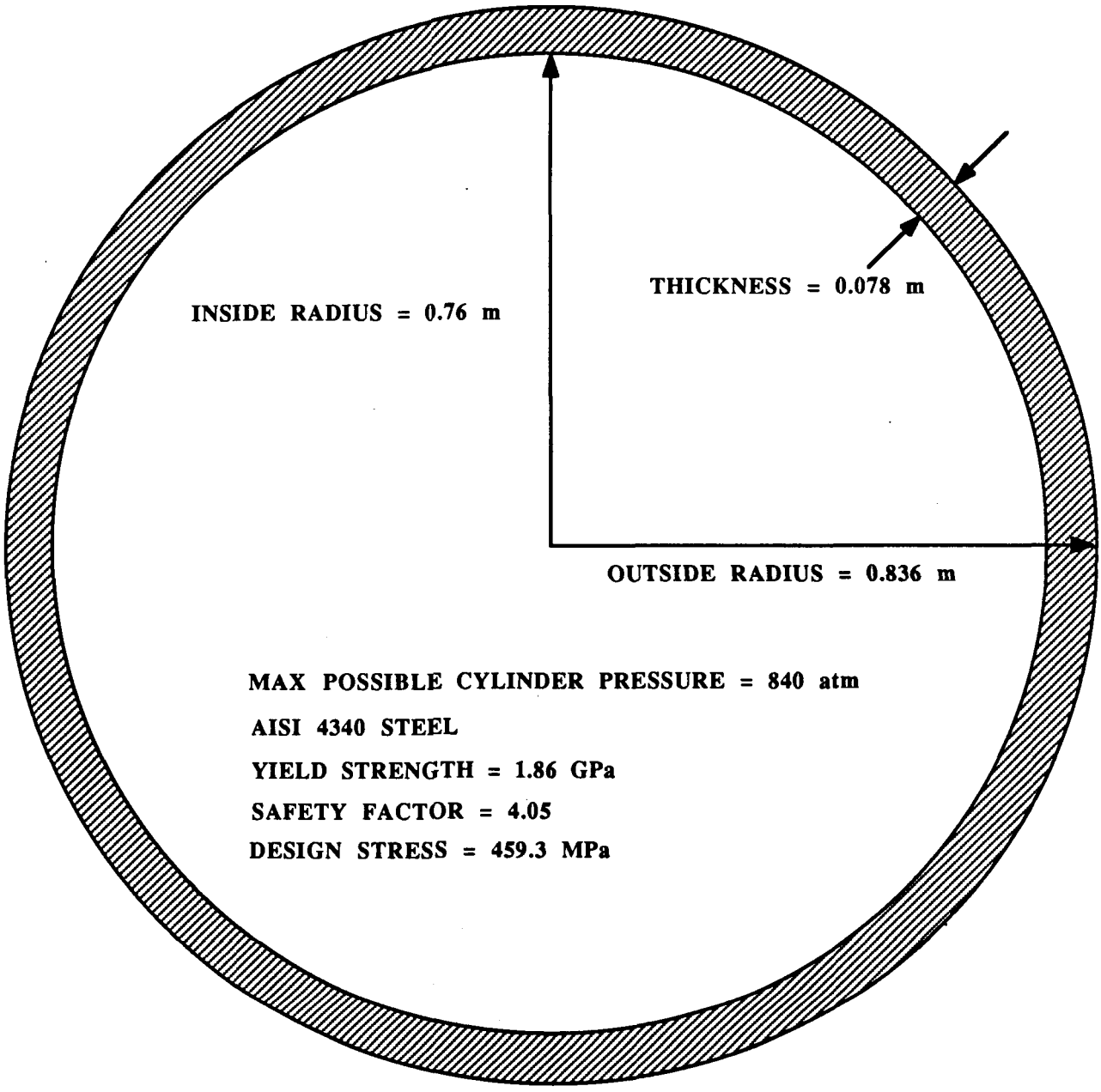

FIG. II-4. CROSS-SECTIONAL DIMENSIONS OF THE COMBUSTION CHAMBER AND BARREL.

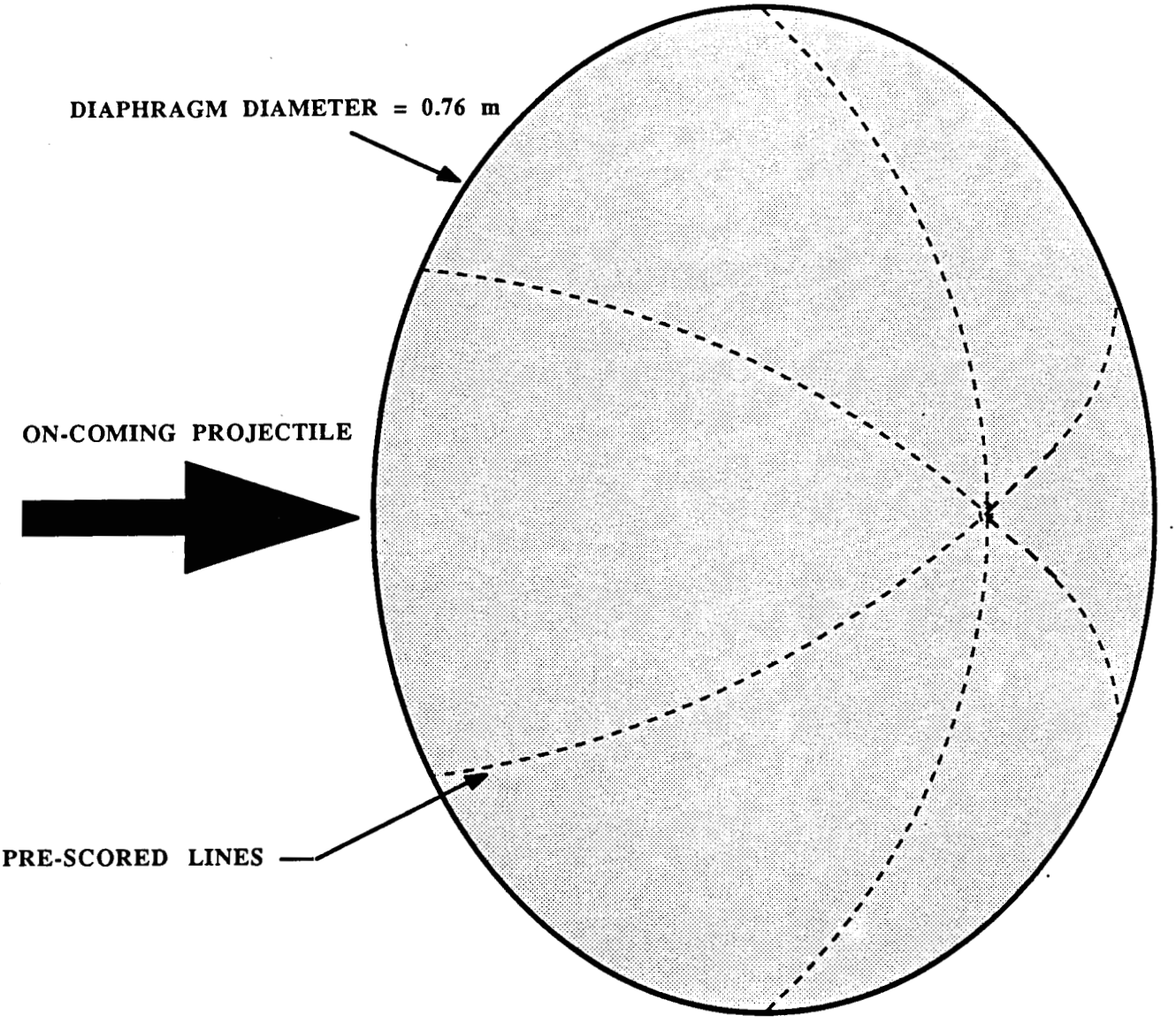

DRAWING TO SCALE: 1cm = 0.02 m

FIG. II-5. PETALING DIAPHRAGM BETWEEN THE COMBUSTION CHAMBER AND BARREL.

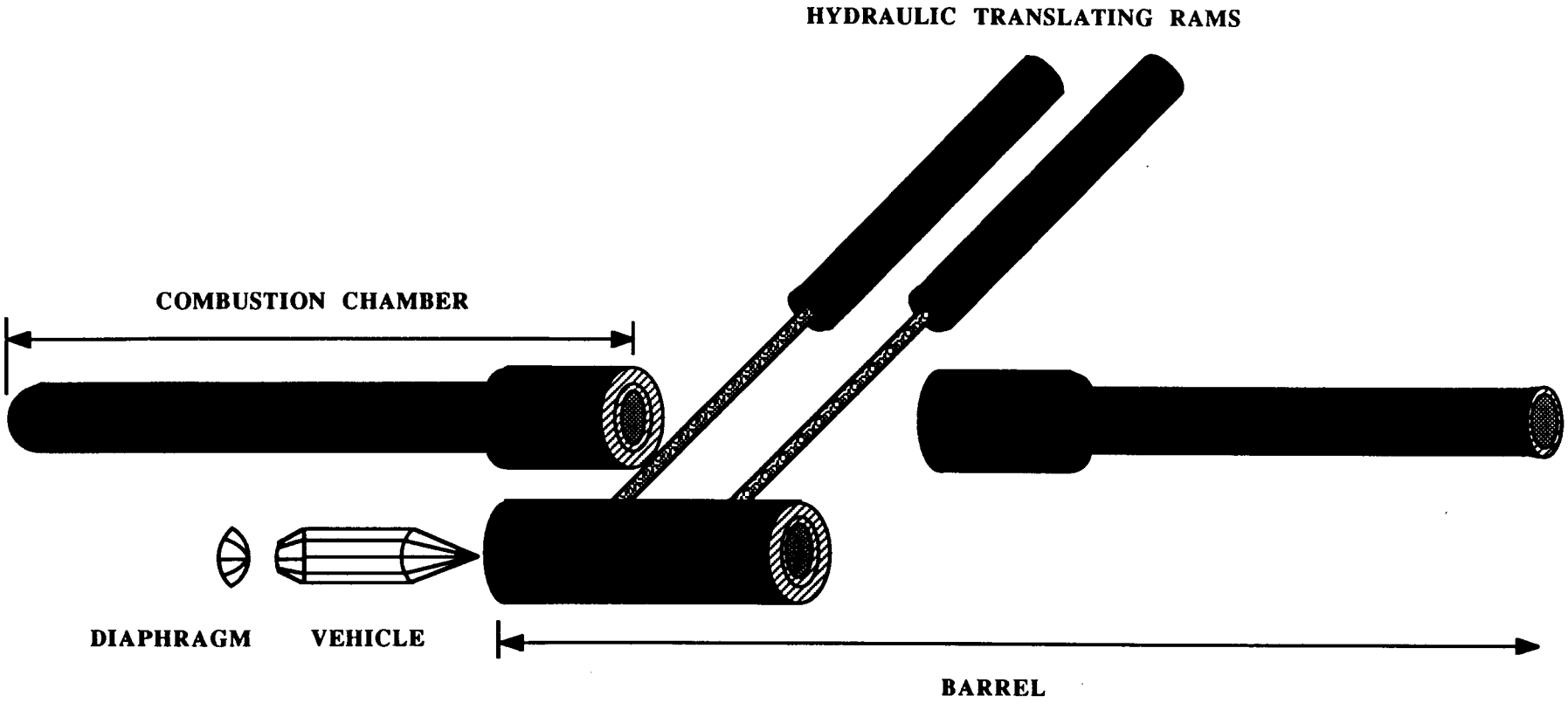

FIG. II-6. DIAPHRAGM AND VEHICLE REPLACEMENT USING TRANSLATING BARREL SECTION.

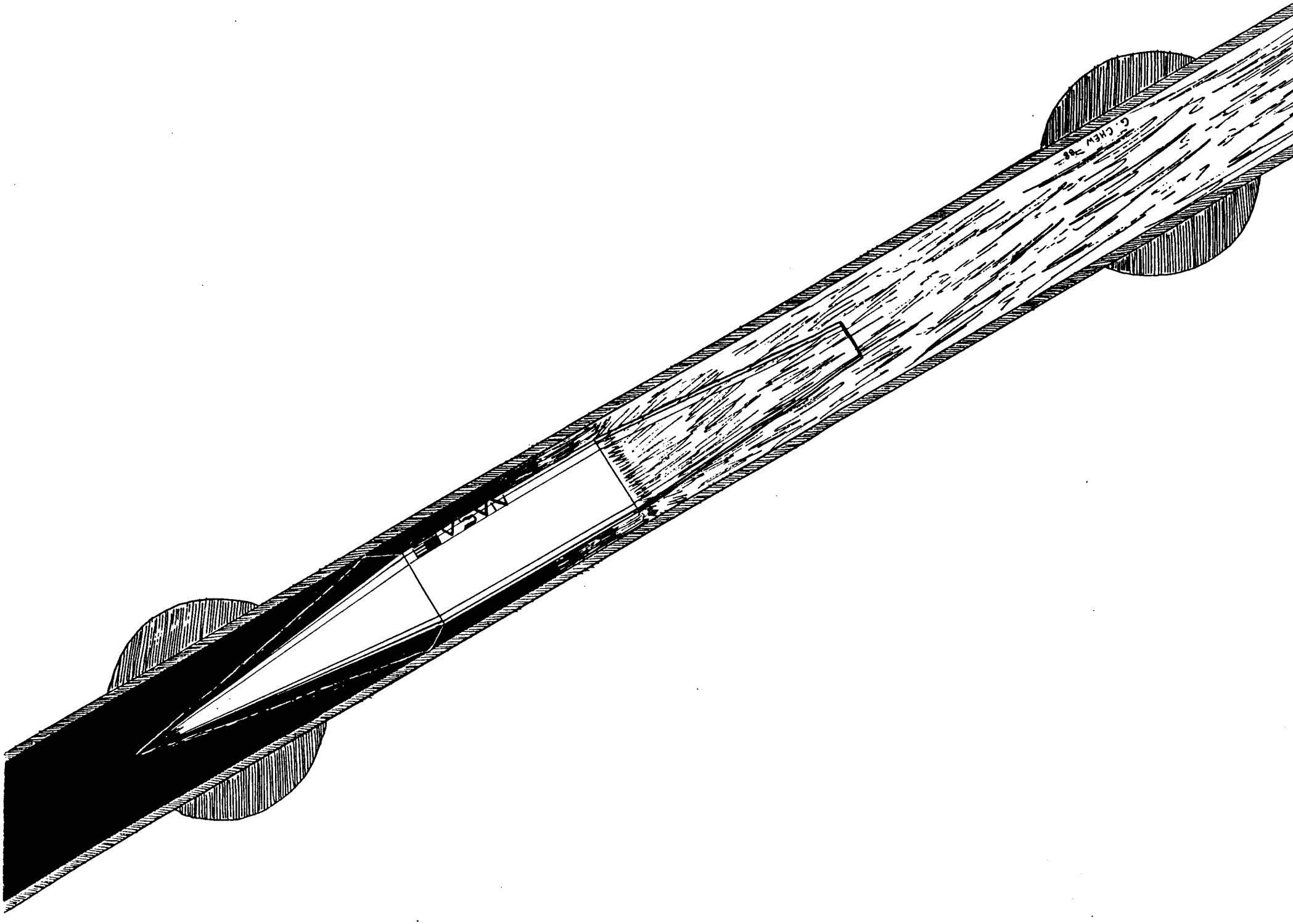
G. CHEW
NASA

III. IN-TUBE PROPULSION

Andrew Berschauer
Jesse Vickers

INTRODUCTION

The ram accelerator is a concept developed at the University of Washington for direct launch of space cargo into orbit [1-6]. The propulsion configuration of the ram accelerator resembles that of a conventional, airbreathing ramjet. The projectile acts as the centerbody, and the stationary launch tube serves as the outer cowling of the ramjet. The launch tube is filled with premixed gaseous fuel and oxidizer, and the energy release process, i. e., combustion travels with the projectile. In this manner it is possible to specifically tailor the fuel/oxidizer mixtures to each velocity increment, thus serving to increase the overall performance of the propulsion process. Because it is not necessary for the vehicle to carry any primary on-board propellant to launch into orbit, a much greater fraction of the total projectile mass can be allotted for payload [1].

Two modes of ram accelerator propulsion have been investigated: a thermally choked, subsonic combustion mode (Fig. III-1) to propel the vehicle from 0.7 km/s to 2.5 km/s, and a "superdetonative" mode (Figs. III-2 and III-3) which uses an oblique detonation wave for combustion to propel the vehicle from 2.5 km/s up to 10 km/s.

The subsonic combustion mode utilizes thermally choked combustion to provide thrust to the vehicle. As with a conventional ramjet, an initial velocity is required to start the propulsive process. Therefore, the vehicle must be accelerated by conventional means, i.e., a combustion-driven gas gun, to the velocity where the thermally choked mode is operational. This velocity has been determined to be 0.7 km/s [3]. The composition of the pressurized gas mixture is chosen such that the vehicle Mach number is sufficient to ensure that the flow remains supersonic through the throat of the diffuser. The nose cone angle is designed to ensure that the oblique shock system in the diffuser does not initiate combustion. A weak

normal shock is located downstream of the diffuser throat, and the flow behind this shock is subsonic. The base of the vehicle acts as a flame holding dump combustor and the premixed propellant gas burns in the tube behind the vehicle. The normal shock is stabilized on the vehicle by the thermal choking of the flow in the full tube area [3, 4]. This propulsion mode is being experimentally investigated at the University of Washington. Velocities up to 2400 m/s have recently been achieved.

The oblique detonation (superdetonative) mode requires a strong oblique shock wave to raise the propellant temperature high enough for combustion to occur. The Type I oblique detonation supersonic combustion mode (Fig. III-2) uses a reflected bow shock to form the detonation wave which ignites the propellant mixture. For highest efficiency and assured detonation, this mode requires that the reflected detonation wave intersect precisely at the shoulder of the vehicle [6]. It was concluded that this mode is undesirable as it requires a varying tube radius and/or stringently controlled freestream Mach number for this requirement to be satisfied as the velocity of the vehicle increases.

The Type II oblique detonation mode (Fig. III-3) operates on the same principle as the Type I mode, except that a small protuberance located on the vehicle triggers the detonation wave. This mode requires that the nose cone half-angle be small enough to ensure that the bow and reflected bow shocks do not ignite the propellant. This design allows for better flexibility, as the performance need not rely on the precarious placement of the reflected bow shock. Both oblique detonation drive modes operate at vehicle velocities which exceed the local propagation speed of a Chapman-Jouguet detonation wave [4-6], hence the term "superdetonative".

The constraints on designing the propulsion configuration include the tolerable peak acceleration of the vehicle and the maximum pressures on the projectile and tube wall. The total mass of the vehicle was set at 2000 kg, and it was desired that 50% of this mass be devoted as payload mass. Vehicle accelerations were restricted within the limits of 600 g to 1000 g for rapid acceleration while permitting practical structural design. The launch tube was initially taken to be of 1.0 m internal diameter and the tube fill pressure and temperature

were set at 33 atm and 300 K, respectively. The design fill pressure results in the desired acceleration of this vehicle mass and acceptable pressures on the body and tube wall, while the temperature is typical ambient temperature. The tube diameter was chosen to accommodate practical size considerations and desired vehicle performance.

The focus of this chapter is on the analysis of the two ram accelerator propulsion modes necessary to propel the vehicle from 0.7 km/s to 10 km/s. This velocity range spans the minimum design velocity of the thermally choked combustion mode to the practical velocity limits of the superdetonative mode.

THEORY

Thermally Choked Mode

The subsonic, thermally choked mode of combustion (Fig. III-1) is modeled by a one-dimensional, inviscid, quasi-steady analysis [4]. The gasdynamic conservation equations (continuity, momentum, and energy) are applied to a control volume framed by stations 1 and 6 as well as the launch tube. Station 1 is located just forward of the projectile nose tip and station 6 coincides with the plane where thermal choking occurs. These conservation equations are applied in the frame of reference of a stationary vehicle. Consequently, the tube wall moves relative to the vehicle with the same velocity as the gas upstream of the vehicle [4].

The thrust on the vehicle is determined by the fill pressure of the launch tube, the amount of heat released during combustion, and the properties of the fuel mixture. It can be shown that the thrust is directly proportional to the tube fill pressure [4]. Diluents can be added to the propellant mixture to change the vehicle Mach number and the energy per unit mass; thus controlling the thrust on the vehicle.

The minimum velocity for a given propellant mixture is determined by the ratio of diffuser throat area to tube area and the heat released during combustion. The normal shock

must remain behind the diffuser throat for shock stability. As the vehicle Mach number increases the normal shock moves away from the throat, thus decreasing the vehicle thrust via increased shock losses and stagnation temperature with constant area heat addition [4]. The maximum vehicle velocity (for a vehicle tapering to a point at its base) is limited, in principle, by the Chapman-Jouguet (C-J) detonation velocity of the propellant [4]. Because the vehicle rear cone is truncated to provide a recirculation region for flame retention, the maximum velocity attainable is approximately 85-95% of the C-J detonation velocity.

Applying the conservation of momentum over the control volume defined by the tube wall and stations 1 and 6 yields the equation for thrust [10]:

$$F = (PA+\dot{m}U)_6 - (PA+\dot{m}U)_1 - D \qquad (1)$$

Where D is the drag on the body due to skin friction (wave drag appears in the other terms) and is found from [2]

$$D = 1/2\ C_f \rho U^2 S \qquad (2)$$

Combining Eq. 1 with the mass and energy conservation equations over the control volume results in a non-dimensional thrust on the vehicle (F/P_1A) given by the equation [4]:

$$F/P_1A = \gamma_1 M_1/\gamma_6\{2((\gamma_6^2-1)/(\gamma_1-1))[1+((\gamma_1-1)/2)M_1^2+ \Delta q/Cp_1T_1]\}^{1/2} - (1+\gamma_1 M_1^2) \qquad (3)$$

The ballistic efficiency is defined as the rate of change of projectile kinetic energy divided by the rate of heat addition to the flow. Using continuity, the ideal gas law, and the definition of the speed of sound it can be shown that [4]:

$$\eta = (F/P_1A_1)a_1^2/\gamma_1\Delta q \qquad (4)$$

A parameter useful in determining thrust performance is the thrust pressure ratio [4]. The thrust pressure ratio (TPR) is defined by the ratio of effective thrust pressure on the projectile to the maximum cycle pressure. The effective thrust pressure is the thrust divided by the maximum projectile frontal area [3,4,6].

In addition to the performance parameters listed above it is also very important to monitor the temperature of the gas along the body. This is especially true between station 4, just after the normal shock, and station 5, the aft end of the vehicle, where the temperatures are highest in the uncombusted flow. The purpose of monitoring the temperature is to ensure that the propellant does not self ignite. For instance, when a hydrogen mixture is used, any temperature beyond 1200 K risks ignition, whereas methane will ignite around 1500 K [11]. In general, by keeping the vehicle Mach number lower than 4.5, temperatures can be kept low enough so that the gas will not ignite prematurely. The vehicle Mach number should also be kept above about 2.6 to ensure that the diffuser does not unstart [11]. The Mach number is kept within the required limits by dividing the launch tube into several segments filled with different propellant mixtures whose speed of sound increases towards the muzzle of the launch tube.

The subsonic thermally choked analysis was performed with the aid of several computer programs. C. Knowlen's "COMB-3" [7] and A. P. Bruckner's "TCRC11" [8] programs were utilized for the high velocity, hydrogen mixtures. In addition, C. Knowlen's program, "CHOKE" [9], was used for methane mixtures. In this manner, appropriate mixtures for accelerating the projectile between the mentioned velocity limits were determined.

Oblique Detonation Mode

Oblique detonation is a complex combustion process, however, this process can be effectively modeled by assuming that complete combustion and heat release take place instantaneously in a thin region directly behind the oblique shock wave. This approximation

is actually quite good and was used in the calculations [12]. The compression across the detonation wave raises the propellant temperature sufficiently so that combustion occurs immediately. Since the vehicle is travelling at superdetonative speeds, i. e., faster than the local speed of propagation of a C-J detonation wave, the detonation wave occurs at an oblique angle, allowing the flow to remain supersonic over the entire body.

After the thermally choked mode reaches its upper velocity limit of approximately 2.5 km/s, the oblique detonation mode is used. Transition from thermally choked to oblique detonation mode is affected by a sudden change in propellant mixtures. The oblique detonation mode's mixture has a much lower speed of sound than the preceding thermally choked mixture, thus causing the Mach number to suddenly increase, resulting in rapid transition. Mixtures must be chosen so that the freestream velocity of the projectile is faster than the C-J detonation velocity and combustion occurs immediately behind the oblique detonation wave generated by the protuberance on the body.

The pressure distribution on the vehicle results from the flow characteristics over the body. The flow is initially compressed by the bow shock and the reflected bow shock. Further compressive shocks also occur but are partially canceled by the expansion fan over the shoulder of the front end. The flow then passes over the body's constant area portion until it reaches the oblique detonation wave, across which a large pressure rise results from the oblique shock and the supersonic heat addition. The pressure on the body then decreases as the flow passes through the expansion fan which is characteristic of detonation waves [11]. After detonation of the propellant mixture by the oblique detonation wave, the flow passes through the reflected shock from the detonation wave which raises the pressure, and is expanded supersonically over the rear of the projectile resulting in thrust on the vehicle [6].

Predetonation of the mixture can occur if the temperature after the bow or reflected bow shock is too high (1200 K) [3]. Predetonation would cause higher pressure on the front of the body than on the back, i.e., negative thrust. To prevent this, the nose cone angle has to be small enough to keep the temperature jump across the bow shocks low, yet high enough

so that when the flow hits the protuberance, a detonation wave forms. A nose cone half-angle of 7-10° works well for this purpose [2] and has the added advantage of low aerodynamic drag. An angle of 7° was used in this analysis.

As defined, the thrust pressure ratio (TPR) is the ratio of the effective thrust pressure to the peak pressure in the cycle. This peak cycle pressure occurs on the barrel wall, immediately following the reflected detonation wave.

A FORTRAN program [6,13] was used to calculate the performance of the oblique detonation mode. For simplicity the flow is assumed to be isentropic up to the oblique detonation wave. Here, the equations of continuity, momentum, and energy are applied across the detonation wave, with a heat addition term added to the energy equation. The flow calculations are performed assuming an ideal gas with one set of values for molecular weight and specific heat ratio before combustion and a second set after [6]. The approximation of isentropic compression over the forebody of the vehicle, up to the detonation wave, affects the results in that the accelerations and efficiencies will be somewhat overestimated and the TPR will be somewhat underestimated because no bow shock losses are included. This assumption, however, is valid as a first approximation, and leads to results very close to those of more sophisticated flow models [14].

A more complex, two-dimensional, CFD code [15] was used to confirm the results of the 1-D code. The flow over the body was modeled at one chemistry and freestream velocity. This program was not used extensively in the analysis because of the extreme computational time requirements (typically 80 hours of CPU time on a DEC Microvax II computer).

The thrust is calculated using the momentum equation (Eq 1). Both the vehicle's acceleration and the peak cycle pressures increase linearly with increasing tube fill pressure [4]. From the accelerations, the launch tube length is calculated by simple kinematic equations applied over specified velocity increments.

With increasing tube fill pressures, rising peak pressures on the body require a stronger structure to support the increased loading; hence, a compromise between higher

accelerations and a larger, heavier structure is required. Lowering the tube fill temperature increases the density of the mixture, giving an increase in thrust; however, temperature manipulation is not a practical means for controlling vehicle acceleration. Consequently, another design compromise needs to be made. If the cone angle is increased the bow shock becomes correspondingly stronger, resulting in a larger temperature jump across the bow shock [16]. The larger temperature jump causes predetonation to occur at a lower velocity; hence, the upper velocity limit of the oblique detonation mode will be lower. Decreasing the tube diameter while keeping the body the same size increases the peak pressures and lowers the TPR because the flow is being isentropically compressed into a smaller area. By changing the propellant mixtures (thereby increasing the speed of sound and the ratio of specific heats along the launch tube), the performance of the vehicle can be tailored to meet specific design restrictions.

RESULTS

Thermally Choked Mode

In order to accelerate a 2000 kg projectile from 0.7 km/s to 2.5 km/s several different propellant mixtures are used to maintain flow conditions within the design parameters mentioned previously. By varying the composition for each segment, optimum mixtures for each velocity range are achieved (Table 1).

Table 1: Propellant Mixtures for Vehicle Propulsion in the Thermally Choked Combustion Mode

	Velocity Range (km/s)	Propellant Mixture	Speed of Sound (m/s)
1)	0.7 - 1.1	$0.5CH_4 + O_2 + 3CO_2$	291
2)	1.1 - 1.59	$0.8CH_4 + O_2 + 2.65N_2$	357
3)	1.59 - 1.9	$2.25H_2 + O_2 + 1.2N_2$	682
4)	1.9 - 2.1	$3H_2 + O_2 + 0.65N_2$	799
5)	2.12 - 2.5	$4H_2 + O_2$	960

Figure III-4 shows a plot of acceleration versus vehicle velocity. It can be seen that the accelerations are kept within the range of 600 to 1000 g, with an average acceleration of 857 g. A transition is made to another propellant mixture as the temperature behind the shock reaches the design limit of 1500 K for methane and 1200 K for hydrogen (Fig. III-5). Above these limits, the propellant mixtures can self ignite at the normal shock, resulting in a detonation wave propagating ahead of the vehicle. This, in turn, would produce negative thrust on the vehicle--a highly undesirable consequence.

Although the second methane mixture in Fig. III-5 does not reach its maximum design temperature of 1500 K, it was determined that higher accelerations, ballistic efficiencies, and TPR's could be reached by changing to another propellant mixture prior to attaining this temperature limit. By optimizing the propellant mixtures, an average ballistic efficiency of 14.4% is achieved for the thermally choked mode. A maximum efficiency of 19.2% occurs in mixture 2 (Fig. III-6).

Figure III-7 shows that the TPR was kept between 30 and 70% over the velocity range of the thermally choked mode. The average TPR here is 48.5%. The TPR for a given mixture is not allowed to fall below approximately half of its initial value to ensure that a maximum thrust efficiency is maintained. This was not of major concern, however, as in most of the mixtures the temperature design constraint is reached before the TPR falls to half its initial value.

The Mach number for the vehicle is kept approximately between 2.6 and 4.5 (Fig. III-8). As noted earlier the reason for a minimum of 2.6 is to ensure that the flow in the diffuser does not unstart. Depending on the propellant mixture and the initial velocity, unstarting of the diffuser occurs in the range of M = 2.3 - 2.6. Figure III-8 also shows a plot of the Mach number at the throat of the vehicle. Its value is not allowed to drop below approximately 1.5. The maximum vehicle Mach number of 4.5 corresponds to the shock temperature limit to prevent detonation of the propellant immediately behind the shock (Fig. III-5).

In Fig. III-9 it can be seen that a maximum static pressure on the vehicle and the wall is 1007 atm and occurs just before the transition between mixtures 2 and 3. The average peak static pressure is 770 atm on the vehicle and launch tube wall.

Figure III-10 shows a plot of velocity as a function of distance along the launch tube. Here, it can be seen that the projectile is accelerated from 0.7 km/s to 2.5 km/s within a distance of 345 m.

Smoother profiles of the performance parameters could be achieved if the number of mixture segments were increased; however, the ratio of body length to segment length could not be allowed to exceed one due to the computational methods used (for this analysis a body length to segment length ratio of approximately 1/5 was used). Alternatively, it might be possible to fill the tube with a continuously graded mixture composition.

Oblique Detonation Mode

The lower limit of the velocity range for the oblique detonation mode is defined by the C-J detonation velocity of the propellant mixture. To ensure combustion, however, a limiting value of 15 - 20% greater than the C-J velocity was set at the low end of the desired velocity range. This limit was determined to be 2.4 km/s for a detonable mixture of methane, oxygen, and argon. It was decided, however, that the thermally choked mode of propulsion would transition to the oblique detonation mode at a velocity of 2.5 km/s. This velocity was used because it fell between the two limiting values for each mode. Also, the acceleration of the thermally choked mode falls rapidly beyond 2.5 km/s. Table 2 shows the mixtures used for this mode of propulsion and their corresponding velocity ranges as determined by an analysis based on 1-D flow assumptions.

Table 2: Propellant Mixtures for Vehicle Propulsion in the Oblique Detonation Mode

Velocity Range (km/s)		Propellant Mixture	Calculated Detonation Speed (km/s)
1)	2.5 - 3.15	$CH_4 + O_2 + 5Ar$	1.650
2)	3.15 - 4.75	$2.4H_2 + O_2 + 2N_2$	2.723
3)	4.75 - 7.2	$5H_2 + O_2$	3.510
4)	7.2 - 10	$8H_2 + O_2$	3.749

The mixtures used in this analysis were tailored to meet the given acceleration parameters while, at the same time, yielding satisfactory efficiencies. Figure III-11 shows the acceleration profile of the projectile as a function of freestream velocity. It was desirable to maintain as low freestream Mach numbers as possible (Fig. III-12) in order to minimize in-tube heating of the vehicle, as projectile heating varies as the square of the Mach number. Therefore, an arbitrary upper limit of M = 11 was set and changes in mixture were made primarily to keep the Mach number below this value, as the acceleration does not vary strongly with vehicle velocity. Some encroachment of this constraint does occur at velocities in the vicinity of 9 km/s; however, this is near the design exit velocity and the remaining time of vehicle transit in the tube is small enough that the increased heating effect is negligible, especially when compared to the ensuing flight Mach numbers of atmospheric transit, which are well into the hypersonic regime. In Chapter IV the problem of in-tube aerodynamic heating is treated.

The maximum temperature on the body was found to occur immediately following the oblique detonation wave and reached a maximum value of 4100 K for mixture 2 (Fig. III-13). It was found that with the final propellant mixture, the vehicle acceleration did not meet the established design criteria with a tube diameter of 1.0 m. To remedy this situation, an investigation into the effects of varying the tube diameter was performed (Figs. III-14 - III-16).

If the tube inner diameter is decreased, the flow must be compressed into a smaller annular area; hence, the pressures on the body (Fig. III-14) and tube (Fig. III-15) increase greatly with decreasing tube diameter and vehicle acceleration improves slightly (Fig. III-16). In addition to increased acceleration, the ballistic efficiency of the process increases, and the TPR decreases as the peak cycle pressure increases with decreasing tube diameter. It was found that an inner tube diameter of 0.9 m yields satisfactory vehicle acceleration while keeping the maximum pressures on the tube and body within reasonable structural limits. The smaller tube diameter was used only for the final propellant mixture ($8H_2 + O_2$) because of the inadequate performance of this mixture with the typical tube dimensions.

The maximum static pressure on the vehicle (Fig. III-17) was found to occur immediately following the oblique detonation wave prior to expansion. This pressure was calculated to be approximately 1667 atm, occurring during the initial and final phase of transit (mixtures 1 and 4, respectively). The peak pressure on the barrel wall occurs immediately following the reflected detonation wave and is 3467 atm. After the detonation wave the pressure drops abruptly as the flow passes through the expansion wave following the shock.

Figure III-18 shows that the Type II oblique detonation mode operates at ballistic efficiencies ranging from 20.1% to 29.6%, and averaging 25.1%. The thrust pressure ratio (Fig. III-19) ranges from 8.1% to 14% and averages 11%. These figures compare to an average ballistic efficiency of 22.7%, and an average thrust pressure ratio of 13.1% for the Type I oblique detonation mode used in a previous study [2]. It should be reiterated that the model used for computation neglects the bow shock; hence, the efficiency calculated is overestimated and the thrust pressure ratio is underestimated due to the omission of shock losses prior to detonation; however, the error incurred is small [14].

In Fig. III-20 the launch tube length required for a given exit velocity is shown for vehicle propulsion from initial acceleration to launch tube exit. For a design exit velocity of 9.0 km/s, a tube length of 5.1 km is required. Of this length, 4.78 km (approximately 93%) is required for the oblique detonation mode alone. For higher exit velocities, this distance increases rapidly, as shown. As can be seen, the oblique detonation mode is the dominant factor in determining overall launch tube length.

2-D CFD Results

The two-dimensional analysis was performed only at a vehicle velocity of 7.2 km/s (mixture 5, oblique detonation mode) to confirm the validity of the 1-D analysis. CPU time

requirements precluded a full analysis of the oblique detonation propulsion mode over the entire velocity range of interest.

The 2-D analysis yields accelerations which are 12% lower than what 1-D approximations predicted. The ballistic efficiency calculated with 2-D approximations is 32.4%, and the thrust pressure ratio is 12.0%. These are 12.1% and 44.6% higher, respectively, than the 1-D values.

The 2-D analysis also shows the peak pressures on the vehicle and barrel wall to be 1939 and 1872 atm, respectively. These values differ by +18.1% and -46.2%, respectively, from the 1-D calculations. These differences occur because of the two-dimensionality of the flow over the vehicle.

The 1-D analysis calculated pressures quite well in the immediate vicinity of the vehicle (CFD values average a difference of 15% from 1-D approximations); however, near the tube wall the differences were much greater. As a result, the 2-D value for peak pressure on the launch tube wall (1872 atm) was used to determine tube wall thicknesses for the detonation propulsion mode. The 2-D pressure values were chosen since the CFD code provides a much more realistic description of the flow field. The thermally choked subsonic combustion peak pressure values are quite accurate, though, since 1-D approximations are quite good behind the body (where combustion takes place) and since the exact solution for the pressure here is readily available in closed form (Eq. 3).

CONCLUSIONS

The ram accelerator is a concept designed to efficiently propel acceleration-insensitive payloads into space. The gasdynamics of the ram accelerator resembles that of a conventional airbreathing ramjet. The projectile serves as the centerbody of the ramjet while the outer cowling of the ramjet is provided by the launch tube. The launch tube is filled with premixed propellants so that the energy release travels with the vehicle, and no on-board propellant is required. This design allows the propellant mixtures to be graded so that the performance can be optimized to meet specific design requirements.

This chapter has analyzed the propellant mixtures necessary to accelerate a projectile from 0.7 km/s to 10.0 km/s. A total of nine mixtures and two combustion modes are required to propel the projectile to the design exit velocity (9.0 km/s). The thermally choked subsonic combustion mode is used for velocities ranging from 0.7 km/s to 2.5 km/s, and requires 345 m of the accelerator length. The second combustion mode utilized is the Type II oblique detonation mode. This mode propels the projectile from a velocity of 2.5 km/s to 9.0 km/s (with the capability for further acceleration), and requires 4.78 km (approximately 93%) of the total launcher length.

Ram acceleration can be performed with satisfactory efficiency. The thermally choked mode efficiency averages 14.4%, while the oblique detonation mode averages 25.1% for an overall average of 24.4%. The overall thrust pressure ratio averages 13.6%. Peak pressures on the vehicle are 1007 atm and 1939 atm for the subsonic and detonation propulsion modes, respectively. Also, the peak pressures on the wall of the launch tube are 1007 atm and 1872 atm for these modes.

REFERENCES

1. Bruckner, A.P. and Hertzberg, A., "Ram Accelerator Direct Launch System for Space Cargo," IAF Paper 87-211, 38th Congress of the International Astronautical Federation, Brighton, England, October 10-17, 1987.

2. Hertzberg, A. and Bruckner, A.P., eds., "The Ram Accelerator Concept: A Method for Direct Launch of Space Cargo to Orbit," Final Report, AA420/AA499, NASA/USRA Advanced Space Design Program, University of Washington, Seattle, WA, June 1987.

3. Bruckner, A.P., Bogdanoff, D.W. and Knowlen, C., "Investigation of Gasdynamic Phenomena Associated with the Ram Accelerator Concept," AIAA Paper 87-1327, AIAA 19th Fluid Dynamics, Plasma Dynamics and Laser Conference, Honolulu, HI, June 8-10, 1987.

4. Hertzberg, A., Bruckner, A.P. and Bogdanoff, D.W., "The Ram Accelerator: A New Chemical Method for Accelerating Projectiles to Ultrahigh Velocities," AIAA Journal, 26, 195(1988).

5. Hertzberg, A., Bruckner, A.P., Bogdanoff, D.W., and Knowlen, C., "The Ram Accelerator and its Applications: A New Chemical Approach for Reaching Ultrahigh Velocities," Proceedings of the 16th International Symposium on Shock Tubes and Waves, Aachen, West Germany, July 26-30, 1987, pp 117 - 128.

6. Knowlen, C., Bruckner, A.P., Bogdanoff, D.W., and Hertzberg, A., "Performance Capabilities of the Ram Accelerator," AIAA Paper 87-2152, AIAA/SAE/ASME/ASEE 23rd Joint Propulsion Conference, San Diego, CA, June 29 - July 2, 1987.

7. Knowlen, C., "COMB-3," Computer Program for Combustion Analysis of the Thermally Choked Ram Accelerator, Department of Aeronautics & Astronautics, University of Washington, Seattle, WA, November, 1983.

8. Bruckner, A.P., "TRCR11," Computer Program for Thermally Choked Ram Accelerator Analysis, Department of Aeronautics & Astronautics, University of Washington, Seattle, WA, February, 1987.

9. Knowlen, C., "CHOKE," Computer Program for Thermally Choked Ram Accelerator, Department of Aeronautics & Astronautics, University of Washington, Seattle, WA, 1984.

10. Oates, G.C., Aerothermodynamics of Gas Turbines and Rocket Propulsion, American Institute of Aeronautics and Astronautics, New York, 1984.

11. Bruckner, A.P., Department of Aeronautics & Astronautics, University of Washington, Seattle, WA, Private Communication, February 1988.

12. Pratt, D.T., Humphrey, J.W., and Glenn, D.E., "Morphology of a Standing Oblique Detonation Wave," AIAA Paper 87-1785, AIAA/SAE/ASME/ASEE 23rd Joint Propulsion Conference, San Diego, CA, June 29 - July 2, 1987.

13. Bogdanoff, D.W., "OBLI2", Computer Program for Type II Oblique Detonation Ram Accelerator Analysis, Department of Aeronautics & Astronautics, University of Washington, Seattle, WA, June 1987.

14. Bogdanoff, D.W., NASA Ames Research Center, Private Communication, February 1988.

15. Bogdanoff, D.W. and Brackett, D., "A Computational Fluid Dynamics Code for the Investigation of Ramjet-in-Tube Concepts," AIAA paper 87-1978, AIAA/ASME/SAE/ASEE, 23rd Joint Propulsion Conference, San Diego, CA June 29 - July 2, 1987.

16. Liepmann, H.W., Roshko, A., Elements of Gas Dynamics, John Wiley, New York, 1957.

NOMENCLATURE

a	speed of sound
A	tube cross-sectional area
C_f	coefficient of friction
C_p	specific heat at constant pressure
D	drag
F	thrust
g	acceleration due to gravity
m	mass flow rate
M	Mach number
P	pressure
Δq	heat release due to combustion
S	surface area
T	static temperature
U	velocity
γ	ratio of specific heats
η	ballistic efficiency
ρ	density

Subscripts

i	i^{th} station
1	freestream conditions
6	conditions at point of thermal choking

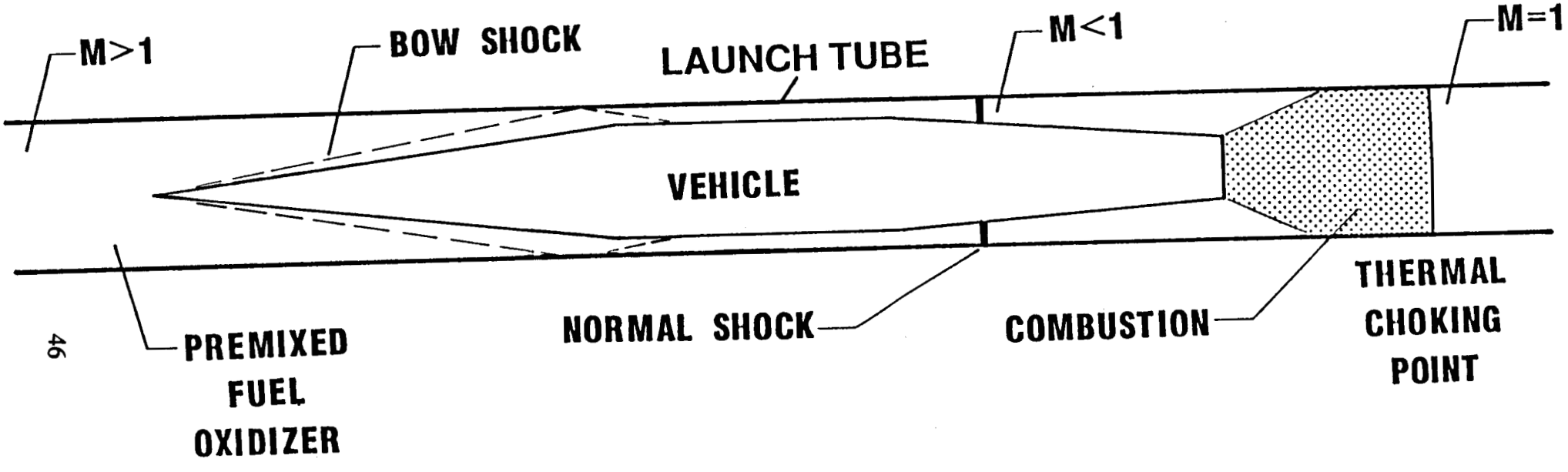

Fig. III-1: Thermally choked subsonic combustion ram acceleration mode.

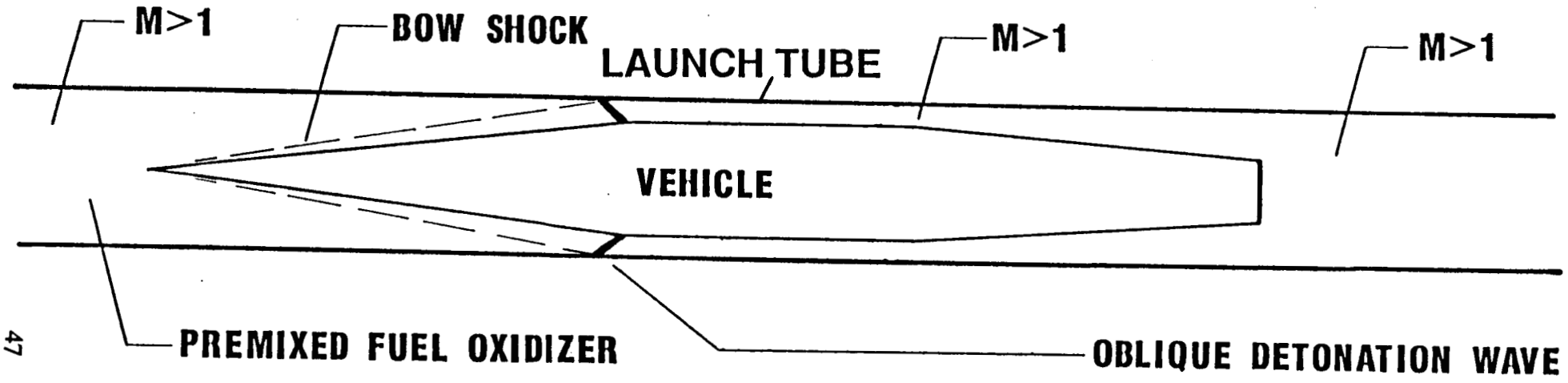

Fig. III-2: Type I oblique detonation ram acceleration mode.

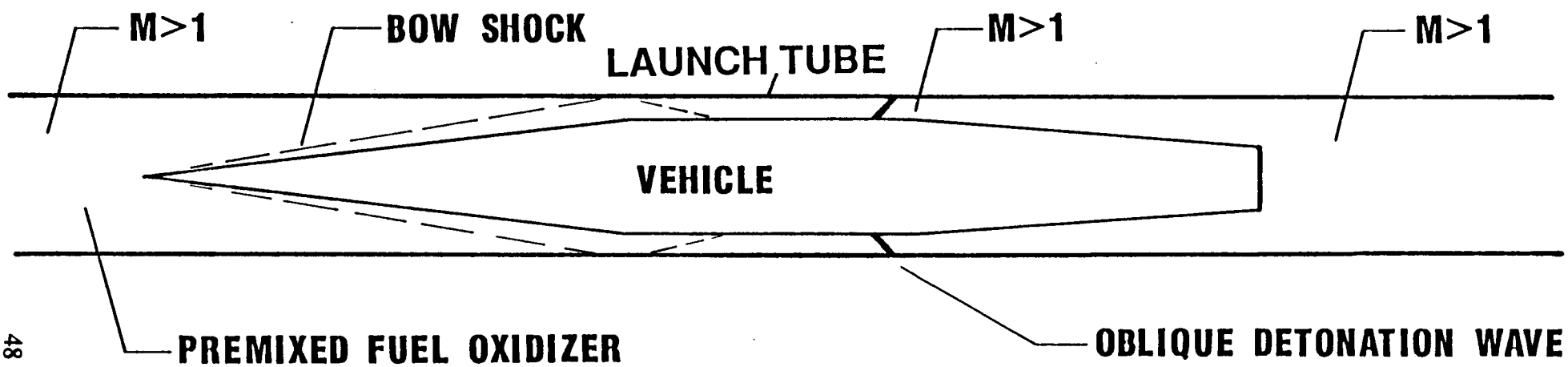

Fig. III-3: Type II oblique detonation ram acceleration mode.

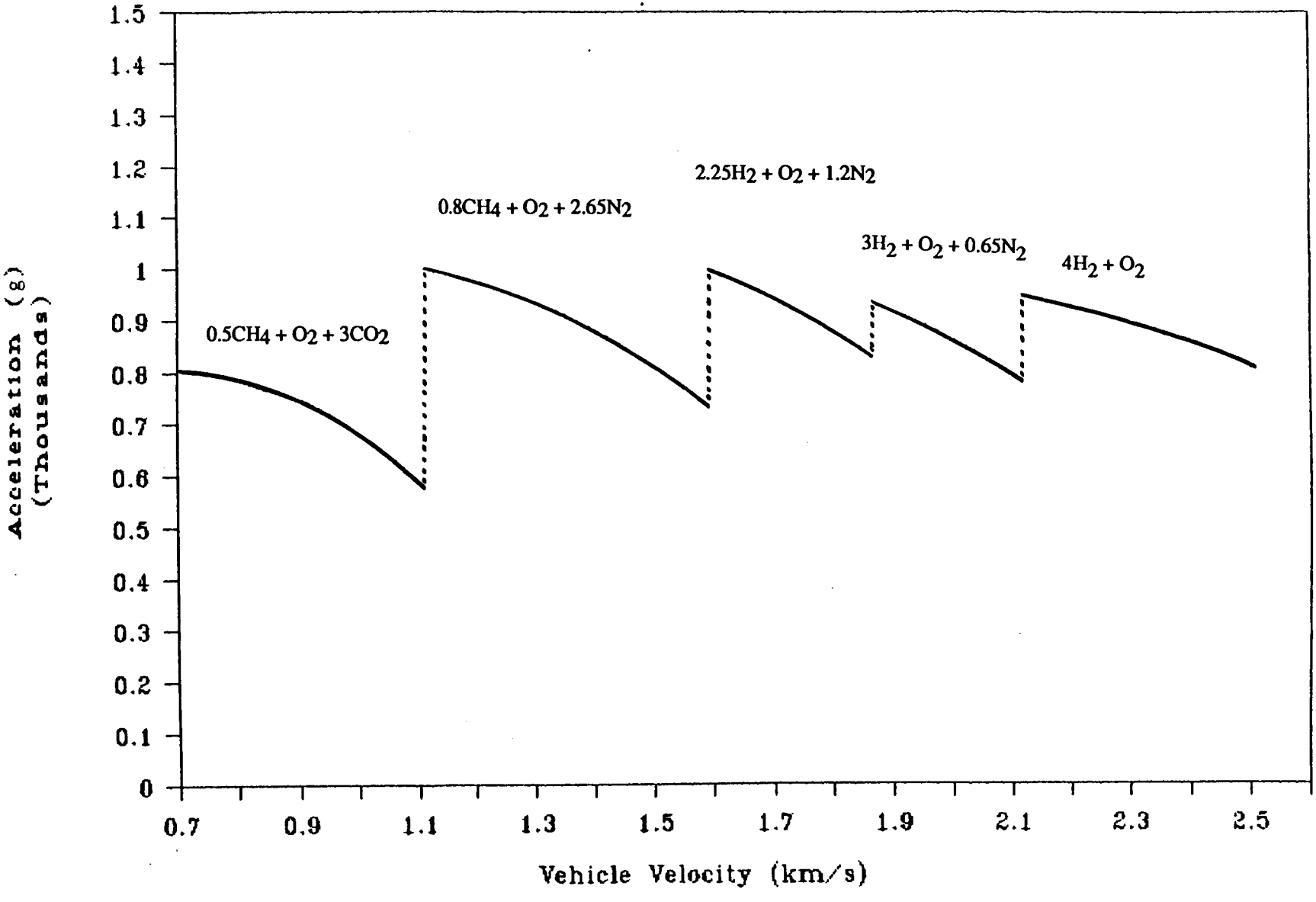

Fig. III-4: Acceleration profile of the thermally choked combustion mode. Acceleration values are for a 2000 kg, 0.76 m O.D. vehicle, 1.0 m I.D. launch tube, and 33 atm propellant fill pressure. Acceleration jumps indicate mixture transitions.

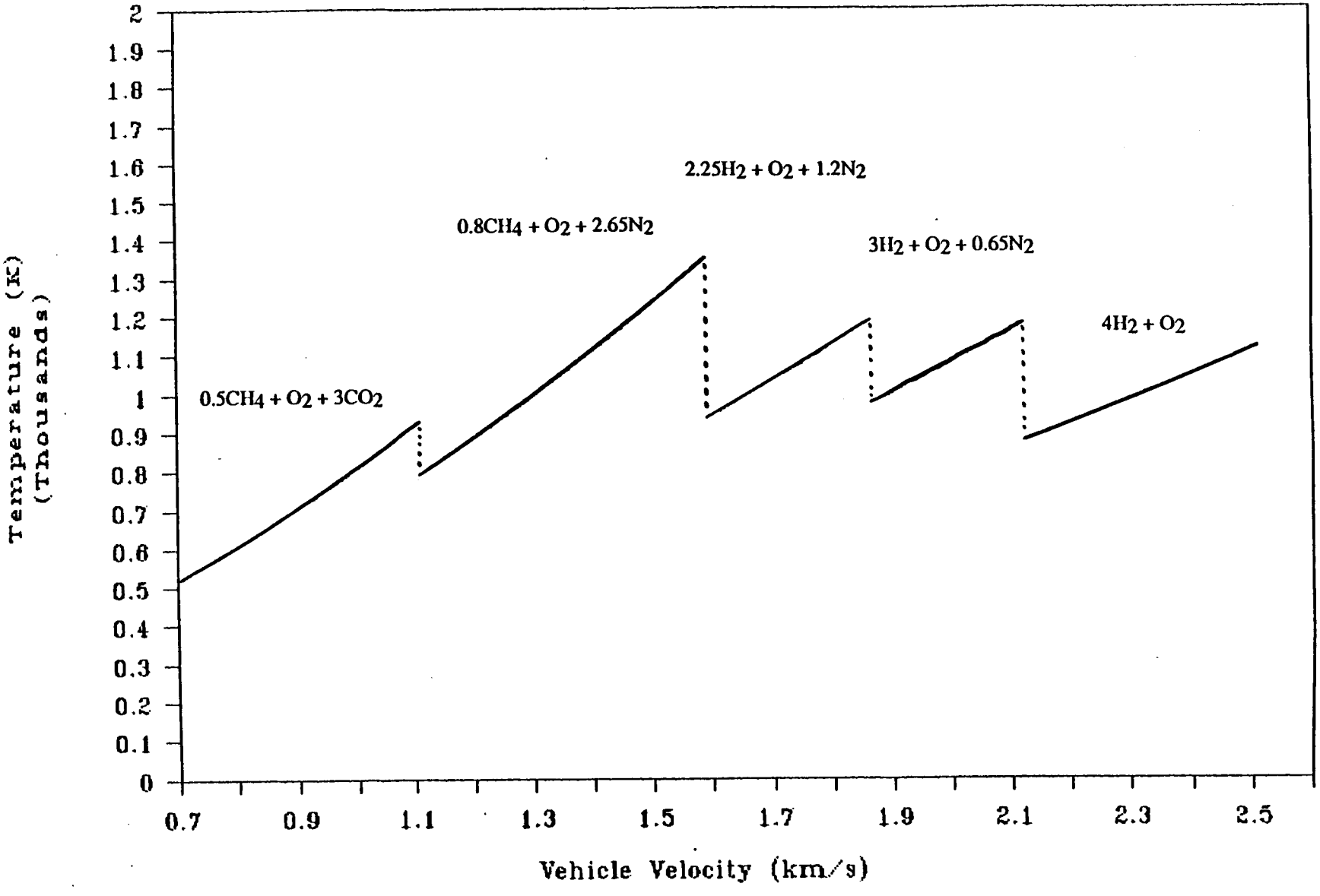

Fig. III-5: Temperature profile of the flow on the ram accelerator body immediately behind the normal shock for the thermally choked mode. Values are for a 2000 kg, 0.76 m O.D. vehicle, 1.0 m I.D. launch tube, and 33 atm propellant fill pressure. Temperature jumps indicate mixture transitions.

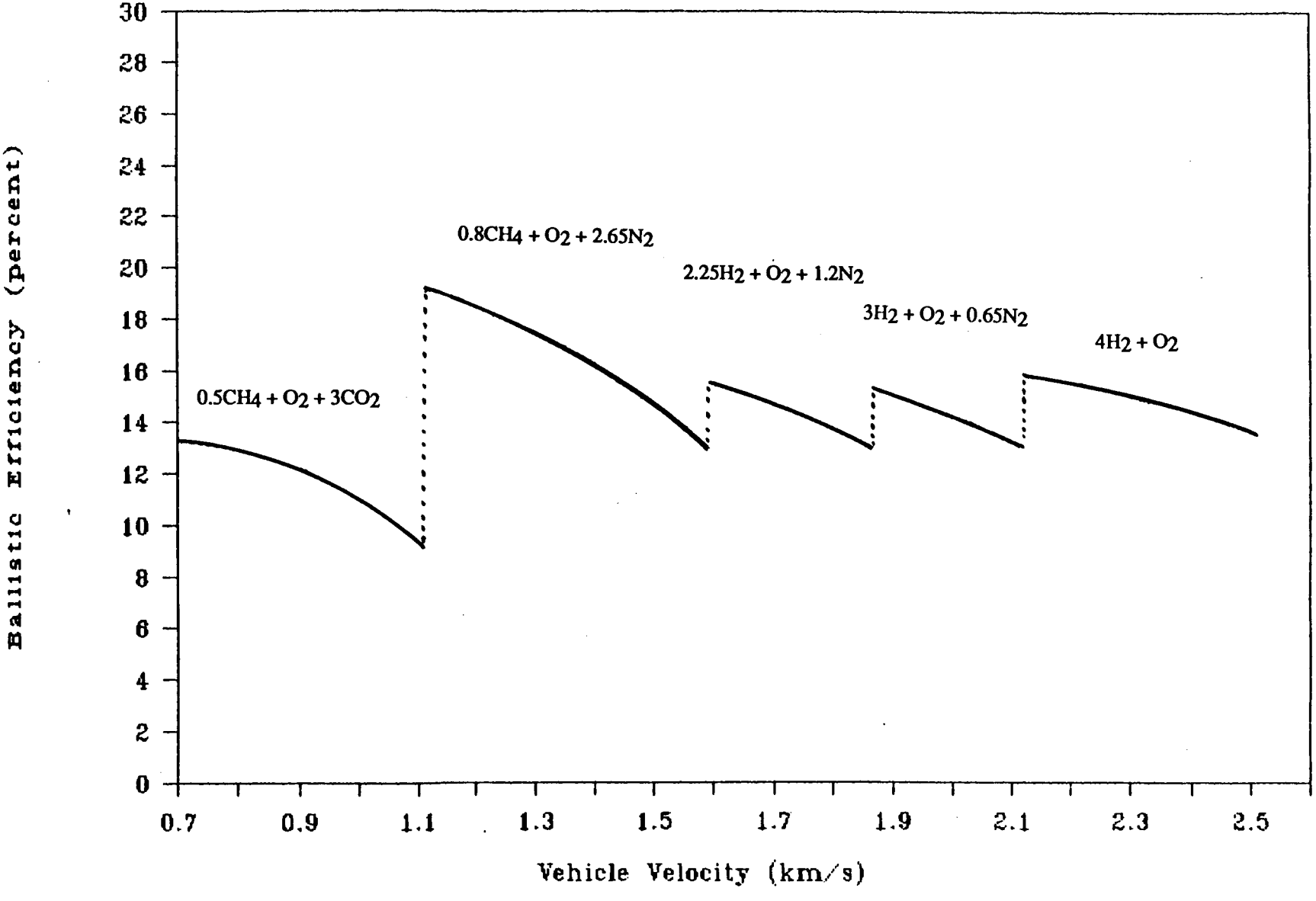

Fig. III-6: Ballistic efficiency profile of the thermally choked combustion mode. Values are for a 2000 kg, 0.76 m O.D. vehicle, 1.0 m I.D. launch tube, and 33 atm propellant fill pressure. Efficiency jumps indicate mixture transitions.

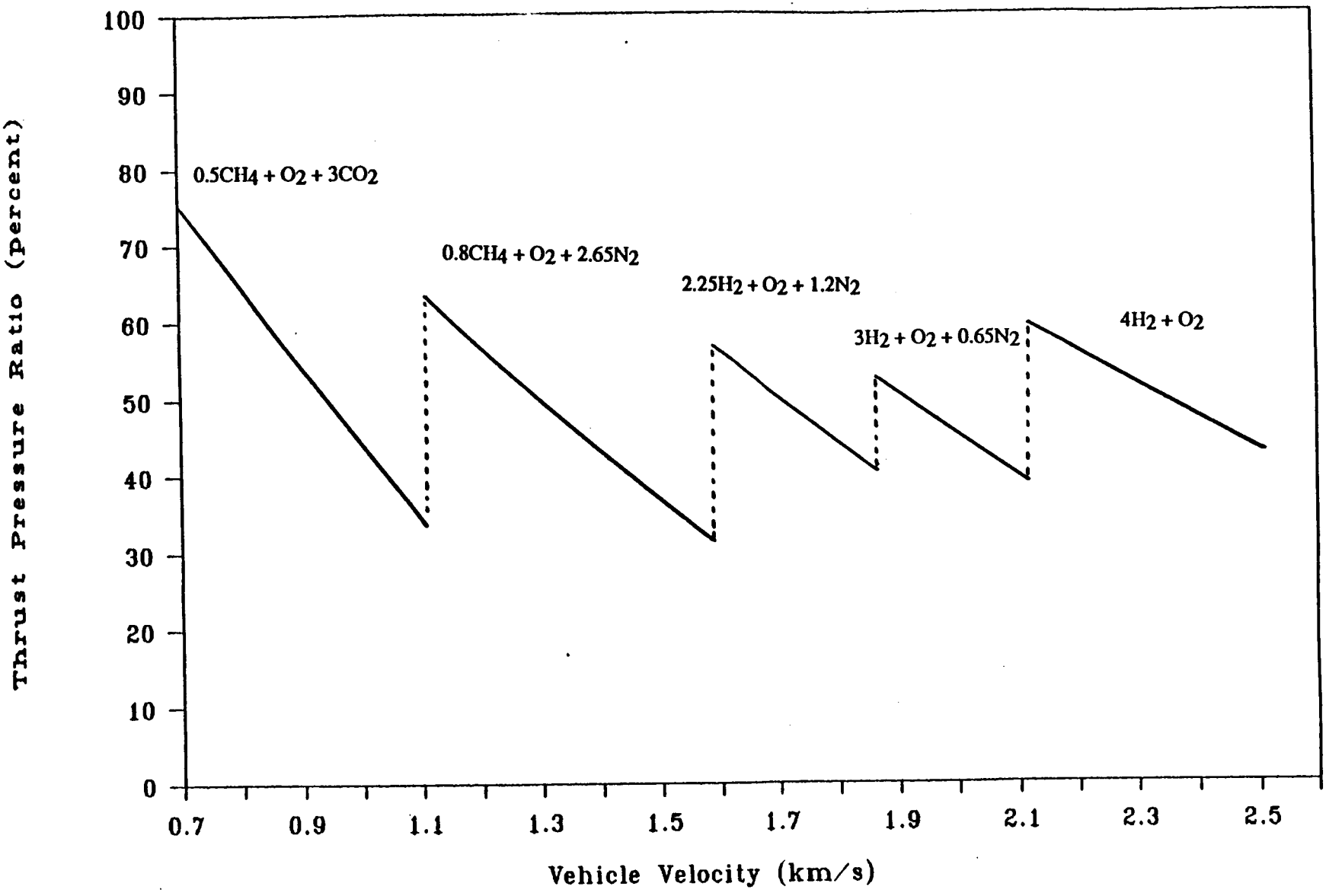

Fig. III-7: Thrust pressure ratio (TPR) profile of the thermally choked combustion mode. Values are for a 2000 kg, 0.76 m O.D. vehicle, 1.0 m I.D. launch tube, and 33 atm propellant fill pressure. TPR jumps indicate mixture transitions.

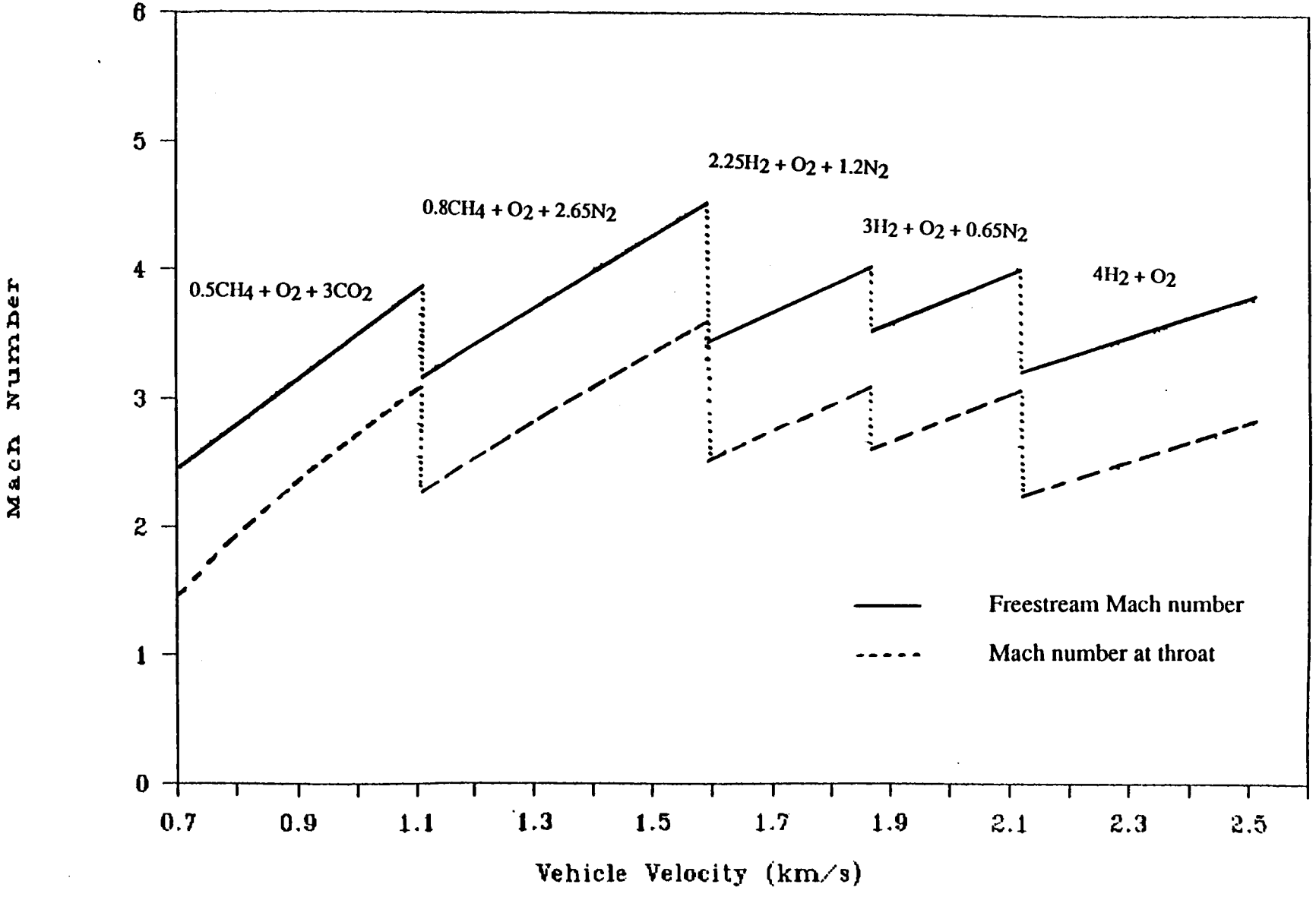

Fig. III-8: Mach number profile of the vehicle in the freestream and at the throat for the thermally choked combustion mode. Values are for a 2000 kg, 0.76 m O.D. vehicle, 1.0 m I.D. launch tube, and 33 atm propellant fill pressure. Jumps in Mach number indicate mixture transitions.

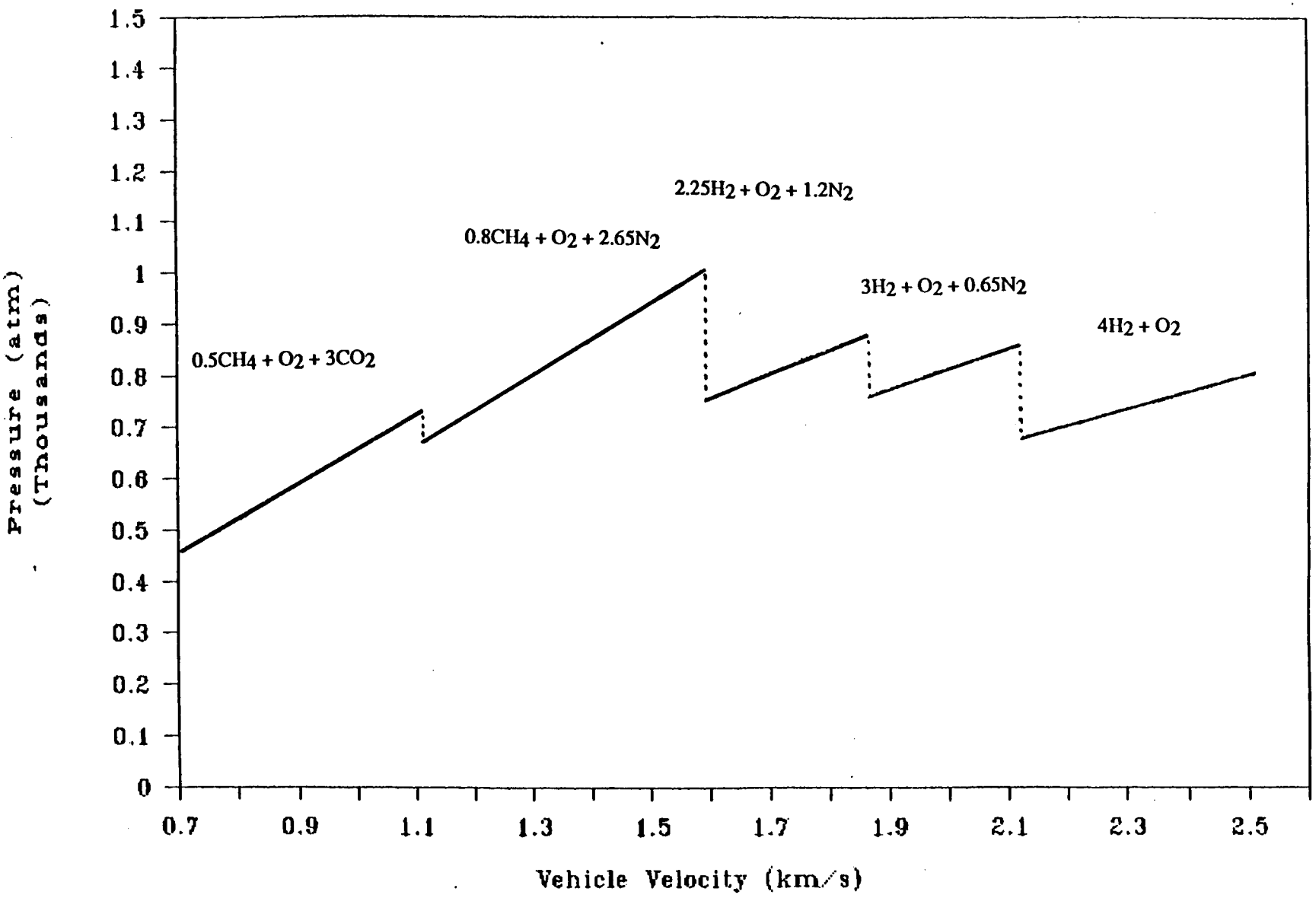

Fig. III-9: Peak static pressure profile at the base of the ram accelerator vehicle for the thermally choked combustion mode. Pressure values are for a 2000 kg, 0.76 m O.D. vehicle, 1.0 m I.D. launch tube, and 33 atm propellant fill pressure. Pressure jumps indicate mixture transitions.

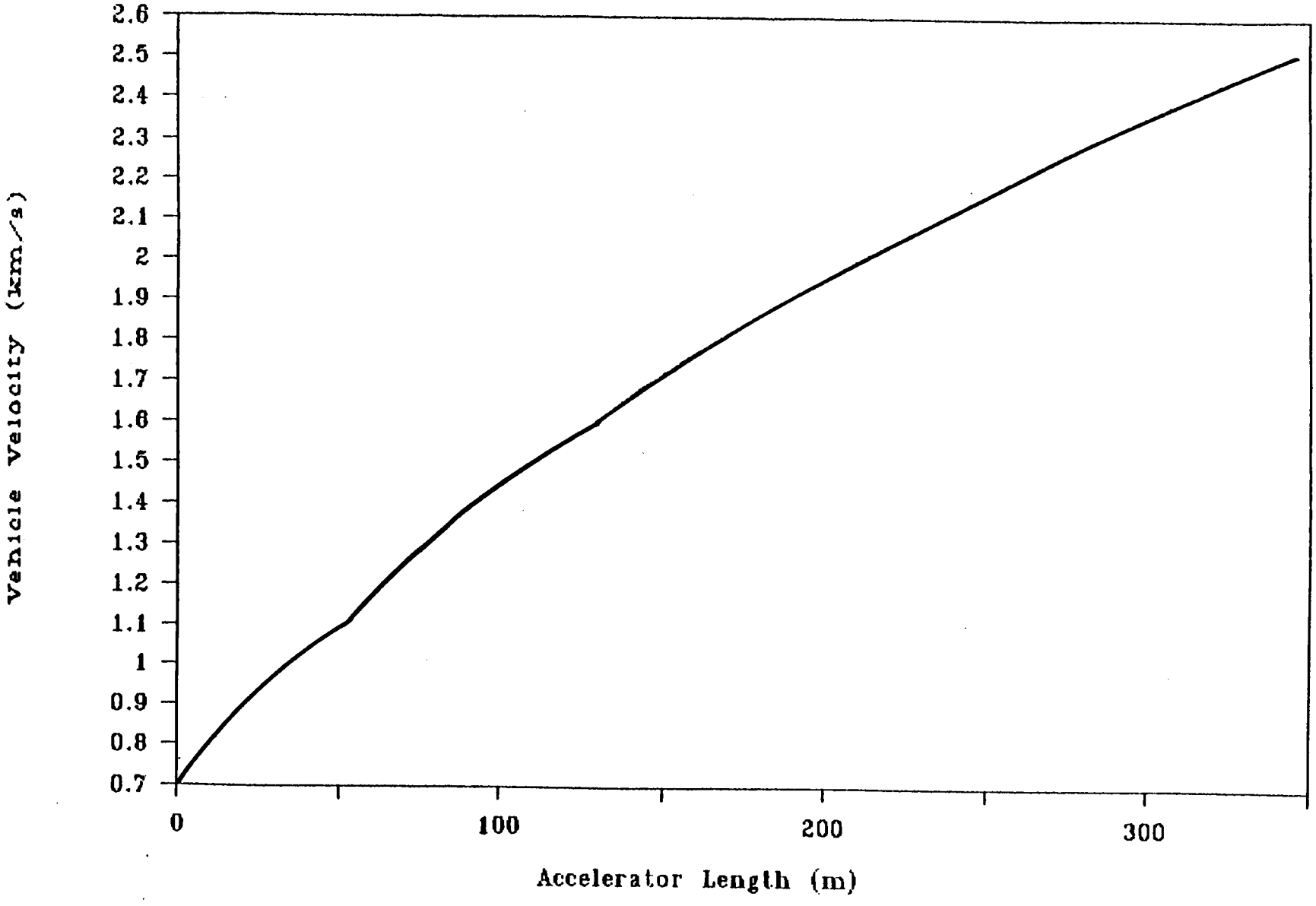

Fig. III-10: Velocity profile of the thermally choked combustion mode. Velocities are for a 2000 kg, 0.76 m O.D. vehicle, 1.0 m I.D. launch tube, and 33 atm propellant fill pressure.

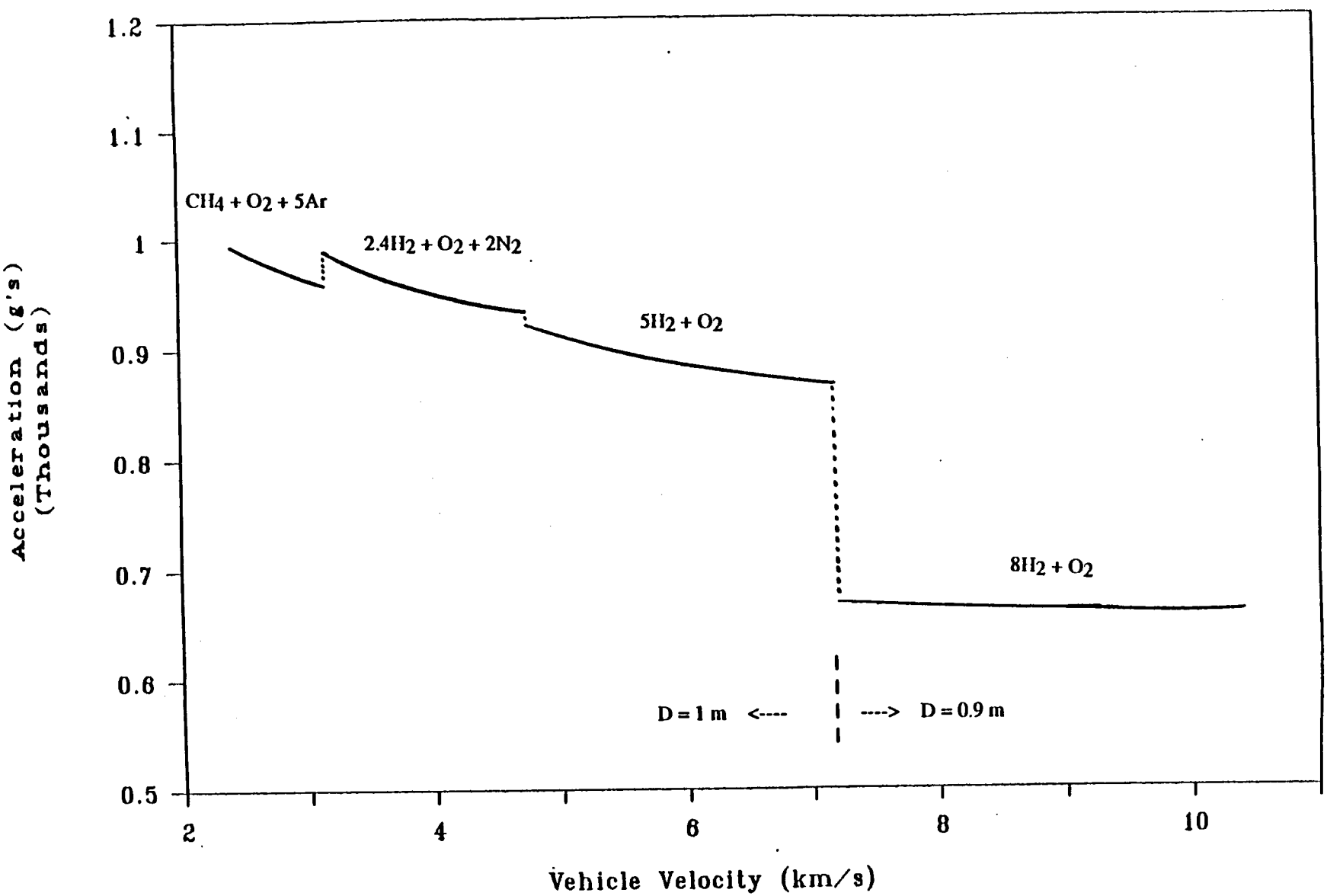

Fig. III-11: Acceleration profile of the oblique detonation mode. Values are for a 2000 kg, 0.76 m O.D. vehicle, and 33 atm propellant fill pressure. D is the launch tube diameter. Acceleration jumps indicate mixture transitions.

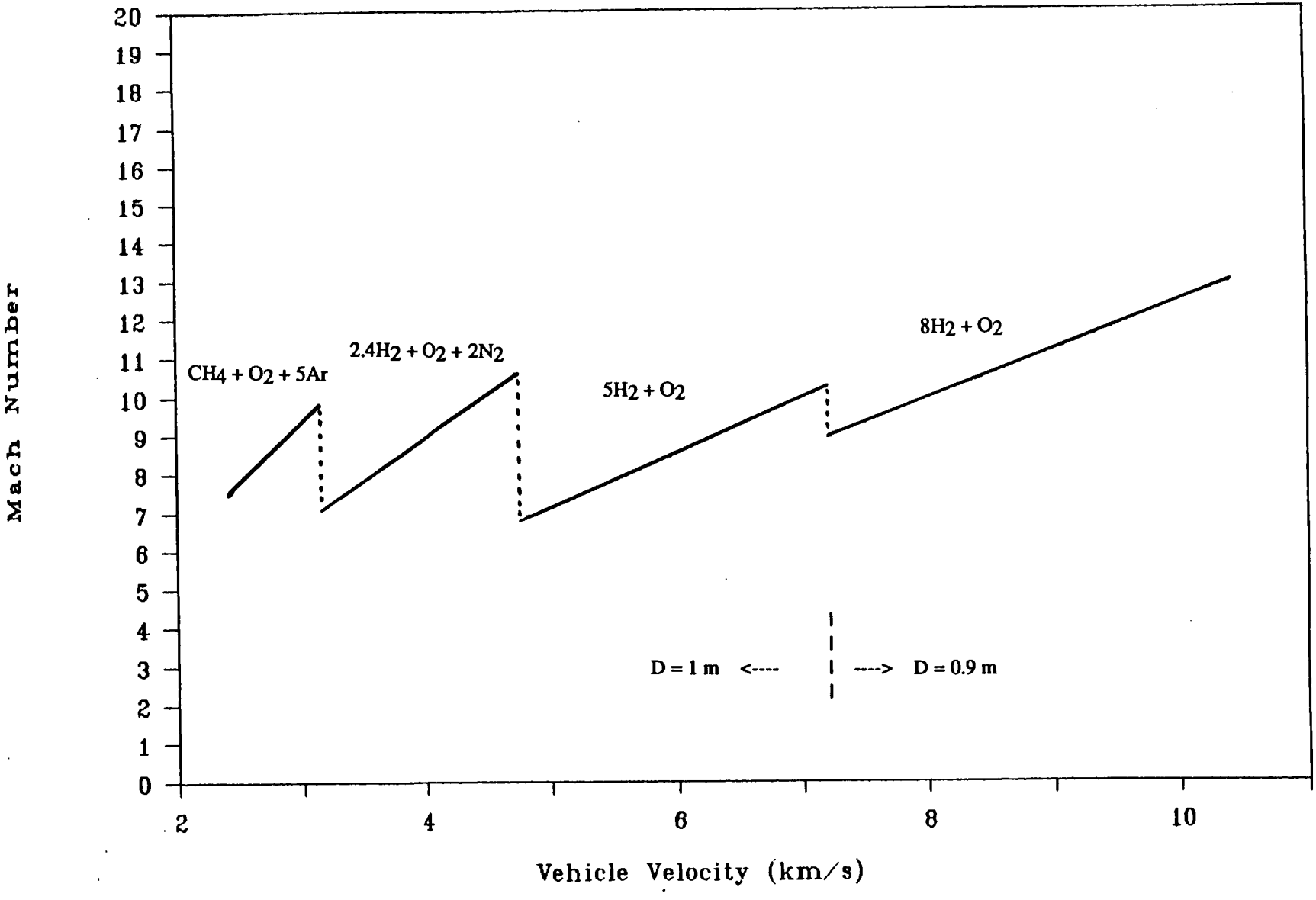

Fig. III-12: Freestream Mach number profile for the oblique detonation mode. Values are for a 2000 kg, 0.76 m O.D. vehicle, and 33 atm propellant fill pressure. D is the launch tube diameter. Jumps in Mach number indicate mixture transitions.

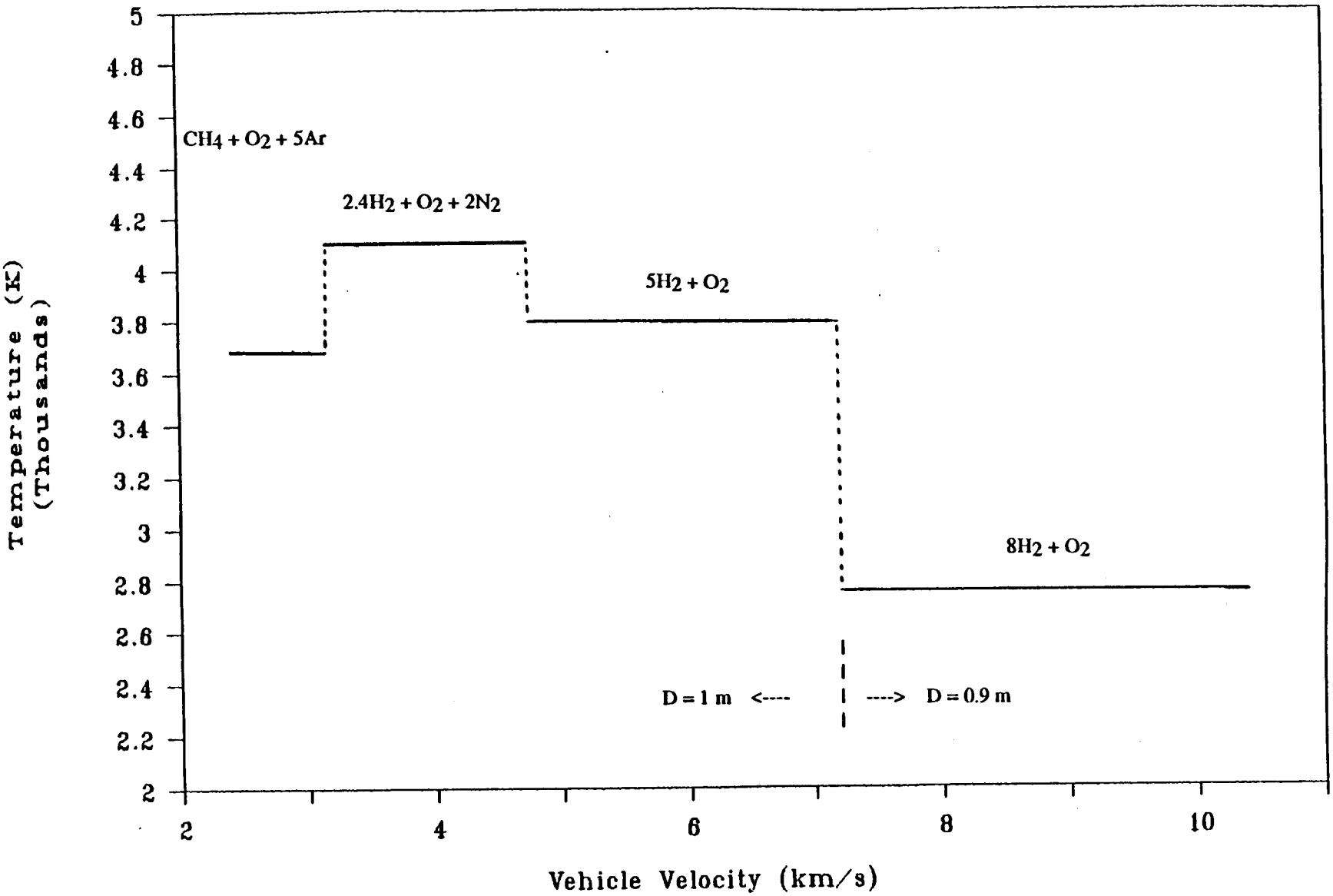

Fig. III-13: Profile of static temperature on the body directly behind the oblique detonation wave for the oblique detonation mode. Values are for a 2000 kg, 0.76 m O.D. vehicle, and 33 atm propellant fill pressure. D is the launch tube diameter. Temperature jumps indicate mixture transitions.

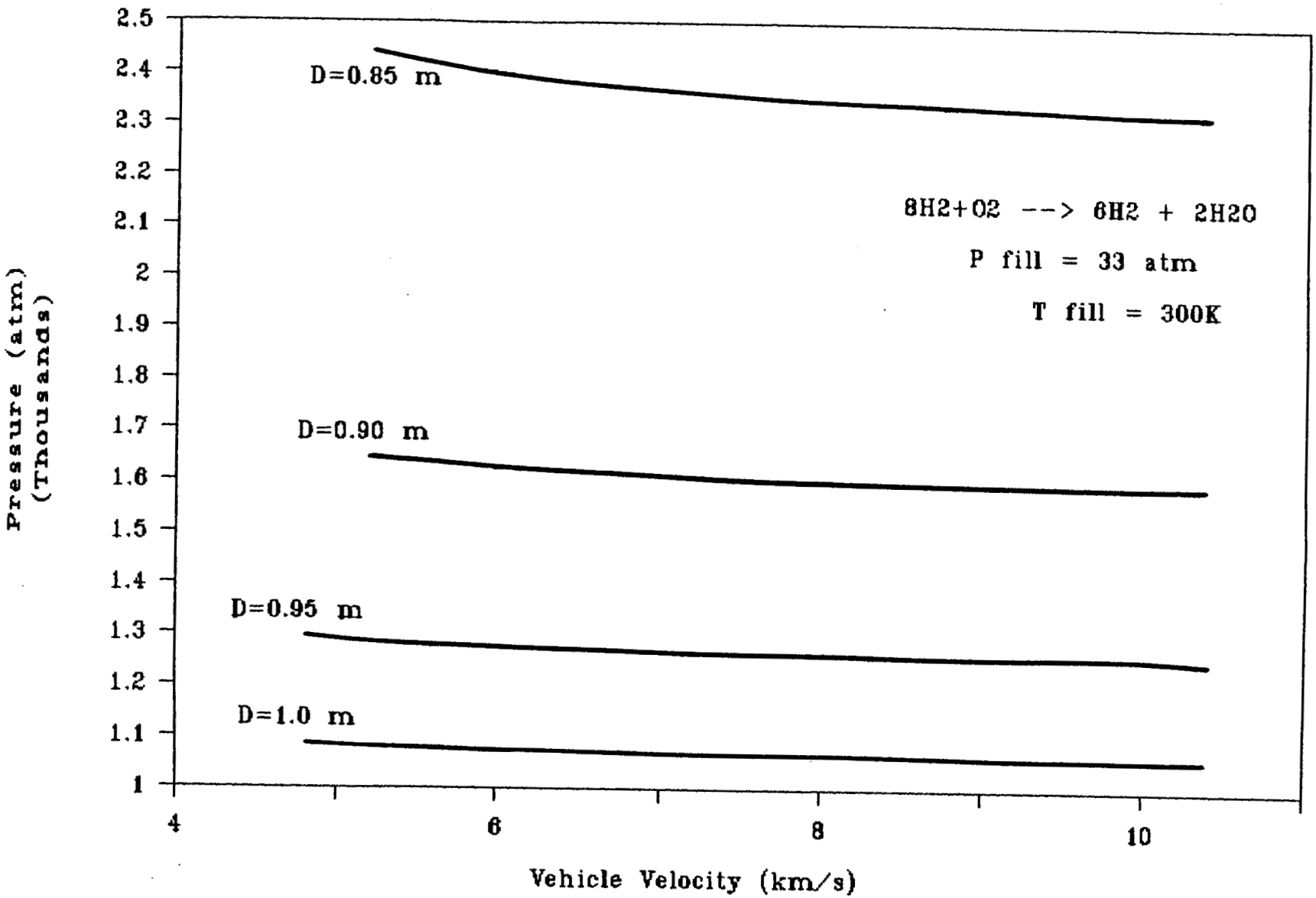

Fig. III-14: Comparison of the maximum peak pressure on the body behind the oblique detonation wave as a function of vehicle velocity when the diameter of the launch tube is varied, using the indicated propellant mixture.

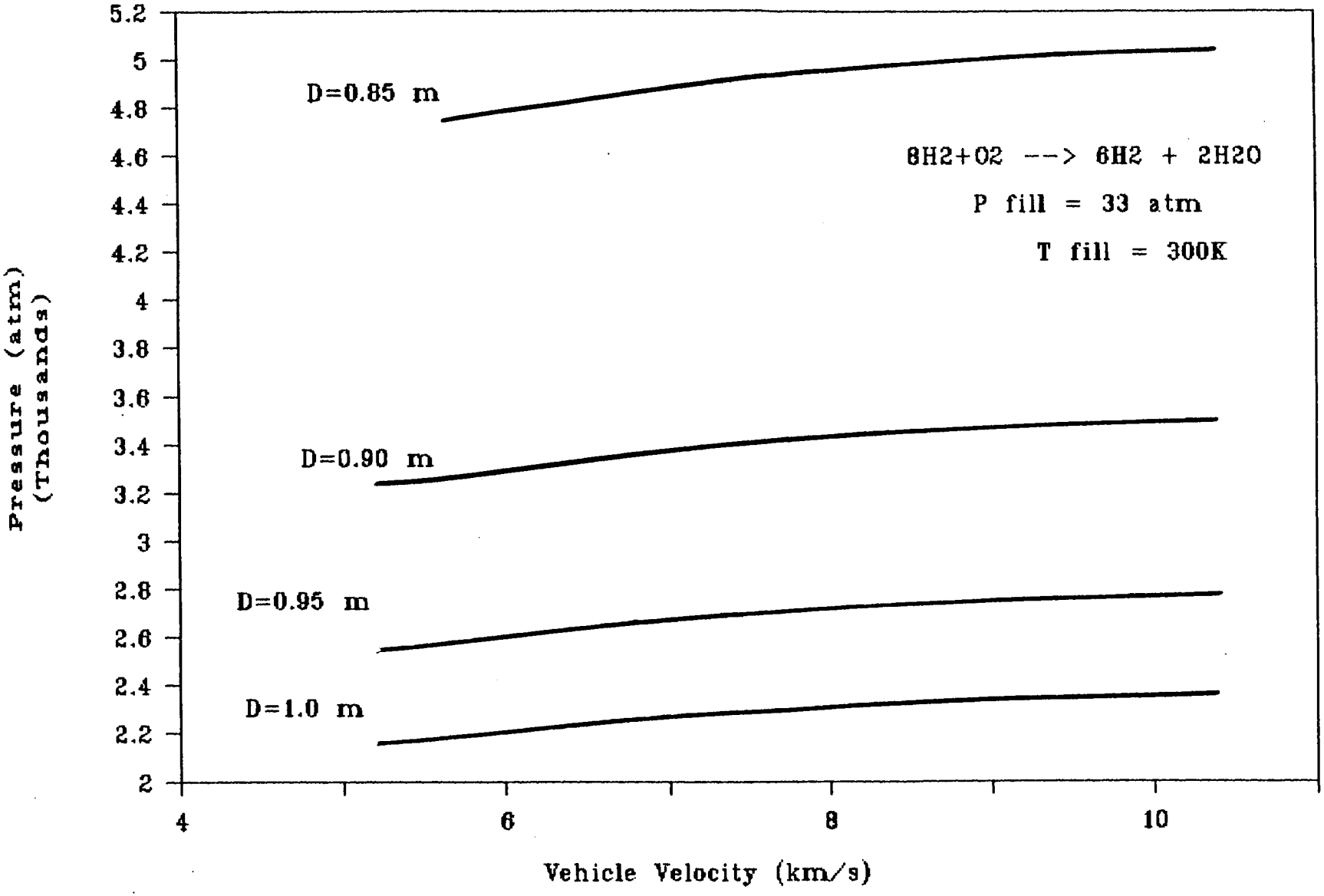

Fig. III-15: Comparison of the maximum peak pressure on the launch tube as a function of vehicle velocity when the diameter of the launch tube is varied, using the indicated propellant mixture.

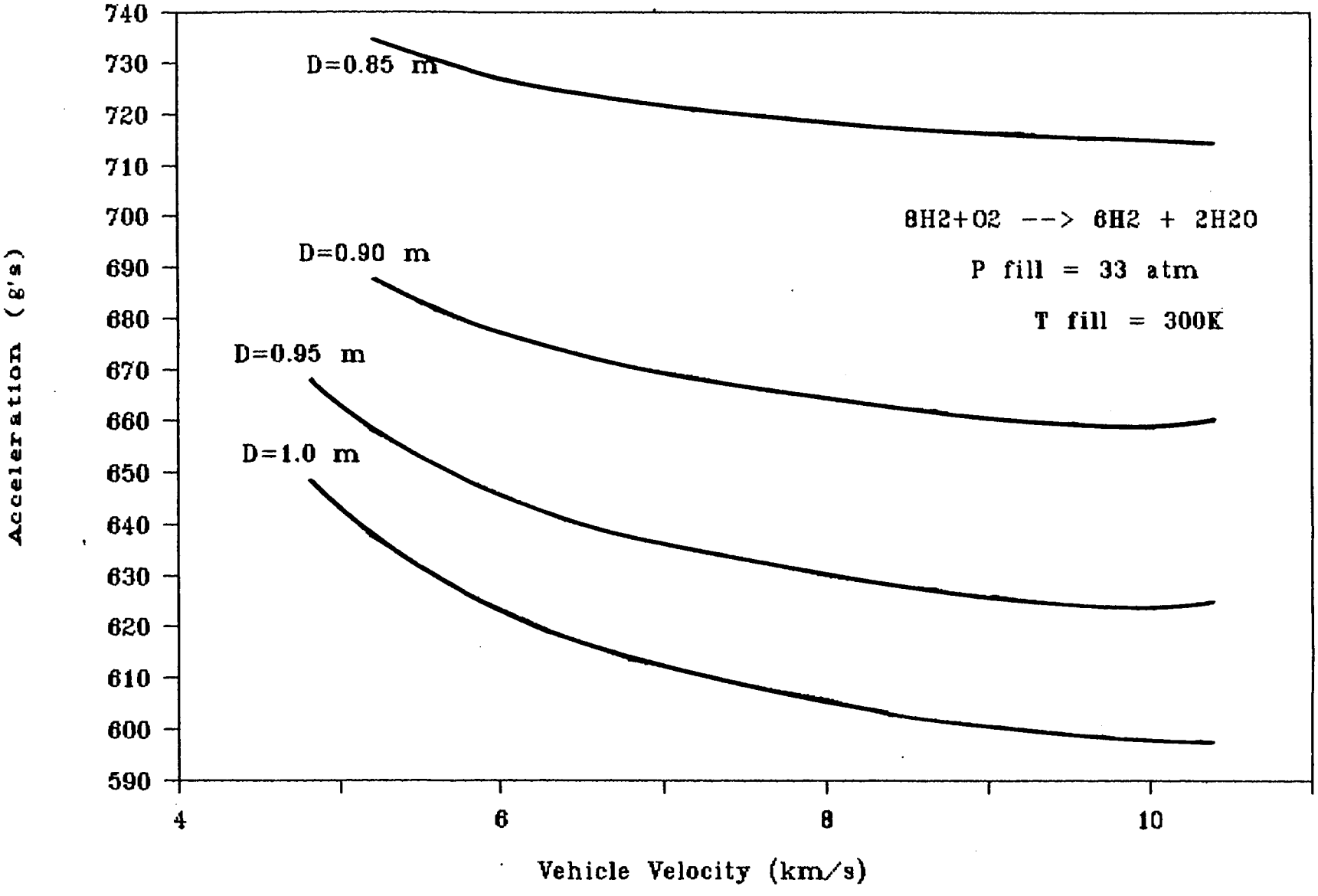

Fig. III-16: Comparison of the vehicle acceleration changes caused by varying the diameter of the launch tube as a function of vehicle velocity for the oblique detonation mode, using the indicated propellant mixture.

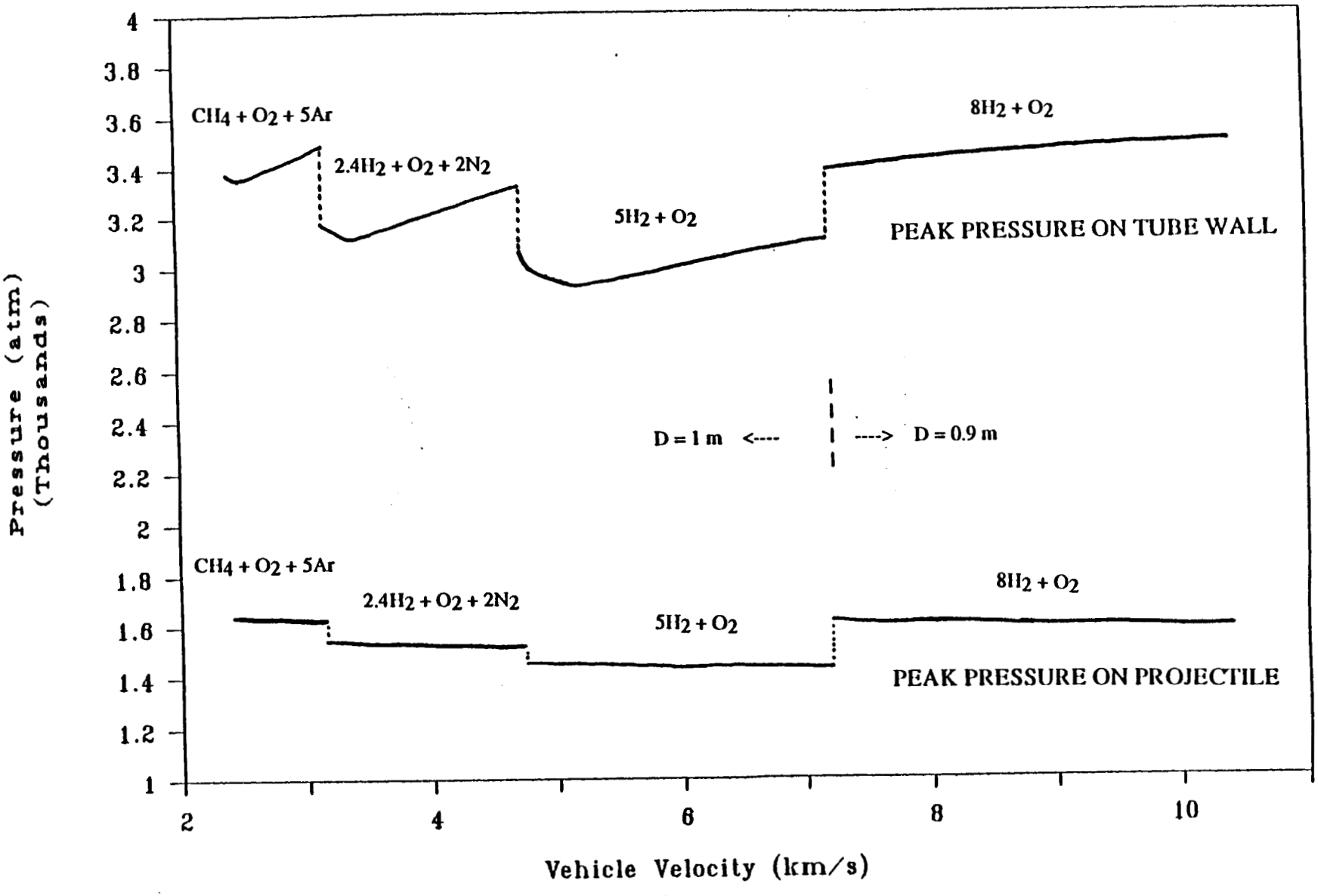

Fig. III-17: Profile of the peak pressures on the tube and body for the oblique detonation mode. Values are for a 2000 kg, 0.76 m O.D. vehicle, and 33 atm propellant fill pressure. D is the launch tube diameter. Efficiency jumps indicate mixture transitions..

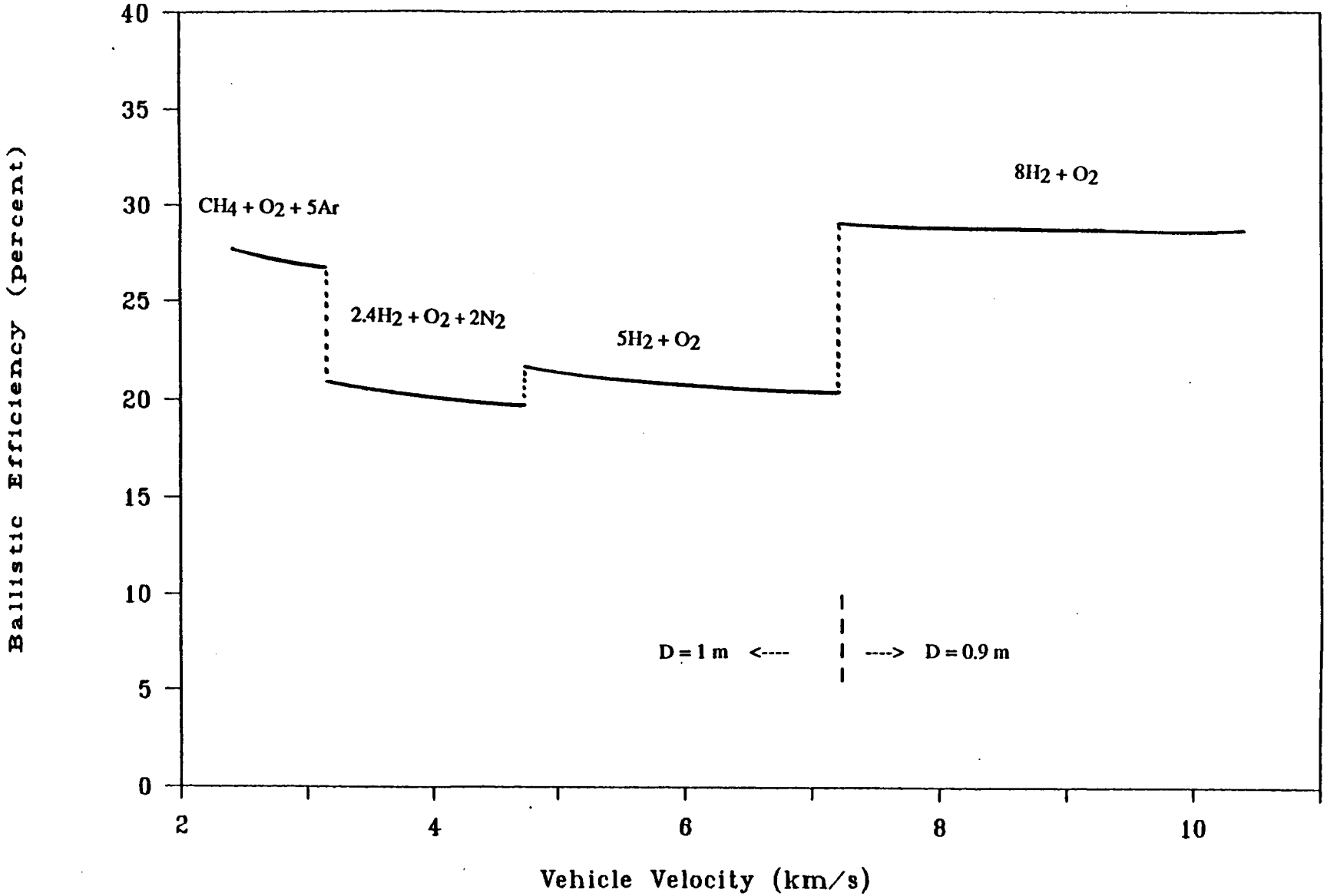

Fig. III-18: Ballistic efficiency profile for the oblique detonation mode. Values are for a 2000 kg, 0.76 m O.D. vehicle, and 33 atm propellant fill pressure. D is the launch tube diameter. Efficiency jumps indicate mixture transitions.

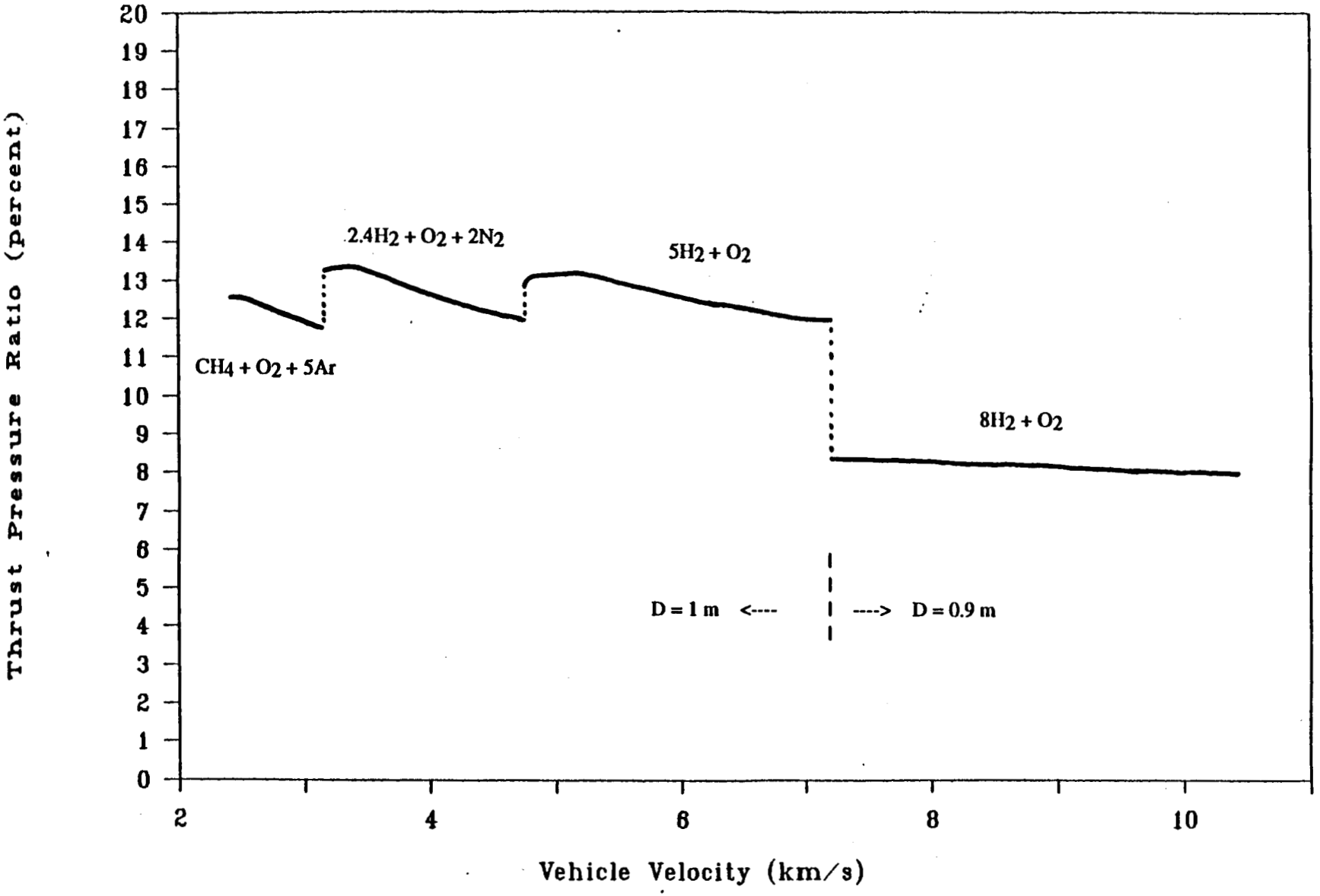

Fig. III-19: Thrust pressure ratio (TPR) profile for the for the oblique detonation mode. TPR values are for a 2000 kg, 0.76 m O.D. vehicle, and 33 atm propellant fill pressure. D is the launch tube diameter. TPR jumps indicate mixture transitions.

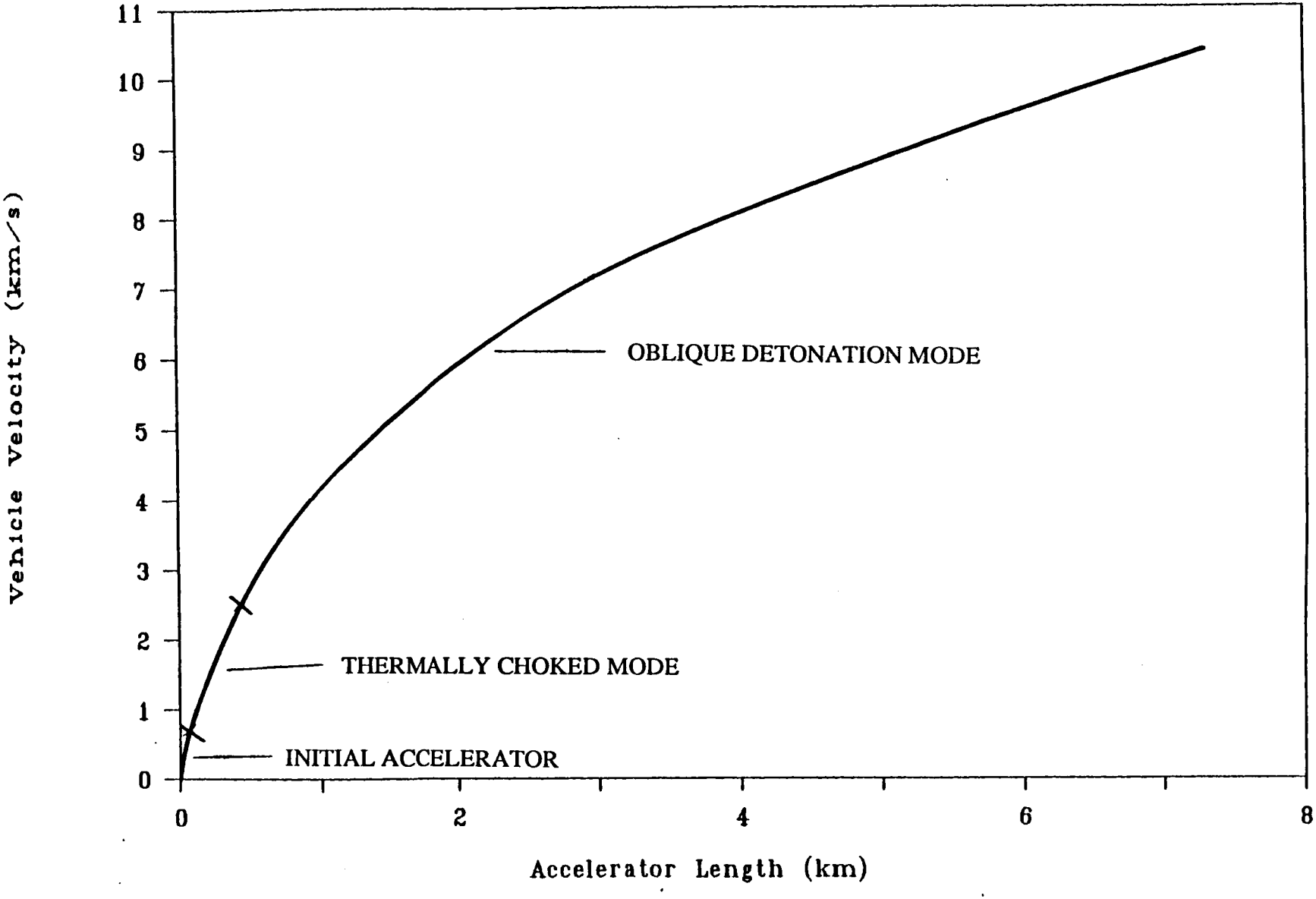

Fig. III-20: Velocity profile for the ram accelerator direct launch concept. Velocities are for a 2000 kg, 0.76 m O.D. vehicle, and 33 atm propellant fill pressure.

IV. ATMOSPHERIC TRANSIT

Erik Christofferson
Bret Neely
Fred Swanstrom

INTRODUCTION

The purpose of the atmospheric transit study is to determine the change in velocity and the thermal protection requirements, and to examine the dynamic stability of the vehicle from the exit of the ram accelerator tube at 4 km to an altitude of 40 km, at launch angles ranging from 16° to 30°. As elevated a launch altitude as possible is desired in order to reduce the atmospheric heating and drag, and thus minimize mass and velocity loss. An altitude of 4 km is considered to be the most feasible altitude for launch (see Appendix A). An altitude of 40 km is assumed to be the edge of the sensible atmosphere due to the low density, the onset of slip flow, and the fact that aerodynamic heating becomes negligible. The 16° to 30° launch angle constraint is the consequence of parameters specified by orbital mechanics. Beyond 40 km, an orbital mechanics approach can be used to follow the progress of the vehicle into low earth orbit, as discussed in chapter V. The cylindrical, non-lifting vehicle has a nose cone half angle of 7°, a diameter of 0.76 m, and an initial mass of 2000 kg (Fig IV-1).

Upon exit from the launch tube, the vehicle will be traveling at 8 - 10 km/sec which results in a Mach number range of 25 - 31. These hypersonic velocities will subject the vehicle to severe aerodynamic heating and forces which will require adequate thermal protection and stability augmentation for a controlled ascent. Convective heating dominates the heat input to the nose cone, and radiative heating, even at the high velocities considered, can be shown to be negligible in comparison to the convective heating.[1] Due to convective heating alone, the nose of the vehicle will experience severe stagnation temperatures that are on the order of 9,000 - 14,000 K, even after considering equilibrium dissociation of the air across the bow shock wave and in the boundary layer.

There are a number of possible approaches to the thermal protection problem. One possibility is transpiration cooling. This method, which involves injecting a coolant through a porous nose cone to keep the nose at a relatively low constant temperature, was previously examined.[2,3] Although this cooling method would theoretically render the vehicle unharmed by the atmospheric heating, leaving it re-usable, transpiration hardware is heavy, complicated and expensive.

Another method for thermal protection is to employ an ablative nose cone. Ablation has been defined as a "self regulating heat and mass transfer process in which incident thermal energy is expended by sacrificial loss of material"[4]. If an ablative nose cone with low thermal conductivity is used, a large amount of heat can be absorbed through the chemical charring and sublimation of the ablator; The heat absorbed will not reach the virgin material below the charred layer of the ablator, thus in effect ablation leaves the payload portion of the vehicle unharmed. Even though ablation blunts the shape of the nose cone and destroys the re-usability of the front portion of the vehicle, it will be cheaper to use ablation, in the long run, due to the manufacturing complications and decreased allowable payload associated with transpiration cooling hardware [3]. Preliminary studies have indicated that the mass loss due to ablation is not substantial [5], and thus the weight of the thermal protection system is low, which allows for a large payload fraction. The focus of this study is on employing ablative cooling, using a replaceable ablative nose cone, to provide the needed thermal protection.

The ablative material chosen for the nose cone is carbon-carbon composite. Carbon-carbon represents a composite fiber reinforced with internal carbon deposits as a binder. This material approximates the ablative performance of homogeneous graphite while retaining a much higher thermal shock resistance [4]. It is relatively durable and readily available.

The use of an ablative nose cone directly affects the total change in velocity during atmospheric transit. Ablation results in variation of body shape during ascent. The drag of

the vehicle, being primarily pressure drag, is affected almost exclusively by body shape. The blunting nose cone shape increases the drag, thereby increasing the velocity loss. An accurate investigation of the changing C_D and the simultaneous mass loss must therefore be conducted in order to determine the velocity loss of the vehicle.

Vehicle instability is investigated by using small perturbation theory. The effect of changing atmospheric density on the magnitude of instability is also of primary concern. The need for stability augmentation schemes, such as control surfaces, to provide the needed stability is discused.

Since propulsive requirements require that the nose cone shape remain unchanged while in the launch tube, a first order examination of heating in the tube is performed. The in-tube heat transfer to the nose is calculated using an analysis similar to the method utilized for the heating due to the atmosphere.

This paper addresses the problem of heat transfer on the body to find the ablative mass loss required to protect the integrity of the vehicle. The heat transfer to the vehicle is analyzed in two regimes, non-stagnation and stagnation regions. From the heat transfer analysis the mass loss of the ablator is established, and consequently the change in body shape is determined. This blunting of the vehicle's nose increases the drag coefficient and reduces the velocity the vehicle will retain during atmospheric transit.

ANALYSIS OF HEAT TRANSFER

Heat Transfer on the Non-Stagnation Region of the Body

The relation that governs the convective heat transfer from the air to the surface of a body in hypersonic flow is [5]

$$dH/dt = h_l \cdot (T_R - T_W) \tag{1}$$

where dH/dt is the heat transferred per unit area per unit time, h_l is the local convective heat transfer coefficient, T_R is the recovery temperature, and T_w is the wall temperature. The heat transfer coefficient h_l can be found by using a modified Reynolds analogy[5]

$$h_l = \frac{C_f \cdot \rho_l \cdot V_l \cdot C_{pl} \cdot \Gamma \cdot Pr^{2/3}}{2} \tag{2}$$

where C_f is the local skin friction coefficient, ρ_l is the local gas density, V_l is the local velocity, C_{Pl} is the local specific heat, and Γ is the blowing factor given by [3]

$$\Gamma = \frac{1}{1 + (k \cdot V^2/\zeta)} \tag{3}$$

In Eq. 3, ζ is the heat of vaporization of carbon-carbon (2.28×10^7 J/kg) [4], and k is a constant that depends on the flow conditions at the body surface. Due to the large Reynolds numbers, turbulent flow is assumed for which $k \approx 0.1$.[3] In Eq. (2), the local skin friction coefficient is assumed to be 0.00056. This value of C_f has been determined from previous work on the ram accelerator vehicle.[3] The local conditions needed to find the heat transfer coefficient, and ultimately the convective heat transfer, are obtained by examining the effects of the oblique shock wave on the flow. The focus of this study is on determining the effects of dissociation through the shock on the flow conditions which comprise the heat transfer coefficient.

To calculate the local conditions, a CFD normal shock code, which includes the effects of dissociation, is utilized in order to obtain accurate post-shock static temperatures, velocities, densities and molar fractions of the gas.[6] The code is run using free stream conditions taken from the standard atmospheric tables[7] at altitudes varying from 4 km to 40 km. It is also assumed that dissociation reaches equilibrium between the

shock and the vehicle body. In the normal bow shock (stagnation region) dissociation equilibrium will occur within the thickness of the shock at the lower altitudes where most of the ablation occurs.[8] Conversely, through the oblique shock dissociation is not very significant, however, dissociation will occur within the boundary layer along the nose cone sidewalls (non-stagnation region). Figure IV-2 shows the stagnation and non-stagnation regions of the nose cone and the associated shock structure. The dissociation is caused by the exchange of kinetic to thermal energy as the flow stagnates within the boundary layer, reaching a no slip condition at the sidewall surface. The effect of dissociation is to lower the static temperature rise of the gas across the shock by approximately 75%.

The total temperatures were calculated from the conservation of post-shock energy defined by

$$C_p \cdot T_t = C_p \cdot T + \frac{(u^2 + v^2)}{2} - h_D \tag{4}$$

where T and T_t are the static and total post-shock temperatures, C_p is the specific heat of air after dissociation, and u and v are the normal and tangential components of post shock velocities, respectively. h_D is defined as[9]

$$h_D = \sum (h^o \cdot C_a)_i \tag{5}$$

where h^o is the heat of formation of the ith species of the dissociated air and C_a is the concentration of atoms of the ith species defined by[9]

$$C_a = \frac{n}{(n+2m)} \tag{6}$$

where m is the mole fraction of diatomic gas, n is the mole fraction of monatomic gas.

The recovery temperature at the surface of the nose cone is calculated using[1]

$$T_R = R_f(T_t - T) + T \tag{7}$$

where T_t and T are the post-shock total and static temperatures previously calculated, and R_f is the recovery factor[5]

$$R_f = Pr^{1/3} \tag{8}$$

and Pr is the Prandtl number. The Prandtl numbers for dissociated air range from 0.5 to 5.8 and are a strong function of temperature and how much dissociation has occurred.[10] The high total temperatures and Mach numbers encountered in this study resulted in Prandtl numbers which varied only between 0.55 and 1. Thus for a conservative ablation calculation, a constant Prandtl number of 0.7 is used.

Recall that the heat input per unit area per unit time dH/dt on the nose cone is found with Eq. (1). The wall temperature, T_W, is taken to be constant at the value of the sublimation temperature of the carbon-carbon composite (3850 K). Subsequently, h_l can be calculated using Eq. (2) and the local conditions already described.

Heat Transfer at the Stagnation Region

At the stagnation region of the vehicle, the bow shock wave is detached and normal to the flow (Fig. IV-2). The normal shock wave in this region converts the high speed flow to a low speed (subsonic) high temperature flow; thus the heat transfer at this point may be treated as for a hemisphere in a low speed flow field.[1] The heat transfer rate per unit area at the stagnation region, dH_S/dt is thus governed by the relation[5]

$$\frac{dH_S}{dt} = - \frac{Nu_r \cdot k_r \cdot (T_W - T_R)}{\sigma} \qquad (9)$$

where σ is the nose radius, k_r is the thermal conductivity of the gas at the recovery temperature, and Nu_r is the Nusselt number of the flow.[9] To determine this value, the wall and recovery temperature discussed earlier can be used, and only a Nusselt number and a thermal conductivity need to be found. Because the Reynolds number referenced at the nose radius is fairly large (on the order of 10^7), and the surface roughness of the carbon-carbon material under ablation is significant, the flow is assumed to be fully turbulent. As mentioned earlier, the boundary layer is comprised of mainly dissociated air, and Nu_r for a turbulent dissociating boundary layer can be found from[9]

$$Nu_r = .029 \cdot (Re_r)^{.8} \cdot (1 + (Le^{\beta} - 1) \cdot (h_D/h_s) \cdot Pr^{1/3} \qquad (10)$$

where the Lewis number, Le, and the parameter β for a dissociating gas in equilibrium are typically 1.4, and .52 respectively,[9] and h_D is defined by Eq. (5). The stagnation enthalpy h_s, from hypersonic similarity, can be assumed to be[9]

$$h_s = \frac{V_o^2}{2} \tag{11}$$

where V_o is the freestream velocity of the vehicle. The thermal conductivity was found by looking up its value at the recovery temperature of the gas.[10]

For the hemispherical nose considered, any position on the stagnation region of the nose can be identified by the body angle x/r, where x is the longitudinal position measured from datum to the nose tip, and r is the radius of the hemispherical portion of the nose (Fig. IV-4)[9]. The datum position is shown in Fig. IV-4, and is located at the center of the hemispherical nose. The position determined by x/r is simply the cosine of the angle between the center-line of the nose cone and the point under investigation, and can be given in degrees. The x/r position is used only to determine position on the hemispherical portion of the nose. In general, the heat transfer rate, dH/dt, at any x/r position on the hemisphere will decrease from the stagnation value, dH_S/dt, where x/r = 1 at the tip, to the non-stagnation value, dH/dt, where x/r = 0.

To find dH/dt at every x/r position would increase the complexity of analysis beyond the scope of this study, and thus a simplifying assumption is required. Studies done by Schreier have determined a relation between $\dot{H}/\dot{H}_S$ and the body angle, x/r.[9] Using these relations and the range of x/r for the hemispherical portion of the nose, an average value of $\dot{H}/\dot{H}_S$ can be calculated, thereby allowing the total heat transfer to the hemispherical portion of the nose to be represented by some fraction of the stagnation heat transfer rate. For this study, $\dot{H}/\dot{H}_S$ was calculated from Schreier's results to be approximately 0.65. The heat transfer rate to the entire hemispherical portion of the nose is then calculated by multiplying the result for stagnation point heat transfer (Eq. (9)) by 0.65, and this "average" heat transfer rate is applyed to determine the resulting ablative mass loss.

COMPUTATIONAL PROCEDURE

The transit of the vehicle through the atmosphere is broken down into a series of small increments of altitude (Fig IV-3). The mass and velocity loss of the vehicle is determined at the beginning of each altitude increment, and due to the small size of each increment, variable parameters such as the mass of the vehicle, C_D, V_o, and local flow conditions can be assumed constant as the vehicle transits through each increment. The altitude increment used in this study is 100 m. The transit is started at 4 km and continues to 40 km where an orbital mechanics approach can be used. 40 km is the altitude where mass loss and drag induced velocity loss become negligible. For each altitude increment mass loss and velocity loss can be calculated, and thus by summing up the mass and velocity loss for each increment a total result can be obtained. A computer program is utilized to carry out the computations.

Shape Change and Mass Loss Due to Ablation

The shape change of the body is dependent on the heat transfer rate at the body surface, which is different for the stagnation and non-stagnation regions (Fig. IV-2). Therefore, the shape change of the nose cone can be found using the heat transfer rate at the stagnation region, Eq. (9), and the non-stagnation regions, Eq. (1). The heat transfer rate at every point on the nose cone in actuality is different, and ideally a finite element analysis of the heat transfer over the nose cone would be desired. Nonetheless, a finite element analysis of the ablation process is beyond the scope of this study, and a simplifying assumption is required. The simplifying assumption made for this study is that the ablation of the nose cone is axisymmetric with a hemispherical nose tip of uniform radius (Fig. IV-4). The assumption of an axisymmetric model for mass loss can be shown to be a valid assumption for two reasons. First, using previously discussed theory it can be shown that the heat transfer on the side walls of the nose cone is not high enough to cause significant ablation (a recession of only 0.5 cm occurs at a 9 km/s, 20° launch), and thus

the angle of the nose cone remains essentially constant during ablation. Second, studies done for reentry vehicles undergoing ablation have found that the vehicle retains its basic shape and only encounters increasing bluntness.[1] Using the assumption of an axisymmetric model, a method can be derived to obtain the length of recession of the nose cone tip from the mass loss, and ultimately a new nose cone radius. Figure IV-4 shows the recession model used in this study.

The ablative heat shield vaporizes during the aerodynamic heating with an incremental mass loss given by

$$dm_l = \frac{dH \cdot S}{\zeta} \tag{12}$$

where dm_l is the incremental mass loss, dH is the incremental heat input, ζ is the heat of vaporization per unit mass of the ablator, and S is the surface area of the stagnation region of the nose cone. For the model utilized, a new radius r_2 can be found for each time increment dt from the mass loss dm_l and the radius before mass loss r_1:

$$r_2 = \left[\frac{r_1^3 + dm_l \cdot (.1448)}{\rho_{c\text{-}c}}\right]^{1/3} \tag{13}$$

where $\rho_{c\text{-}c}$ is the density of the carbon-carbon ablator.

Each incremental mass loss yields a new radius and ultimately a new body shape. This process is then repeated through the entire transit for each increment of altitude and results in a total ablated mass loss and a final body shape.

Drag Coefficient Calculation

Once the new vehicle shape after incremental ablation is calculated, a new drag coefficient must be found in order to enable a velocity loss for the increment to be calculated. This can be achieved by using a tangent cone method[11] as shown in Fig. IV-5. Given the new nose cone radius, a numerical expression for the curve describing the new nose shape is found. Looking at x as a longitudinal location, (using the nose tip as datum), and y as the cone radius at position x, the cone geometry is described by y as a

function of x. Thus a three-dimensional cone body can be described with a two-dimensional Eq. due to its symmetry. This function is then differentiated to find dy/dx which represents the local angle of attack, α at each longitudinal position x. The drag of the body acts through the longitudinal axis; thus, if the vehicle's longitudinal axis is parallel to the free stream, i.e. the vehicle body is at a zero incidence angle, the α at all radial points at a specified longitudinal location can be viewed as equal when examining the drag (Fig. IV-5). In other words, the elemental surface highlighted in Fig. IV-5, will be at the same angle of attack at every radial position. The coefficient of pressure, C_P, is found using the α defined at these elemental surface areas. This is achieved for a 3-D axisymmetric body at zero angle of attack to the free stream if $\alpha < 57.6^\circ$[12]. It is known that with an axisymmetric body the maximum allowable α is 57.6° for $\gamma = 1.4$. Greater angles will result in a detached bow shock[13], thereby making the above analysis invalid at these high angles. This problem is resolved by using modified newtonian flow theory to find the C_P at α's greater than 57.6° where C_p is defined by[11]

$$C_P = 1.89 \cdot (\sin^2(\alpha)) \tag{14}$$

By using both the tangent cone approximation and modified newtonian flow, a good approximation for the pressure drag coefficient, which is the dominant component of the total C_D, can be found. With this geometry the C_D due to pressure drag only (the drag due to skin friction will be addressed shortly) at any longitudinal station can be found using[11]

$$C_D = C_P \cdot (\sin(\alpha)) \tag{15}$$

The nose cone finite radius will result in a variation of α from 90° to 7°. The nose cone radius gives a surface perpendicular to the flow at the very tip of the cone. Conversely at the point where the hemispherical tip becomes tangent with the 7° cone, α is 7°. Thus, one can appropriately weight each area's respective C_D using the following expression[11]

$$C_D = \frac{C_P \cdot dS \cdot \sin(\alpha)}{dA} \tag{16}$$

where dS is the elemental surface area and dA is the elemental cross sectional area of the nose cone. By integrating the C_D's over the entire length of the cone a total C_D over the body can be obtained. This weighting method is known as the tangent cone approximation[11].

With the vehicle geometry used, the skin friction drag component also needed to be addressed. Using a skin friction coefficient of 0.00056,[3] the C_D due to skin friction is given by

$$C_{Df} = \frac{C_f \cdot S}{A} \tag{17}$$

where S is the surface area of the cylindrical portion of the vehicle. This C_f approximates the flow conditions on the cylindrical portion of the vehicle, as determined by a previous study on the ram accelerator[3]. The weighting of the C_{Df} uses only the surface area of the cylindrical main body and not the nose cone surface area. The skin friction drag on the nose cone is negligible compared to the pressure drag, and thus only pressure drag is considered on the nose cone. The C_{Df} is normalized by the frontal area, as is the coefficient of drag due to pressure, to allow summation with the pressure coefficient of drag. By combining the appropriately weighted pressure and skin friction drag coefficients the total C_D is given as

$$C_D = \sum \frac{C_p \cdot S \cdot \sin(\alpha)}{A} + \frac{C_f \cdot S}{A} \tag{18}$$

The drag calculation process is repeated for the next increment in altitude by modifying the body using the change in mass that was calculated. The new vehicle shape is then redefined for the next altitude increment and so on. During each incremental altitude, the C_D is assumed to be constant.

Velocity Loss Calculation

Using the drag coefficient and vehicle's mass calculated for the increment, a velocity loss for the increment is obtained. The deceleration during each increment of altitude traveled is assumed to be constant, which again is a good assumption for the small increments used. The deceleration is given by

$$a = - \frac{C_D \cdot V_o^2 \cdot \rho_o \cdot A}{2 \cdot m} \tag{19}$$

With this deceleration, the velocity loss can be found from

$$V_e = V_i + a \cdot dt \tag{20}$$

This process is then repeated for each altitude increment.

RESULTS FOR MASS AND VELOCITY LOSS

Using the previously discussed theory for non-stagnation heat transfer, it can be shown that the heat transfer on the side walls of the nose cone is not high enough to cause significant ablation. The non-stagnation heat transfer yields a total mass loss of only 7 kg at a 9 km/s, 20° launch, and did not change appreciably with variations in launch angle. The mass loss on the sidewalls, upon initial investigation, does not appear to be negligible; however, this total mass loss corresponds to only a 0.5 cm recession over the total transit. This small recession is what is considered negligible when compared to the nose tip recession occurring in the stagnation region. The small recession does not appreciably alter the nose cone shape during transit, and thus does little to change the drag coefficient. The primary location where heat transfer is a significant changing factor is at the stagnation region of the cone, and thus only heat transfer in the stagnation region is considered further.

The vehicle design considered for all computations consists of a 2000 kg, 0.76m diameter, 7.5 m long vehicle, with a 7° nose cone half angle. The initial conditions for the launch are velocities of 8000, 9000 and 10,000 km/s at an altitude of 4000 m which were

specified as initial design conditions for this study. The transit phenomena are investigated at the various launch velocities for launch angles ranging from 16° to 30° in order to provide a parametric study for the orbital mechanics calculations. The initial coefficient of drag is found to be 0.058.

From the orbital mechanics study on the ram accelerator vehicle, optimal launch angles were determined for the three initial launch velocities considered. The optimization parameters used in this study are discussed in Chapter V, and will not be discussed here. At 8 km/s a launch angle of 22° is optimal, at 9 km/s 20° is optimal, and at 10 km/s 18° is optimal. The results for these optimal launch angles are tabulated in Table IV-1 for convenience.

Table IV-1. Results for optimal launch angles

Launch angle	Initial velocity	Mass loss	Final C_D	Final velocity
22°	8,000 m/s	22 kg	0.123	6899 m/s
20°	9,000 m/s	25 kg	0.111	7623 m/s
18°	10,000 m/s	29 kg	0.115	8276 m/s

At these optimal launch angles, the ablator mass needed for thermal protection is small, and thus the integrity of the vehicle is maintained.

To investigate the effects of atmospheric transit, plots relating to mass and velocity loss are shown versus altitude for the various launch angles considered in this study. The general conclusions derived from these plots are similar for the three initial launch velocities considered. For this reason, the plots are shown only for the 9000 m/s initial launch velocity at specific launch angles. Results for the three initial launch velocities at all the investigated launch angles can be found in Table IV-2.

Table IV-2. Final transit conditions at 40 km
For launch angles from 16° - 30°
At launch velocities of 8,000 m/s, 9,000 m/s, and 10,000 m/s

	8,000 m/s			9,000 m/s			10,000 m/s		
LA	m_l kg	C_D	V m/s	m_l kg	C_D	V m/s	m_l kg	C_D	V m/s
16°	40	.131	6377	38	.128	7191	36	.126	8007
18°	32	.119	6599	30	.118	7437	29	.115	8276
20°	26	.111	6767	25	.111	7623	24	.109	8481
22°	22	.123	6899	21	.104	7770	20	.103	8642
24°	19	.101	7004	19	.099	7887	17	.098	8771
26°	17	.097	7090	16	.095	7983	15	.094	8876
28°	15	.093	7162	14	.092	8063	13	.091	8963
30°	13	.090	7222	13	.089	8129	12	.088	9037

A plot of the rate of mass loss versus altitude is shown in Fig. IV-6. It is seen that the peak rate of mass loss does not occur at the exit of the launch tube where the atmospheric density is greatest, but occurs at somewhat greater altitudes. This phenomenon is a result of the surface area of the stagnation region increasing as the atmospheric density is decreasing. These two factors work against each other to result in a maximum mass loss rate at approximately 10 km. A plot of the integrated mass lost up to a given altitude as a function of that altitude is shown in Fig. IV-7. The integrated mass loss is seen to increase with decreasing launch angle as a result of longer transit time in the lower, denser regions of the atmosphere. The mass loss curve is seen to flatten out above about 30 km, and thus supports the assumption that 40km is the altitude where mass loss rate can be considered negligible. A plot of C_D versus altitude is shown in Fig. IV-8. The curves again follow the same pattern as the integrated mass loss curves. In comparing Fig. IV-7 and Fig. IV-8 can be seen that the variation in C_D is similar to the variation in

mass loss. This phenomenon is due to the direct relation between body shape and the drag coefficient. Thus, as the body shape changes due to ablation, the C_D changes similarly. A plot of V/Vo versus altitude is shown in Fig. IV-9. This figure shows that the change in velocity is very small at altitudes above 40 km., thus again verifying the assumption that atmospheric effects at altitudes above 40 km need not be considered. In a plot of final V/Vo versus launch angle (Fig. IV-10), velocity losses, as expected, are seen to decrease with increasing launch angles. Figure IV-10 is shown for all three initial launch velocities, and all the curves are very similar, showing that the fractional velocity loss is approximately the same for all launch conditions.

Obviously, as the launch angle is increased, the aerodynamic heating is reduced, the ablative losses decrease, the C_D remains smaller, and the final velocity is increased. For the system considered, there are many conflicting design considerations. Lower launch angles achieve a more energy-efficient means of orbital transfer, but in turn result in higher mass and velocity losses. Conversely, keeping the launch angle high to minimize mass and velocity losses results in excessive amounts of on board propellant required to achieve the desired orbit. Strictly examining the atmospheric transit characteristics, the different initial launch velocities do not significantly affect the final conditions; however, chapter V will show that the effect of launch velocity on the orbital mechanics is substantial.

Realizing that there are conflicting design constraints for the complete ram accelerator system makes an optimization of any single aspect impossible. Thus, examining only atmospheric transit characteristics, a maximum launch angle is desired to achieve a minimal mass and velocity loss. The smaller ablative mass loss is desirable in order to reduce the overall structural mass of the vehicle to allow for a larger payload fraction.

STABILITY AND CONTROL

To examine the problem of stability and control, the vehicle geometry and mass distribution must be defined. For the ram accelerator mass launch concept the current vehicle has a length of 7.5 m, diameter of 0.76 m and a nose half angle of 7°. The center of gravity, CG, for such a vehicle is found to be at 5.3 m from the vehicle nose tip. The result was obtained from the structural design of the vehicle (see Chapter VII). The center of pressure, CP, is at 33% of the body length or 2.4 m from the nose tip. Due to the fact that the CP is located in front of the CG the vehicle is inherently unstable. The effects and magnitudes of the instability can be estimated by examining small perturbation effects on a simple dynamic model of the vehicle.

The Eq. of the vehicle's motion is found by summing the moments acting about the CG of the vehicle using,

$$\Sigma M_{CG} = 0 = I \cdot \ddot{\Theta} - x \cdot F \tag{21}$$

where x is the moment arm of the applied force, (Fig. IV-11). The moment of inertia, I, for the vehicle is 6350 kg-m^2. To find the resultant angular acceleration, the magnitude of the applied force must be examined.

For a slender body of revolution the lift coefficient, C_L, and the lift-induced drag coefficient, C_{Di} are approximated as

$$C_L = 2 \cdot i \tag{22}$$

$$C_{Di} = i^2 \tag{23}$$

where i is the incidence angle of the body, (Fig. IV-11).[14] These coefficients are based on the frontal area of the vehicle. The magnitude of the applied force is

$$F = 2 \cdot i \cdot q \cdot A \cdot \cos(i) + i^2 \cdot q \cdot A \cdot \sin^3(i) \tag{24}$$

where q is the dynamic pressure and A is the cross-sectional area of the vehicle. Assuming a small perturbation (such that, $\cos(i) \approx 1$ and $\sin(i) \approx i$), the force can be approximated by

$$F = 2 \cdot i \cdot q \cdot A + i^3 \cdot q \cdot A \tag{25}$$

For small i, the second term on the right is much smaller than the first term and can be neglected.

The dynamic pressure on the vehicle varies by three orders of magnitude from an altitude of 4 km to 40 km, and a 1° incidence angle. Thus, the altitude is the dominant factor in the magnitude of the vehicles' dynamic response to perturbations. At an altitude of 4 km, the angular acceleration is approximately 164 rad/sec^2 , while at 40 km, the angular acceleration is about .16 rad/sec^2.

In order to counter the angular accelerations, an active stability augmentation is necessary. It is suggested that a ring of control surfaces mounted on the vehicle as far aft as possible would provide one possible solution. Assuming control surfaces of 0.1 m^2 area located 6.4 m from nose cone tip, the required moment for zero rotation could be achieved by a 17° deflection of one of these control surfaces.

This stability analysis is at best an order of magnitude study. It is apparent that at the lower altitudes the instability of the vehicle is severe. A more detailed investigation of this problem is clearly required, and possible alternative stability augmentation schemes must be considered.

IN-TUBE HEATING

Propulsive cycles in the launch tube require that the nose cone of the vehicle retain a constant geometry throughout acceleration in the tube. It is necessary to determine whether convective in-tube heating results in significant ablation of the vehicle nose before it exits the launch tube. Such vehicle ablation occurring inside the launch tube would have a deleterious effect of the propulsive cycles.

To examine the problem of in-tube heating, an analysis similar to that used in stagnation region for atmospheric transit is used. Equations 9 - 11 are used to calculate the stagnation region heating and Eqs. 12 and 13 are used to determine the mass loss and increased nose tip radius due to ablation. Several assumptions and simplifications that

facilitate a conservative heating calculation were made. Since forced convective heating increases with Mach number, the analysis was carried out for the final 2.5 km section of where the propellant mixture is $8H_2 + O_2$ and the Mach number range is the highest. The Mach number range varies from 7 to 11 to achieve an exit velocity of 9.0 km/sec, and from 7 to 13 to achieve an exit velocity of 10 km/sec (see chapter III). It is also approximated, as it was with atmospheric transit, that the entire spherical nose tip region experiences 65% of the stagnation heating. As a first order approximation, the CFD normal shock code was used to calculate post shock temperatures for in-tube conditions of 33 atm pressure and a temperature of 300 K, at the highest in-tube Mach number. Recovery temperatures were then calculated with Eqs. 7 and 8 using a Prandtl number of 0.7. The recovery temperature (calculated with the greatest Mach number value) was assumed to remain constant throughout the last section of the accelerator tube. All parameters in the Nusselt number calculation (Eq. 10) were calculated for the in-tube gas mixture also at fill pressure and temperature.

To account for heating that already occurs up to the last mixture, it is conservatively assumed that the nose cone has just reached the sublimation temperature of carbon-carbon, 3850 K, and is taken to be constant thereafter. The thermal conductivity for use in Eq. 9 was approximated for the in-tube gas using the following relationship[10]

$$k = \frac{95 \cdot \sqrt{\pi} \cdot (R \cdot T/MW)^{1/2} \cdot k_o}{64 \cdot N \cdot S_O} \tag{26}$$

where N is Avogadro's number, k_o is a reference thermal conductivity[10] and S_O is the molecular cross sectional collision area. An average Reynolds number is used in Eq. 9 and the total heat input is calculated using the total elapsed time of transit for the last section of tube. After the mass loss is calculated using Eq. 12, the new nose tip radius is found using Eq. 13.

Results from the first order analysis indicate that ablation due to in-tube heating is minimal. Using an initial nose tip radius of 3 cm, the total ablative mass loss for a launch velocity of 9 km/sec and 10 km/sec is 0.23 kg and 1.4 kg, respectively, while the

corresponding new nose tip radius is 3.6 cm and 5.2 cm respectively. When repeating the analysis for a nose tip radius of 5 cm, the ablative mass loss for 9 km/sec and 10 km/sec is 0.55 kg and 3.3 kg with a corresponding new radius of 5.5 cm and 7.2 cm, respectively. In either case it is clear that if an ablative nose cone is utilized for thermal protection during atmospheric transit, no additional thermal protection will be needed to guard against in-tube ablation.

IN-TUBE STABILITY

The vehicle is aerodynamically unstable during its acceleration in the launch tube, for the same reasons that it is inherently unstable during atmospheric transit. Even if the vehicle were stable any oscillations in response to perturbations in the pressure field would be unacceptable. Therfore, in order to keep the projectile centered in the tube and to prevent any rotational oscillations it is proposed to install a set of three equally-spaced rails in the bore of the tube. These rails would touch only very lightly on the vehicle. Additional details are provided in Chapter VII.

CONCLUSION

The investigation of the atmospheric transit phase of the ram accelerator mass launch concept has included a study of an ablative nose cone as a thermal protection system, as well as an examination of the dynamic stability of the vehicle. Velocity lost in transit due to aerodynamic drag is also an important parameter which has been considered in order to determine the orbital characteristics of the vehicle (Chapter III).

In the ablation study, only convective heat transfer was considered, and the nose cone was found to ablate predominantly in the stagnation region. Most of the ablation was found to occur in the lower atmosphere, with a peak mass loss rate encountered at an

altitude of ≈ 10 km. The mass loss due to ablation was found to be negligible above an altitude of 40km.

At an optimum launch angle of approximately 18° for a 10,000 m/s launch, 20° for a 9,000 m/s launch, and 22° for a 8,000 m/s launch the vehicle retained approximately 85% of its initial velocity, and suffers a mass loss of only 22-29 kg to ablation for all initial launch velocities. These results support the assumption that a carbon-carbon ablative nose cone is a viable option for the thermal protection of the vehicle.

The vehicle, as suspected, is highly unstable at low altitudes. At the 4 km launch altitude the angular acceleration of the vehicle was found to be 164 rad/sec^2. At higher altitudes the magnitude of the instability is less with the angular acceleration, approaching 0.16 rad/sec^2 at 40 km. The possible use of stability augmentation systems was briefly discussed, and plausible methods of vehicle stabilization given.

In-tube heating was found to cause minimal mass loss and shape change. For a nose radius of 3 cm at a launch velocity of 9 km/sec, the in-tube mass loss was 0.23 kg and the nose radius increased to 3.6 cm. For a launch velocity of 10 km/sec, the mass loss was 1.4 kg and the nose radius increased to 5.2 cm.

REFERENCES

1. Allen, H.J., "The Aerodynamic Heating of Atmosphere Entry Vehicles - A Review", Fundamental Phenomena in Hypersonic Flow: Proceedings of the International Symposium Sponsored by Cornell Aeronautical Laboratories, Cornell University Press, New York, 1966. pp. 5-14.

2. Ghosh, S., "A Study of Transpiration Cooling for Sharp Conical Bodies in Hypersonic Flow," MSC Thesis, Department of Aeronautics and Astronautics, University of Washington, Seattle WA., May 1988.

3. Hertzberg, A., Bruckner, A.P, eds., "The Ram Accelerator Concept: A Method for Direct Launch of Space Cargo to Orbit," Final Report, NASA/USRA Advanced Space Design Program, University of Washington, Seattle WA., June 1987. pp. 38-52.

4. Roshenow, W.M., Hartnett, J.P., Handbook of Heat Transfer, McGraw Hill Book Company, New York, 1973. sects. 17, 19.

5. Allen, H.J., and Eggers, A.J. Jr., "A Study of the Motion and Aerodynamic Heating of Missiles Entering the Earth's Atmosphere at High Supersonic Speeds", NACA TN 4047, 1957.

6. "CHEMKIN", a computational fluid dynamic code for solution of normal shock waves. Sandia Laboratories, June 1981.

7. Anderson, J.D. Jr., Introduction to Flight, 2nd ed., McGraw Hill Books Company, New York, 1985. pp 507-516

8. Eberhardt, S., Department of Aeronautics and Astronautics, University of Washington, Seattle WA, private communication, February 1988.

9. Schreier, S., Compressible Flow, John Wiley and Sons, New York, 1982. pp 406-455.

10. Hansen, F.C., "Approximation for the Thermodynamic and Transport Properties of High-Temperature Air," NASA Technical Report R-50, 1968.

11. Eberhardt, S. "Tangent wedge approximations in Hypersonic flow", AA400 class notes, University of Washington, Fall, 1987.

12. Taylor, G.I. and Maccoll, J.W., "The Conical Shock Wave Formed by a Cone Moving at High Speed", Proceedings of the Royal Society of London, Cambridge University Press, London, 1937. no. 898 vol 159, pp 459-472.

13. Taylor, G.I. and Maccoll, J.W., "Air Pressure on a Cone Moving at High Speeds", Proceedings of the Royal Society of London, Cambridge University Press, London, 1933. Vol. 139, pp 298-311.

14. Liepmann, H.W., Roshko, A., Elements of Gas Dynamics, John Wiley and Sons Inc., New York, 1957. pp. 305-313, 348-352.

NOMENCLATURE

A	Area
a	Acceleration
C_a	Molar fraction of dissociated gas
C_D	Coefficient of drag
C_{Df}	Drag coefficient due to skin friction
C_f	Coefficient of skin friction
CG	Center of gravity
C_L	Coefficient of lift
CP	Center of pressure
C_P	Coefficient of pressure
C_P	Constant pressure specific heat
F	Force
dH/dt	Rate of heat input
h	Enthalpy
h_l	Local heat transfer coefficient
h^o	Heat of formation
I	Moment of inertia
i	Incidence angle of vehicle to the freestream
k	Thermal conductivity
k_o	Reference thermal conductivity
l	Recession length
Le	Lewis number
m	Mole fraction of diatomic gas
m_l	Mass loss
M	Moment
MW	Molecular weight
m	Mass
n	Mole fraction of monatomic gas
N	Avogadro's number
Nu	Nusselt number
Pr	Prandtl number
q	Dynamic pressure
r	Radius
R	Universal gas constant

C-2

Re	Reynolds number
Rf	Recovery factor
S	Surface area
S_O	Molecular cross section collision area
T	Temperature
T_R	Recovery temperature
t	Time
u	Normal velocity to shock
v	Tangential velocity to shock
V	Velocity
x	Longitudinal body position
y	Altitude
α	Angle of attack
β	Constant dependent of flow conditions dissociated air
Γ	Blowing factor
ρ	Atmospheric density
$\ddot{\Theta}$	Angular acceleration
σ	Nose radius
Σ	Summation
ζ	Heat of vaporization of ablator

Subscripts

a	monatomic
c-c	Carbon-carbon composite
e	Final conditions
i	Initial conditions
l	Local conditions
m	Diatomic
o	Freestream conditions
r	Conditions referenced at the nose radius
s	Stagnation region
w	Conditions at the wall

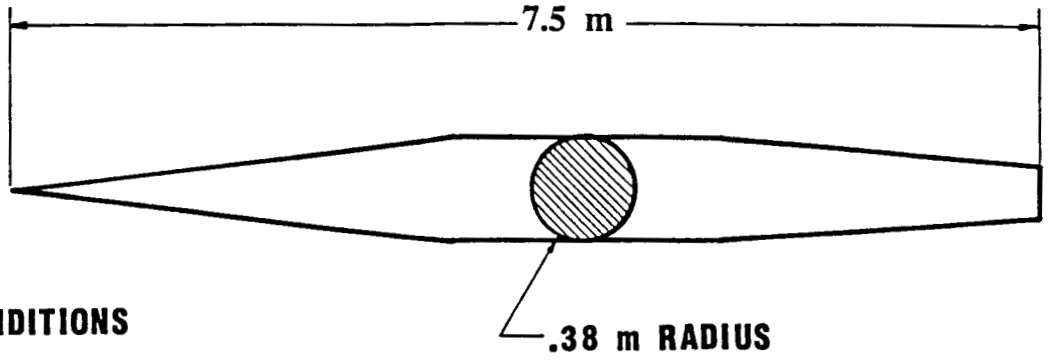

INITIAL CONDITIONS

20°-30° DEGREE LAUNCH ANGLE
4000 m ALTITUDE
9000 m/s
2000 Kg
7 DEGREE NOSE CONE HALF ANGLE

Fig. IV-1 The Ram Accelerator Vehicle

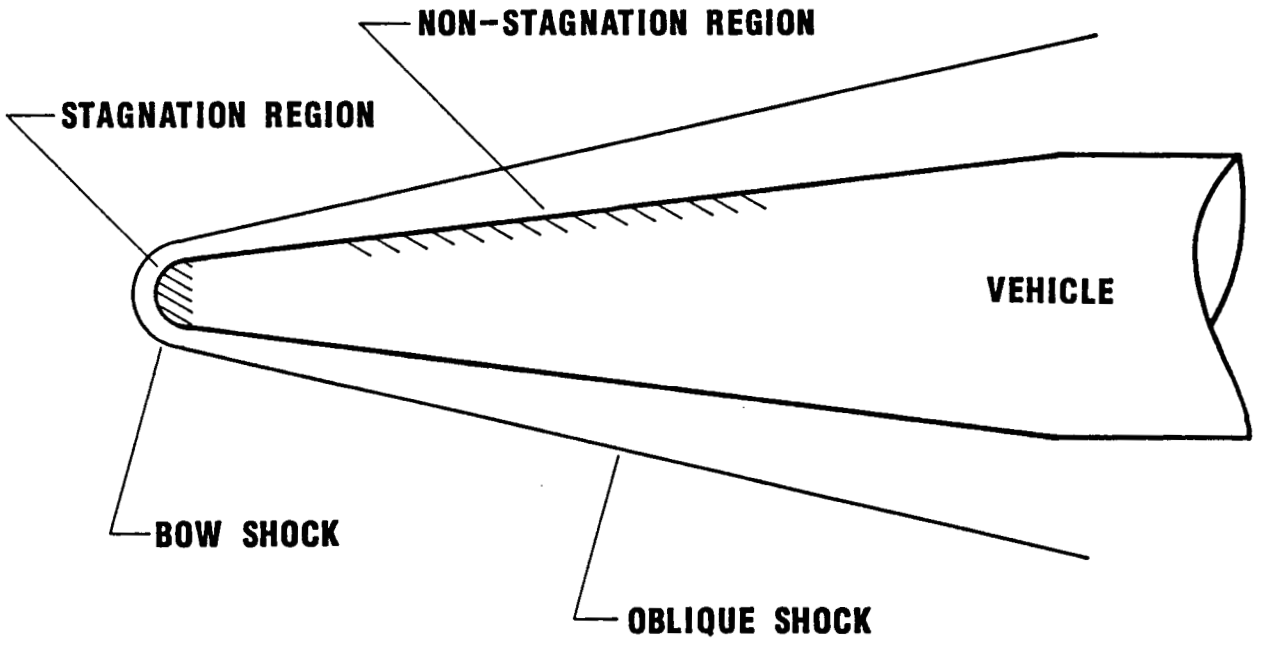

Fig. IV-2 Ablative Regions on the Ram Accelerator Vehicle

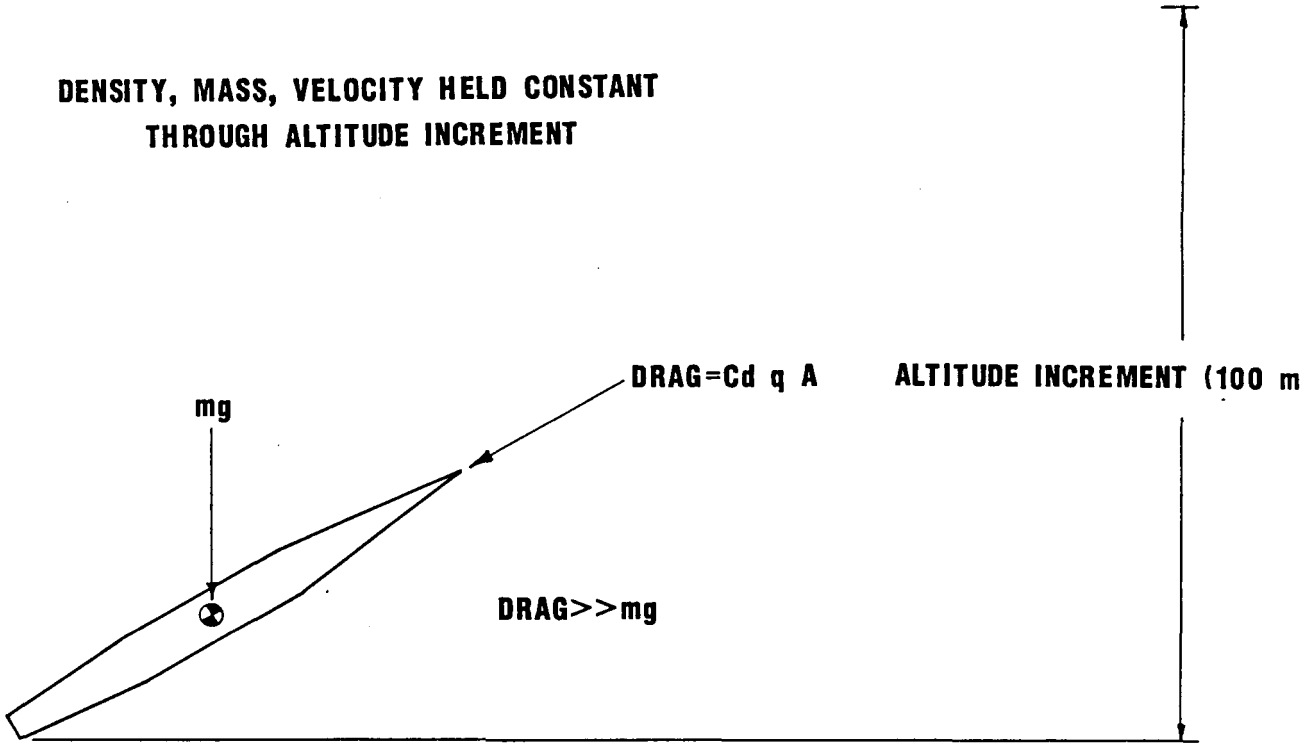

Fig. IV-3 Ram Accelerator Vehicle Traveling Through Altitude Increment

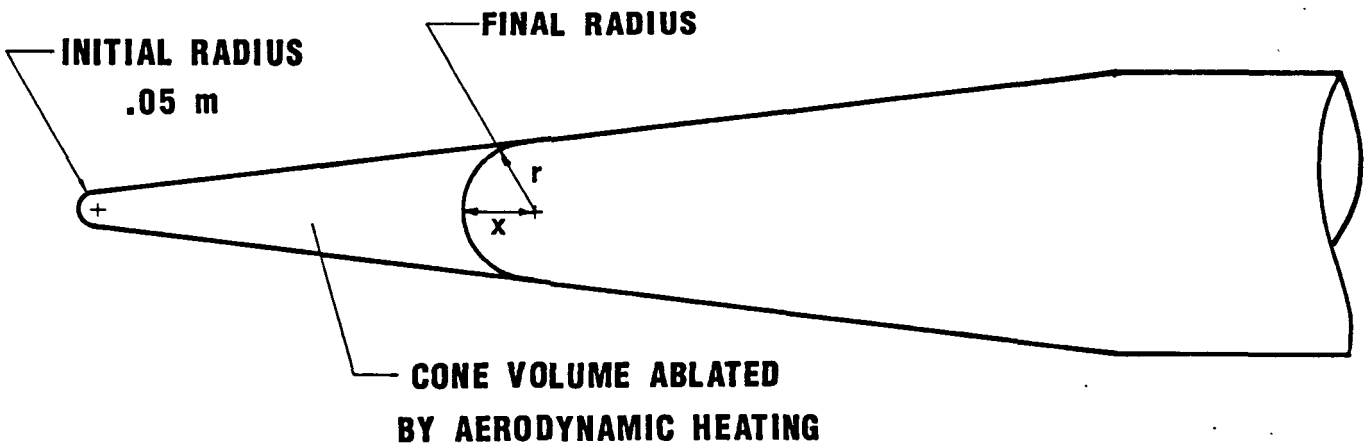

Fig. IV-4 Model for Nosecone Ablation

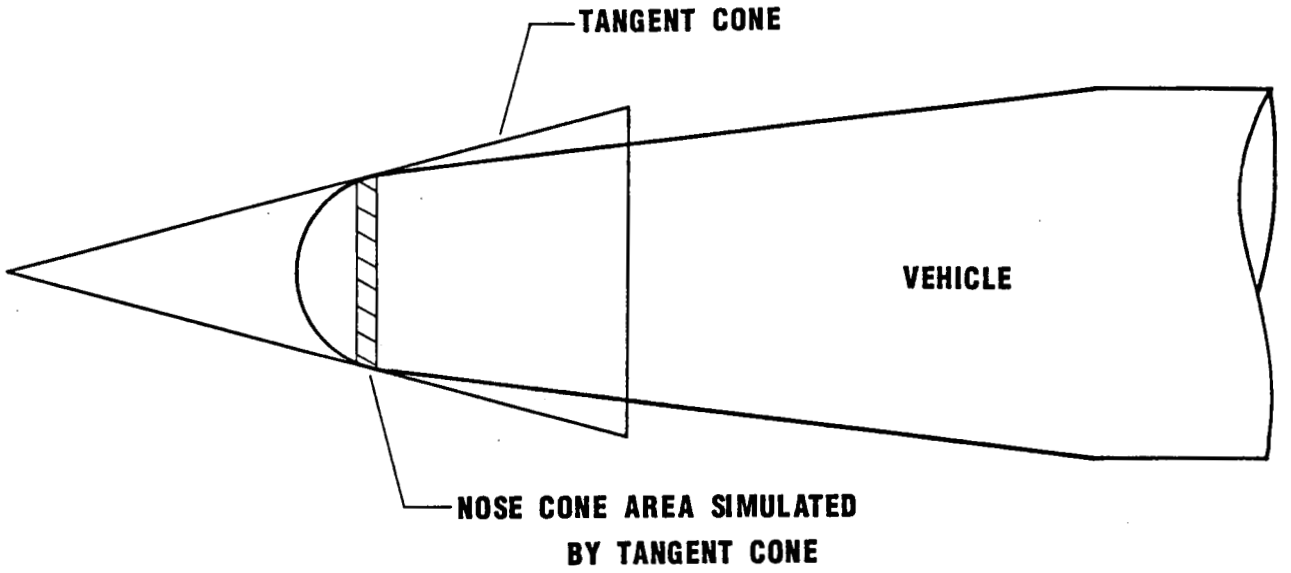

Fig. IV-5 Method of Tangent Cone Approximation

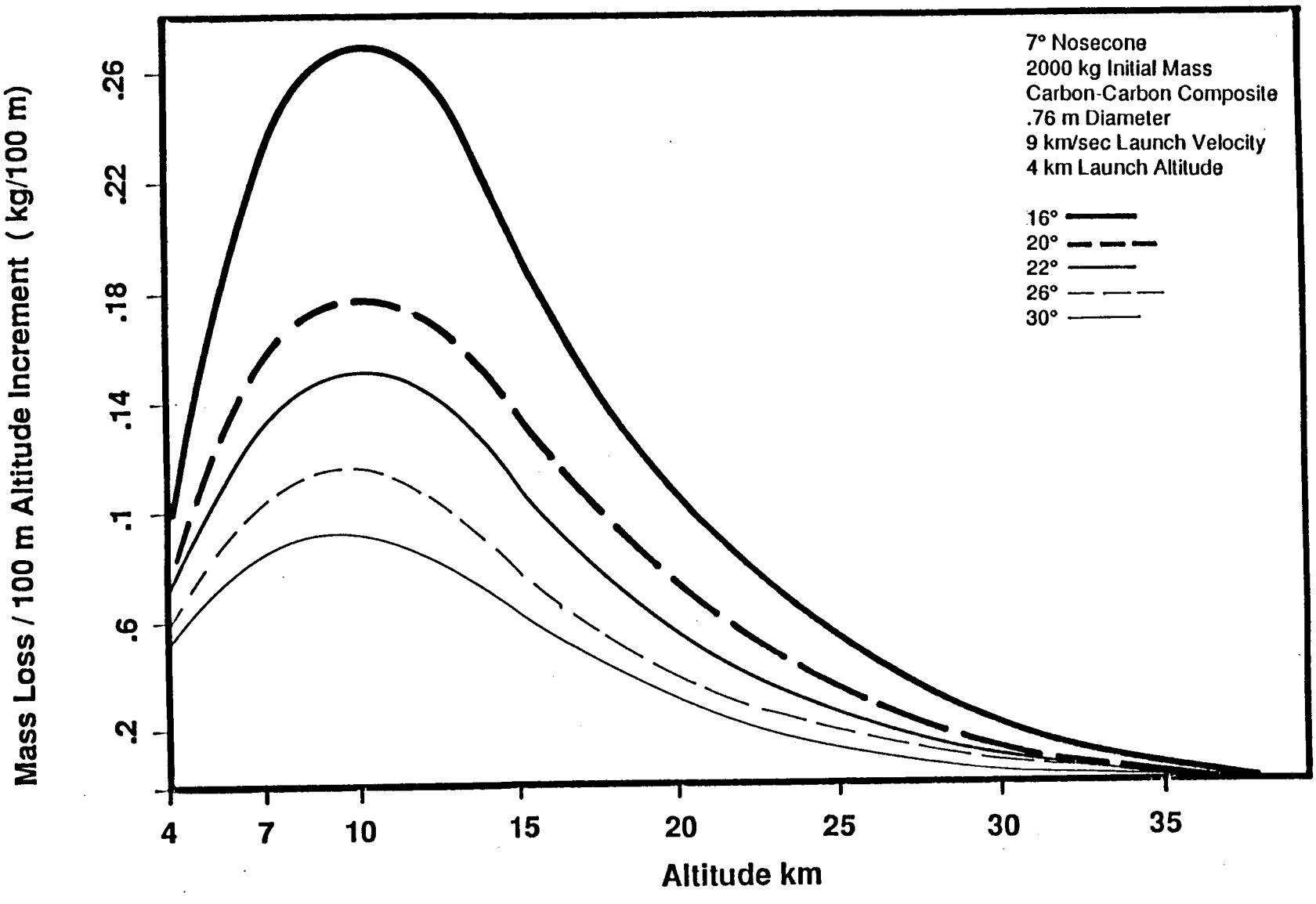

Fig. IV-6 Mass Loss vs. Altitude

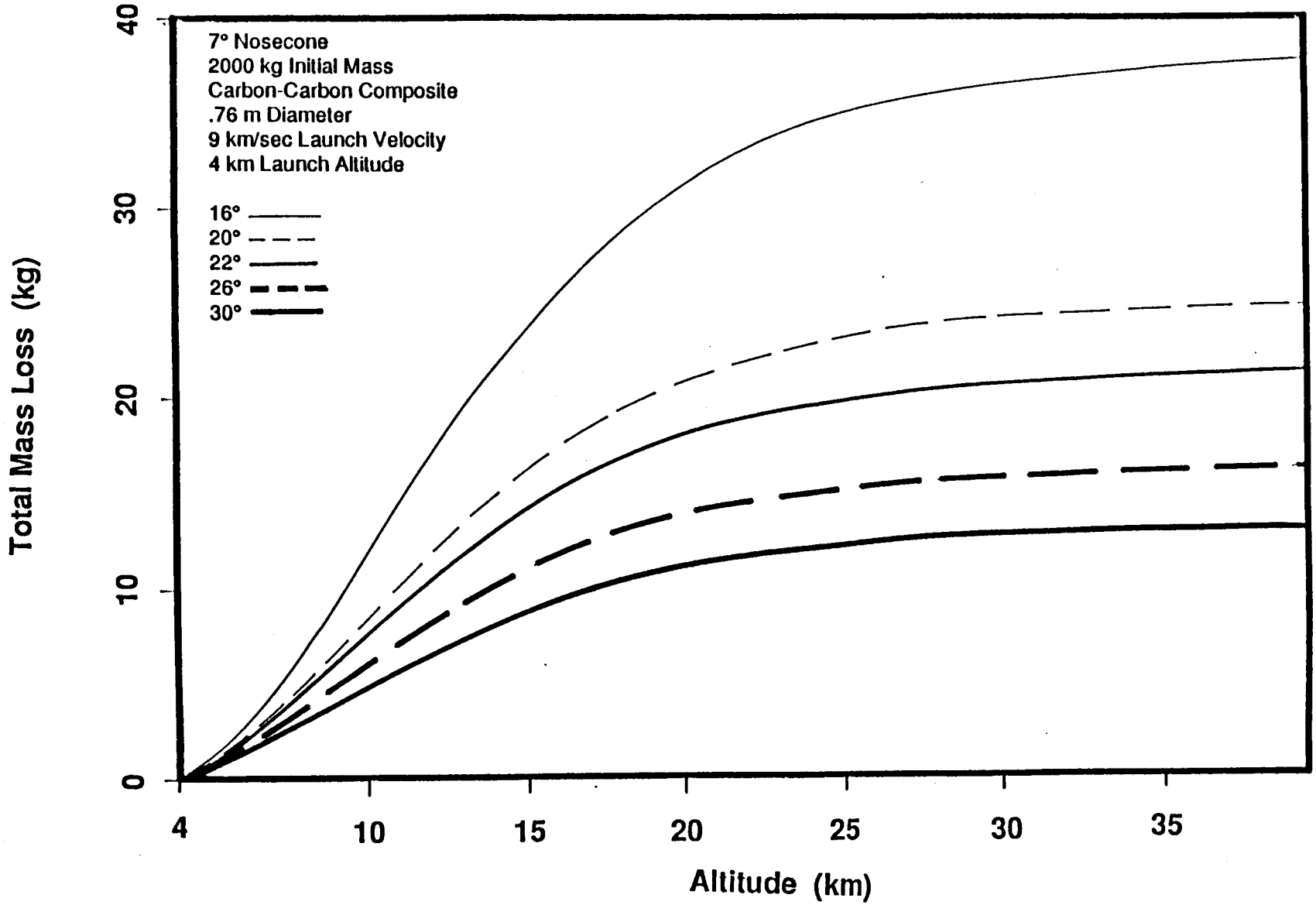

Fig. IV-7 Mass Loss vs Altitude

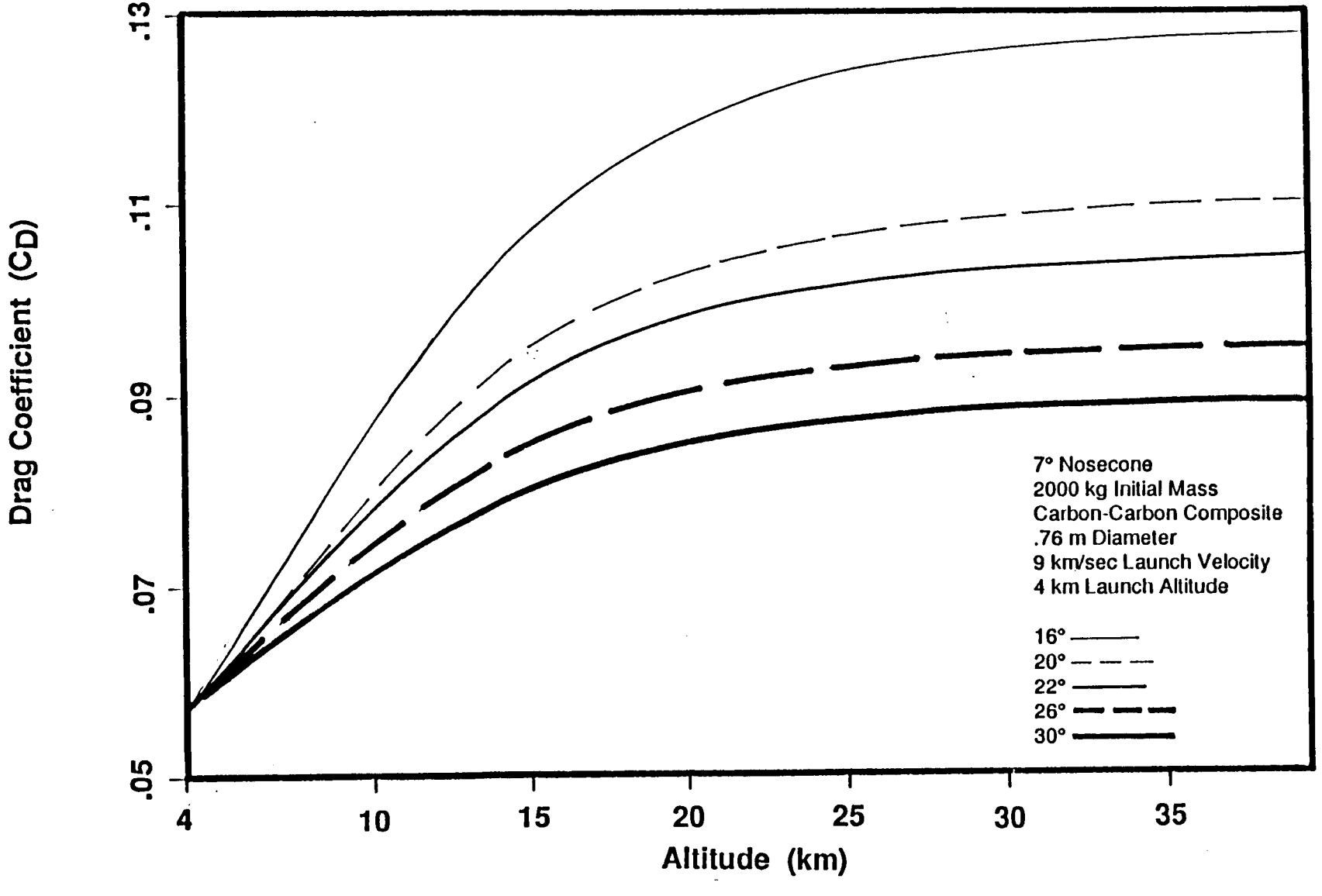

Fig. IV-8 Drag Coefficient vs. Altitude

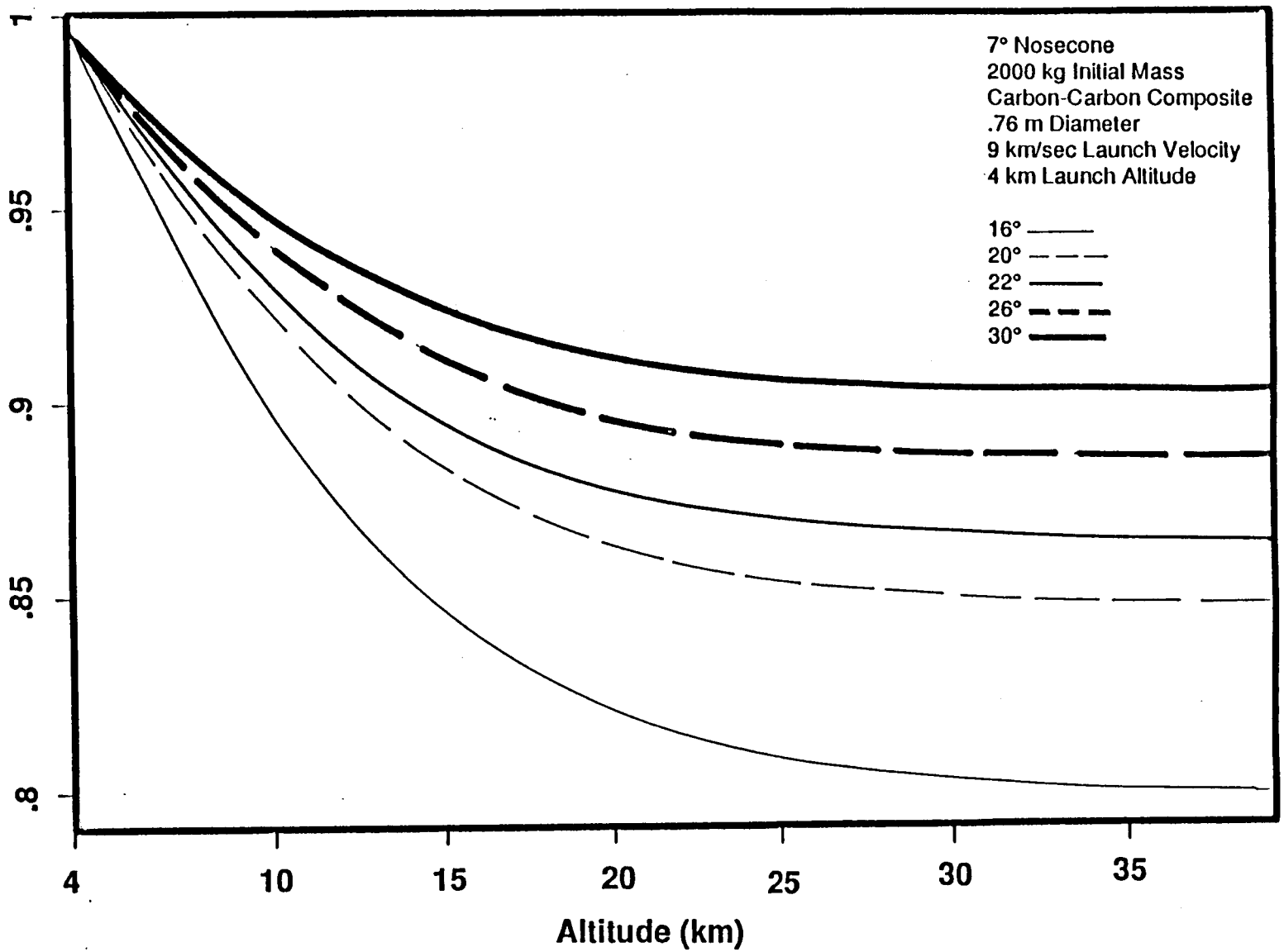

Fig. IV-9 V/Vo vs. Altitude

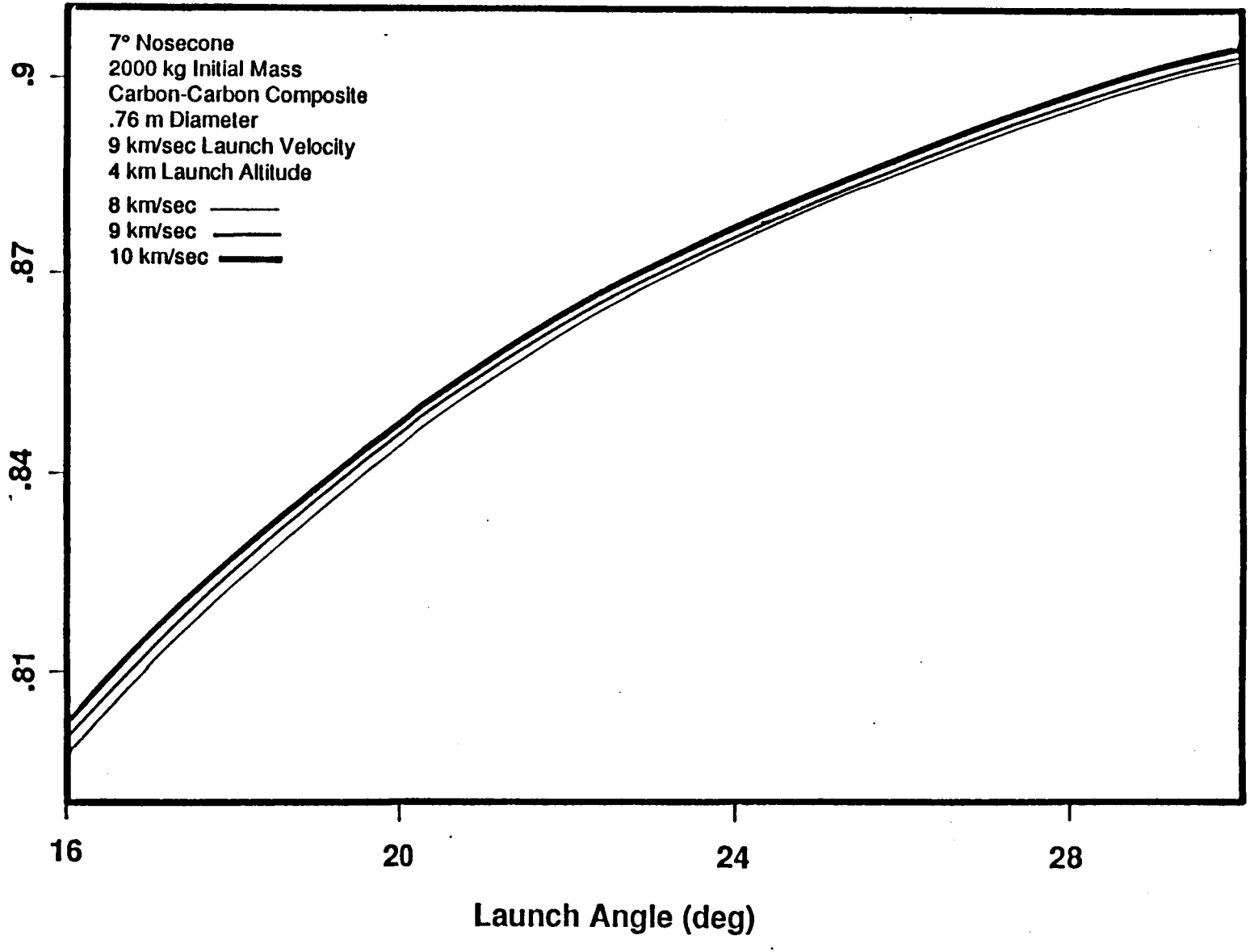

Fig. IV-10 V/Vo vs. Launch Angle

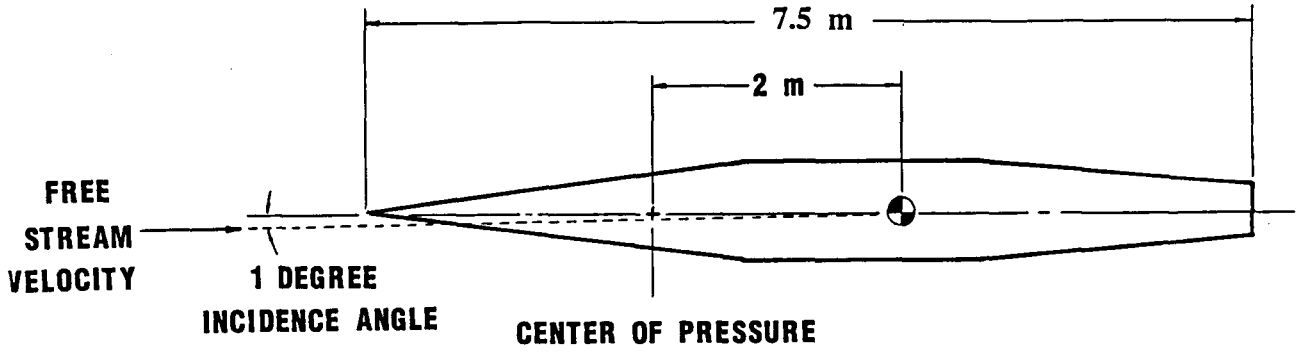

Fig. IV-11 Stability of the Ram Accelerator Vehicle

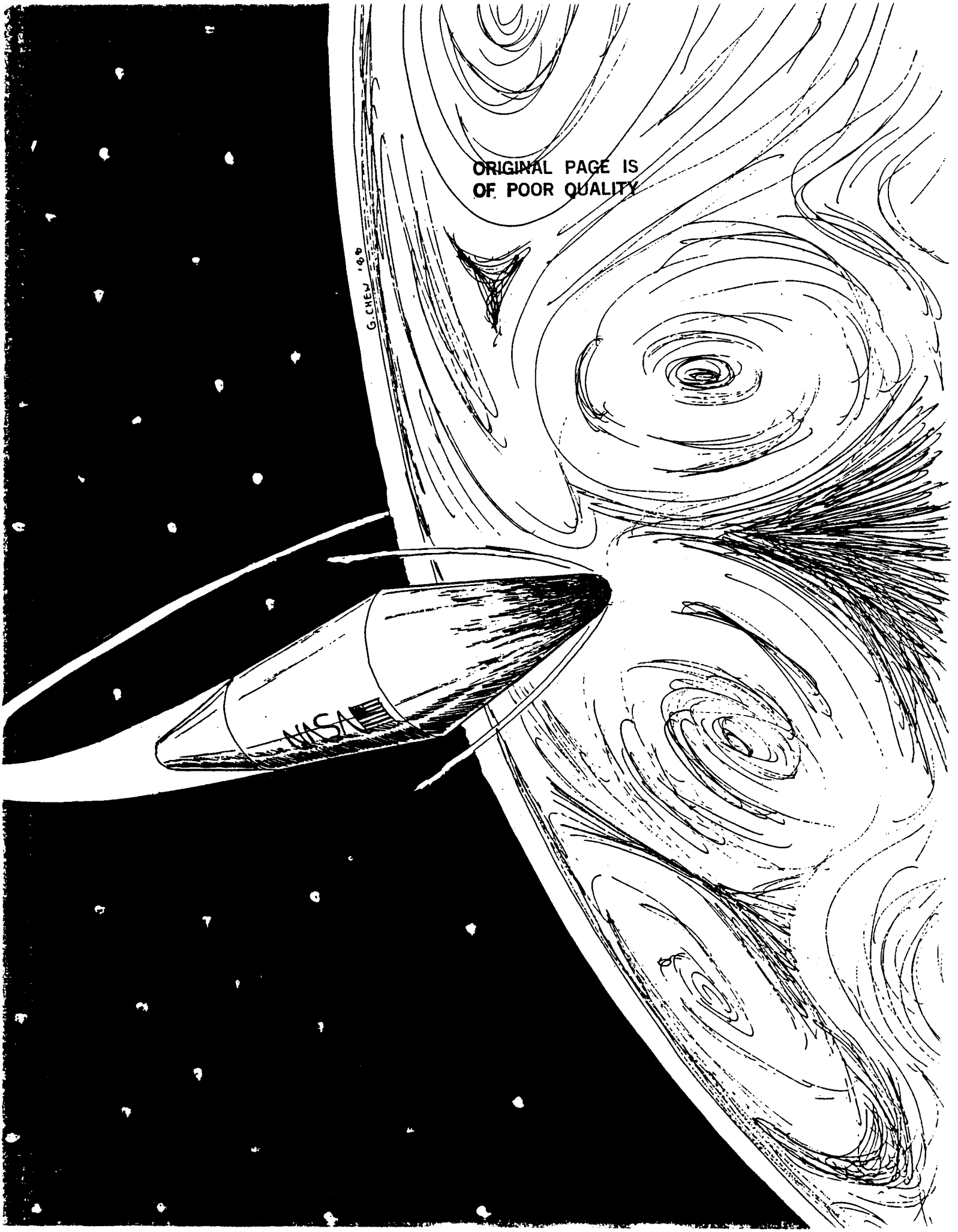
ORIGINAL PAGE IS
OF POOR QUALITY
G.CHEW '88
NASA

V. ORBITAL MECHANICS

Rob Gohd
Dave Reed
Seshu Vaddey
LeAnne Woolf

INTRODUCTION

Once the ram accelerator vehicle exits the atmosphere it pursues a ballistic trajectory which, if left undisturbed, would intersect the earth (see Fig. V-1). Therefore, to place the vehicle into low earth orbit (LEO) an appropriate circularization maneuver or series of maneuvers must be carried out. This requires the vehicle to carry an on-board rocket and sufficient propellant to accomplish the desired mission. Clearly, the mass of the on-board propulsion system must be kept to a minimum to maximize the payload carrying capacity of the vehicle.

A number of possible orbital insertion scenarios for the ram accelerator mass launcher have been proposed [1], including direct circularization at the ballistic apogee and a multi-step maneuver involving aerobraking. Preliminary investigations have indicated that the latter offers the potential for lowest on-board propulsion system mass, and is discussed in detail in this chapter. Figure V-1 illustrates the various phases of the vehicle trajectory for this orbital scheme.

To increase the flexibility of this launch concept the use of a parking orbit below the desired final orbit, e.g. a space station orbit, has been proposed. The parking orbit would be used to "store" the vehicles until they would be needed in the final orbit, at which time an orbital transfer would be performed. This would allow the continuous launching of vehicles without having to synchronize the vehicle launch with the orbital position of the space station in orbit.

Before the vehicle's orbital path can be studied, a launch site must be chosen. The primary factors to be considered are maximizing the velocity imparted by the earth's rotation by launching as close to the equator as possible and minimizing the amount of atmosphere to

be traversed by choosing a site with a high altitude. In addition, an equatorial launch site is desirable to permit all vehicles to be inserted into the same orbit regardless of when launched. This permits a frequent and flexible launch schedule. A launch site matching these and other criteria is proposed at Mt. Kenya in Kenya. This site offers a launch altitude of about 4000 m and lies very near the equator. A detailed discussion of the launch site selection process is presented in Appendix A.

The development of an accurate atmospheric model is presented in this chapter along with the orbital mechanics involved in the ascent of the vehicle from the earth's atmosphere to its initial ballistic apogee, through aerobraking, and into a parking orbit. The analysis was done using launch velocities of 8, 9, and 10 km/sec and launch angles from 16-30°. Finally, the ΔV requirements for achieving a parking orbit at approximately 450 km with the use of an aerobraking maneuver is compared to that for reaching a 450 km parking orbit without aerobraking. A Hohmann transfer is used to reach the final orbit altitude of 500 km.

ATMOSPHERIC MODEL

In previous studies carried out on the effects of the atmosphere on orbital maneuvers performed "near" the earth's surface (e.g., aerobraking) an isothermal exponential density profile was assumed for the entire atmosphere [1]. However, the sensitivity of aerobraking called for a model more closely based on experimental values of density taken from atmospheric tables [2]. Using various curve-fitting routines, an equation for the density variation as a function of altitude could be determined. Initial estimates that aerobraking would probably occur at altitudes in the range of 30 to 100 km were confirmed when further studies indicated that most of the vehicle drag occurs between 30 and 50 km. The best curve fit from 30-100 km was found to be an exponential

$$\rho = 1.3815\, e^{-y/6880} \tag{1}$$

For altitudes under 30 km the following correlation was used [3]:

$$\rho = 1.225\, e^{-y/7170} \tag{2}$$

The scale heights of 6880 and 7170 are in m.

This combined atmospheric model is illustrated in Fig. V-2a. A comparison between a standard isothermal atmosphere [1] and the empirical atmosphere is provided in Fig. V-2b.

MULTI-STEP METHOD WITH AEROBRAKING

As indicated in Fig. V-1, the vehicle trajectory can be investigated in several phases. The first phase encompasses the vehicle's atmospheric transit from the muzzle of the ram accelerator tube to approximately 40 km above the earth's surface. At the end of atmospheric transit, the velocity and flight path angle are corrected for the earth's rotation [4]. In Phase 2 standard orbital mechanics equations [4,5] are used to find the ballistic apogee. A velocity change is made at this initial apogee by the use of an on-board propulsion system. The vehicle then coasts toward the atmosphere and undergoes aerobraking (Phase 3). In Phase 4 the vehicle coasts to a second, lower, apogee where a burn is made to place it into a circular parking orbit. A Hohmann transfer from parking orbit to final, space station, orbit comprises the final maneuver (Phase 5).

Phase 1: Atmospheric Transit

During atmospheric transit, drag reduces the velocity of the vehicle from the initial launch velocity as discussed in the preceding chapter. At the upper edge of the atmosphere, the component of velocity contributed by the earth's rotation at launch is added to the vehicle velocity and the flight path angle adjusted [4].

$$V_h^2 = (R_0\,\omega\cos\lambda)^2 + (V_1^*\cos\phi_0)^2 + 2R_0\,V_1^*\,\omega\cos\lambda\cos\phi_0\cos\gamma \qquad (3)$$

$$V_1^2 = V_h^2 + (V_1^*\sin\phi_0)^2 \qquad (4)$$

$$\phi_1 = \cot^{-1}(V_h/(V_1^*\sin\phi_0)) \qquad (5)$$

The orbital mechanics calculations proceed from these values of V and ϕ.

Phase 2: Coast to Initial Apogee

Given the altitude, velocity and flight path angle at the edge of the atmosphere, the orbit's radius at apogee is calculated by [4]

$$r_a = (gR_0^2 + (g^2R_0^4 - h^2\eta)^{0.5})/\eta \quad (6)$$

where

$$h = r_1 V_1 \cos \phi_1 \quad (7)$$

$$\eta = (2gR_0^2)/r_1 - V_1^2 \quad (8)$$

The velocity at apogee is found from [5]

$$V_a = h/r_a \quad (9)$$

In order to demonstrate the general trend of how conditions at this first apogee depend on conditions at launch, the altitudes and velocities at apogee for launch velocities of 8, 9, and 10 km/s and launch angles of 16-30° were calculated using Eqs. (6) and (9). Figures V-3 and V-4 illustrate the changes in these apogee altitudes and velocities at apogee, respectively, as functions of the launch conditions. Note that as launch angle increases, velocity at apogee decreases more slowly than apogee altitude increases. This seems to indicate that apogee altitude will dominate further orbital maneuvers.

Phase 3: Aerobraking

Because the details of aerobraking are dependent upon the conditions at the initial ballistic apogee, Phase 3 combines the coast phase to the atmosphere and the aerobraking into one phase. The two portions are listed as Phases 3a and 3b, respectively. The factors that affect aerobraking are:

1. the altitude of the initial ballistic apogee,
2. the velocity at apogee,
3. the change in velocity needed at apogee to raise the perigee to the desired altitude,
4. the vehicle dimensions and mass,
5. the drag coefficient of the vehicle,
6. the desired altitude of the parking orbit.

The first three factors determine the orbital parameters as the vehicle enters the atmosphere. The body dimensions, mass, and C_D determine the amount of drag the vehicle experiences and thus how much velocity is lost during the aerobraking maneuver. The

altitude of the parking orbit, when combined with the other parameters, determines the altitude at which aerobraking occurs. The altitude of initial ballistic apogee, the velocity at that apogee, and the drag coefficient vary with initial launch angle and launch velocity, as noted earlier, and with launch altitude. As noted earlier a launch altitude of 4000 m was selected.

A simple model, called the impulsive model, was developed to gain insight into the mechanics of aerobraking so as to guide a more comprehensive analysis. In this model the following assumptions are made:

1. Aerobraking occurs over a small angular distance and short time duration; thus it can be considered as an impulsive ΔV at perigee.
2. The flight path angle is virtually zero during aerobraking and the velocity vector is tangent to the earth's surface.
3. The flight path is defined by orbital parameters alone.

With these assumptions and the initial apogee altitude, an initial estimate of perigee altitude for aerobraking is made. From [5]

$$a = (r_a + r_p)/2 \tag{14}$$

$$\varepsilon = -\mu/(2a) \tag{15}$$

$$V_3 = (2(\varepsilon + \mu/r_a))^{0.5} \tag{16}$$

The ΔV at apogee is found by subtracting the initial velocity at apogee from V_3. The orbital parameters for the elliptical path (see Fig. V-5) to aerobraking are then calculated [5].

$$e = (r_a - r_p)/(r_a + r_p) \tag{17}$$

$$p = a(1 - e^2) \tag{18}$$

Although this model assumes an impulsive ΔV, it is actually based upon the loss of velocity across incremental steps of true anomaly, ν. The velocity loss in each increment is calculated by

$$\Delta V_j = -1/2\ (C_D\ V^2\ A\ \ \Delta t\ \ \rho)/m_3 \tag{19}$$

where the density is modeled by Eqs. (1) and (2) and

$$\Delta t = (\Delta \nu\, r)/V \tag{20}$$

The velocity, V, at the upper edge of the atmosphere before aerobraking begins is given by

$$V = (\mu/p)^{0.5} [-\sin \nu \underline{P} + (e + \cos \nu)\underline{Q}] \tag{21}$$

where $\underline{P}$ and $\underline{Q}$ are shown in Fig. V-6. The velocity is updated after every increment in time by

$$V = V - \Delta V_j \tag{22}$$

By summing the change in velocity for each increment across a range of true anomaly the total velocity decrement, ΔV_t, for aerobraking can be calculated.

$$\Delta V_t = \Sigma\ \Delta V_j \tag{23}$$

This ΔV_t is then applied at perigee as an impulsive change to yield an orbit with a new specific mechanical energy. This approach is justified because the kinetic energy lost is much smaller than the total specific mechanical energy of the orbit. The specific mechanical energy is used to calculate a new value of a from

$$a = -1/2\ \mu/\varepsilon \tag{24}$$

and then the new apogee r_6 is found by using the same value for r_p as was chosen at the beginning of aerobraking.

$$r_6 = 2a - r_p \tag{25}$$

If this apogee altitude is not that of the design parking orbit, a new radius of perigee is chosen and the process repeated until convergence is achieved.

The major contribution of this model to an understanding of the aerobraking process is in finding the range of true anomaly, ν, over which aerobraking is significant. It was found that the velocity change outside the range of -20° to +20° is negligible. Figure V-7 illustrates the ratio of the aerobrake ΔV for each degree of true anomaly to the total ΔV_t calculated over $\pm$20° for the case of a 20° launch angle at a launch velocity of 9 km/s. As can be seen from the graph, approximately 75% of aerobraking occurs within $\pm$5° of perigee and about 98% occurs within $\pm$10° of perigee. This supports the model's assumption of an impulsive

change in velocity during aerobraking. For all cases, a ν of 20° corresponds to a flight path altitude of about 100 km.

From the insight gained using the impulsive model, the study proceeded to a model which took the effects of atmospheric drag on the flight path into account. This more complex model uses numerical integration of the equations of motion

$$d^2r/dt^2 - r(d\theta/dt)^2 = -g(r_0/r)^2 - 1/2(C_D\ \rho\ V^2\ A\ \sin\phi)/m_3 \quad (26)$$

$$r(d^2\theta/dt^2) + 2(dr/dt)(d\theta/dt) = -1/2(C_D\ \rho\ V^2\ A\ \cos\phi)/m_3 \quad (27)$$

to determine the change of velocity during aerobraking. Equations (26) and (27) represent accelerations in the radial and tangential directions, respectively [6]. For nose-first entry C_D depends on the launch angle and the amount of ablation that results from atmospheric transit (see chapter IV).

After choosing a ΔV to be made at initial apogee, r_a and V_3 give the angular momentum and specific mechanical energy of the orbit [5].

$$h = r_a\ V3 \quad (28)$$

$$\varepsilon = V_3^2/2 - \mu/r_a \quad (29)$$

At the upper edge of the atmosphere, as defined by the impulsive model, the velocity and flight path angle can be found by [5]

$$V_4 = (2(\varepsilon + \mu/r_4))^{0.5} \quad (30)$$

$$\phi_4 = \cos^{-1}(h/(r_4\ V_4)) \quad (31)$$

Based on the initial conditions, V_4 and ϕ_4, at the start of aerobraking, Eqs. (26) and (27) can be numerically integrated using a Runge-Kutta 4th order method. The integration proceeds until the vehicle is back at an altitude of 100 km as it moves away from the earth and provides the net change in velocity due to aerobraking is found.

Aerobraking Results

Figure V-8 illustrates the perigee altitude reached during aerobraking. The perigee altitude decreases with increasing launch angle for two reasons: For higher launch angles the projectile travels through less atmosphere during ascent and thus ablates less. This means

the vehicle retains a lower drag coefficient which in turn requires the projectile to dip deeper into the atmosphere to obtain the appropriate velocity loss during aerobraking. However, the effects of C_D are minimal compared to the second reason. As the launch angle increases the initial apogee altitude and apogee velocity also increase, leading to higher velocities at the beginnning of aerobraking. In order to reduce the projectile velocity enough to attain the desired parking orbit altitude, the vehicle must go deeper into the atmosphere to obtain the desired velocity loss from aerobraking.

Another parameter of interest is the velocity, and thus kinetic energy, lost during aerobraking. The dissipation of energy will generally be in the form of aerodynamic heating of the vehicle. Figure V-9 shows the absolute value of the ΔV occurring as a result of aerobraking. As the velocity loss increases, so must the amount of energy to be dissipated. The length of time over which the velocity loss occurs, however, determines the rate of heat load to the vehicle. The aerobraking procedure lasts approximately 15-20 minutes, thus allowing ample time for energy dissipation.

A major problem which has emerged from the study of aerobraking is that the projectile will crash to earth if the change in velocity at the ballistic apogee is not done accurately. Variations of as small as 0.1 m/s in the velocity change applied at apogee meant the difference between whether the projectile crashed into the earth or successfully coasted toward parking orbit. This is within the limits of most propulsion systems used today, however the problem of sensitivity will require the vehicle to have an accurate guidance and control system on board.

Phase 4: Reaching Parking Orbit

Based on the velocity V_5 and flight path angle ϕ_5 at the end of the aerobraking maneuver, r_6 can be found using Eq. (10) after replacing V_1 with V_5 and r_1 with r_5 in Eqs. (11) and (12). Similarly, V_6 is calculated with Eq. (13). The velocity required to maintain an object in a circular orbit is [5]

$$V_{CS} = (\mu/r_{CS})^{0.5} \tag{32}$$

The difference between V_6 and V_{CS} is the amount of velocity change needed to finally place the projectile into a parking orbit.

DISCUSSION OF RESULTS

The goal of the orbital mechanics study was to minimize the propellant ΔV requirements, as opposed to the ΔV due to aerobraking. Provided in Figure V-10 are the results for the comprehensive model for total propellant ΔV required to deliver the vehicle to the space station. This includes the primary burn at the initial ballistic apogee, the circularization burn into the parking orbit and the Hohmann transfer to the space station orbit.

As one can see from the graph there is an optimal launch angle corresponding to each launch velocity considered. The velocity retention of the vehicle as it traverses the atmosphere is the primary factor in the performance of the orbital maneuvers. Based on purely orbital considerations, lower launch angles are preferred because the vehicle's initial flight path is more circular, which reduces the propellant ΔV requirements. However, at the lower launch angles the vehicle travels through more of the atmosphere which results in greater losses in velocity, which in turn requires a greater propellant ΔV. At the higher launch angles the vehicle retains more of its initial velocity but the vehicle's flight path becomes more eccentric, which offsets the benefits of the higher velocity retention. Thus, a compromise or optimal launch angle occurs somewhere between the two extremes. Table V-1 lists the optimal launch angle for each launch velocity analyzed and provides the corresponding orbital maneuver performance for each case.

Figure V-10 also indicates, as expected, that higher launch velocities are more desirable for orbital mechanics purposes. As the launch velocity increases, the optimal launch angle decreases and so does the corresponding propellant ΔV requirement. The other point of interest which can be noted from the graph is that at higher launch velocities the curves become shallower, thus permitting a wider latitude of acceptable launch angles.

Table V-1. Optimal performance parameters for the orbital maneuvers

	Launch Velocity		
	8 km/sec	9 km/sec	10 km/sec
Optimal launch angle	22°	20°	18°
1st apogee burn	1149 m/s	630 m/s	320 m/s
Circularization burn (parking orbit)	117 m/s	120 m/s	123 m/s
Transfer from parking to final orbit	43 m/s	30 m/s	30 m/s
Total ΔV	1309 m/s	780 m/s	473 m/s
ΔV(aerobraking)	-252 m/s	-507 m/s	-909 m/s
Perigee altitude	50.2 km	44.4 km	39.6 km

The total velocity change required from the on-board propulsion system is the measure of how efficient a set of orbital maneuvers is. In order to determine whether or not the method emphasized in this study is optimal, a brief analysis of other possible scenarios is necessary. Two other methods were evaluated, direct insertion and a multi-step method without aerobraking.

For direct insertion into a circular parking orbit from initial ballistic apogee, the projectile must be fired at a very low launch angle in order to have an apogee altitude at 450 km, as can be seen from Fig. V-11. This increases the amount of time the projectile spends in the atmosphere, reducing the velocity retention leading to the need for additional heat shielding (see Chapter IV). This reduces the amount of payload that can be carried and thus increases the cost of launch [1].

Another approach is to impart a change in velocity at the initial ballistic apogee to raise the perigee altitude to the desired parking orbit altitude. A subsequent burn is then made to circularize the orbit. This approach allows higher launch angles and launch velocities than does the use of direct insertion at initial apogee and thus its flexibility approaches that of the multi-step maneuver with aerobraking. Figure V-12 illustrates the total ΔV requirements to

place the projectile into the space station orbit at an altitude of 500 km given a launch angle of 16-30°, for a launch velocity of 9 km/sec. This ΔV is the sum of the absolute values of the velocity change made at initial ballistic apogee and the velocity change made to circularize the orbit. Also shown on the figure is the total ΔV requirement to be provided by the on-board rockets for the multi-step maneuver with aerobraking. It can be seen that the use of aerobraking significantly reduces the amount of ΔV needed, and thus the amount of on-board propellant. At the optimal launch angle of approximately 20° for the 9 km/sec launch velocity, the method using aerobraking requires about 40% less on-board propellant (assuming $I_{sp} = 297$) than using the multi-step approach without aerobraking.

CONCLUSIONS

The ram accelerator mass launch system was initially conceived as a means of economically launching payloads into low earth orbit. A key part of this concept is the reduction of the on-board propulsion system mass by minimizing the mission's total change in velocity in order to increase the payload mass ratio. To reach this goal a multi-step maneuver using aerobraking has been proposed. The study of the aerobraking process was first performed with a simple model to gain an understanding of the parameters involved in an atmospheric drag maneuver. This model indicated that aerobraking occurs almost impulsively near the perigee. These results led to the development of a more comprehensive model based on spacecraft re-entry analysis. Both models gave similar results, supporting the approaches taken. Results using aerobraking were then compared with two other methods of inserting the vehicle into the desired parking orbit. The multi-step maneuver using aerobraking proved to be more efficient than a direct insertion at first apogee or a multi-step process without aerobraking. Based on these findings, it is felt that aerobraking can be integrated successfully into the ram accelerator mass launch concept.

REFERENCES

1. Bruckner, A.P., and Hertzberg, A., "Ram Accelerator Direct Launch System for Space Cargo," IAF Paper 87-211, 38th Congress of the International Astronautical Federation, Brighton, United Kingdom, October 10-17, 1987.

2. U.S. Standard Atmosphere, 1976, NOAA, NASA, USAF, Washington, D.C., October 1976.

3. Vincenti, W.G., and Kruger, C.H., Jr., Introduction to Physical Gas Dynamics, Robert E. Krieger Publishing Company, Malabar, FL, 1965..

4. Ball, K.J., and Osborne, G.F., Space Vehicle Dynamics, Clarendon Press, Oxford, 1967.

5. Bate, R.R., Mueller, D.D., and White, J.E., Fundamentals of Astrodynamics, Dover Publications, Inc., New York, 1971.

6. Allen, H.J., and Eggers, A.J., Jr., "A Study of the Motion and Aerodynamic Heating of Missiles Entering the Earth's Atmosphere at High Supersonic Speeds," NACA TN 4047, Washington, D.C., October 1957.

NOMENCLATURE

a	semi-major axis
A	cross-sectional area
C_D	drag coefficient
e	eccentricity of orbit
g	gravitational acceleration at earth's surface, 9.81 m/sec
h	angular momentum of orbit
m_3	mass of projectile after burn at initial apogee
p	semi-latus rectum of orbit
$\underline{P}$	radius vector to $\nu = 0$
$\underline{Q}$	radius vector perpendicular to $\underline{P}$
r	radius from center of earth
r_a	radius of initial ballistic apogee
r_{cs}	radius of circular orbit
r_p	radius of perigee
r_1	radius at edge of atmosphere after atmospheric transit
r_4	radius at edge of atmosphere before aerobraking
r_5	radius at edge of atmosphere after aerobraking
r_6	radius of second apogee
R_0	mean radius of earth
t	time
V	velocity
V_a	velocity at initial apogee
V_{cs}	velocity required to maintain object in circular orbit
V_h	horizontal velocity contributed by earth's rotation
V_1^*	velocity after atmospheric transit but before correction for earth's rotation
V_1	velocity corrected for earth's rotation after atmospheric transit

V_3	velocity after rocket burn at initial apogee
V_4	velocity at edge of atmosphere at beginning of aerobraking
V_5	velocity at edge of atmosphere after aerobraking
V_6	velocity at second apogee
y	altitude above earth's surface
γ	launch direction with respect to east = 0
ε	specific mechanical energy of an orbit
η	constant of integration in calculating velocity contributed by earth's rotation
λ	launch latitude
μ	gravitational parameter
ν	true anomaly, angle between vector from center of earth to perigee and radius vector to actual position
ρ	air density
ϕ	flight path angle
ϕ_0	launch angle
ϕ_1	flight path angle after atmospheric transit following launch, corrected for earth's rotation
ϕ_4	flight path angle at entry into atmosphere for aerobraking maneuver
ϕ_5	flight path angle at exit from atmosphere after aerobraking maneuver
θ	angular position
ω	angular velocity of earth

All units are MKS

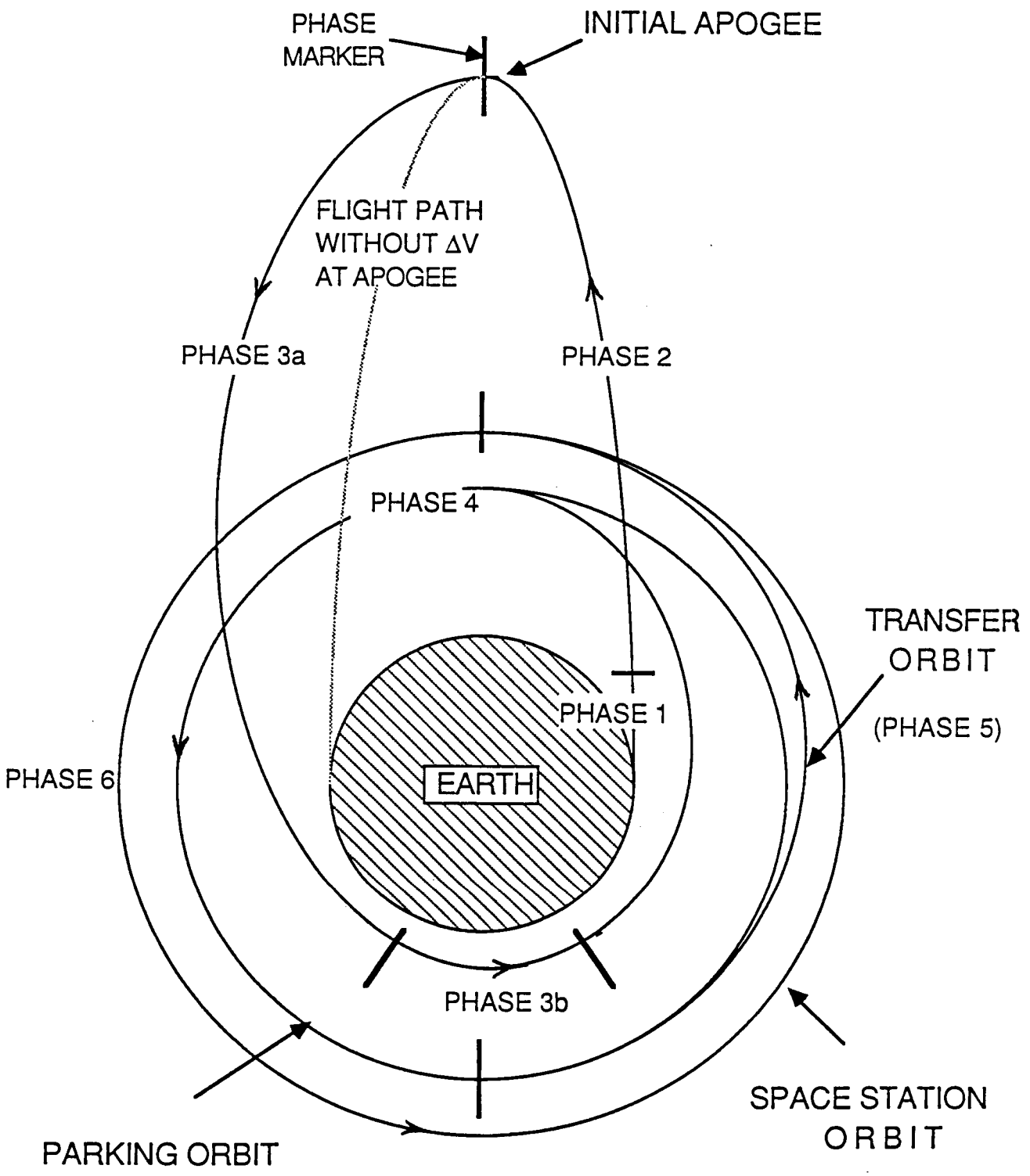

Fig. V-1 Proposed trajectory of the Ram Accelerator vehicle

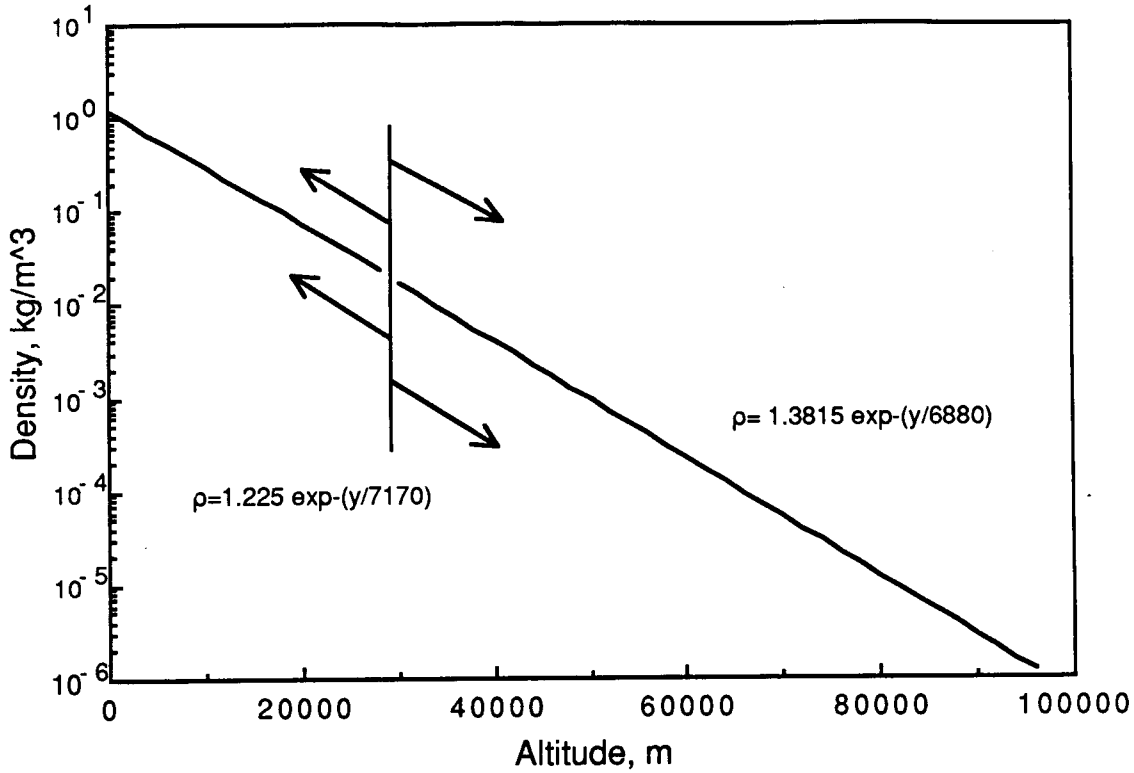

Fig. V-2a Curve fits of density variation of atmosphere with altitude

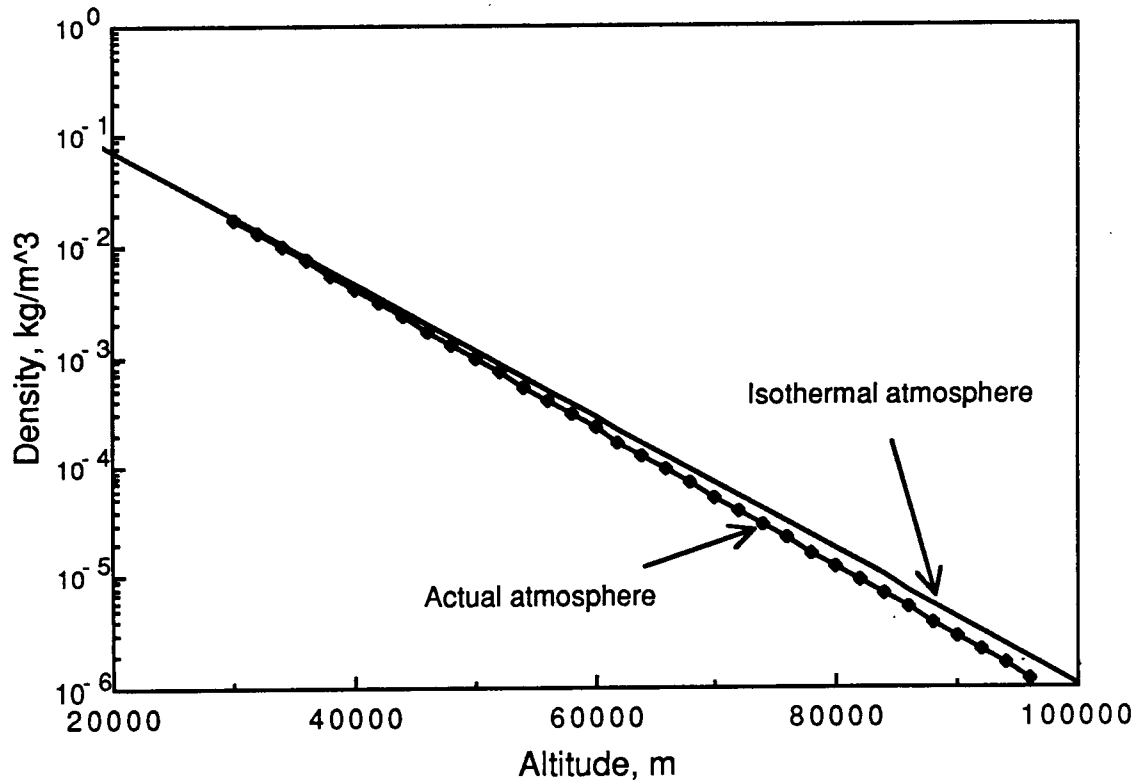

Fig. V-2b Comparison between actual and isothermal atmospheres

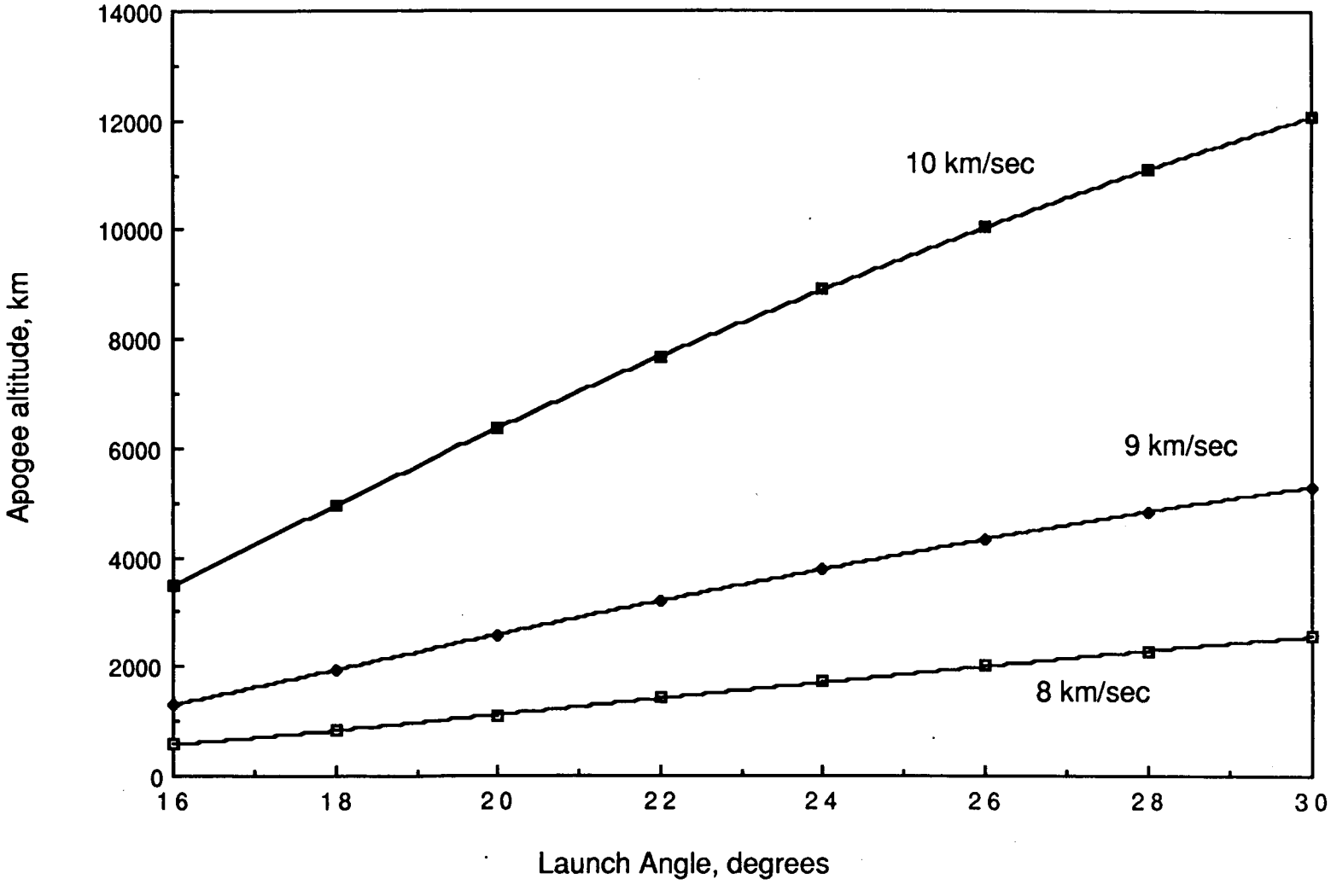

Fig. V-3 Initial apogee altitude variation with launch velocity and launch angle

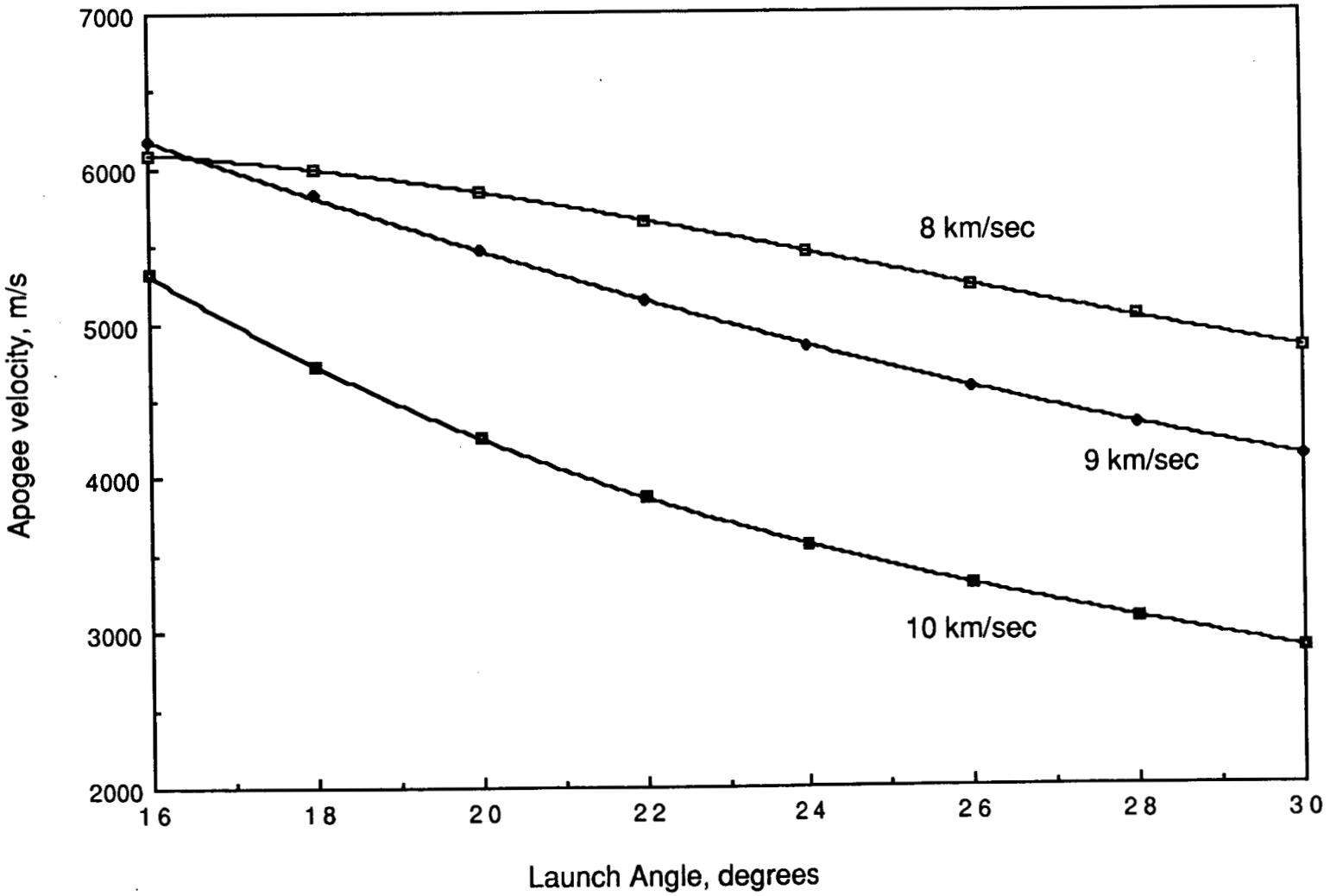

Fig. V-4 Initial apogee velocity variation with launch velocity and launch angle

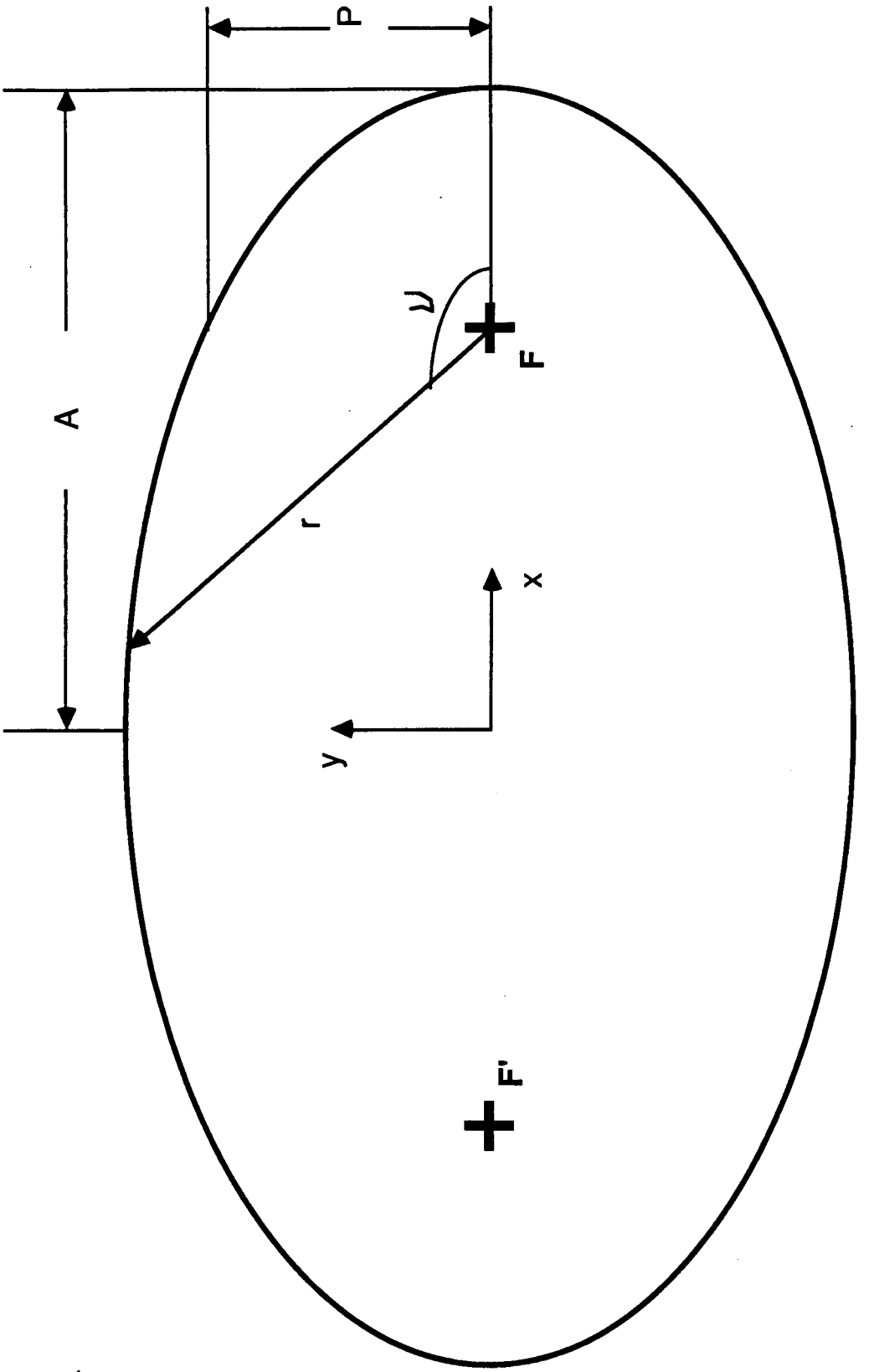

Fig. V-5 Geometry of an ellipse

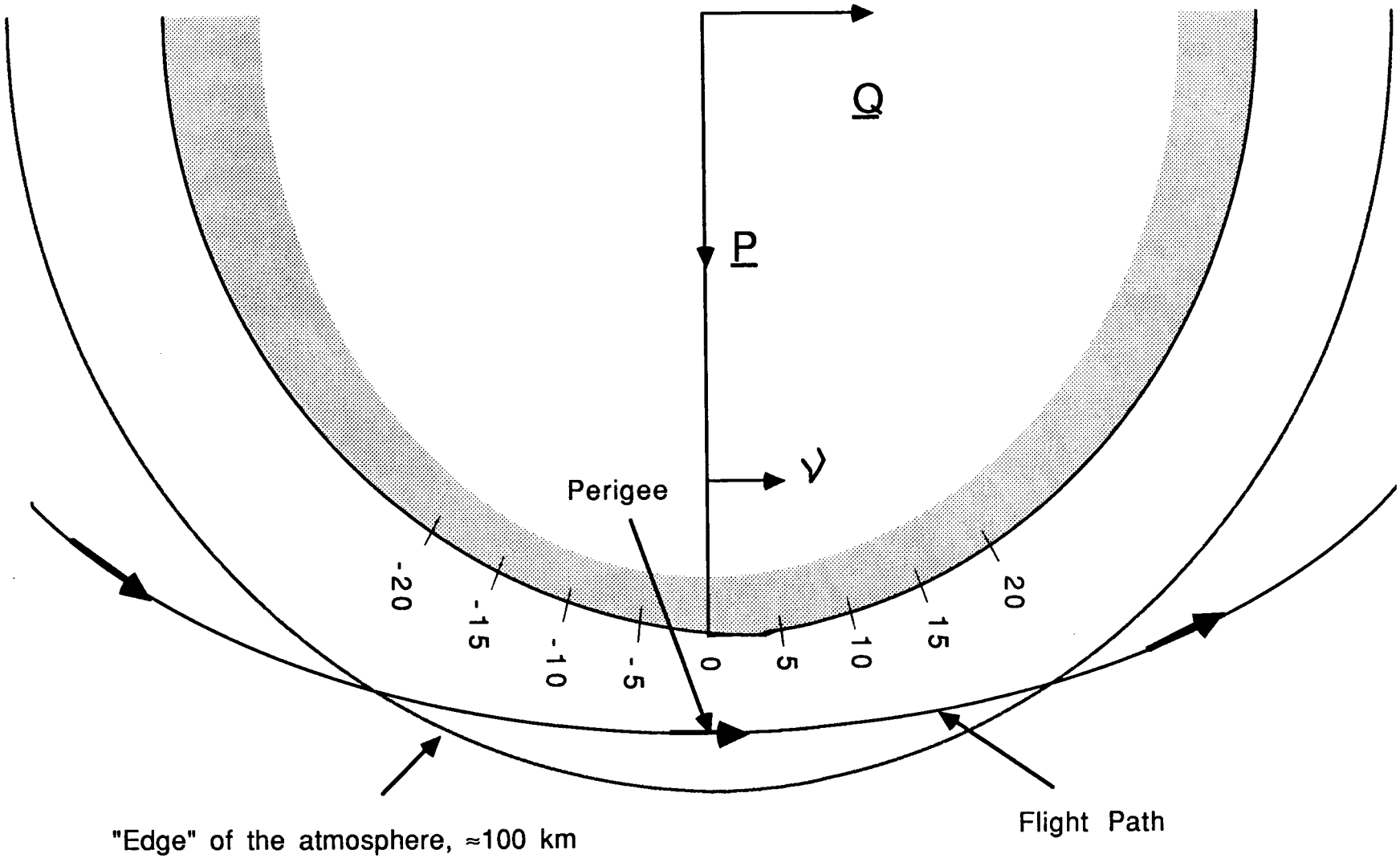

Fig. V-6 Impulsive aerobraking schematic.

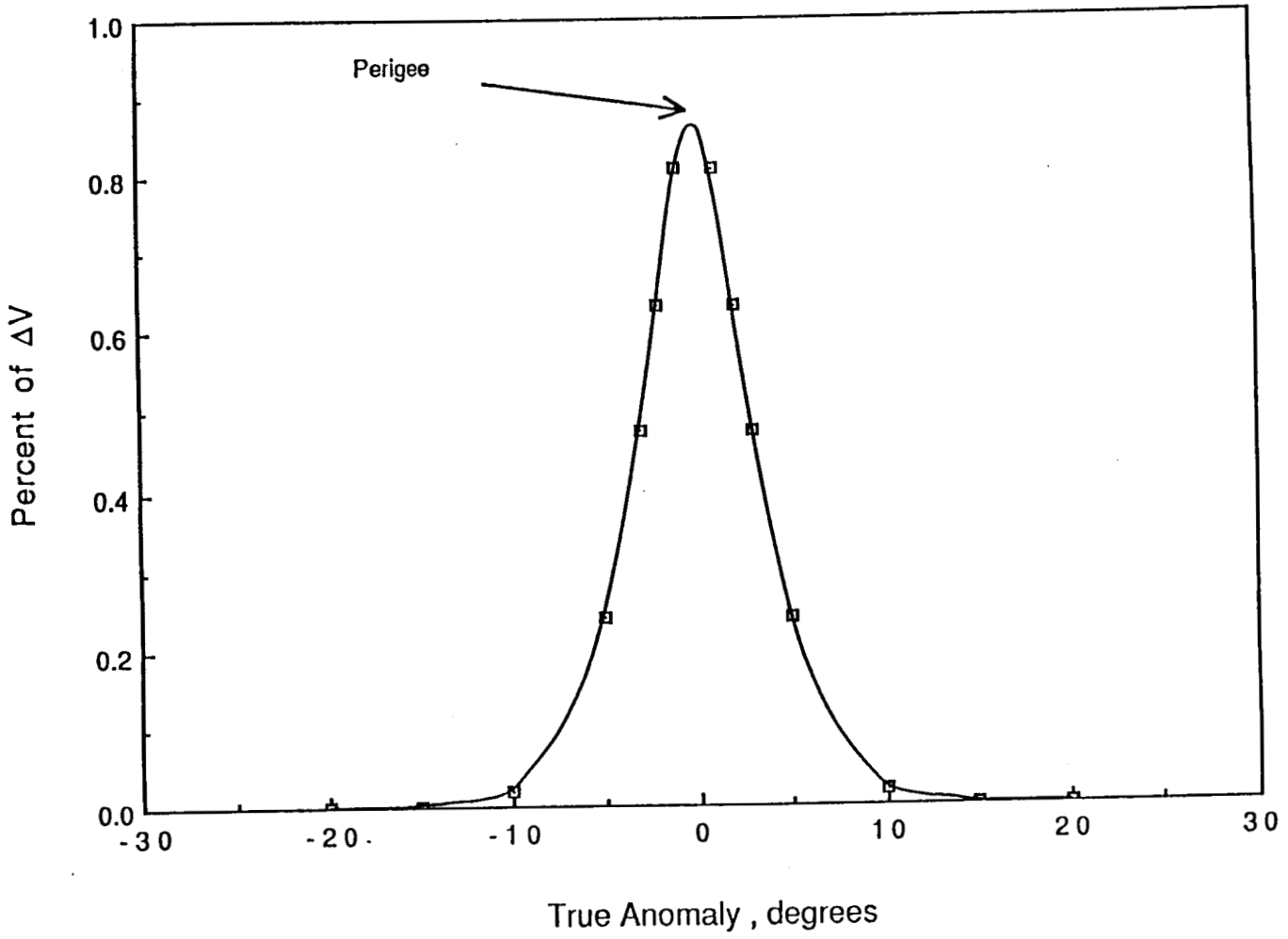

Fig. V-7 Distribution of velocity loss in impulsive aerobraking model.

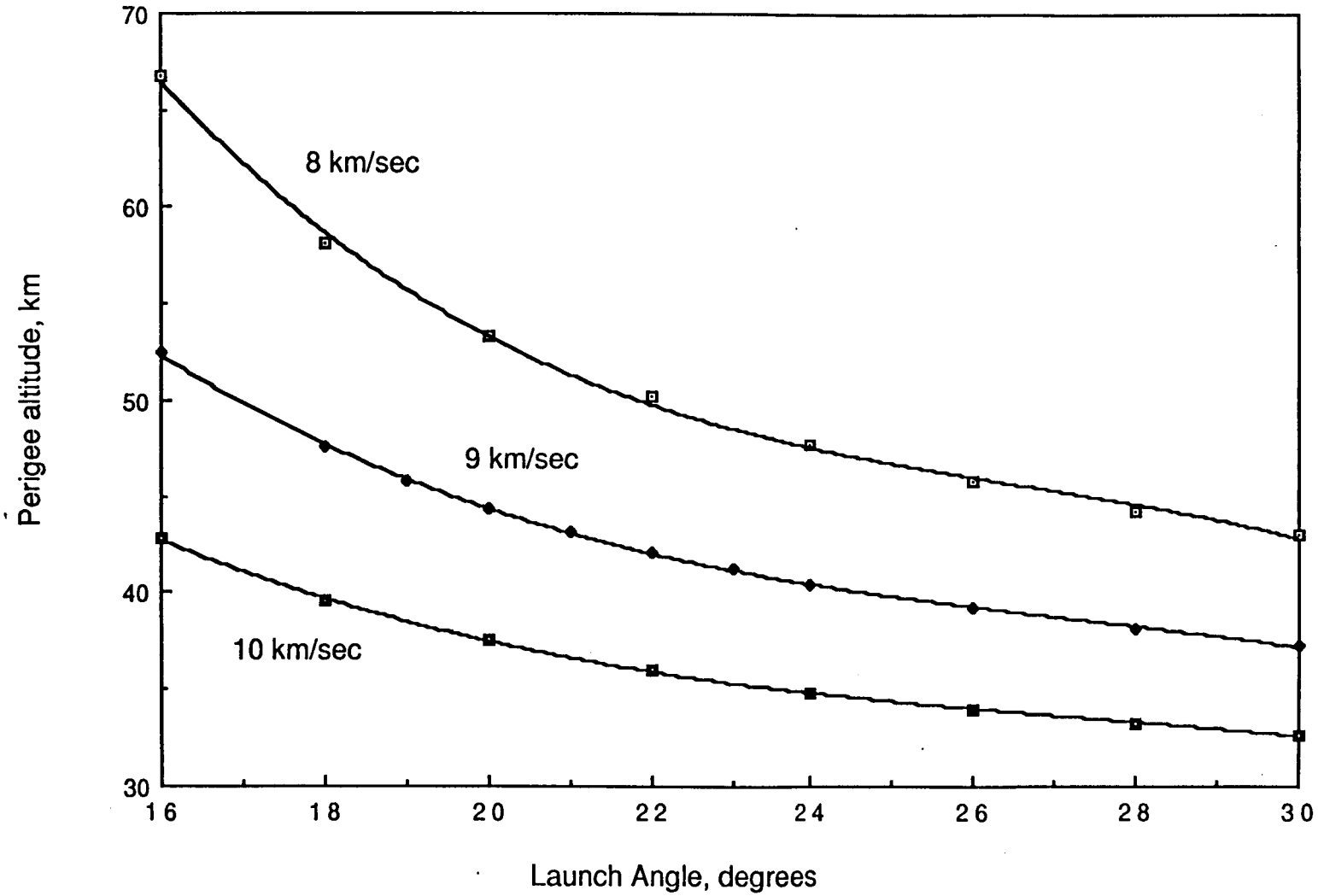

Fig. V-8 Relation of perigee altitude to launch angle for various launch velocities

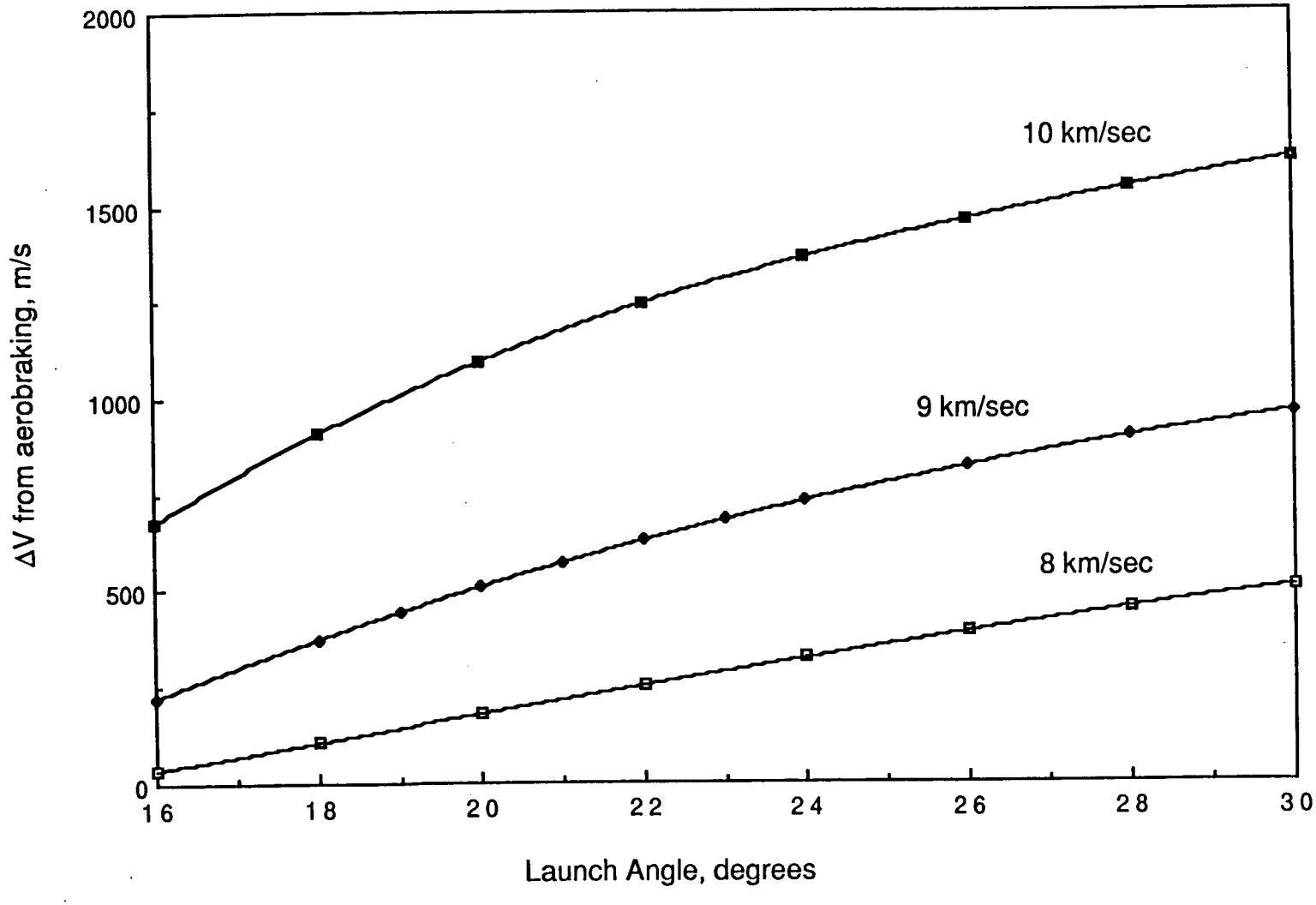

Fig. V-9 Velocity loss from aerobraking

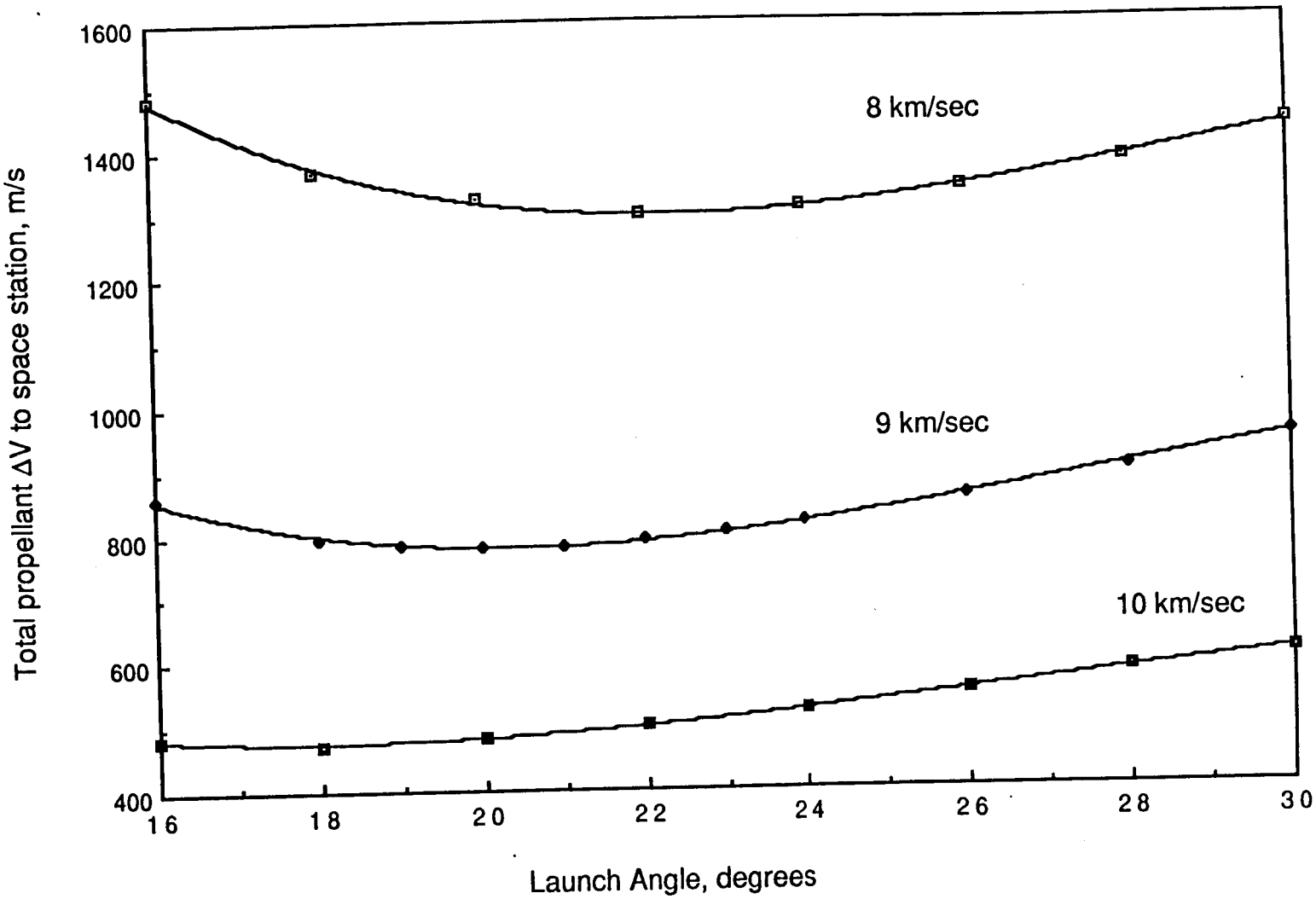

Fig. V-10 Total propellant ΔV required as a function of launch angle and launch velocity

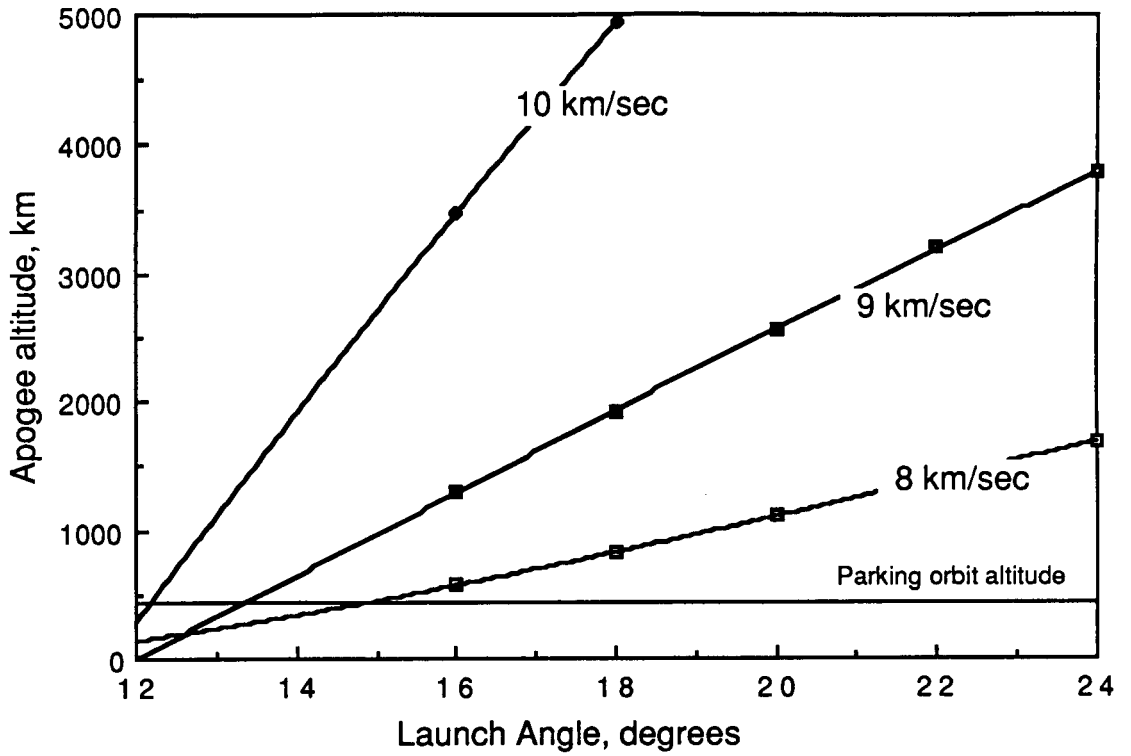

Fig. V-11a Apogee altitude extrapolated to lower launch angles

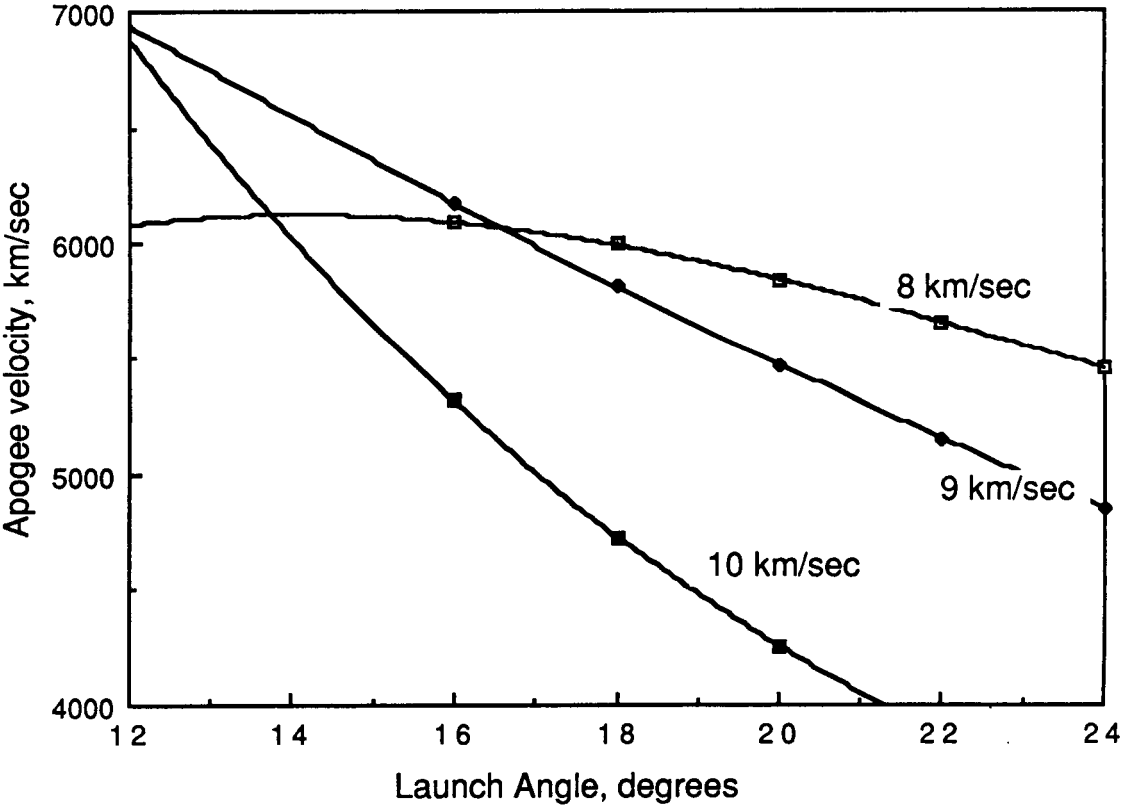

Fig. V-11b Apogee velocity extrapolated to lower launch angles

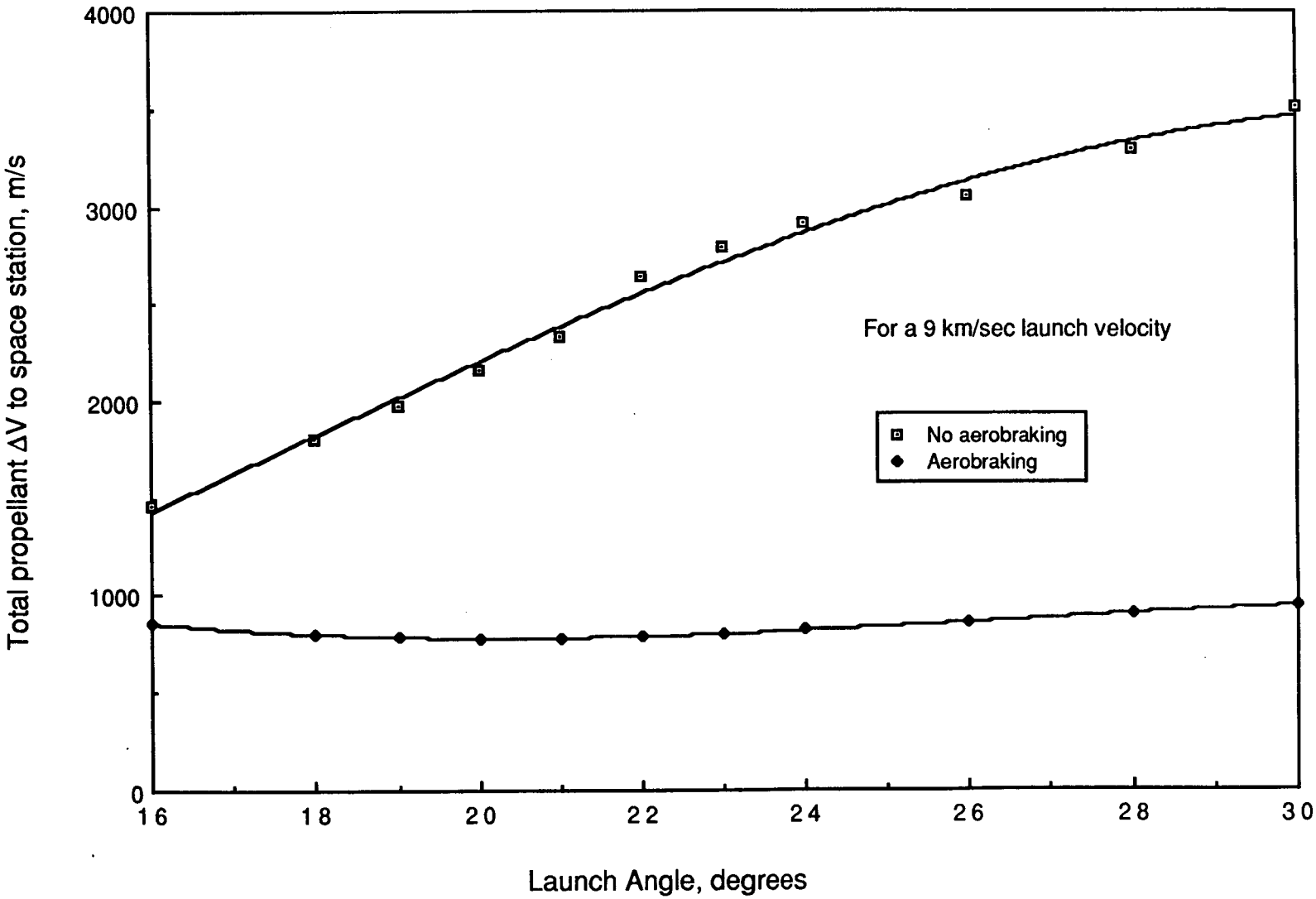

Fig. V-12 Comparison of orbital performance with and without aerobraking

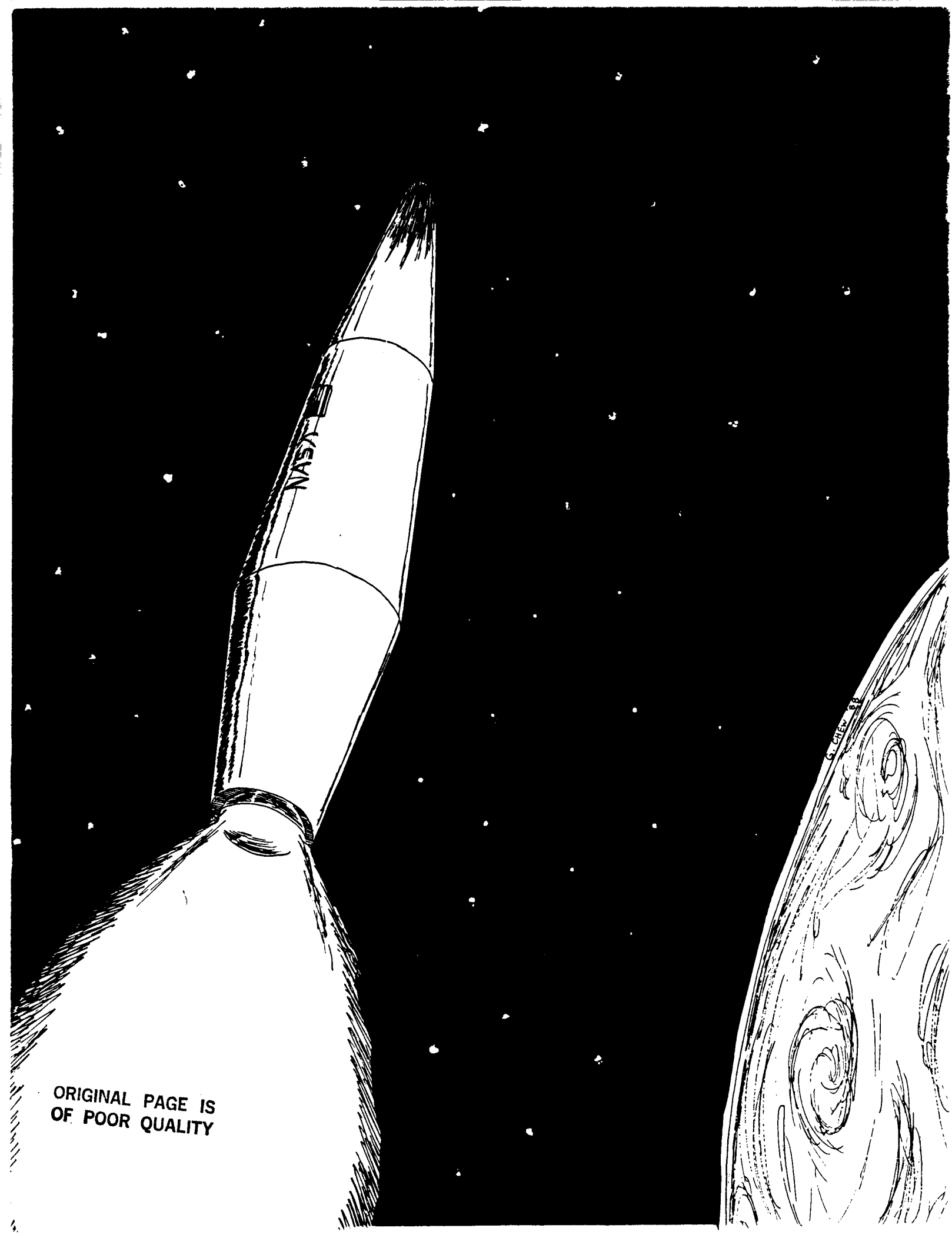

VI. ON-BOARD PROPULSION SYSTEM

Calvin Armerding
Michael Aarnio

INTRODUCTION

An on-board propulsion system for the ram accelerator vehicle is needed so that the vehicle can be maneuvered to a practical parking orbit. Since the vehicle is initially launched into a ballistic trajectory which intersects the earth, it is necessary to change the velocity of the vehicle in order to change the trajectory to an elliptical orbit, which can then be circularized. The basic requirements of the on board rocket system are established by the orbital mechanics (see Figure V-1 Chapter V). These include the capability to deliver four separate burns: the initial burn at ballistic apogee, the circularization burn at the parking orbit, and two burns for the Hohmann transfer from parking orbit to space station orbit. Another requirement is that the system deliver sufficient thrust to provide a minimum one-half g acceleration. This is needed to reduce inaccuracies in the final orbit which are a consequence of finite burn times (the ideal burn is an impulse, from which no orbital error results). An additional requirement, for practical reasons, is that the propulsion system be simple and of a proven design. Out of the broad range of available propulsion options, several meet these criteria and are worthy of consideration.

The velocity change requirements, the small size of the vehicle, and the desire to achieve the greatest possible payload fraction necessitates the use of a propulsion method which offers high specific impulse and low system mass. The vehicle is moving at high velocity (on the order of 6 km/sec) when passing through first apogee, where the largest of the velocity changes is required. The Δv's required must be delivered over short time

spans, preferably less than two minutes. In an ideal situation the burn would be instantaneous so that there would be no error due to the changing velocity and attitude of the vehicle. However, it is impossible to instantaneously change the velocity of a vehicle, therefore the burn time must be minimized. Decreasing the allowable burn time increases the required thrust level, and thus the need for a high thrust level becomes as important as the need for a high specific impulse.

Chemical propellants are generally classified into three principle groups: solid propellants, liquid propellants, and hybrids. Hybrids are solid fuels with liquid oxidizers and promise high performance levels; however, they have not been used commercially and their technology is not sufficiently developed for consideration here.

SOLID PROPELLANTS

Solid propellants are attractive because of their great simplicity. A solid propellant rocket is a canister filled with a combustible solid. Once ignited, the rocket burns until the propellant is exhausted. Typical I_{sp} values for solid propellants are less than 280 seconds, though thrust levels can be quite high due to the rapid combustion.

However, the use of solid propellants in the ram accelerator vehicle introduces a number of problems. The initial acceleration of the projectile during launch is as high as 1000 g's and exerts great stresses on the internal components. Solid propellants range from brittle to viscoelastic in behavior. A brittle propellant runs the risk of fracture under the initial loadings, while a propellant that is partially viscous will flow under a 1000 g acceleration, introducing containment difficulties. In addition, the propellant must be completely supported during high acceleration periods, as the wall-to-grain bonds are not capable of supporting such high G loads. This eliminates the possibility of using an aft mounted propulsion system and requires the use of an end burning grain.

Another problem lies in the performance characteristics of suitable solid propellants. For typical I_{sp}s of 230 to 250 sec and for apogee Δvs of 550 to 750 m/s, propellant masses of 401 to 557 kg are required (see Table 1) [1]. In addition, it is worth noting that: 1) the figures of Table 1 do not include the masses of the propellant casings, nozzle, piping, etc; 2) the solid rocket would only provide the first burn; 3) a liquid propellant system would be required for circularization and orbital transfer to the space station orbit, as well as attitude adjustment, since both these systems would require an on-off capability. Heat removal could also pose a problem, since the solid propellant has an end burning grain that burns at approximately 3300 K, which could cause excessive heating of the surrounding components.

TABLE 1: SOLID ROCKET PERFORMANCE CALCULATIONS

I_{sp}=230 sec

ΔV m/s	Propellant kg
550	433
650	501
750	557

I_{sp}=250 sec

ΔV m/s	Propellant kg
550	401
650	465
750	519

Propellant properties

Chemical formula approximately 70% AP, 15% Al, 15% binder
Density - 1664.3 to 2496.3 kg/m^3
Combustion temperature - 3300 K

LIQUID PROPELLANTS

The main restriction on a liquid propellant system is that the propellants must be storable. This eliminates the highest specific impulse propellants which are all cryogenic, but it is still possible to obtain reasonably high specific impulses with available storable propellants. The use of cryogenic propellants requires refrigeration systems or large amounts of insulation. This would add significant weight and undesired complexity and cost to the rocket system. Storable propellants can keep the design simple and can reduce maintenance.

Currently available storable propellants are the fuels hydrazine, N_2H_4, monomethylhydrazine, $CH_3N_2H_3$, known simply as MMH; unsymmetrical dimethylhydrazine, $(CH_3)_2N_2H_2$, known as UDMH; ammonia, NH_3; diethylenetriamine, $(H_2NC_2H_4)_2NH$; chlorine trifluoride, ClF_3; bromine pentafluoride, BrF_5; and the oxidizer nitrogen tetroxide, N_2O_4, known as NTO [2]. The decision to use only the most proven propellants limits this selection to hydrazine, MMH, UDMH, and NTO.

When NTO is used with any of the three hydrazine-based fuels the propellant combination is hypergolic. With the capability of the propellants to react spontaneously upon contact with each other, the need for external sources of power to initiate combustion is eliminated [3]. Hypergolic propellants also provide uniform ignition in the combustion chamber [2] and combustion instability problems are reduced as a consequence.

NTO is very dense (1448 kg/m^3), which makes it a good choice as an oxidizer because it will then require minimal storage volume. Other advantages include good performance, immediate availability, and low cost [2]. The only major disadvantage of NTO is that it has a relatively high vapor pressure and so its container must be slightly stronger and heavier than an oxidizer with a lower vapor pressure.

Hydrazine provides the best performance of the three fuels [4]. It has the highest specific impulse and also has the greatest density. Hydrazine also has some very important disadvantages. When exposed to mechanical shocks hydrazine can violently decompose at temperatures as low as 360 K [2]. This phenomenon can be reduced by the addition of large amounts of UDMH. Aerozine-50, a 50-50 mixture of hydrazine and UDMH, has suitable resistance to shock decomposition but at the cost of a 4% reduction in specific impulse and a decrease in density to 900.7 kg/m^3. In addition to its uses as a bipropellant, hydrazine may be used as a monopropellant by utilizing iridium as a catalyst in the decomposition process. This type of a propellant system is very attractive in its simplicity and is very often used in attitude control thrusters [3,5].

MMH offers performance close to that of hydrazine but is safer for applications where pressure shocks could occur. The specific impulse of an MMH system is only 2% lower than that of a hydrazine system. Under a pressure shock, MMH undergoes only a moderate decomposition and then only at temperatures above 490 K [2]. The density of this propellant is 874 kg/m^3. The performance and characteristics of UDMH are similar to those of MMH. UDMH offers the same shock insensitivity but at a slightly lower specific impulse and an even lower density, 786 kg/m^3.

With the possibility of pressure shocks, large amounts of hydrazine are undesirable due to safety considerations. Small amounts of hydrazine are acceptable and will be required for the attitude control thrusters. The main rocket engine will utilize MMH and NTO, as this combination offers the best performance of the shock insensitive propellants. The ratio of oxidizer to fuel is set at 1.75, which results in a ratio of specific heats, γ, of 1.25 in the combustion products.

MAIN ROCKET MOTOR DESIGN

Theory

The rocket performance equations are well known, and a simplified presentation of the formulas used follows. The thrust of a rocket in terms of mass flow, m, and effective exhaust velocity, C, is

$$T = \dot{m}\, C \tag{1}$$

where the effective exhaust velocity is given in terms of the specific impulse, I_{sp}, and earth's gravitational constant, g_o, as

$$C = I_{sp}\, g_o \tag{2}$$

Thrust may also be expressed in terms of throat area, A_t, thrust coefficient, C_f, chamber pressure, P_c, and thrust correction factor, ζ_f, as

$$T = A_t\, C_f\, P_c\, \zeta_f \tag{3}$$

where C_f depends on γ and the pressure ratio such that

$$C_f = \gamma\sqrt{\frac{2}{\gamma-1}}\left(\frac{2}{\gamma+1}\right)^{\frac{(\gamma+1)}{2(\gamma-1)}}\left(1-\left(\frac{P_e}{P_c}\right)^{\frac{(\gamma-1)}{\gamma}}\right)^{-\frac{1}{2}}\left[1+\frac{(\gamma-1)}{2\gamma}\left(\frac{P_c}{P_e}\right)^{\frac{1}{\gamma}}\frac{\left(\frac{P_a}{P_c}-\frac{P_a}{P_c}\right)}{\left(1-\left(\frac{P_e}{P_c}\right)^{\frac{(\gamma-1)}{\gamma}}\right)}\right] \tag{4}$$

The thrust correction factor is used to account for losses arising from nozzle boundary layers and the use of a nonideal nozzle. For this design it is reasonable to assume a thrust

correction factor of 0.96 [6].

The pressure ratio should be as high as possible to attain a large thrust coefficient. The maximum value of the thrust coefficient, corresponding to a pressure ratio (P_c/P_e) of infinity when $P_a=0$, as is the case in orbit, is 2.08 for $\gamma=1.25$. In addition to determining the thrust coefficient, the pressure ratio also sets the area ratio (A_e/A_t).

$$\frac{A_e}{A_t} = \sqrt{\frac{\gamma-1}{2}} \left(\frac{2}{\gamma+1}\right)^{\frac{(\gamma+1)}{2(\gamma-1)}} \left(1 - \left(\frac{P_e}{P_c}\right)^{\frac{(\gamma-1)}{\gamma}}\right)^{-\frac{1}{2}} \left(\frac{P_c}{P_e}\right)^{\frac{1}{\gamma}} \qquad (5)$$

From Eq's. 4 and 5, it is apparent that once the pressure ratio is set, the area ratio and thrust coefficient become fixed.

Another useful quantity is the characteristic velocity, C*. It can be expressed as a function of the effective exhaust velocity and the thrust coefficient. The definition of the characteristic velocity is [7].

$$C^* = C / C_f \qquad (6)$$

where

$$C^* = \left(\frac{\gamma+1}{2}\right)^{\frac{(\gamma+1)}{2(\gamma-1)}} \sqrt{\frac{RT_t^*}{\gamma}} \qquad (7)$$

The characteristic velocity is determined chiefly by propellant properties and partially by chamber pressure. Once the propellant is selected, the thrust and specific impulse can be altered by tailoring the pressure ratio.

PROPULSION SYSTEM CONFIGURATION

In addition to the main rocket engine, the onboard propulsion system consists of propellant tanks, valves and tubing, attitude control thrusters, a control package, and a propellant delivery system. The two types of propellant delivery systems currently in use are pump fed and pressure fed. For use in the ram accelerator, pump fed systems are impractical because it is unlikely that the pumps could withstand the high acceleration loadings to which the vehicle will be subjected at launch. An attractive alternative to pump systems is found in pressurized propellant delivery systems, which are virtually insensitive to high accelerations.

Propellant Delivery

The standard method for pressurizing a propellant tank is to use an inert gas, such as helium, stored in a separate tank. This gas is released into the propellant tanks during flight by means of an explosive valve (Fig VI-1). The helium flow into the three propellant tanks is controlled by a pressure regulator, and each tank is isolated by a check valve which allows the helium to enter the tank but prevents the propellant from escaping. Once the explosive valve is opened the helium flows into the tanks and forces the propellants out the other side.

The helium-pressurized system carries an extra tank for storing the helium. The volume of the helium container is given by [5]

$$V_{He} = V_P P_r \lambda / (P_i - P_f) \qquad (8)$$

The polytropic expansion coefficient, λ, which corrects for effects of heat flow to the helium container, has an approximate value of 1.2 for this application [5]. The regulated pressure to the system must be higher than the chamber pressure, (the maximum chamber pressure delivered by a pressure fed system is typically 2.0 MPa or about 20 atm), and the helium residual pressure should be slightly higher than the regulated pressure. The

regulated pressure was chosen as 2.8 MPa (28 atm); the final helium pressure as 3.1 MPa (31 atm); and the initial helium pressure as 17.2 MPa (170 atm). The mass of the helium container is dependant upon its configuration and the initial pressure.

A relatively new idea in the field of pressurized propellant delivery systems is the use of a small hydrazine gas generator as an alternative method of pressurizing the tanks during flight (Fig VI-2). The system is started with a pressure charge which initially pressurizes the hydrazine tank, forcing some hydrazine across an iridium catalyst embedded in aluminum oxide. The gas generated by the catalytic decomposition of the hydrazine is then fed into the propellant tanks to pressurize them. The mass of hydrazine required to pressurize the tanks is given by [5]

$$m_h = V_P P_r / 850{,}000 \qquad (9)$$

One problem with the gas generator method of pressurization is the heat generated by the decomposition of the hydrazine. In tests run by Rocket Research Company this heat was negligible [6], but if long gas generation times occur, heating could be a considerable problem. Further study of heat generation needs to be performed.

Another problem is the need to prevent the helium or the hydrazine-generated gases used to pressurize the tanks from mixing with the liquids in the tanks. This is prevented by a simple, flexible diaphragm which is initially flush with the tank wall on the side of the pressurizing gas inlet. As the contents are consumed the diaphragm traverses the tank pushing propellant ahead of it. Due to the reactivity of rocket propellants, the diaphragm is most commonly made of stainless steel [5]. This choice of material requires that tanks be of spherical or quasi-spherical design to reduce the strains on the diaphragm as it meets corners. The corrosive effects of the propellants also require that the tanks be made of a material which resists reaction. Most propellant tanks

have been constructed of titanium, but it is possible to build the tanks of composites with an inner lining of titanium.

In addition to the check valves discussed above, each tank is equipped with an isolation valve which keeps the propellants in the tanks until just prior to the initial burn. This isolation valve is provided as a safety device to prevent leakage of the propellants.

Attitude Control Thrusters

The propulsion system also requires attitude control thrusters. Eight 220 N thrusters will be sufficient for the vehicle [5]. These thrusters use hydrazine as a monopropellant and are very simple and reliable. They are very light (approximately 1 kg) and small (roughly 20 cm long by 4 cm in diameter) but cost $15,000 to $20,000 each [8]. A good estimate of the amount of hydrazine required to run these thrusters is 5% of the mass of the main propulsion fuel, MMH [4].

A control system is required to activate the main rocket and the attitude control thrusters at the appropriate moments. A simple timer could activate the main engine when needed, and accelerometers can measure the Δv to a very high degree of accuracy. Gyroscopes could measure the projectile's attitude, and these measurements could signal when the attitude thrusters need to be used. Such systems are in common use and are relatively lightweight and inexpensive.

RESULTS

Main Rocket Motor

Most nozzles built today are contour nozzles, and this type is employed here also. The exit diameter of the nozzle is taken as 40 cm so that the engine can be placed in either the forward or rear tapered section of the projectile without wasting excessive amounts of volume (See Fig VII-1 in Chapter VII). Figure VI-3 shows the relationship

between thrust and area ratio at various chamber pressures for a contour nozzle having a fixed exit area. From this graph it is evident that the highest possible chamber pressure (2.069 MPa or 20 atm), corresponding to the maximum value attainable with a pressure feed system, should be used.

Figure VI-4 shows the relationship between specific impulse and area ratio for several characteristic velocities typical of hydrazine-based propellants. The theoretical characteristic velocities of the hydrazine based propellants considered in this study range from 1700 m/s to 1750 m/s [6]. On the other hand, a Rocketdyne publication [9] on real hydrazine-based rocket motors, similar to the type required for the present vehicle, lists characteristic velocities between 1530 m/s and 1630 m/s. Based upon the Rocketdyne information, a characteristic velocity of 1580 m/s is assumed.

The minimum thrust, T, that the main engine must produce is determined from

$$T \geq m_o a \tag{10}$$

where m_o is the mass after atmospheric transit and a is the desired acceleration. An acceleration of one-half g, 4.9 m/s^2, results in a minimum thrust of 9710 N. The design value for thrust is taken as 10,000 N, which gives a nozzle area ratio of 46.0, a throat diameter of 5.90 cm, and a specific impulse of 297 sec. Thrusts exceeding 10,000 N yield specific impulses which rapidly decrease for the fixed nozzle exit area (see Figs VI-3 and VI-4).

The nozzle length can be approximated by assuming a conical nozzle with a 15^o half-angle. Figure VI-5 shows nozzle length versus area ratio. For an area ratio of 46.0 the length is 63.6 cm. A contour nozzle would be slightly shorter than this. Rockets of a size similar to this design typically have a nozzle length which is approximately two-thirds of the total length of the engine [9]. The overall length of the engine is thus approximately 95 cm. Similarly, the engine mass and thrust are related [9] in such a way that for 10,000 N thrust the engine mass is about 60 kg, including the extra mass required

to make the engine restartable. Engine cooling was not studied but most engines which would fit the ram acceleartor application are radiation cooled [9]. The approximate cost of such an engine is $500,000 to $1,000,000 [8], however, significant cost reductions may be possible due to the large number of units that will be required for the ram accelerator mass launch system.

Propulsion System

The first burn (at the ballistic apogee) is the longest and most critical one, as a small error in the velocity increment can dangerously affect the aerobraking maneuver. The burn time is found as follows. The velocity change of the vehicle is the integral of the acceleration over the burn time

$$\Delta v = \int_0^{\tau} a \, dt \tag{11}$$

The acceleration is the ratio of thrust, which is constant, to the instantaneous mass.

$$\Delta v = \int_0^{\tau} T/m \, dt \tag{12}$$

However, the mass at any point in time is the mass after atmospheric transit minus the mass flow rate of propellants multiplied by the time into the burn.

$$\Delta v = \int_0^{t} T/[m_o - \dot{m} t] \, dt \tag{13}$$

The mass flow rate is simply the total amount of propellant burned divided by the total burn time, assuming a constant mass flow.

$$\Delta v = \int_0^{\tau} T/[m_o - (m_{p1} t / \tau)] \, dt \tag{14}$$

Integrating yields,

$$\Delta v = (T \tau / m_{p1}) \{\ln[m_o] - \ln[m_o - m_{p1}]\} \tag{15}$$

Solving for the burn time:

$$\tau = (\Delta v\, m_{p1} / T)\, \{\ln[m_o] - \ln[m_o - m_{p1}]\}^{-1} \qquad (16)$$

expressed in terms of Δv, pre-burn vehicle mass, m_o, and mass of propellant burned, m_{p1}. A plot of Eq. 16 is shown in Fig VI-6. For example, for Δv's of 500 m/s to 800 m/s (possible first burns) the burn times are 92 to 140 seconds. Not only is the one-half g acceleration requirement met, but the short burn times indicate the finite burn time errors will be minimized.

The mass ratio, i.e, the ratio of vehicle mass before burns to vehicle mass after all burns have been completed, is [7].

$$MR = e(\Delta v/C) \qquad (17)$$

Using this equation, the total amount of propellant consumed varies from 290 kg to 560 kg for velocity changes of 450 to 990 m/s (Fig VI-7).

Masses of the various valves and other hardware were obtained from the Rocket Research Company [5] and quantities are tabulated in Tables VI-2 and VI-3. Required helium and hydrazine masses for the two types of propellant delivery systems are calculated using Eqs. 8 and 9. An additional 1% must be added to Helium, fuel, and oxidizer masses as current diaphragm technology is capable of removing only slightly over 99% of the propellant from the tanks [3]. A summary of these calculations is given in Tables VI-2 and VI-3. The total mass of the pressurized helium propulsion system is 146.2 kg, excluding the propellant tanks. With propellant and tanks, the mass of this system is 543.0 kg for a ΔV of 500 m/s and 740 kg for a ΔV of 800 m/s. The system using the gas generator to pressurize the propellant tanks has a total mass of 490 and 670 kg for ΔVs of 500 and 800 m/sec respectively, including propellant and propellant storage tanks. This is 50 to 70 kg lighter than the Helium pressurized system, and is an advantage of the gas generator system.

TABLE VI-2:TOTAL PROPULSION SYSTEM MASS PRESSURIZED HELIUM CONFIGURATION

MAIN ENGINE SPECIFICATIONS

THRUST	10,000 N
MASS	60 kg
LENGTH	95 cm
I_{sp}	297 sec
O/F RATIO	1.75

PROPULSION SYSTEM DATA

P_r	2.76 MPa
P_i	17.24 MPa
P_f	3.10 MPa

ATTITUDE CONTROL THRUSTERS	8 @ 1.0 kg each	8.0	kg
CONTROL SYSTEM		10.0	kg
FILL VALVES	4 @ 0.1 kg each	0.4	kg
EXPLOSIVE VALVE	1 @ 0.5 kg each	0.5	kg
CHECK VALVES	3 @ 0.3 kg each	0.9	kg
ISOLATION VALVES	3 @ 0.5 kg each	1.5	kg
PRESSURE REGULATOR	1 @ 1.0 kg each	1.0	kg
TUBING	20 m @ .2 kg/m	4.0	kg

TOTAL ΔV (m/s)	500	650	800
BURN TIME (sec)	92.0	116.5	140.4
NTO MASS (kg)	197.2	254.4	298.9
MMH MASS (kg)	112.8	145.6	171.8
N_2H_4 MASS (kg)	5.6	7.3	8.6
He MASS (kg)	113.4	214.7	172.2
MASS OF PROPELLANT AND HELIUM TANKS (kg)	106.1	130.3	136.8
TOTAL MASS (kg)	**621.4**	**838.6**	**874.6**

TABLE VI-3:TOTAL PROPULSION SYSTEM MASS
GAS GENERATOR CONFIGURATION

MAIN ROCKET SPECIFICATIONS

THRUST	10,000 N
MASS	60 kg
LENGTH	95 cm
I_{sp}	297 sec
O/F	1.75

PROPULSION SYSTEM DATA

ATTITUDE CONTROL THRUSTERS	8 @ 1.0 kg each	8.0	kg
CONTROL SYSTEM		10.0	kg
FILL VALVES	3 @ 0.1 kg each	0.3	kg
PRESSURE CHARGE	1 @ 0.5 kg each	0.5	kg
CHECK VALVES	3 @ 0.3 kg each	0.9	kg
ISOLATION VALVES	4 @ 0.5 kg each	2.0	kg
GAS GENERATOR	1 @ 0.5 kg each	0.5	kg
TUBING	20 m @ .2 kg/m	4.0	kg

TOTAL Δv (m/s)	500	650	800
BURN TIME (sec)	92.0	116.5	140.4
NTO MASS (kg)	197.2	254.4	298.9
MMH MASS (kg)	112.8	145.6	171.8
N_2H_4 MASS (kg)	5.3	6.8	7.1
MASS OF PROPELLANT TANKS (kg)	79.0	93.1	103.9
TOTAL MASS (kg)	**480.5**	**586.1**	**667.9**

CONCLUSION

This study has shown that the onboard propulsion system for the ram accelerator vehicle does not require new technology or present any major technical problems. A liquid propellant rocket engine using monomethylhydrazine and nitrogen tetroxide appears to be the most practical choice. Such a system would employ a gas generator propellant delivery system to reduce system mass. The remaining propulsion system components are commercially available at reasonable costs. The cost of the main engine and the attitude control thrusters could approach $1.2 million, which indicates that engine recovery and re-use is necessary for the ram accelerator to be cost effective. However, the large number of units required would most likely reduce the costs significantly. The entire propulsion system mass is approximately 30% of the proposed vehicle launch mass of 2000 kg, which is very promising. Further studies need to be performed in the area of heat generation by the main engine and the gas generator system, but preliminary studies do not indicate a problem.

REFERENCES

1. Micheli, Paul, formerly of Aerojet General, Private Communication, March 1988.

2. Holzman, R.T., Chemical Rockets, Marcel Dekker, New York, 1969, pp. 171-182.

3. Landel, R.F., Rembaum, A., Chemistry in Space Research, American Elsevier Publishing Company, Inc., New York, 1972, pp. 267, 465-593

4. Schmidt, E.W., Hydrazine and Its Derivatives, John Wiley & Sons, New York, 1984, p. 807.

5. Schmitz, Bruce, Rocket Research Company, Private Communication, February 1988.

6. Sutton, G.P., Ross, D.M., Rocket Propulsion Elements, John Wiley & Sons, New York, 1976, pp. 76-78.

7. Oates, G.C., Aerothermodynamics of Gas Turbine and Rocket Propulsion, American Institute of Aeronautics and Astronautics, Inc., New York, 1984, pp. 52, 61-72.

8. Peineman, Fred, Rockwell International, Rocketdyne Division, Private Communication, February 1988.

9. "A Past to Build a Future On", Rockwell International, Rocketdyne Division, Publication 571-N-2 NEW 9-84.

NOMENCLATURE

a	acceleration of vehicle
A_e	nozzle exit area
A_t	nozzle throat area
C	effective exhaust velocity
C_f	thrust coefficient
C^*	characteristic velocity
g_o	gravitational acceleration at Earth's surface
I_{sp}	specific impulse
m	vehicle mass at any point in time
$\dot{m}$	mass flow rate
m_o	vehicle mass after ablation
m_{pl}	mass of propellant burned during initial burn
MR	mass ratio, total mass to payload mass
P_c	combustion chamber pressure
P_e	nozzle exit pressure
P_f	final Helium pressure
P_i	initial Helium pressure
P_r	regulated pressure of propulsion system
R	gas constant
t	time
T	thrust
T_t^*	total temperature at the throat
γ	ratio of specific heats
Δv	velocity change
τ	burn time
ζ_f	thrust correction factor

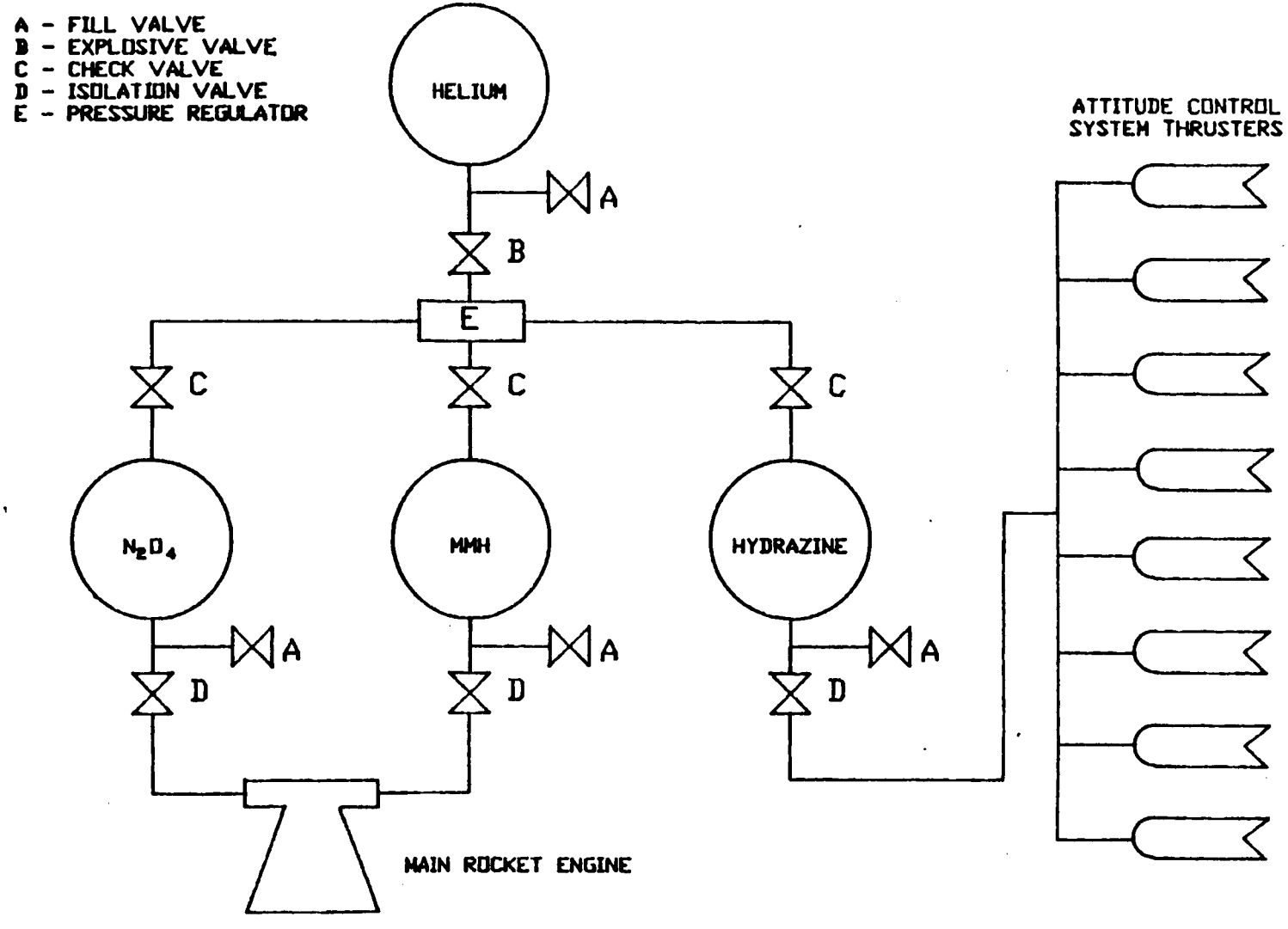

Fig VI-1 Schematic of Helium Pressure Fed Propulsion System

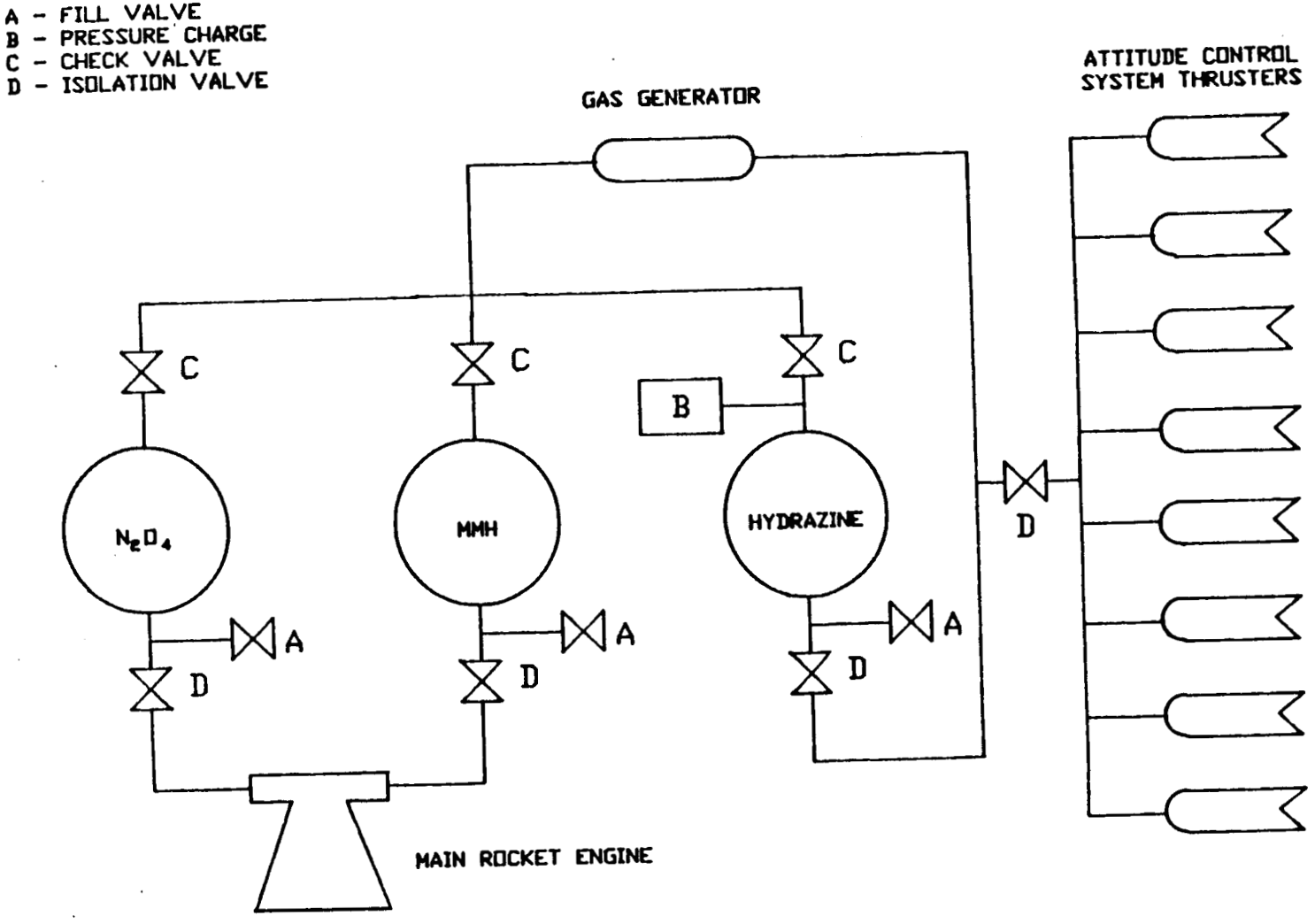

Fig VI-2 Schematic of Gas Generator Pressure Fed Propulsion System

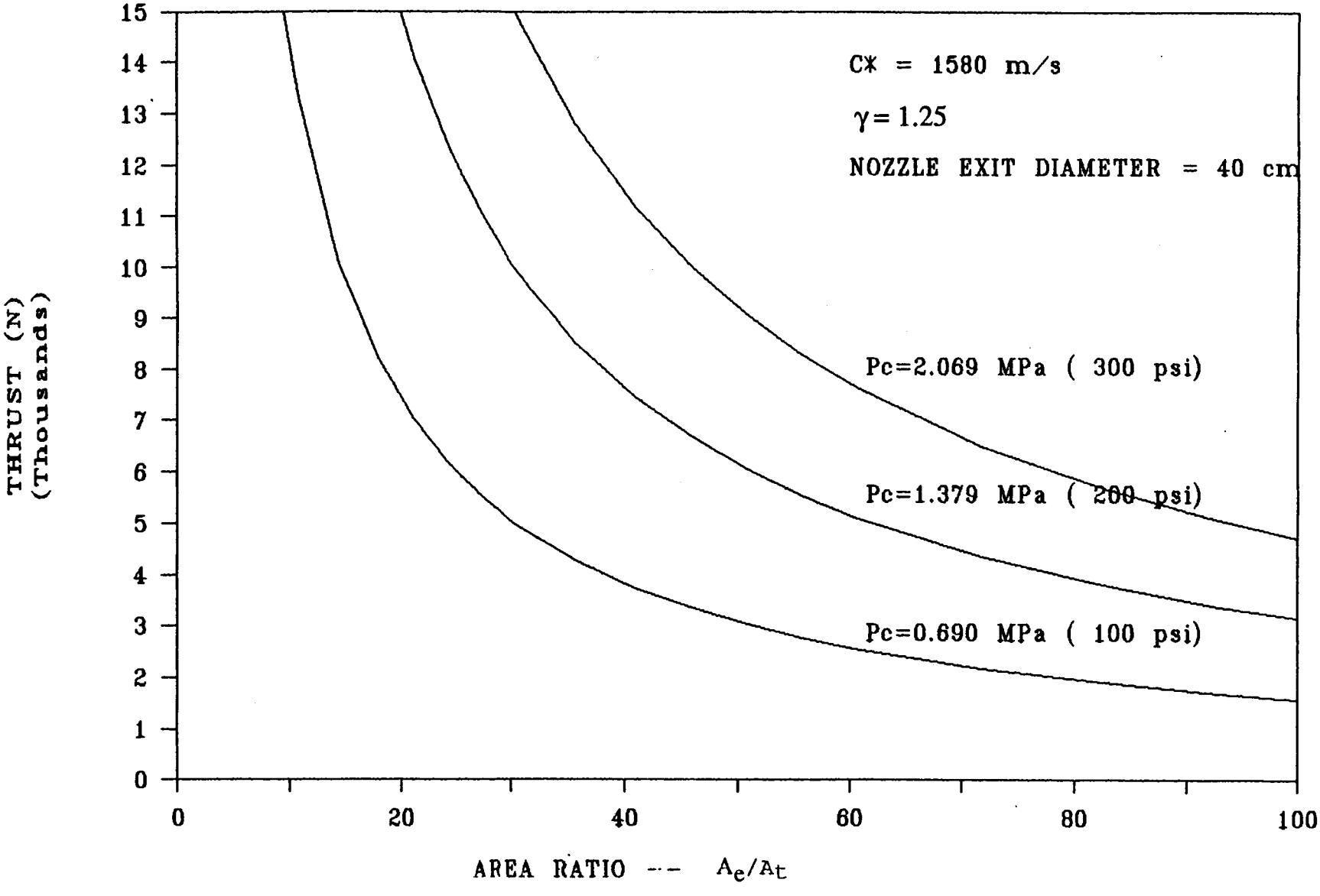

Fig VI-3 Variation of Thrust with Area Ratio for Several Different Chamber Pressures and Fixed Exit Area

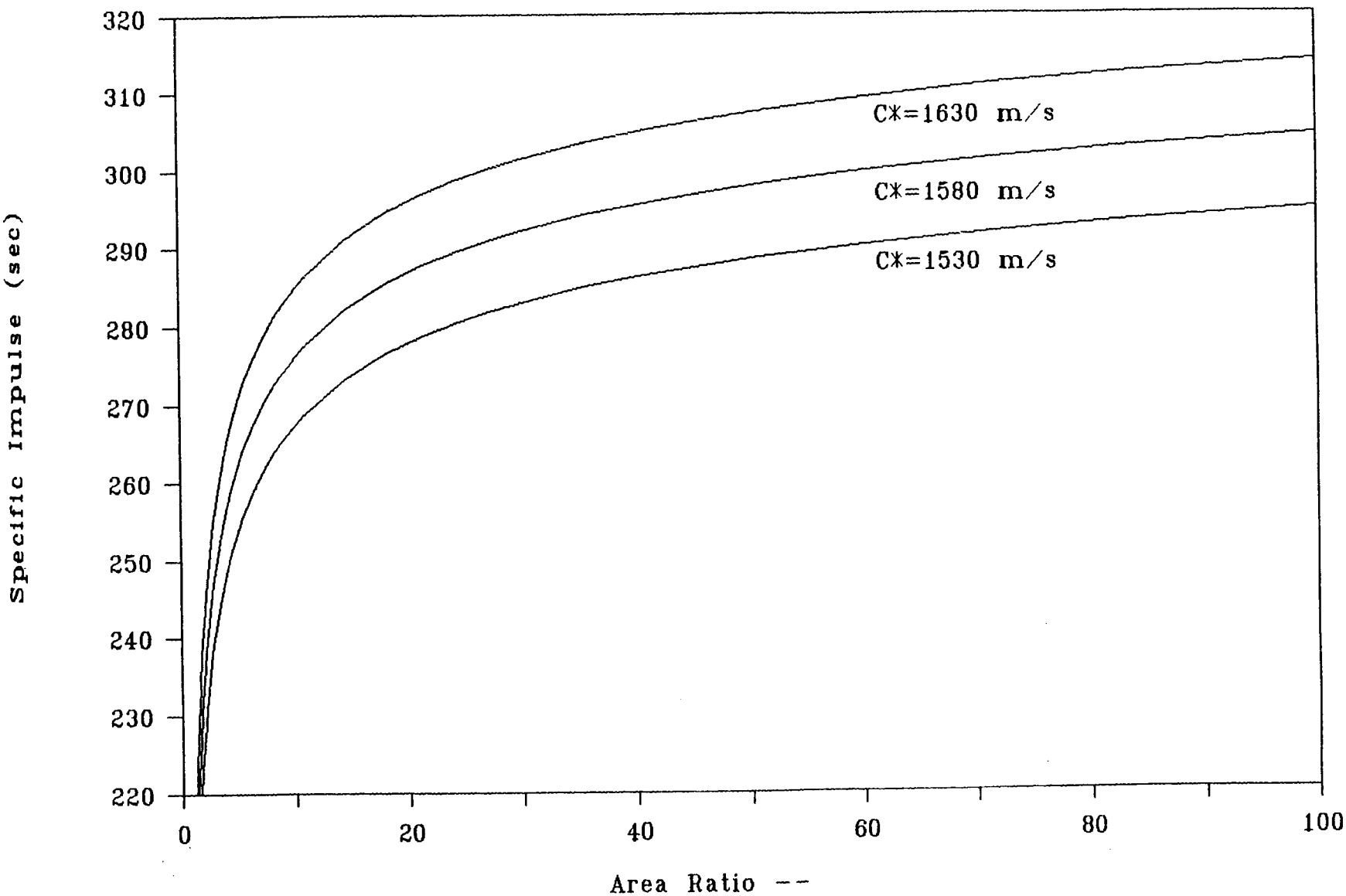

Fig VI-4 Variation of Specific Impulse with Area Ratio for Several Different Characteristic Velocities

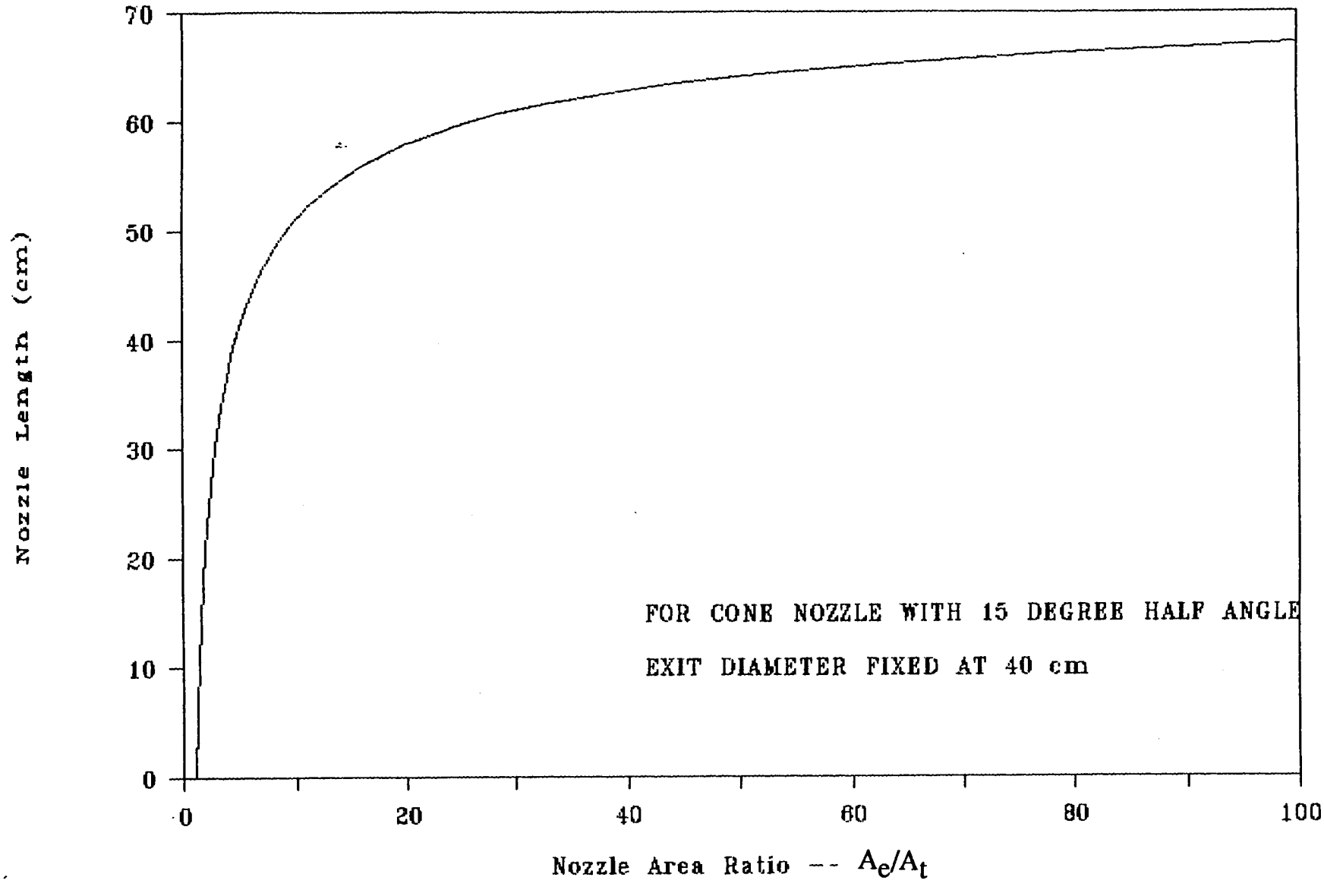

Fig VI-5 Required Nozzle Length for a Cone Nozzle with a 15 Half Angle and an Exit Diameter = 40 cm

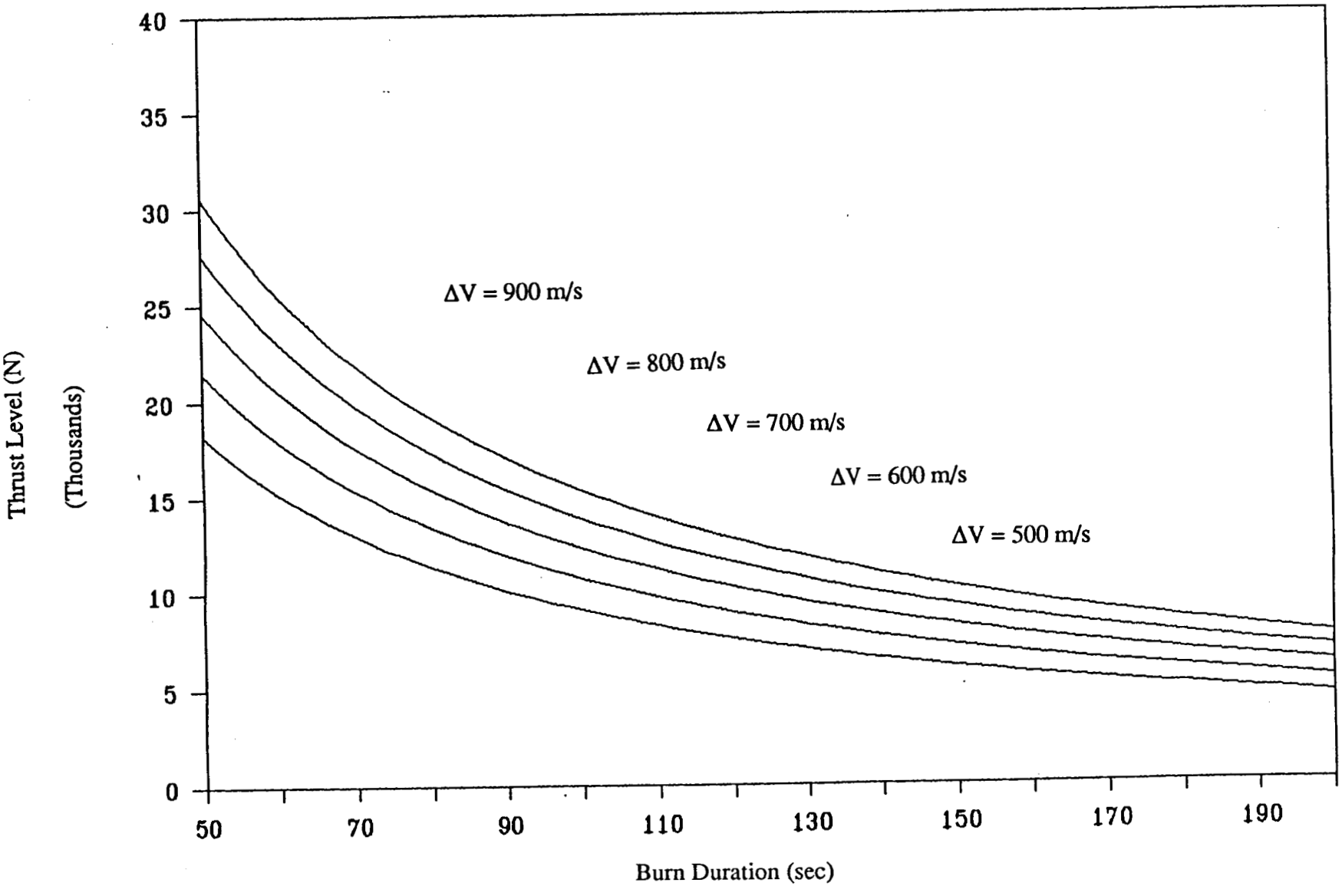

Fig VI-6 Variation of Burn Time with Thrust for Initial Burn at Various Required Velocity Increments

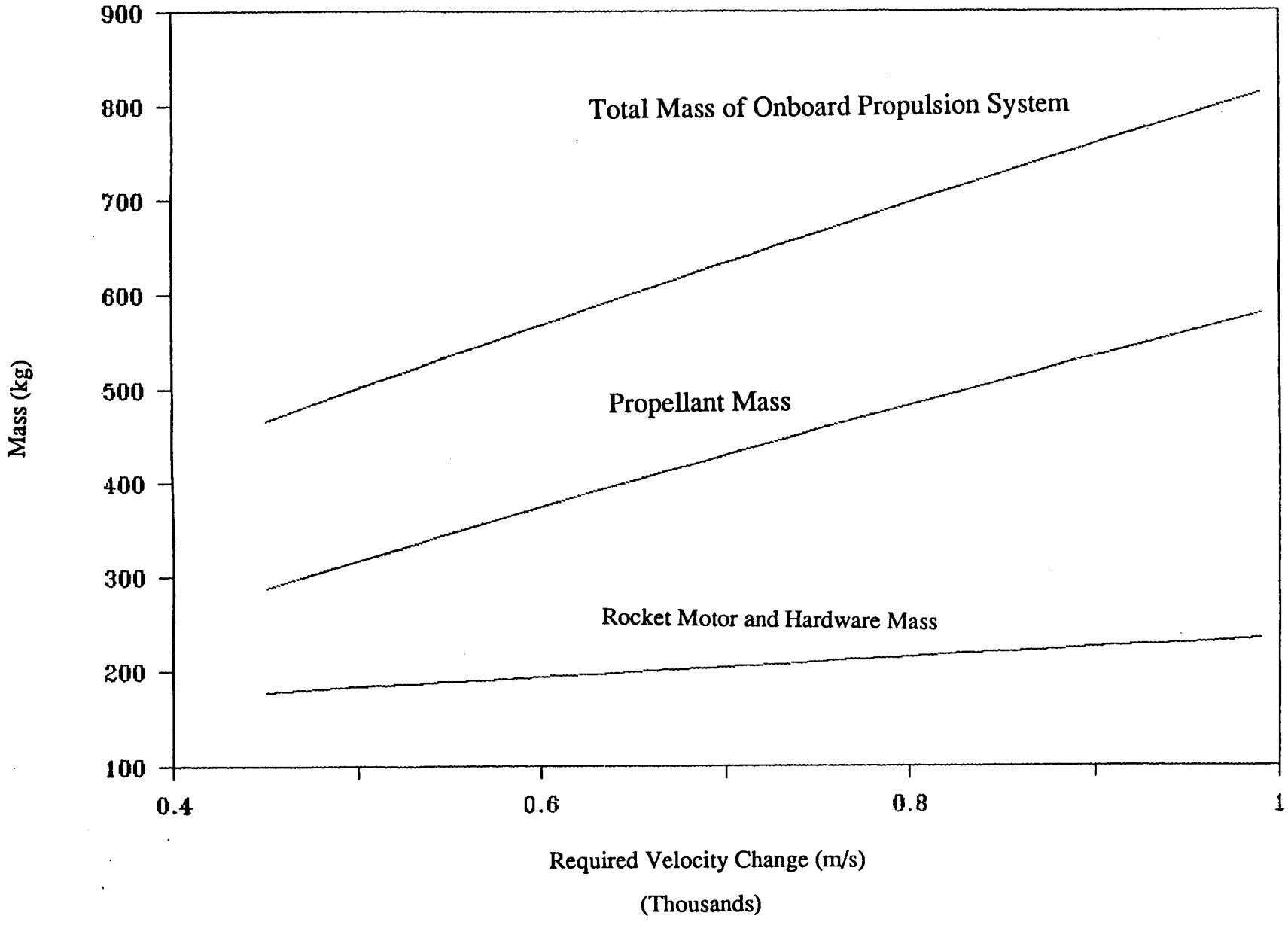

Fig VI-7 Mass of On-board Propulsion System for Varying Velocity Change Requirements

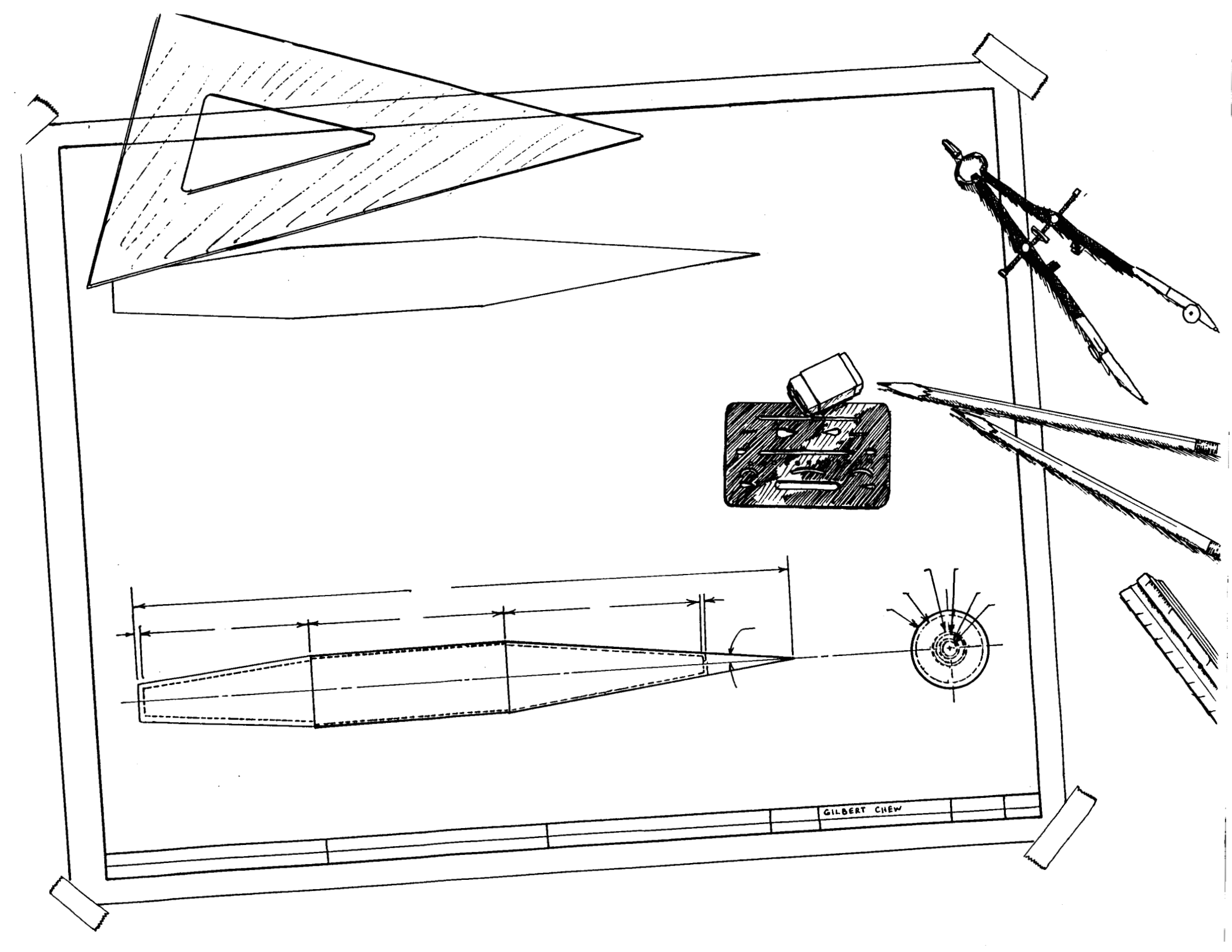
GILBERT CHEW

VII. STRUCTURAL DESIGN OF THE PAYLOAD VEHICLE AND LAUNCH TUBE

Carlos Rodriguez
Jack Wolda

INTRODUCTION

The overall success of the ram accelerator concept depends ultimately on the successful design of a payload vehicle. In the design process, it becomes evident that on-board propulsion, flight mechanics, orbital mechanics and aerobraking, and launch tube design are all highly sensitive to vehicle mass and geometry. To optimize the performance of the ram accelerator, the vehicle must meet the following requirements:

The vehicle must withstand a 1,000g acceleration, a maximum pressure of 169 MPa (25 Ksi), and temperatures of the order of 3,000 °K to 4,200 °K for brief periods (~1 sec). The total mass is 2,000 kg, and a payload fraction of 50% is desired. This vehicle must accommodate a rocket and propellants for circularization maneuvers and attitude controls for stability.

This chapter emphasizes the design of the payload vehicle and presents a simple approach to launch tube design. In the preliminary analyses, simplified models are used to determine stress components and, ultimately, shell thicknesses. These results then serve as a starting point for a finite element analysis. The cargo vehicle is similar to the centerbody of a conventional ramjet; a fixed launch tube is used as the outer cowling of the ramjet and is filled with a premixed fuel and oxidizer mixture. A point-design outside diameter of 0.76 for the payload vehicle was chosen as noted earlier in this report.

VEHICLE CONFIGURATION COMPARISON

This section discusses the effect of the location of various internal components on the physical and structural properties of the vehicle. The physical properties include mass, total length, center of gravity, and other geometric characteristics. The structural design criteria

address vehicle resistance to axial buckling, resistance to pressure collapse, and overall structural soundness. Two basic configurations were proposed and examined: 1) the rocket nozzle is located in the rear with the payload compartment in the front, 2) the rocket is in the front with the payload compartment aft. These two configurations are shown in Fig. VII-1. Before addressing the advantages and disadvantages of each configuration, some of the constraints placed by other than structural considerations are discussed.

One of the requirements for vehicle stability is that the center of gravity be placed as far forward as possible to minimize the extent of attitude control needed. This suggests that the payload be placed immediately behind the nose cone ablator (type 1 in Fig. VII-1) since the mass of the payload is expected to be approximately half of the launch mass. This would place the rocket motor in the tail of the vehicle, since the rocket nozzle must be located either in the nose or the tail of the vehicle so that the circularization burn can be performed. This configuration requires the removal of either part of the nose or part of the tail section so that the nozzle may be exposed.

One of the disadvantages of locating the rocket motor in the rear is that the blunt shape of the tail cannot be used in the aero-braking maneuver currently being studied. However, it was decided that the stability problem is more serious than the aero-braking inconvenience, and that nose first aerobraking is acceptable. Since no major advantages in the type 2 configuration could be found, the type 2 configuration was discarded.

The propellant tanks must be arranged in such a way that the center of gravity be as far forward as possible. If the payload is placed in the front, then the propellant tanks must be located between the rocket motor and payload (in the middle). For stability considerations, the three propellant tanks should be arranged such that the densest propellant is closest to the front. Another approach is to put the N_2O_4 tank ahead of the payload compartment since it is has a density of 1443.7 kg/m^3.* This would help move the center of gravity forward, but there would be increased complexities in propellant tubing and a

*It was assumed for present purposes that the payload is water.

corresponding increase in total launch mass. These complexities were avoided since, as will be seen later, any unnecessary increase in total launch mass is undesirable.

PRESSURE AND TEMPERATURE DISTRIBUTIONS

The worst case pressure distributions over the vehicle of the ram accelerator were found for both the thermally choked mode and the oblique detonation mode. These pressure distributions were obtained from computer simulations of the two in-tube launch modes of the ram accelerator [1], as discussed in Chapter III. For the thermally choked mode, the maximum pressure was obtained at a velocity of 1.6 km/sec with $0.8CH_4 + O_2$. Fig. VII-2 shows the pressure distribution as a function of percent body length. The graph reveals that the pressure increases from 3 MPa (.4 Ksi) to 12 Mpa (1.74 Ksi) along the cone, and then stays constant until the point in front of the normal shock. This shock causes the pressure to jump to 90 MPa (13 Ksi), and the pressure then slowly increases towards the rear of the body to a value of 94 MPa (14 Ksi).

In the oblique detonation drive, the peak pressure distribution occurs at a velocity of 7.2 km/s with a fill mixture of $8H_2 + O_2$ (Fig. VII-3). The pressure along the nose cone and body is relatively constant at 20 MPa (2.9 Ksi). For this simulation, the frustum that creates the strong shock wave used to ignite the gas mixture is at 72% body length. Nevertheless, the optimum location and height of the frustum remains to be determined. Here the pressure jumps to a maximum of 169 (25 Ksi), decreases to 140 MPa (20 Ksi) at the rear corner, and then decreases linearly along the rear cone to 17 MPa (2.4 Ksi).

From the same computer simulations, the temperature distribution along the body for the oblique detonation drive was obtained and is shown in Fig. VII-4. The temperature on the body before the frustum remains constant at about 360 °K. After the oblique shock, it jumps to 4,200 °K, and decreases linearly along the rear cone to a value of 2,900 °K. The temperature effects on the design of the vehicle are discussed in the following section.

CHOICE OF MATERIAL

After extensive research as to which material to use for the main frame of the vehicle, the following two were chosen: graphite/epoxy (T300/5208) and titanium alloy (Ti-8Mo-8V-2Fe-3Al). The graphite/epoxy's favorable characteristics are its light weight, high ultimate strength, high modulus, and low production cost compared to other composites. High-strength T300/5208 (ρ = 1550 kg/m^3) was chosen from the group of graphite/epoxy composites because it is approximately 50% stronger in transverse and longitudinal compression than high-modulus or ultrahigh-modulus graphite/epoxy. Titanium, although it is three times denser than graphite/epoxy, is two and a half times stronger, thus requiring a thinner body wall and increasing the payload volume. Titanium is also easier to manufacture and machine although it is more expensive than graphite/epoxy. The general properties of T300/5208 are compared to those of titanium alloy in Table VII-1.

Composites are directional in nature, and as a result, it is possible to construct the material so that it will meet specific load requirements without wasting material and weight, and provide stiffness and strength only where needed. Although allowing the designer to tailor the material for the specific loading conditions, the anisotropic nature of composites creates the problem of selecting the proper orientation for the design application. This, however, does not occur in metal design because metal is isotropic. Therefore, the analysis and design for composites must be refined to higher orders to provide a basis for selecting proper orientation and for defining stresses on the body. Thus, the average properties of a layup orientation of $(0^\circ/90^\circ)_s$ were chosen for the isotropic approximation because this gives the highest strength, considering the biaxial loading conditions imposed on the body [2]. This layup is shown in Fig. VII-5. By convention, the 0° direction is defined in the direction of the acceleration and the layup is indicated to be symmetric by the subscripted s.

TABLE VII-1: COMPARISON OF PROPERTIES OF GRAPHITE/EPOXY AND TITANIUM ALLOY

PROPERTIES	GRAPHITE/EPOXY (T300/N5208)	TITANIUM ALLOY (Ti-8Mo-8V-2Fe-3Al)
Ultimate Transverse Compression Strength	526 MPa (76.3 Ksi)	1310 MPa (190 Ksi)
Ultimate Longitudinal Compression Strength	517 MPa (75 Ksi)	1310 MPa (190 Ksi)
Longitudinal Compression Modulus	60.9 GPa (9.1 Msi)	113 GPa (16.5 Msi)
Transverse Compression Modulus	60.1 GPa (9.0 Msi)	113 GPa (16.5 Msi)
In-Plane Modulus $(0/\pm45/90)_s$	69.9 GPa (10.1 Msi)	N/A
Out-of-Plane Modulus $(0/\pm45/90)_s$	9.65 GPa (1.4 Msi)	N/A
Density	1550 kg/m^3 (.056 lb/in^3)	4844 kg/m^3 (.175 lb/in^3)
Poisson's Ratio	0.297	0.3

The other options for materials were aluminum, graphite/polyimide composites, metal matrix composites (graphite/aluminum, graphite/titanium), and ceramic matrix composites. These were all discarded for reasons of high cost (metal matrix composites, graphite/polyimide), brittleness (ceramic matrix composites), or comparatively low strength (aluminum).

The only problems foreseen using T300/5208 or ultra strength titanium alloy are their low temperature tolerance. The vehicle sees a maximum temperature of 4200 °K, and the maximum short term temperature, neglecting moisture effects, that T300/5208 can withstand, is 450 °K. The maximum service temperature for titanium is 922 °K. However, because the vehicle sees this temperature for approximately one second, it is possible and feasible to

wrap the vehicle in a thin ablative shield such as carbon/carbon composite which is a standard ablative material.

SHELL ANALYSIS

Isotropic Approximation

Current analytical solutions to shell structures are not applicable to arbitrary shapes, load conditions, or anisotropic stiffnesses. Thus, numerical solutions are necessary for better than first order approximations. However, a first-order approximation for the thickness of the payload vehicle can be made by assuming isotropic properties, constant pressure distributions, and a simple geometry. These preliminary thicknesses can then be used in a finite element analysis to ultimately optimize the vehicle mass.

To begin the first order analysis, a thin shell approximation was made using cylinders with the mechanical properties of the titanium alloy described above. Constant cylinder radii and thicknesses were also assumed. The analysis was performed for four different sections as shown in Fig. VII-6. Since part of the nose cone consists of an ablative material for thermal protection during atmospheric transit, the ablative material is not treated as part of the load bearing structure. Thus, for structural design purposes, the nose cone looks much like the truncated tail cone. This truncation simply results in a reduction in length since the nose cone and tail cone were also assumed to be cylinders for lack of better analytical solutions with the prescribed loading. The radius of each cone was taken to be its mean radius. Since the cone half angles are small (7° and 5° for the front cone and tail cone, respectively), the results should be well within first order accuracy. Thus, the vehicle is divided into four sections as mentioned earlier, all of which are cylindrical. These assumed geometries are also shown in Fig. VII-6. To obtain a conservative estimate, the internal hydrostatic pressure of the liquid payload was assumed negligible. This dictated the thickness of a thin cylindrical shell as given by the hoop stress equation,

$$\sigma_2 = \frac{p\,r}{t} \tag{1}$$

Because the resultant thicknesses at the two sections upstream of the frustum required by the oblique II detonation drive were very thin (on the order of 1 mm), the possibility of buckling failure was recognized. For a long uniform thin-walled cylindrical shell the critical thickness is given by

$$t = (5Nr/3E)^{0.5} \tag{2}$$

For the two sections downstream of the frustum (sections III and IV in Fig. VII-6), the thin shell analysis yielded thicknesses greater than one-tenth the radius and rendered the thin shell approximation invalid. An analysis for thick-walled cylinders was then performed for the more heavily loaded areas from equations presented by Roark [3]. The simple equations for thick walled cylinders are as follows:

$$\sigma_1 = 0 \tag{3}$$

$$\sigma_2 = -q \frac{2a^2}{a^2 - b^2} \tag{4}$$

$$\sigma_3 = - q \tag{5}$$

$$\tau = q \frac{a^2}{a^2 - b^2} \tag{6}$$

Again, sections III and IV were modeled as cylinders of circular cross-section with constant radii and thicknesses.

Note that none of the equations presented above account for stress interactions. Thus, the design is made such that the structure can withstand the highest stress at each section. Section II is designed with the buckling criterion and Sections I, III, and IV are designed for the hoop stress. The thick-wall solutions assume no longitudinal stress. The longitudinal

stress was separately computed by modeling the vehicle as a cylinder with hemispherical caps rather than using the leading and trailing cones. The terms comprising the longitudinal stress were due to the external pressure at the aft end, and the acceleration of the vehicle. It was found that the longitudinal stress is smaller than the hoop stress predicted by Eq. 6. Thus, only the hoop stress entered into the design of sections III and IV. The thicknesses were computed in two ways; either to withstand 1.4 times the largest applied stress using the ultimate strength of the material, or to have the critical buckling thickness using a safety factor of 1.4.

For purposes of optimizing the design, an alternate analysis was made using high strength graphite/epoxy (T300/5208). It was expected that having a body made from this light composite material would save structural mass. Again, a first order analysis was needed before proceeding to a more rigorous one. This analysis was similar to that used for the titanium alloy. In other words, the composite material was modeled as having isotropic properties. These properties were obtained from a flat plate with a ($0^\circ/90^\circ$) layup. The 90° fibers were used to withstand the compressive hoop stress, and the 0° fibers to withstand the longitudinal stress. The assumption of isotropy for a first order analysis is considered a reasonable preliminary design criterion [2].

Of critical importance are the resulting masses for the different cases studied. These are listed in Table VII-2.

TABLE VII-2: WALL THICKNESSES AND MASSES OF STRUCTURAL BODY SECTIONS

Material	Titanium Alloy		Graphite/Epoxy	
Section	t (m)	M (kg)	t (m)	M (kg)
I	.008	114	.020	88
II	.015	345	.015	113
III	.061	84	.140	55
IV	.027	496	.063	343
Total Mass		1039		600

The total structural mass (not including ablator, tanks, seals, or stiffeners) of a vehicle made from titanium alloy (Ti-8Mo-8V-2Fe-3Al), using a 1.4 factor of safety and the ultimate strength of the alloy is 1039 kg. The structural mass of a vehicle built entirely out of high strength graphite/epoxy (T300/5208) is 600 kg. Although both cases require structural masses that are rather high, it is clear that a titanium alloy body is not a viable option because its mass exceeds 50% of total vehicle mass. A reason that titanium turned out inferior (in terms of mass) to graphite/epoxy is that the thin shells (sections I and II) had to be designed using buckling considerations (Eq. 4) rather than collapse pressures (Eq. 3). Although the titanium could withstand the hoop stresses in the front of the vehicle very easily, the longitudinal stress would cause buckling of the cylinder if the design were made on the basis of the hoop stress only. Therefore, these shells are thicker than they need to be to withstand the radial pressure field.

Since the mass of each section is consistently larger for the titanium alloy, any combination of the two materials would yield a greater mass than a body made entirely of graphite/epoxy. It is important to note that since a graphite/epoxy body resulted in greater thicknesses, though lower mass, the internal volume was reduced. To keep the payload volume a constant, it was necessary to increase the length of the vehicle from 7.15 m for the titanium vehicle to 7.5 m for the graphite/epoxy vehicle. However, as stated earlier, this still resulted in the lowest mass.

In previous work, it had been reported that a structural mass as low as 185 kg could be achieved [4]. However, this mass was achieved by assuming an incorrect pressure distribution. The mass reported here results from the design of a vehicle that can realistically withstand the highest pressures at any propulsion mode, along with the 1000g's peak acceleration.

It is feasible to secure a solid disk onto the end of the payload compartment not only to act as the rear end of the payload vessel, but also as a stiffener to enable the vehicle to withstand the radial pressure. This configuration is not treated in this analysis.

Anisotropic Analysis

In order to optimize the structural design, a finite element analysis is required. In particular, an anisotropic finite element analysis can give high order approximations for the graphite/epoxy vehicle and pinpoint stress concentrations. These stresses can be controlled by varying the vehicle thickness until a nominal and more uniform stress distribution exists over the entire body. In the following analysis, the preliminary thicknesses obtained from the isotropic approximation for the graphite/epoxy are used in an anisotropic finite element analysis to obtain displacements, stress distributions, total mass, and moments of inertia.

The code used is SUPERSAP [5]. Because it cannot do fully anisotropic materials, a quasi-isotropic layup was used. Thus, an optimal layup cannot be determined from this code. The quasi-isotropic layup is shown in Fig. VII-7. This layup has the simplicity of equal properties in three directions: along the fibers, perpendicular to the fibers (in the plane of a flat plate), and through the thickness (perpendicular to the plate). The stiffness matrix can be described by three independent parameters as opposed to four. This minimizes computing time and necessary memory.

A total of 804 nodes resulted in 621 four-node two dimensional elements. Four-node elements were selected because the thickness after the frustum does not allow using shell elements. Nevertheless, only the profile of the vehicle needed to be specified with a flag to indicate an axisymmetric structure. This profile is shown in Fig. VII-8. The boundary condition at the base of the body constrains one surface node from motion in the longitudinal direction. This has the effect of making the vehicle appear slightly stiffer than it really is in the region close to the base.

A loading of 1,000 g's and the pressure described earlier produced the deformed configuration in Fig. VII-9 in which the displacement has been magnified 10 times. Displacements are on the order of 1 cm which is a strain of less than 0.3%. The maximum displacement was 1.25 cm at the leading edge of the vehicle, but since there is actually an ablator that precedes it, the displacement is expected to be less. Through inspection of the

computer output, it was evident that the hoop stress was the maximum stress present. Figure VII-10 shows the stress distribution on a distorted body to enhance the detail. The stresses in this mesh (slightly adjusted from the previous preliminary sizing to avoid stress concentrations) resulted in stresses that are smaller than the ultimate compression strength of the Graphite/Epoxy (526 MPa). However, some of these stresses do not meet the 1.4 safety factor. This indicates that slight resizing of the vehicle thickness should be made to lower the maximum stresses and to somewhat increase the minimum stress magnitudes to obtain a more uniform stress distribution, or, alternately, to analyze a ply layup with more fibers in the 90° direction. The mesh presented here resulted in a structural mass of 625 kg which is comparable to the mass from preliminary sizing (600 kg). The center of gravity along the longitudinal axis was found to be 5.3 m from the base with a moment of inertia of 702 kg*m^2 for the structure or approximately 2270 kg*m^2 for the 2000 kg system when the mass is homogeneously distributed in the vehicle compartments as described above. The center of gravity is aft of the center of pressure which makes the vehicle inherently unstable. Although stability problems have previously been recognized, no stability control systems have yet been designed. Thus, no internal volume has been allowed for them and they are not part of the total integral mass of the vehicle system at this time.

FAILURE CRITERIA

Note that the thicknesses of the vehicle shell were found for values that avoided stresses on the body greater than 1.4 the ultimate strength. This simplified criterion for isotropic materials with simple loadings resulted in thicknesses that were computed for buckling or for collapse loads, whichever was greater. However, the mechanisms of failure in composite materials are many and involve interlaminar shear, delamination, buckling, voids, broken chains, thermal expansion, differential elastic properties, etc [6]. It is noted by Chamis that the definition of ply failure is still controversial. Thus, failure criteria provide the basis for establishing the strength of a structure under combined stresses. The existing failure criteria are many and range from the simple (maximum stress or maximum strain with

no stress interaction) to those of greater complexity (three dimensional Huber-Mises yield criterion) [7]. It is argued by some that to fully take advantage of composite materials, a design for the full stress-strain range including the range of considerable nonlinearity be considered [6].

ABLATIVE SHIELD AT VEHICLE REAR

The shock wave of the oblique detonation propulsion mode increases the flow temperature to a magnitude that would melt the titanium alloy or graphite/epoxy in sections III and IV of the body which consist of a small cylinder and a tail cone as was shown in Fig. VII-6. To avoid melting or sublimation of the structures, an ablative heat shield is necessary. A standard carbon/carbon composite ablator was chosen to protect the vehicle. The mass flow rate per unit area ($\dot{m}/A$) of the carbon/carbon ablator being evaporated off and total time, t, for the vehicle to travel through the launch tube are calculated to determine the necessary thickness of the ablator. In the oblique detonation mode, the ram accelerator vehicle goes through four different gas mixtures at different velocities, therefore the mass flow rate per unit area and time must be determined for each section. The mass flow rate per unit area, ($\dot{m}/A$), can be found from:

$$q'' = \Delta H(\dot{m}/A) \qquad (7)$$

where ΔH is the heat of vaporization (2.28×10^7 J/kg) for carbon/carbon, and q" is the heat flux from the surroundings to the ablator. Hertzberg and colleagues [10] have shown that the wall heat flux is very small below 5 km/sec and varies from 3×10^5 W/m^2 at 5 km/sec to about 2×10^6 W/m^2 at 9 km/sec in the propellant mixtures. For present purposes an average heat flux of 1.2×10^6 W/m^2 was assumed. The flight time of the vehicle between the above velocity limits is approximately 1 second and thus the total heat load is 1.2×10^6 J/m^2. Knowing the total surface area of the cylinder and the frustum, the mass and thickness of the carbon/carbon ablator were determined as 2.1 kg and 3 mm.

PROPELLANT TANK DESIGN

A preliminary design (Fig. VII-1, vehicle type 1) has the tanks placed on top of each other with the exception of the N_2H_4 (hydrazine) for the attitude control rockets. This tank, because of its small volume is kept in a spherical or toroidal shell. The tanks are basically cylindrical in shape, however the corners are rounded to accommodate a diaphragm to push the propellant out. This configuration appears to provide the most efficient use of space, with a total volume of 0.245 cubic meters (for a ΔV of 780 m/sec). First approximate calculations show that a titanium vessel of seven millimeters thick is all that is required to safely contain each of the propellants during maximum in-tube acceleration.

CENTER OF MASS AND MOMENT OF INERTIA

For simplicity of calculation, the axisymmetric vehicle was divided into four sections. Each section was assumed to be a solid homogeneous body with dimensions defined by Fig. VII-6. With this assumption, the sectional mass center x and radial moment of inertia I_y' with respect to the sectional mass center were calculated for two different structural configurations. These values are shown in Table VII-3.

TABLE VII-3 : SECTIONAL MASS CENTER AND MOMENT OF INERTIA

STRUCTURE MATERIAL	SECTION	L(m)	X(m)	I_y' (kg·m^2)	M(kg)
CARBON COMPOSITE	I	1.67	2.60	394	88
	II	2.18	3.691	410	110
	III	0.15	5.23	460	55
	IV	2.20	6.00	1016	346
TITANIUM	I	3.10	2.33	270	114
	II	1.38	3.79	176	345
	III	0.35	4.93	15	84
	IV	2.20	5.92	460	496

For the entire vehicle, the mass center can be calculated by

$$\bar{x} = \sum_{i=I}^{IV} \tilde{x}_i M_i / \sum_{i=I}^{IV} M_i. \qquad (8)$$

Also the parallel axis theorem gives the radial moment of inertia I_y with respect to the vehicle's mass center

$$I_y = \sum_{i=I}^{IV} (Iy')_i + M_i(\bar{x}-\tilde{x}_i)^2. \qquad (9)$$

The results for the two different configurations are shown in Table VII-4.

TABLE VII-4 : VEHICLE MASS CENTER AND MOMENT OF INERTIA

STRUCTURE MATERIAL	X(m)	I_y(kg.m2)	TOTAL STRUCTURAL MASS (kg)
CARBON COMPOSITE	4.40	6353	600
TITANIUM	4.28	6363	1039

Good vehicle stability requires the mass center to be located upstream of the aerodynamic center of pressure. However, all configurations considered were unstable, although the degree of instability varied. In Table VII-4 the titanium structure has the best stability but also has a poor payload fraction of 19%. On the other hand the graphite composite structure has poor stability but high payload fraction of about 35%. To improve on stability, the vehicle should have more mass in the front of the body. It is stressed here that the inherent stability problems of the ram accelerator vehicle be addressed in further analyses.

RECYCLING THE VEHICLE MATERIAL

Once the payload has been successfully delivered to the space station, there is a question concerning the reusability of the vehicle's material. The most common and needed material for use in erectable space structures and beam building machines has been cited to be composites, specifically graphite/epoxy [2]. Thus, it would be practical to reuse the composite material of the vehicle for use in a large space structure such as a space antenna.

According to Inoue [8], there are a wide range of techniques for machining composite materials with applications to future use in other structures. Thermally set polymer matrix composites (PMC's), of which graphite/epoxy is a member, can be cut several ways: 1) water jet, 2) abrasive water jet, 3) laser beam, 4) electron beam, and 5) plasma arc. Options 3-5 are quite costly, but options 1 and 2 are impractical. The scarcity of water in space necessitates its conservation, so the water used to cut the composite would have to be recycled. Laser beams however, give the cleanest cuts and incur the least amount of fiber damage to the material.

Since the rocket motor is expected to cost in excess of one million dollars, it is vital to retrieve it. Because the payload will be retrieved, the rocket motor is also accessible for reuse. Details of this procedure have yet to be investigated.

LAUNCH TUBE

The wall thickness for the launch tube wall was determined for AISI 4340 steel (assuming a conservative yield stress of 1.4 GPa) with a safety factor of 3 to assure resistance to fatigue failure and to keep internal deformations small. For thick-walled tube theory, the following equations apply:

When an internal pressure is applied at the tube inner radius, the radial stress, σ_3, is calculated from,

$$\sigma_3 = \frac{P(K^2 - k^2)}{k^2(K^2 - 1)} \qquad (10)$$

where K is the ratio of the tube outer radius and the inner radius, and k is the ratio of the inside radius of the deformed tube to the inner radius of the undeformed tube. Since yielding of the material is undesirable, k was taken to equal unity to assure tube longevity since a vehicle may be launched as often as every two or three hours.

Similarly, the tangential stress is calculated from,

$$\sigma_t = \frac{P(K^2 + k^2)}{k^2(K^2 - 1)} . \qquad (11)$$

The stress in the longitudinal direction of the tube is given by,

$$\sigma_l = \frac{P}{K^2 - 1} . \qquad (12)$$

Lastly, the octahedral equilibrium stress which is a function of the radial, tensile, and longitudinal stresses is obtained from,

$$\sigma_{eq} = P\,[\,(\sigma_3 - \sigma_2)^2 + (\sigma_2 - \sigma_1)^2 + (\sigma_1 - \sigma_3)^2\,]/(2)^{.5} \qquad (13)$$

The equation of interest (the non-dimensional octahedral stress) can finally be used to determine the thickness,

$$\sigma_{eq} / P = [\,(4k^2 - 2k^2K^2 + K^4)^{.5}) / (3k^2(K^2 - 1))] \qquad (14)$$

The wall thickness required for the subsonic combustion portion of the barrel (1.0 m I.D.) is 12.7 cm while the wall thickness of the oblique detonation portion is 27.6 cm for the first 2.3 km and 24.8 cm for the remaining 2.5 km. This results in a total tube mass of 41,700 metric tons. Together with the initial accelerator, the total system tube mass is 41,844 metric tons.

Some alternatives that should be looked into in the future are: Autofretage, multi-layer construction, strip and wire winding, and composite materials. Manning and Labrow [9] have developed information on the first three types. Using one of these alternatives could greatly decrease the overall weight of the launch tube although it would increase its

fabrication complexity and cost. Therefore, the selection of tube wall material is likely to be guided more by economic considerations than by weight.

As noted in Chapter IV, the vehicle is aerodynamically unstable during the acceleration in the launch tube. Accordingly, some means of stabilizing the vehicle within the tube is required. One straightforward approach is to attach a set of three equally spaced guide rails to the bore of the tube as shown in Fig. VII-11. These rails, fabricated of steel or other suitable material, would touch the vehicle only very lightly, and thus would not be expected to wear significantly, or to cause frictional drag or erosion problems for the vehicle.

In order to contain the propellant mixture in the tube, it is necessary to provide end closures similiar to the petaling diaphragm closure discussed in Chapter II. Also, in order to seperate the nine different propellant mixtures thin lightweight plastic diaphragms would be used. These would be sufficiently strong since they would not support a pressure difference (all propellant mixtures are at a fill pressure of 33 atm.). Clearly, diaphragm and closure replacement mechanisms will need to be incorporated into the design. This aspect of launch tube design has not been examined in detail here, but needs to be addressed in future studies.

CONCLUSIONS

In the structural design of a payload vehicle, one configuration was selected. This configuration placed the orbit circularization rocket in the tail cone with the payload in the nose cone and midsection. Three propellant tanks were placed in the remaining volume. An acceleration of 1,000 g's and a maximum pressure of 169.8 MPa (25 Ksi) are the loadings on the vehicle. The vehicle was designed to withstand the maximum pressure on its surface or to withstand buckling, whichever is the greater effect. A titanium alloy (Ti-8Mo-8V-2Fe-3Al) and graphite/epoxy (T300/N5208) composite were considered for the vehicle structural material. It was shown that the titanium alloy was inferior to graphite/epoxy in terms of mass. The graphite/epoxy vehicle had a mass of 600 kg for a 7.5 m long vehicle, and the titanium body resulted in a mass of 1039 kg. A quasi-isotropic finite element analysis was performed on the graphite/epoxy as a higher order analysis. A high correlation was found in

the two analyses but the computer code revealed that the 1.4 safety factor is not met at all the elements and indicates that slight vehicle resizing is required. With the graphite/epoxy vehicle a payload mass fraction of 35% was achieved. It is suggested that further studies emphasize the obtaining of an optimum thickness using a computer code to obtain an optimum layup and ultimately to minimize the mass. Reusability of the vehicle material for other space structures is also proposed. Because the rear portion of the vehicle encountered temperatures of the order of 4,000 °K, an ablative shield over the rear is required to protect the vehicle. This shield has a mass of 2.1 kg yielding a thickness of 3 mm.. Preliminary design of the launch tube resulted in a mass of 41,844 metric tons.

REFERENCES

1. Bogdanoff, D.W. and Bracket, D., "A Computational Fluid Dynamics Code for the Investigation of Ramjet-in-Tube Concepts," AIAA Paper 87-1978, AIAA/SAE/ASME/ASEE, 23rd Joint Propulsion Conference, San Diego, CA, June 29-July 2, 1987.

2. Department of Defense, National Aeronautics and Space Administration, Advanced Composites Design Guide, Wright-Patterson Air Force Base, OH, 1983.

3. Roark, Raymond J., Formulas for Stress and Strain, McGraw-Hill, New York, 1975.

4 Bruckner, A.P. and Hertzberg, A., "Ram Accelerator Direct Launch System for Space Cargo," Paper No. IAF-87-211, 38th Congress of the International Astronautical Federation, Brighton, England, October 10-17, 1987.

5. Algor Interactive Systems Inc., ALGOR SUPERSAP, Finite Element Analysis System, Pittsburgh, PA, 1988.

6. Broutman, L. J. and Krock, R. H., Composite Materials, Vol. 5, Academic Press, New York, 1975.

7. Hinton, E. and Owen, D. R. J., Finite Element Software for Plates and Shells, Pineridge Press, Swansea, United Kingdom, 1984. pp. 235-396.

8. Inoue, H., "The Machinability of Composites", University of Washington Mechanical Engineering Department Seminar, Seattle, WA, March 4, 1988.

9. Manning, W. R. D., and Labrow, S., High Pressure Engineering, CRC Press, Cleveland, Ohio, 1971. pp. 121-130

10. Hertzberg, A., Bruckner, A.P. and Bogdanoff, D.W., An Exploratory Study of Ram Accelerator Principles, Progress Report No. F08635-84-K-0143, Aerospace and Energetics Research Program, University of Washington, Seattle, WA, April 15, 1985.

NOMENCLATURE

a	outside radius
A	unit area
b	inside radius
E	Young's modulus of elasticity
ΔH	heat of vaporization
I_y	vehicle mass moment of inertia about the radial axis
m	ablator mass flow rate
M	Mach Number
M_i	sectional mass
N	axial force/unit length
p	external pressure on the vehicle
q	heat flux per unit area
r	local vehicle radius
t	wall thickness
ΔV	apogee burn
$\bar{x}$	center of mass location along vehicle axis measured from nose cone
$\tilde{x}$	sectional center of mass
ν	Poisson's ratio
ρ	mass density
σ_1	longitudinal stress
σ_2	hoop stress
σ_3	radial stress
τ	shear stress

ν	Poisson's ratio
ρ	mass density
σ_1	longitudinal stress
σ_2	hoop stress
σ_3	radial stress
τ	shear stress

subscripts:

$()_o$	stagnation property
$()_w$	wall property
$()_I$	nose cone structure
$()_{II}$	water payload and container
$()_{III}$	rocket propellant and containers
$()_{IV}$	rocket motor, nozzle and casing

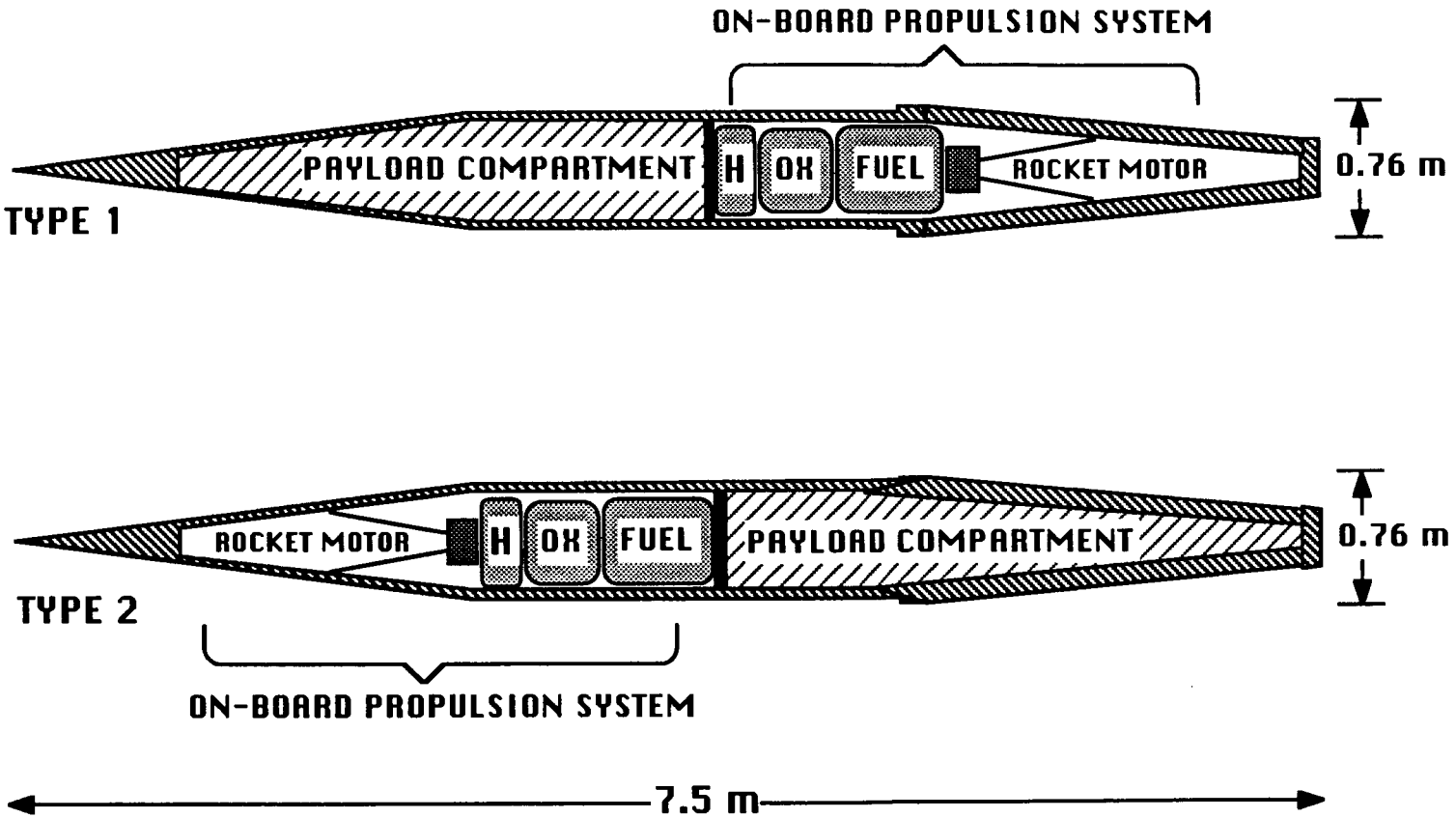

FIG. VII-1: POSSIBLE COMPONENT CONFIGURATIONS FOR THE RAM ACCELERATOR VEHICLE

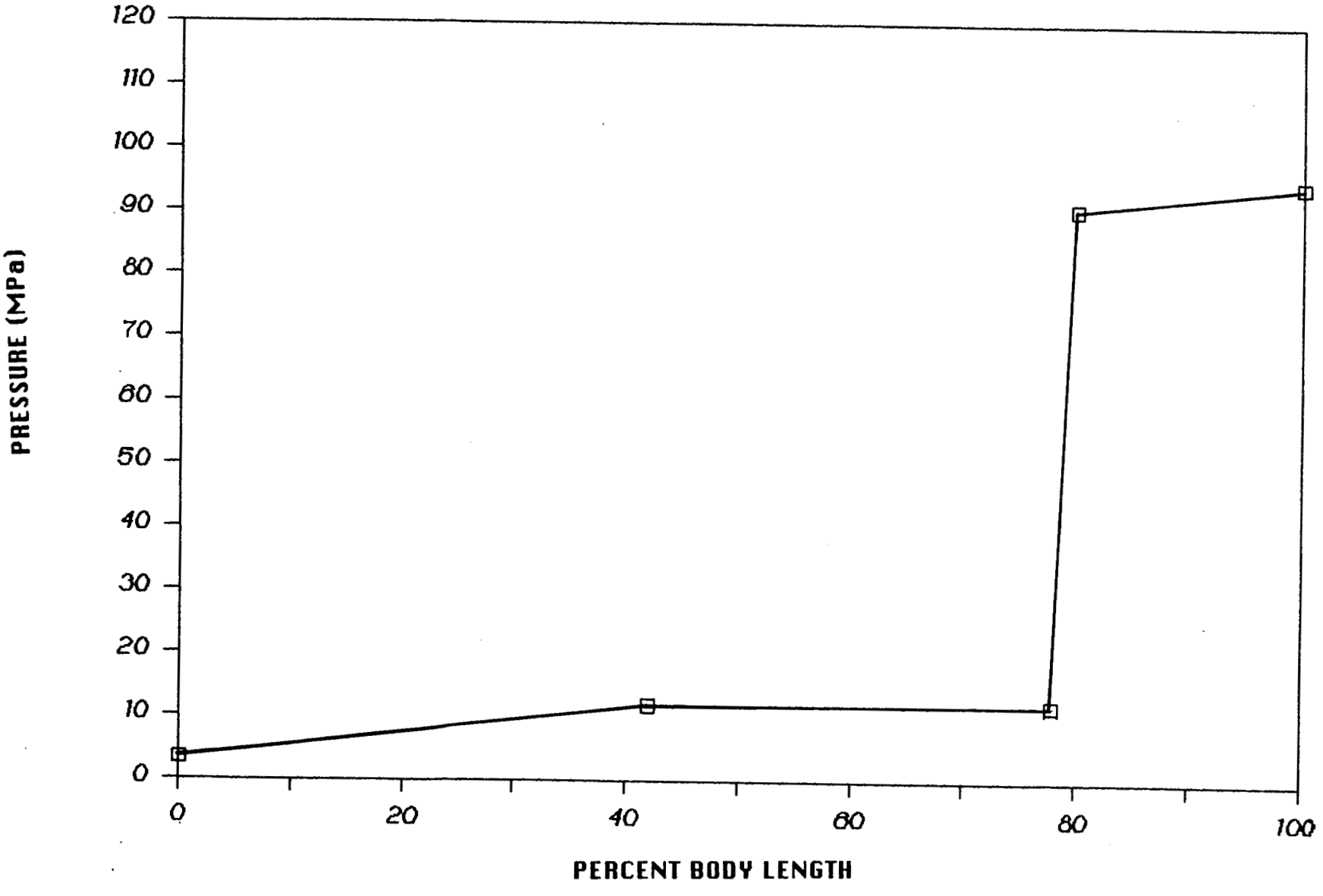

FIG. VII-2: PRESSURE DISTRIBUTION FOR THE 1-D THERMALLY CHOKED MODE

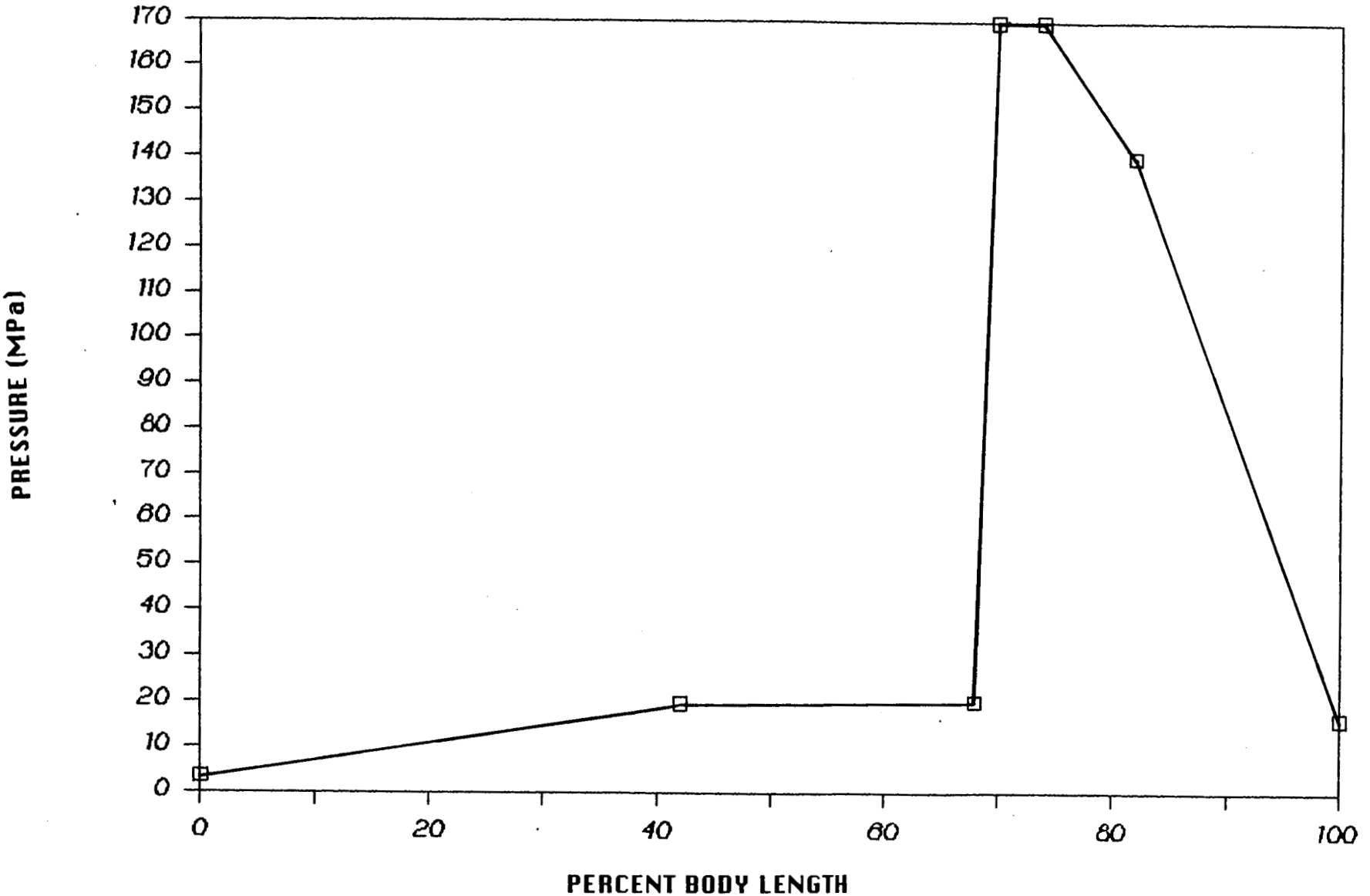

FIG. VII-3: PRESSURE DISTRIBUTION FOR THE 1-D OBLIQUE DETONATION MODE

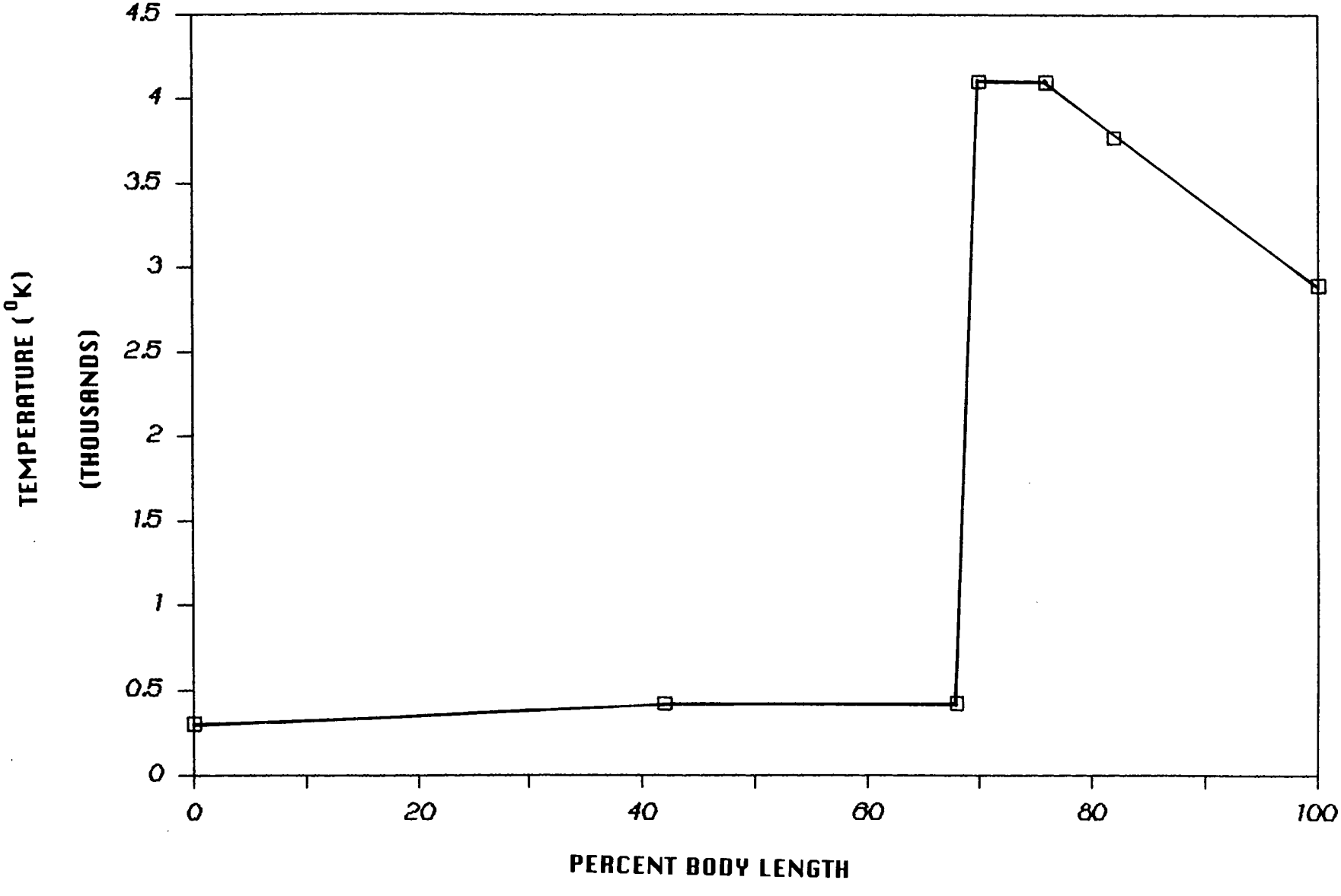

FIG. VII-4: TEMPERATURE DISTRIBUTION FOR THE 1-D OBLIQUE DETONATION MODE

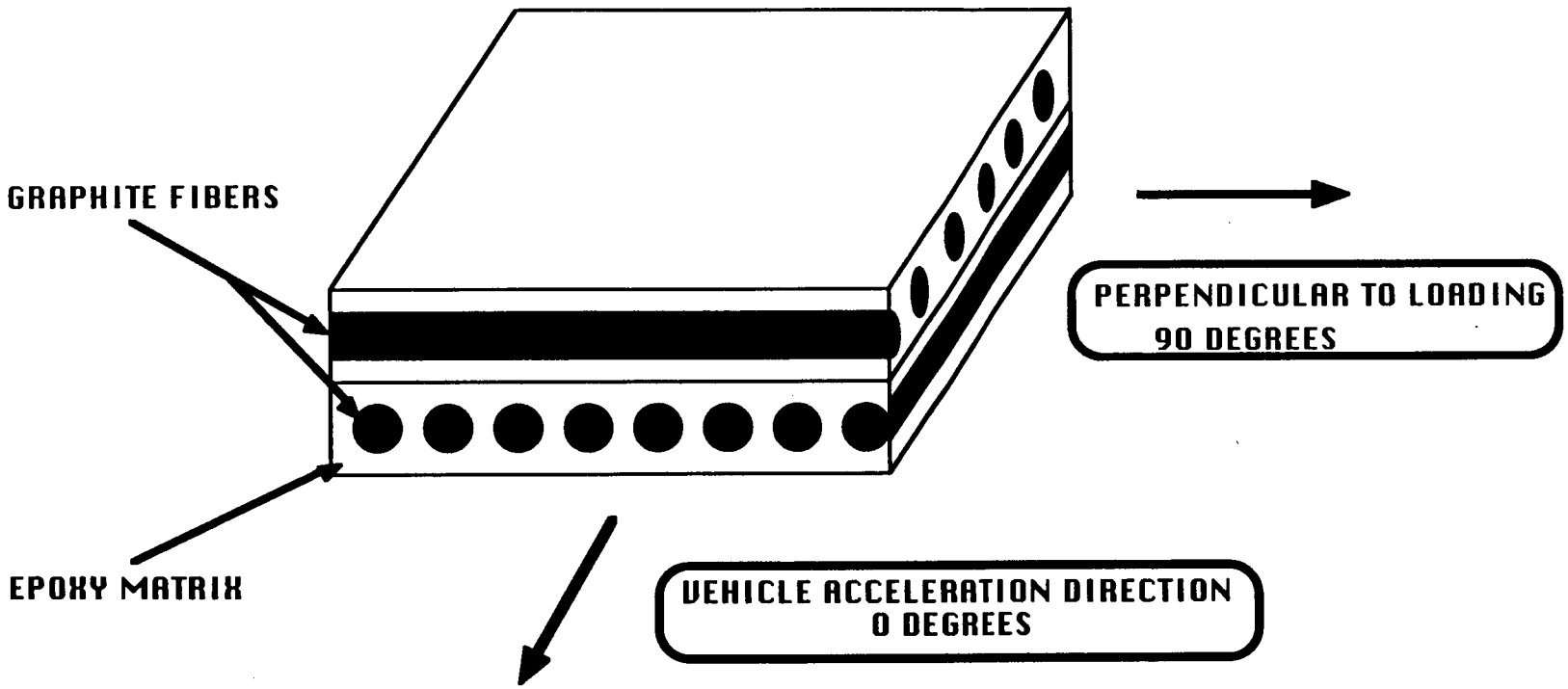

FIG. VII-5: MACROSCOPIC VIEW OF A (0/90) LAYUP

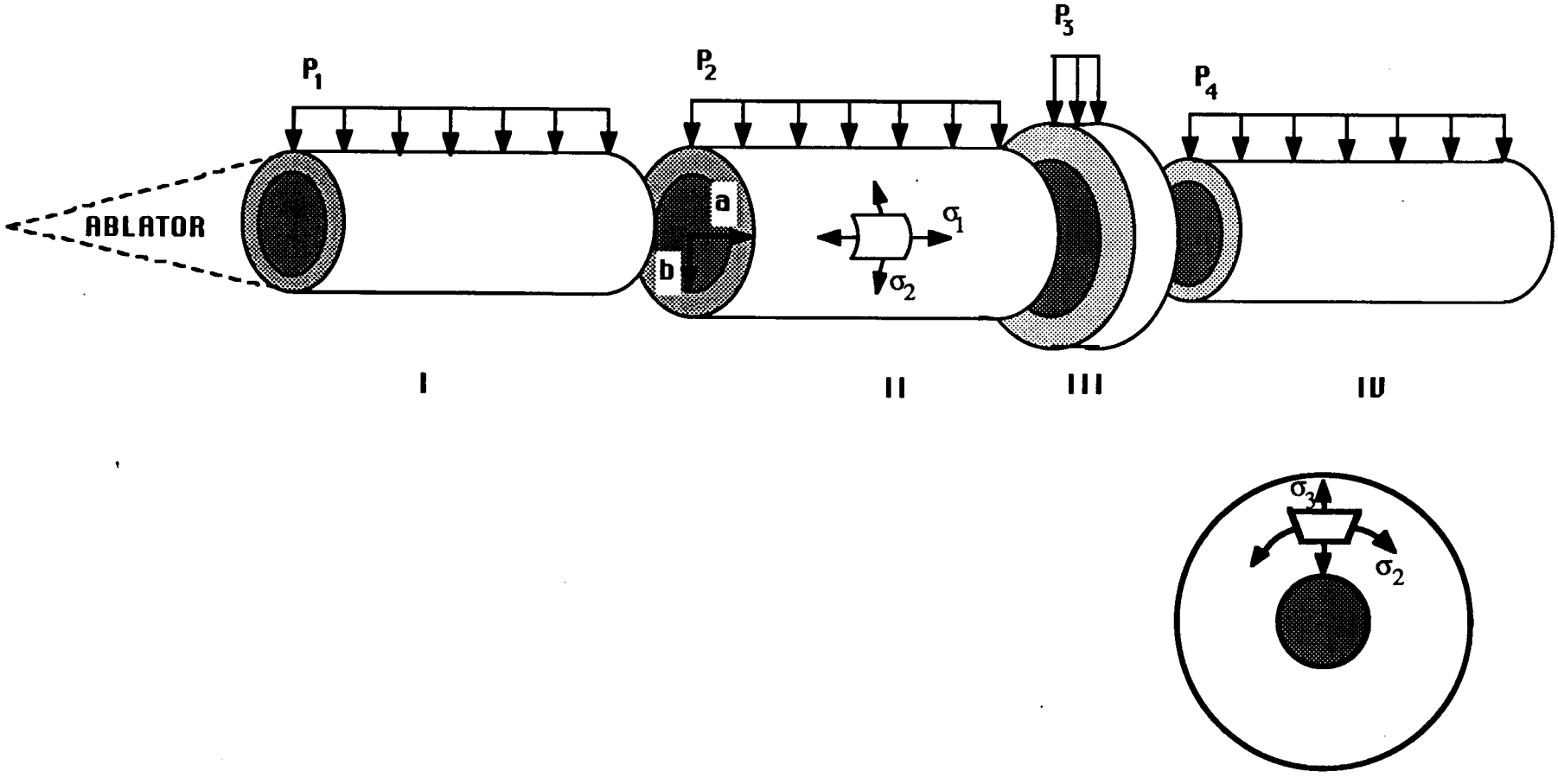

FIG. VII-6: STRUCTURAL MODEL OF THE RAM ACCELERATOR VEHICLE WITH AXISYMMETRIC PRESSURE

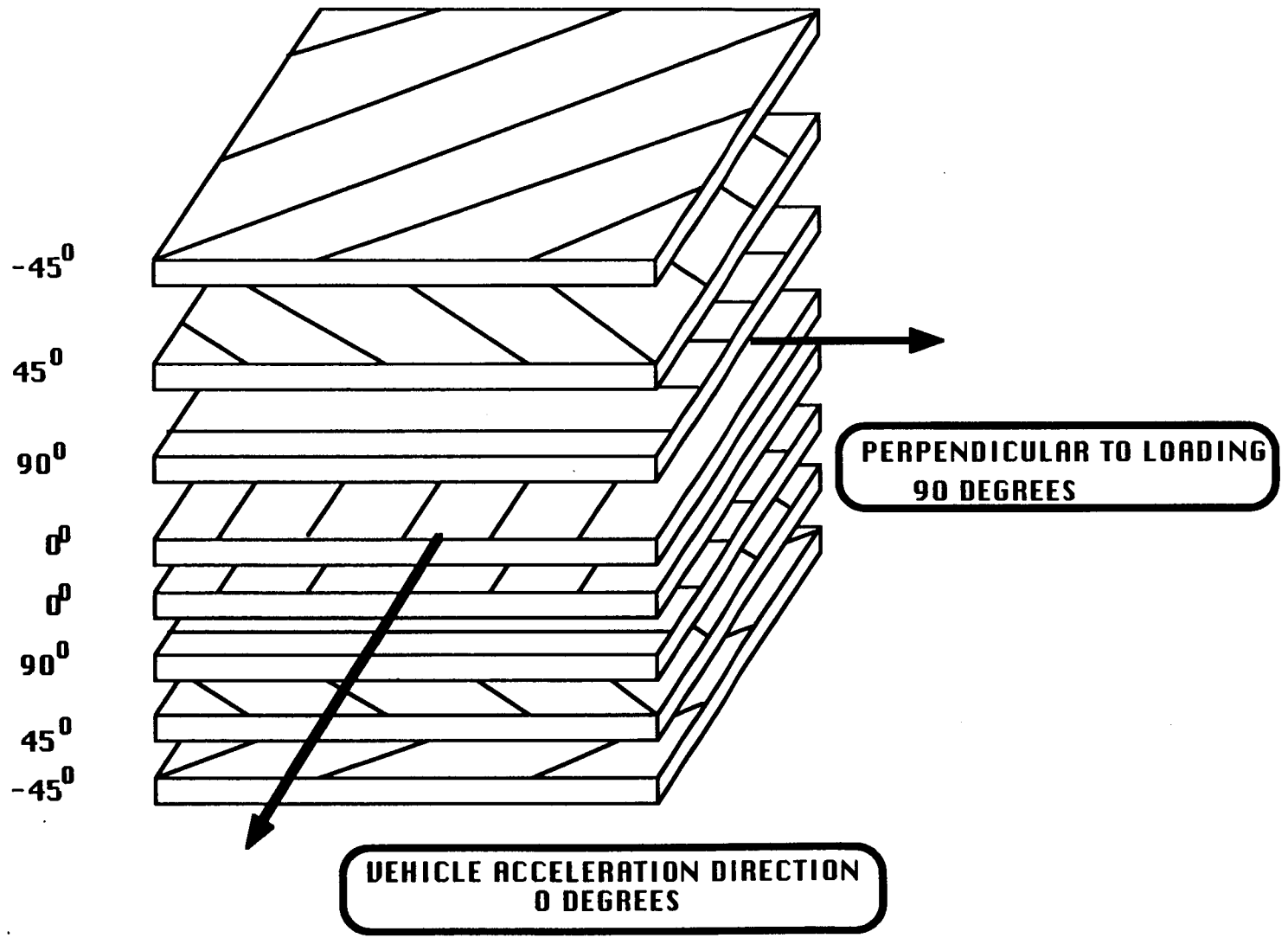

FI. VII-7: MACROSCOPIC VIEW OF A QUASI-ISOTROPIC LAYUP

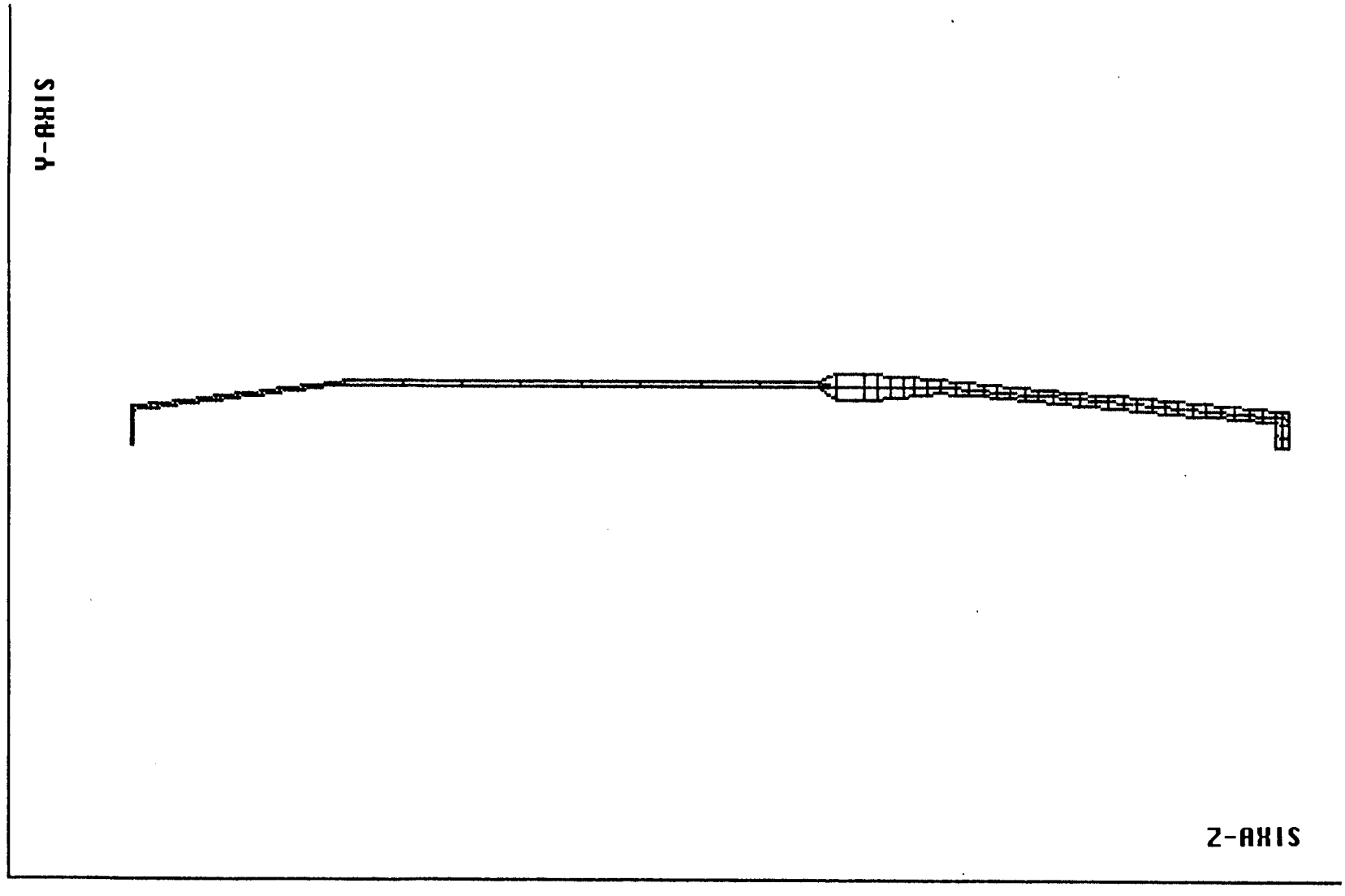

FIG. VII-8: PROFILE OF AN AXISYMMETRIC FINITE ELEMENT MESH FOR THE RAM ACCELERATOR VEHICLE

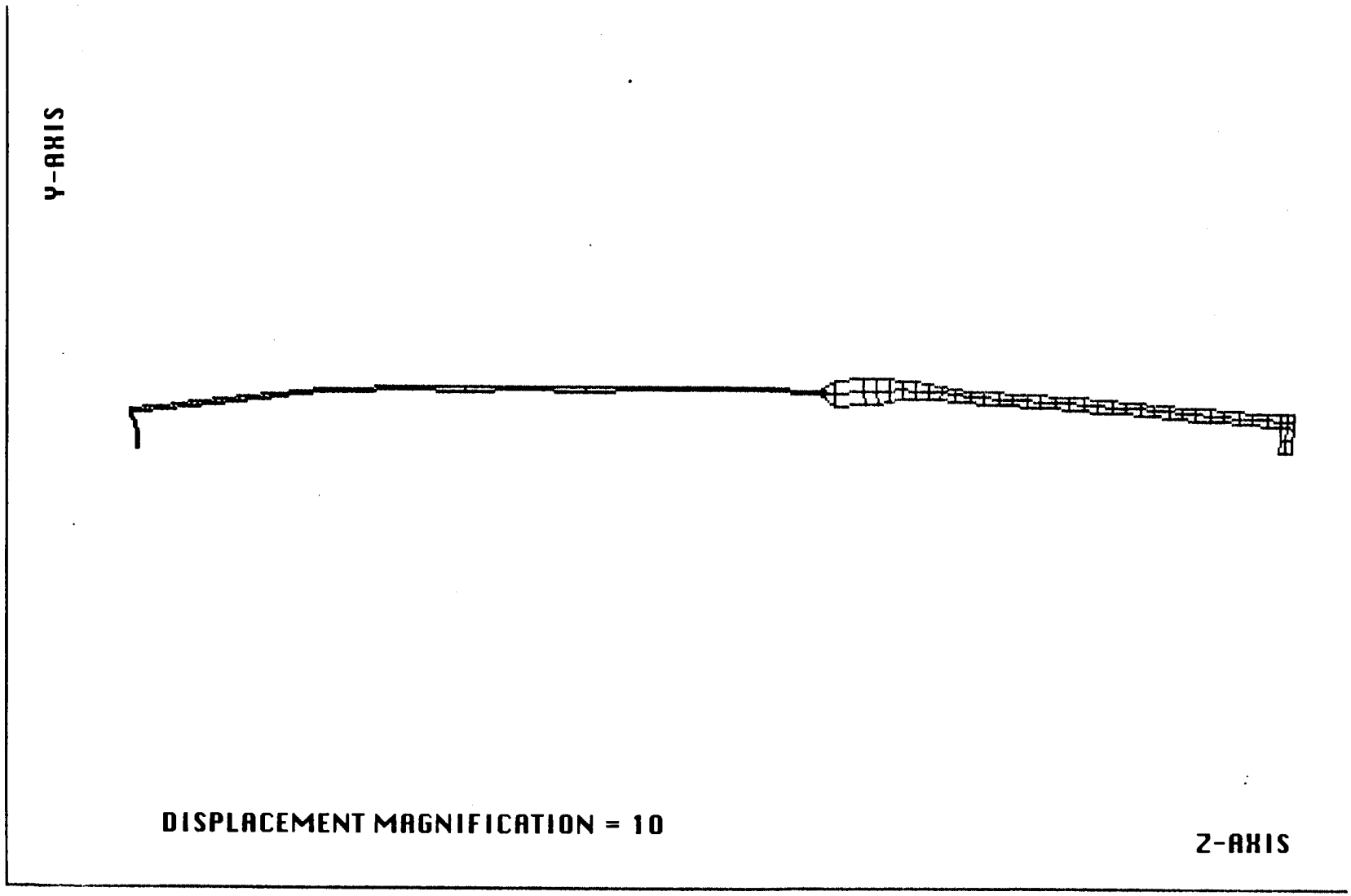

FIG. VII-9: DEFORMED PROFILE OF AN AXISYMMETRIC FINITE ELEMENT MESH FOR THE RAM ACCELERATOR VEHICLE

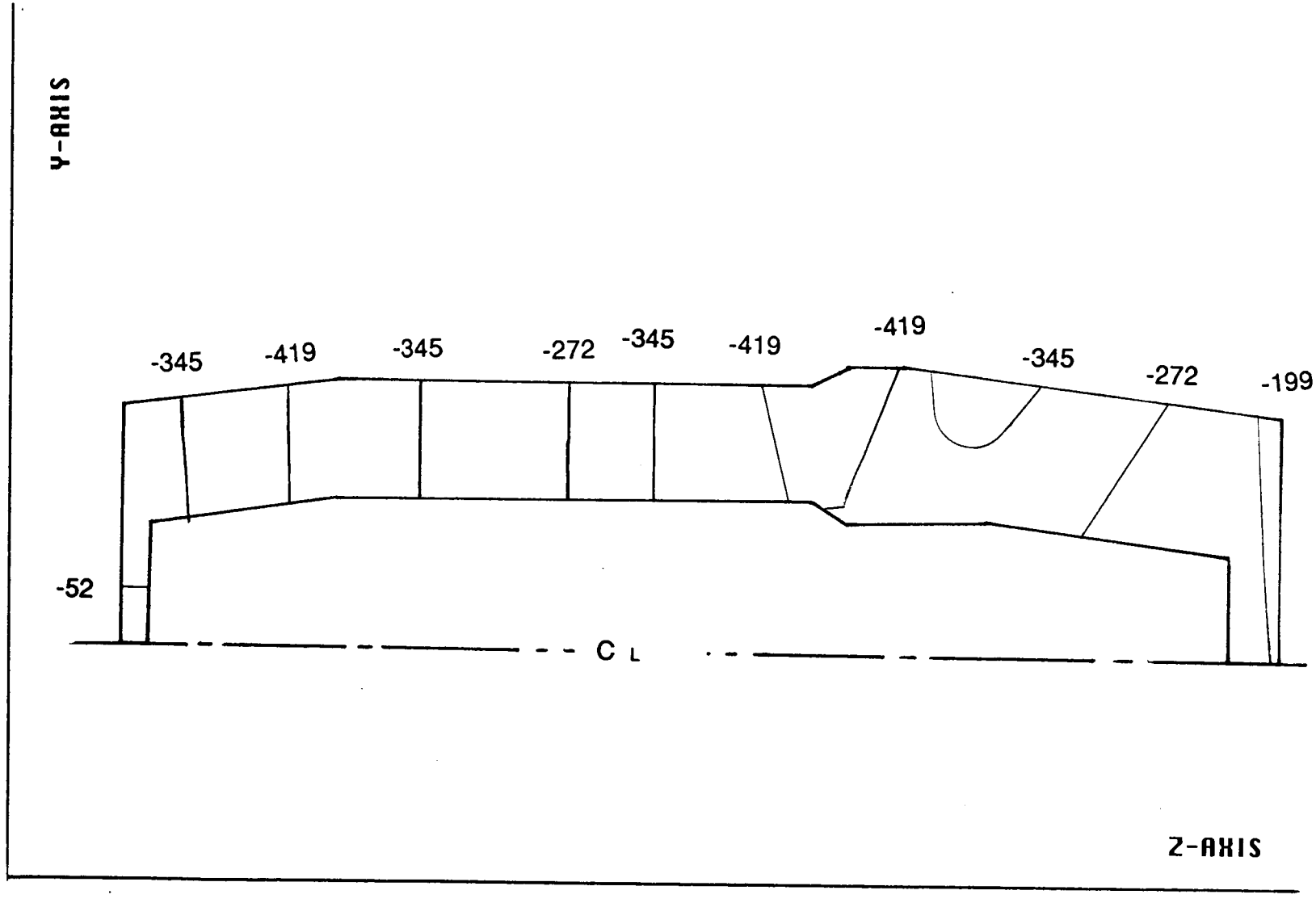

FIG. VII-10: HOOP STRESS DISTRIBUTION FOR THE RAM ACCELERATOR VEHICLE (RADIAL SCALE EXAGGERATED) (MPa)

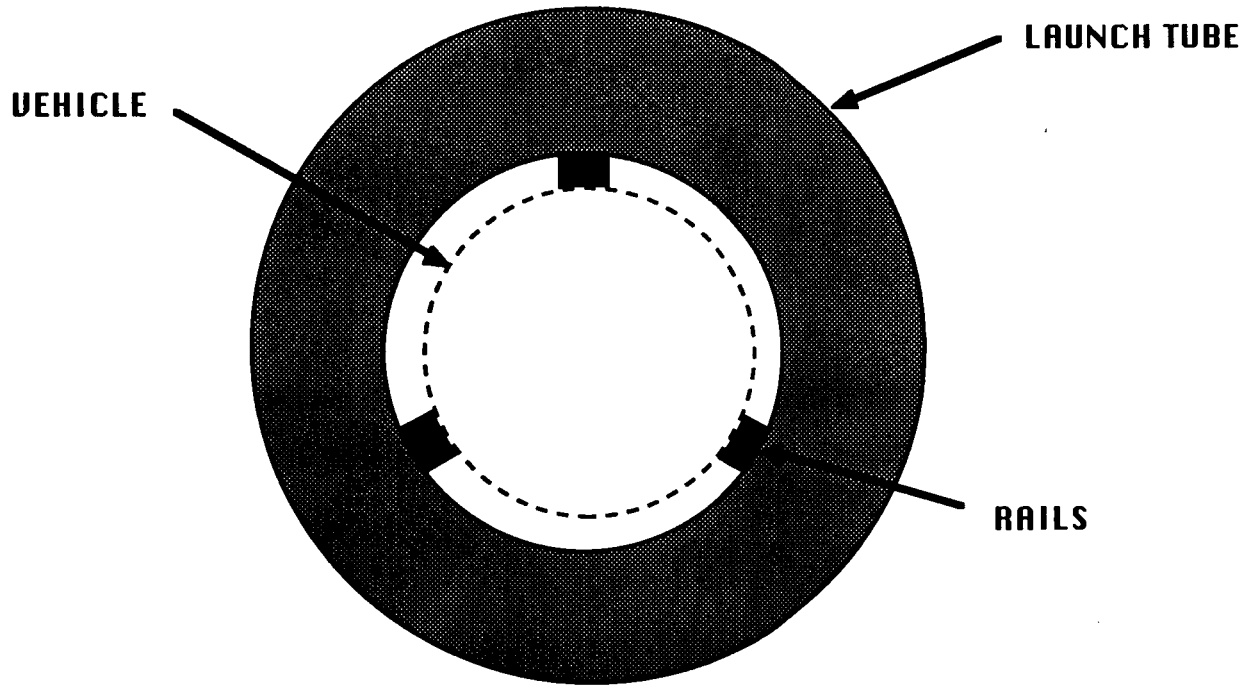

FIG. VII-11: SCHEMATIC OF LAUNCH TUBE CROSS SECTION SHOWING VEHICLE GUIDE RAILS

VIII. CONCLUSION

The ram accelerator mass launch system was conceived as a means of economically launching acceleration insensitive payloads into a low earth orbit. In previous years feasibility studies were done and proposals made on how to best design the systems of this concept. This year the research centered on a systems analysis based on the proposals from previous years. The study was divided into six systems. Each system was researched and designed based on the use of current technology to launch a 2000 kg vehicle into a low earth orbit with as high a payload fraction as possible (the goal being 50%).

The vehicle is initially accelerated to a velocity of 0.7 km/sec using a combustion-driven gas gun. From 0.7 km/sec two ram accelerator propulsive modes are used to propel the vehicle to the necessary launch velocity. They are a thermally choked subsonic combustion mode which propels the vehicle to 2.5 km/sec, where a transition is made to an oblique detonation mode which accelerates the vehicle to 9 km/sec. The total length of the stationary launch tube is 5.1 km for a maximum acceleration within the tube of 1000 g's.

The hypersonic launch velocities required the development of a thermal protection system for the nose cone of the vehicle. A carbon-carbon ablating nose-cone was chosen as the thermal protection system. At an optimal launch angle of 20°, for a launch velocity of 9 km/sec at the equator, the vehicle retains 85% of its original launch velocity and suffers an ablative mass loss of only 26 kg. The stability of the vehicle is another primary concern during the atmospheric transit. It was found that the vehicle is highly unstable right out the end of the launch tube and will require stability augmentation devices such as control surfaces to maintain dynamic stability.

The prior feasibility studies proposed the use of a multi-step maneuver with aerobraking to minimize the on-board propellant requirements. A parametric study was performed using launch velocities from 8 km/sec to 10 km/sec, and launch angles from 16-30°. For the multi-step maneuver with aerobraking the optimal launch angles ranged from

22-18° for launch velocities of 8-10 km/sec, respectively. At these launch angles the propellant ΔV requirements range from 1309-473 m/sec to take the vehicle to a space station in a 500 km orbit. Using an MMH-N_2O_4 bi-propellant rocket with an I_{sp} of 297 sec, the on-board propulsion system, including propellant and tanks, has a mass of approximately 470-1000 kg, depending on the launch parameters.

The structural design of the vehicle centered on the use of lightweight, high yield stress graphite/epoxy composites which could withstand the high pressures and accelerations the launch tube. A vehicle configuration incorporating T300/5208 graphite/epoxy resulted in minimal structural mass when approximating the composite material properties as isotropic. The analysis produced a structural mass of approximately 600 kg for a vehicle length of 7.5 m. Estimates of the vehicle center of gravity place it 3.8 m behind the nose tip with a moment of inertia of 6,200 kg/m^2 about an axis perpendicular to the axis of the vehicle.

At the present stage of the design, the payload fraction of the vehicle is ~40% for a design launch velocity of 9 km/sec. Further refinements of the in-tube propulsion modes and of the structural design are needed to increase the payload fraction to the desired level of 50% or more. Optimization of parking orbit altitude and/or eccentricity may also provide an increase in the payload fraction. Methods for recycling vehicle components or for returning them to earth should be investigated. In addition, a cost analysis of the entire launch system should be carried out. The work done thus far, however, has demonstrated the potential of the ram accelerator mass launch concept.

APPENDIX A

LAUNCH SITE

LeAnne Woolf

In selecting a site for a mass launch system, the primary factors to be considered are maximizing the velocity imparted by the earth's rotation by launching from as close to the equator as possible, minimizing the amount of atmosphere to be traversed by choosing a site with a high altitude, and selecting a site with minimal seismic and volcanic activity. In addition, an equatorial launch site is desirable so that the mass launch vehicles can be placed into the same orbit regardless of when they are launched. Other issues to be considered include the climate (for minimal environmental stress on equipment) and the political stability of the country containing the launch site.

The velocity increment contributed to the projectile's speed by earth's rotation is determined by the cosine of the latitude in degrees and by the cosine of the launch direction with respect to due east (see Chapter V) [1]. For a contribution of about 90% or greater of earth's angular velocity when launching due east, a latitude of less than 30° is needed. To reduce atmospheric drag losses following launch, the higher the launch altitude the better. The atmospheric density at 3500 m is approximately 60% of that at sea level. Furthermore, most of the world's agricultural zones are found below 3500 m and thus the ram accelerator would not be likely to impinge on the host country's agrarian pursuits. In order to avoid permanent ice packs that could be quite detrimental to the ram accelerator installation, an upper limit of 6000 m altitude was chosen. These upper and lower limits of latitude and altitude were chosen, after preliminary studies, to maximize the appropriate parameters while still leaving a wide range of possible launch sites to be investigated.

The countries with latitudes of less than 30° and mountains of 3500 m or taller are listed in Table A-1 [2]. Each of them experiences some sort of seismic or volcanic

Table A-1 Countries with Possible Launch Sites

Africa	
Ethiopia	Kenya
Tanzania	
Asia	
Bhutan	Nepal
Irian Jaya (Indonesia)	Papua New Guinea
North America	
Costa Rica	Panama
Mexico	
South America	
Bolivia	Chile
Colombia	Ecuador
Peru	Venezuela

activity, as must be expected of a mountainous area [3]. The only mountains not associated with the high density earthquake areas marking suspected subduction zones are found in Ethiopia, Kenya, and Tanzania. A subduction zone, in the theory of plate tectonics, is an area where an oceanic plate is being overridden by a continental plate. Mountains are built on the leading edge of the overriding plate [3]. The Andes of South America are an excellent example of mountains built by plate collision and subsequent subduction activity.

Eastern Africa is theorized to be the middle of a plate [3] and the earthquake and volcanic activity there is not as well explained as tectonic theory explains such activity elsewhere. There has been some volcanism in the area since 1700 and the faults of the Great Rift Valley are in this vicinity [2], but in comparison to subduction zones, this activity is minimal. In a random six-year period, Ethiopia, which encompasses most of the Great Rift Valley, experienced about six measurable earthquakes, Kenya one, and

Tanzania, site of Mt. Kilimanjaro and other volcanic peaks, had about eight measurable earthquakes [3]. A measurable earthquake starts at a much lower severity than that which can be felt by most humans. Earthquakes which cause structural damage are even more severe than those which can be felt. A more thorough seismic study, as well as an investigation of soil stability, should be made before construction begins; however, a preliminary site choice is made here.

Several factors work against Ethiopia as a launch site. The flight path of the projectile is much more likely to pass over the main area of the Asian land mass before leaving the atmosphere than if launched from Kenya or Tanzania. Ethiopia's current government is not particularly friendly to United States interests and the drought and famine in the country present logistical supply problems. The several rift valley faults are also a consideration. All mountains of greater than 4000 m height are north of 5°N latitude while Kenya and Tanzaia offer mountains very close to the equator.

Mt. Kilimanjaro and Mt. Kenya are both very attractive possibilities (see Fig. A-1). However, Mt. Kilimanjaro has been volcanically active within the last 300 years, whereas Mt. Kenya has not been active, is not near any major faults, and is nearly on the equator. Thus, the recommendation of the author is to place the launch site at Mt. Kenya.

Mt. Kenya is about 112 km north of Kenya's capital city Nairobi and is one of Kenya's major tourist attractions. The multiple, rugged peaks are surrounded by fifteen permanent glaciers [4]. To have less impact on the tourist industry (an important part of Kenya's economy [4]) and to avoid the glaciers, the launch tube site should be carefully chosen. It is also desirable to have a site which allows for a due-east launch. A study of the contours of the higher slopes of Mt. Kenya has been done and a particular site chosen. The average slope of this site is about 12°. In order to use higher launch angles, a tunnel and dike system will need to be constructed, as shown in the example in Fig. A-2. This construction should not prove to be difficult as tunnels of 9.6 km or longer have been

built since 1882 [6] and the United States is dotted with large, free-standing, cement structures.

The temperatures around the mountain are in the 10-20°C range all year and the launch site, at an altitude of approximately 4000 m, is ice free. Annual precipitation is 50-100 cm. The working environment should be quite satisfactory and environmental stresses on equipment minimal, especially since much of it will be underground. Mombasa has large port facilities and the country has good aerial and highway systems [4] capable of handling the logistics of bringing in equipment, supplies, and personnel. Mt. Kenya seems to be as ideal a launch site as possible and all calculations made in this report are based on its use as such.

REFERENCES

1. Ball, K.J., and Osborne, G.F., Space Vehicle Dynamics, Clarendon Press, Oxford, 1967.
2. The Prentice-Hall American World Atlas, Prentice-Hall, Inc., Englewood Cliffs, NJ, 1984.
3. Press, F., and Siever, R., Earth, W.H. Freeman and Company, San Francisco, 1982.
4. Encyclopaedia Britannica, Encyclopaedia Britannica, Inc., H.H. Benton, Publisher, Chicago, 1975.
5. "Mt. Kenya," map compiled and drawn by Directorate of Overseas Surveys, 1957.
6. "World's Longest Railway Tunnels," Railway Directory and Year Book 1980, 1980.

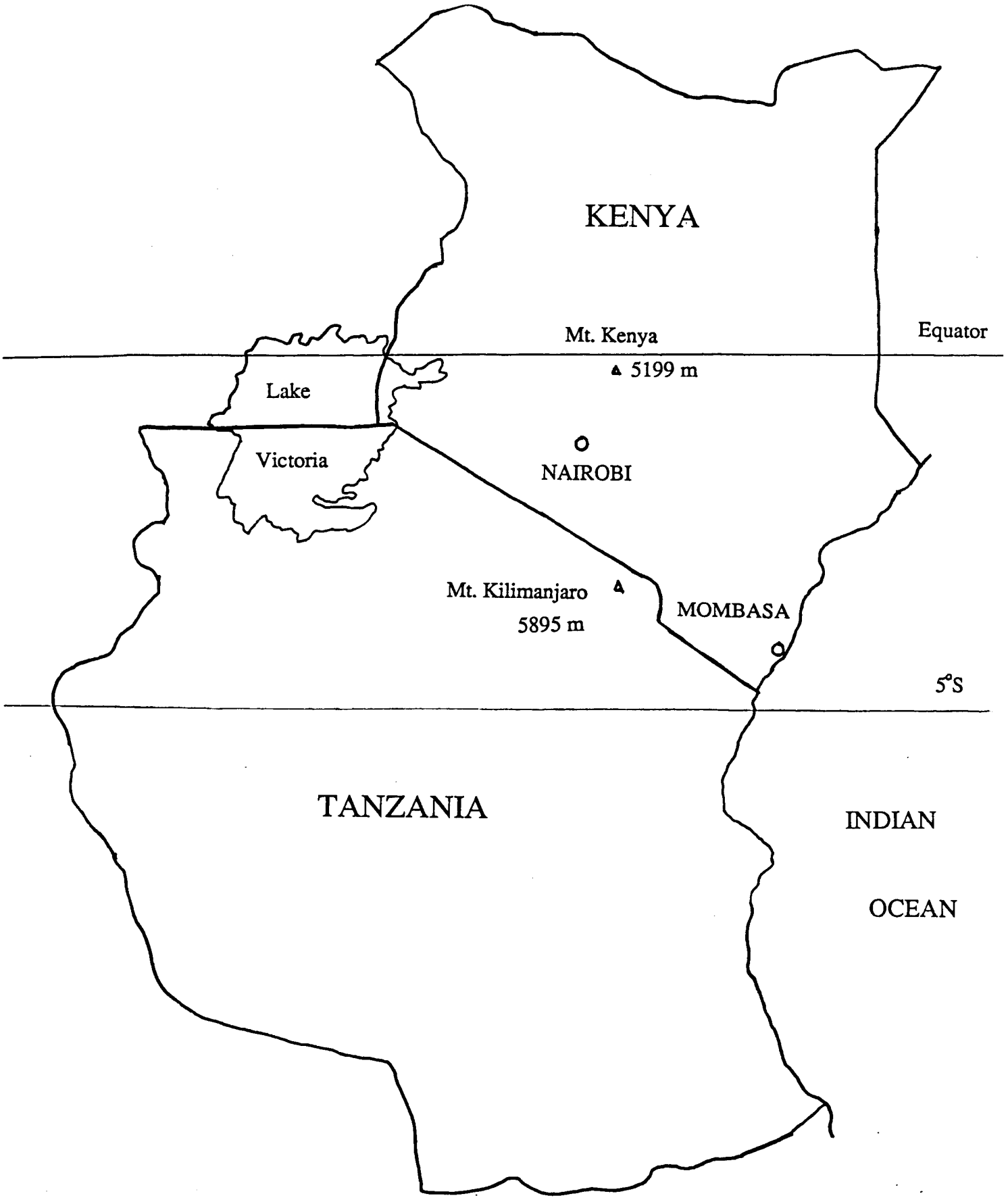

Fig. A-1 Most Likely Launch Sites

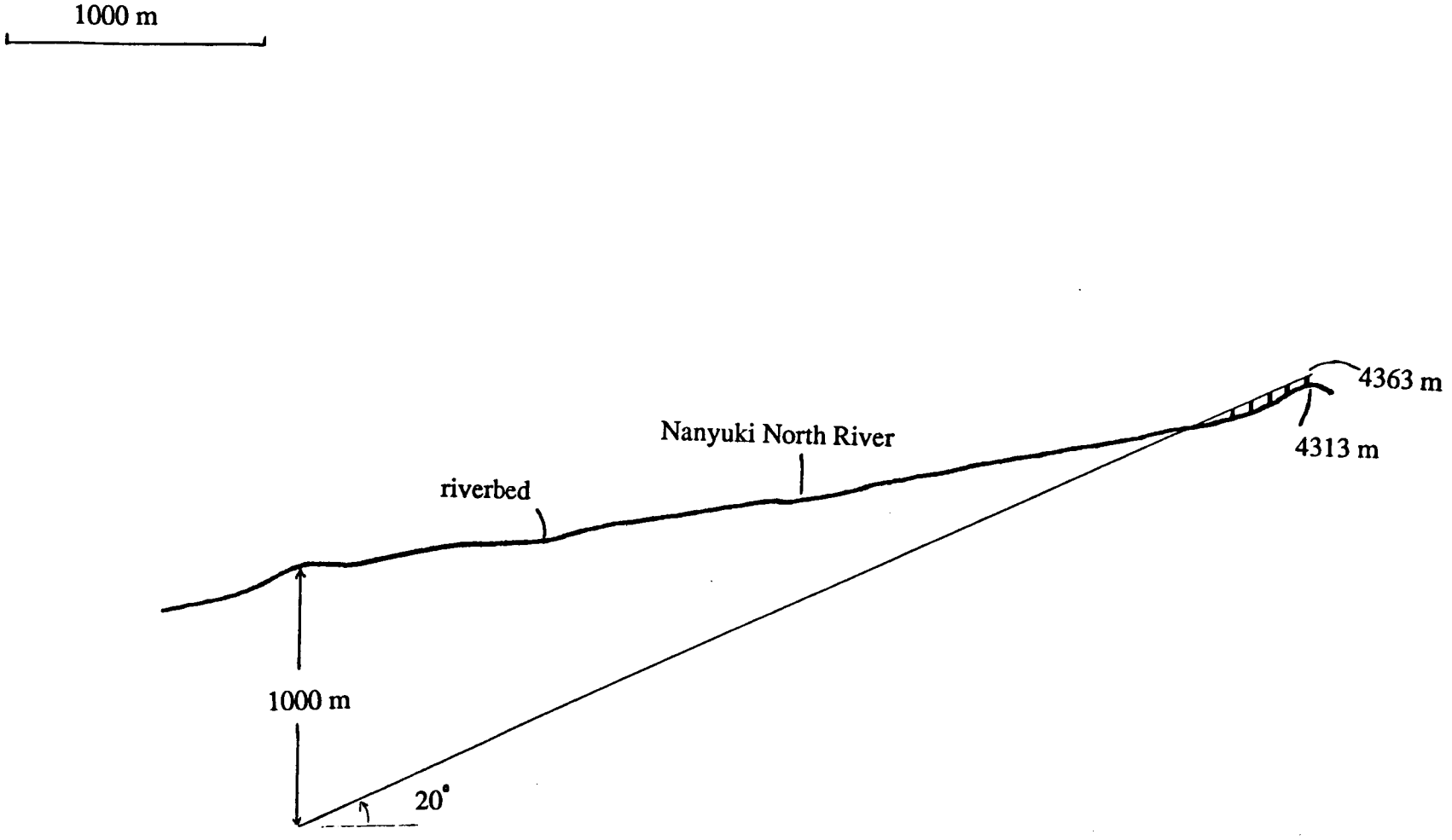

Fig. A-2 Tunnel and Dike Configuration for
Ram Accelerator Launch Tube